Heriot-Watt University

The effect of noise in models of spiny dendrites

Emma Jayne Coutts

May 2010

Submitted for the degree of
Doctor of Philosophy in Mathematics
on completion of research in the
Department of Mathematics,
School of Mathematical and Computing Sciences.

ACADEMIC REGISTRY
Research Thesis Submission

Name*:*			
School/PGI:			
Version: *(i.e. First, Resubmission, Final)*		Degree Sought (Award **and** Subject area)	

Declaration

In accordance with the appropriate regulations I hereby submit my thesis and I declare that:

1) the thesis embodies the results of my own work and has been composed by myself
2) where appropriate, I have made acknowledgement of the work of others and have made reference to work carried out in collaboration with other persons
3) the thesis is the correct version of the thesis for submission and is the same version as any electronic versions submitted*.
4) my thesis for the award referred to, deposited in the Heriot-Watt University Library, should be made available for loan or photocopying and be available via the Institutional Repository, subject to such conditions as the Librarian may require
5) I understand that as a student of the University I am required to abide by the Regulations of the University and to conform to its discipline.

* *Please note that it is the responsibility of the candidate to ensure that the correct version of the thesis is submitted.*

Signature of Candidate*:*		Date:	

Submission

Submitted By *(name in capitals):*	
Signature of Individual Submitting:	
Date Submitted:	

For Completion in Academic Registry

Received in the Academic Registry by *(name in capitals):*			
Method of Submission *(Handed in to Academic Registry; posted through internal/external mail):*			
*E-thesis Submitted (**mandatory for final theses from January 2009)***			
Signature:		Date:	

Abstract

The dendritic tree provides the surface area for synaptic connections between the 100 billion neurons in the brain. 90% of excitatory synapses are made onto dendritic spines which are constantly changing shape and strength. This adaptation is believed to be an important factor in learning, memory and computations within the dendritic tree. The environment in which the neuron sits is inherently noisy due to the activity in nearby neurons and the stochastic nature of synaptic gating. Therefore the effects of noise is a very important aspect in any realistic model.

This work provides a comprehensive study of two spiny dendrite models driven by different forms of noise in the spine dynamics or in the membrane voltage. We investigate the effect of the noise on signal propagation along the dendrite and how any correlation in the noise may affect this behaviour. We discover a difference in the results of the two models which suggests that the form of spine connectivity is important. We also show that both models have the capacity to act as a robust filter and that a branched structure can perform logic computations.

Acknowledgements

The completion of this thesis would not have been possible without the unending support, guidance and patience of my supervisor, Professor Gabriel Lord. For his continuing encouragement and warm advice I am forever grateful. I would also like to thank the other members of staff and PhD students in the Department of Mathematics.

I am thankful to have friends and family who are endlessly supportive and have been understanding throughout all stages of my studies. In particular I am forever indebted to my Mum, Mary, for her relentless encouragement, backing and kindness.

Finally I want to thank everyone at The Stewart Craft Centre in Aberdeen for making me smile and reminding me how fortunate I am to have the opportunity to write this thesis.

Abbreviations

BC	Boundary Conditions
BR	Baer and Rinzel model
CNS	Central Nervous System
CR	Coherence Resonance
FHN	Fitzhugh Nagumo model
HH	Hodgkin Huxley equations
IF	Integrate and Fire
LTD	Long Term Depression
LTP	Long Term Potentiation
ODE	Ordinary Differential Equation
OU	Ornstein Uhlenbeck process
PDE	Partial Differential Equation
PRC	Phase Resetting Curve
SDE	Stochastic Differential Equation
SDS	Spike Diffuse Spike Model
SNR	Signal to Noise Ratio
SPDE	Stochastic Partial Differential Equation
SR	Stochastic Resonance
STDP	Spike Time Dependent Plasticity

Parameter List

This page gives the parameter values used throughout the thesis and their respective units. The values are biologically realistic, where appropriate, and the bracketed values are the non-dimensional values used, for example in the Spike diffuse spike model Section 2.8 and Chapter 4.

Symbol	Name	Value	Unit
V	Cable Voltage	-	mV
U	Spine head Voltage	-	mV
R_m	Transmembrane Resistance	2500 (1)	Ωcm^2
R_a	Intracellular Resistance	70 (1)	Ωcm
C_m	Transmembrane Capacitance	1 (1)	$\mu F cm^{-2}$
$\hat{C}$	Transmembrane Capacitance of Spine head	1 (1)	$\mu F cm^{-2}$
$\hat{r}$	Transmemrane Resistance of Spine head	2500 (1)	Ωcm^2
μ	Strength of additive noise	-	-
ν	Strength of multiplicative noise	-	-
a	Dendritic Diameter	0.36 (1)	μm
$\lambda = \sqrt{aR_m}4R_a$	Electronic Length Scale	(1)	-
$\tau = R_m C_m$	Electonic time constant	(1)	-
$D = \frac{\lambda^2}{\tau}$	Diffusion Coefficient	(1)	-
τ_R	Refractory time	-	-
L	Length of dendrite	1-2	mm
N_{spines}	Number of spines in SDS model	81 or 37	-
τ_s	Length of time pulse lasts in SDS model	-	-
h	Voltage threshold in spine head for SDS model	0.04	-
m	Sodium activation particle	-	-
h	Sodium inactivation particle	-	-
n	Potassium activation particle	-	-
G_{Na}	Maximum sodium conductance	120	$mS cm^{-2}$
G_K	Maximum potassium conductance	36	$mS cm^{-2}$
G_L	Maximum leakage conductance	0.3	$mS cm^{-2}$
V_{Na}	Sodium reversal potential	50	mV
V_K	Potassium reversal potential	-77	mV
V_L	Leakage reversal potential	-54.402	mV
ρ	Spine density	-	-
d	Spine spacing	(0.8 or 1)	μm
η_0	Strength of action potential pulse in SDS model	-	-

Contents

Chapter 1

Introduction

The neuron, or nerve cell, is the building block of the mammalian nervous system; it sends, receives and processes information that ultimately controls functions as fundamental as our breathing and as complex as human consciousness. The brain is so densely populated by neurons that it was long believed that the brain was not a collection of individual cells but one single mass. In the late 19th century Camillo Golgi discovered a stain that highlighted only certain neurons within a sample of brain tissue and this allowed the study of the structure of the individual neuron. It was, however, Ramón y Cajal that used this stain to carry out extensive studies of the structure and interconnections of neurons in many parts of the brain. He produced many detailed and beautiful drawings of neurons, [118], see Figure 1.1 for an example of his work. Through his studies Ramón y Cajal discovered the existence of the axon, dendrite and even dendritic spines. Although there are around 100 billion individual neurons in the human brain [117], [107], with a variety of morphologies, they share a basic structure. As shown in Figure 1.2, the neuron consists of the main cell body, or soma, the axon along which information travels to the synaptic terminals to be transferred onto several other connecting neurons through their dendritic trees. The dendritic tree allows a greater surface area for synaptic connections to be made and around 90% of excitatory synapses in the brain are made onto dendritic spines. Neurons can range in size, anywhere from a couple of millimeters to a meter in length whereas dendrites are typically 1-2 mm long. The dendritic spines are small bulbous protrusions along the length of the dendrite and are usually 1-2 μm long. Spiny dendrites occur in many regions of the brain e.g. CA1 and CA3 pyramidal neurons in the hippocampus (important in long term memory), basal ganglia (used in motor control and learning) and spiny stellate neurons in the cerebral cortex (important in memory, thought and human consciousness) [107], [111], [3]. The density of spines varies depending on the type of neuron and there can be up to 20 spines to each 10μm of dendrite. The spines are thought to be an important component in signal propagation and computations along the dendrite and spine motility and morphology,

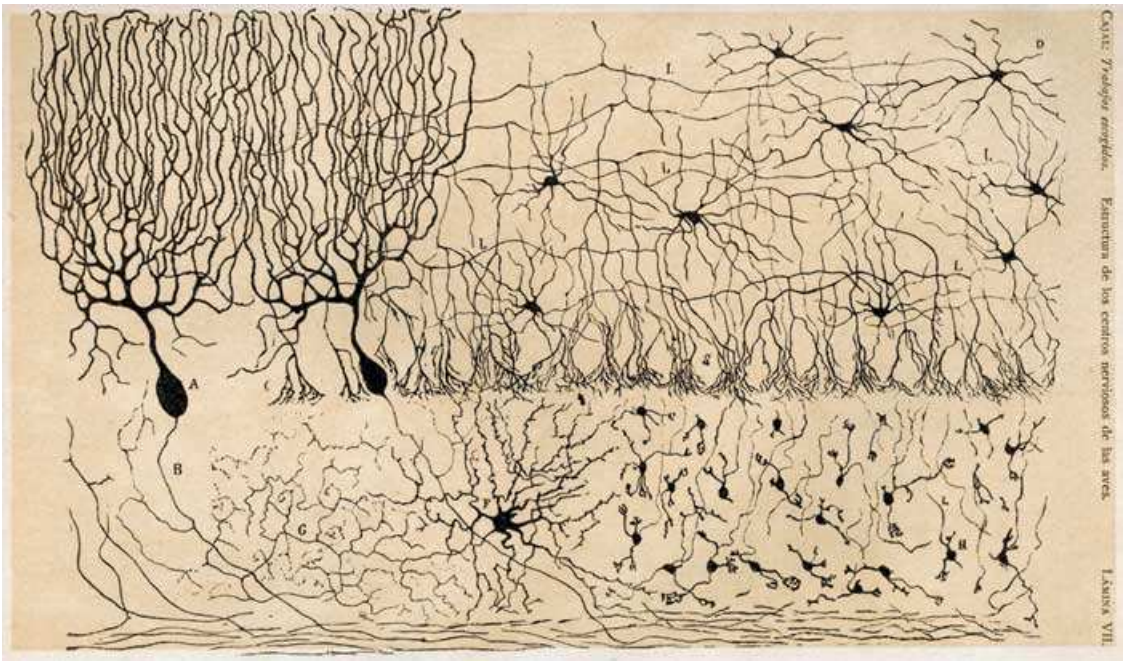

Figure 1.1: An example of the diagrams produced by Ramón y Cajal. This figure shows the structure of several types of neuron. Picture from www.nature.com

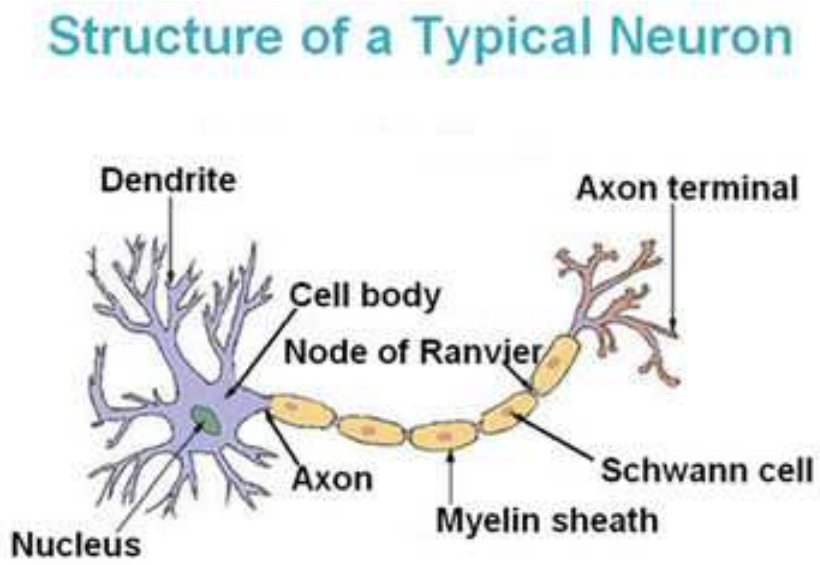

Figure 1.2: Diagram of the basic structure of a neuron, showing the cell body (or soma), axon and dendritic tree with dendritic spines. Picture from www.training.seer.cancer.gov

called spine plasticity, is thought to be an important process in learning and memory. It has been shown that abnormalities in dendritic spines can cause learning difficulties and mental retardation [53].

Measurement of signal propagation in neurons and axons has been possible for some time with a voltage clamp technique, developed in the 1940's, and patch-clamp technique, 1970's. The most famous example is perhaps the Hodgkin and Huxley experiments, [44], which measured voltage changes in the squid giant axon. Due to the small size of the typical dendrite these techniques were not applicable to the measurement of dendritic membrane voltage since the intracellular electrodes used in the measurements are too large, in relation to the dendrite, and damage the sample before any measurements can be made. The advent of the confocal and two-photon microscopy used to image the membrane in dendrites led to the measurement of action potentials in dendrites and proved that action potentials can be generated in dendrites themselves, see Figure 1.3 for an example of an action potential produced by the Hodgkin Huxley model. These new microscopy methods use the fluorescence of

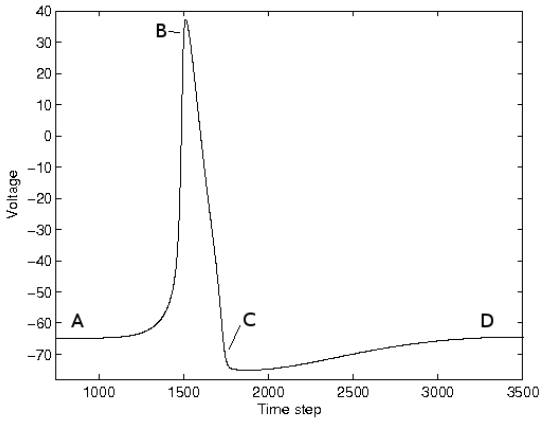

Figure 1.3: Example of an action potential generated by the Hodgkin Huxley equations developed to describe the voltage changes in the squid giant axon. The voltage starts at its resting value of -65V and rises rapidly to a peak before falling below the resting value and eventually settling back at the resting potential. The whole pulse is called an action potential.

voltage sensitive dyes to highlight activity and the microscope measures these changes in the fluorescence as the sample neurons are stimulated. These techniques make it possible to compare experimental, [40], [121], and theoretical results, [115], [95], that predict how voltage will spread throughout a length of dendrite, or a branched dendritic structure, also see review [99]. We consider voltage spread throughout a length of spiny dendrite as a wave propagating from the spines at the distal end, through the main body of the dendrite to the soma without including the effect of the soma. This is an interesting problem as much information processing seems to

happen prior to the action of the soma. We use two dendritic models that describe voltage evolution in a length of spiny dendrite: the Baer-Rinzel (BR) model, Section 2.7, [6], and the Spike-Diffuse-Spike (SDS) model, Section 2.8, [15], [16]. Both these models consist of coupled partial and ordinary differential equations describing the evolution of the voltage in the main cable of the dendrite and the evolution of voltage in the spine heads.

We consider the effect of random fluctuations, or noise, in the BR and SDS models of spiny dendritic tissue. There are two types of noise in a neural system, intrinsic and extrinsic noise, [33], [73]. Intrinsic noise is a source of noise which is always present in the system and is called thermal noise or Johnson noise. Thermal noise arises from the thermal agitation of electric charge carriers, which are of course present in neural systems in the form of electrons and ions. This noise which is present in dendrites can result in voltage fluctuations which can affect the response of the dendrite to a given input. Another source of intrinsic noise, which may be considered particularly

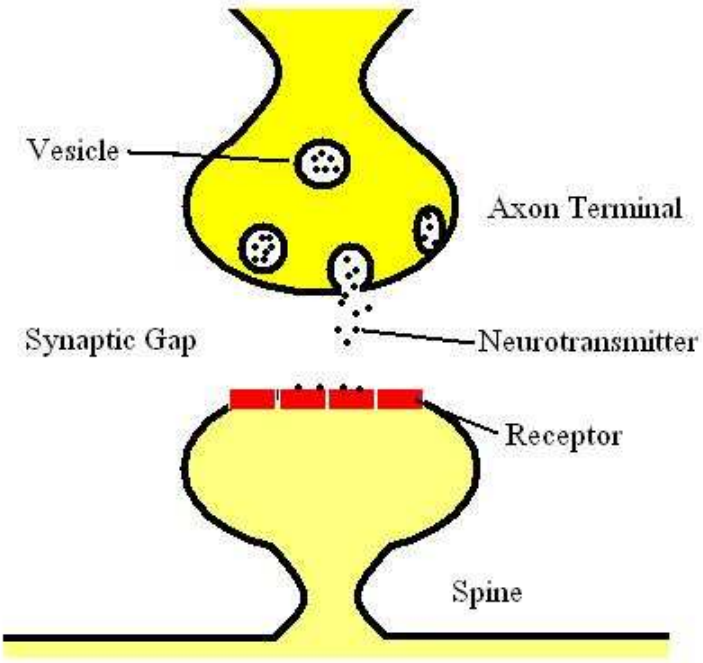

Figure 1.4: Diagram of the basic structure of a synaptic connection, showing the pre-synaptic vesicles of neurotransmitter and post-synaptic receptors on the spine head.

relevant in spiny dendrites, is the process of synaptic gating, see Figure 1.4. When a chemical synapse transmits a signal across the synaptic cleft to the receiving dendrite's spine, tiny vesicles (of which there is a finite number) in the pre-synaptic terminal open in response to sufficient voltage changes. The opening of the vesicles releases a transmitter substance (neurotransmitter) across the synaptic cleft to be absorbed by the spine, which in turn causes a change in voltage and possibly the generation of an action potential in the post-synaptic dendrite. The release of the neurotransmitter

is a stochastic or noisy process; the number of molecules of transmitter released may change from event to event and the arrival of the transmitter at the post-synaptic terminal depends on its diffusion across the synaptic cleft and so may not follow the same path each time. Also due to the finite number of these vesicles, if the potential of the post-synaptic membrane is close to threshold then the opening (or not) of some of the vesicles causes tiny voltage fluctuations which may (or may not) push the membrane voltage above threshold. This creates a stochastic membrane voltage. For more detailed information on synapses see [56], [107]. The second type of noise, extrinsic, emanates from out with the cell itself and one source is other nearby neurons. Any electrically charged object emits an electromagnetic field, [38], and as neurons conduct a current they too emit an electromagnetic field. This field can interfere with any neighbouring neurons and so cause a random effect. As all neurons are part of, usually complex, networks they can be affected by the firing of other neurons in the network that are not necessarily direct neighbours. We include noise into the dendritic models by the formulation of stochastic differential and stochastic partial differential equations (SDE and SPDE's) with different types of noise to describe the stochastic nature of the voltage in the spines and the voltage fluctuations in the cable of the dendrite. We consider the effects of spatio-temporal white noise, temporally correlated noise and spatially correlated noise.

The thesis is structured as follows: first there are two background chapters, Chapter 2 and Chapter 3, which serve as a foundation for the rest of this body of work. It is in these chapters that we introduce the models that are investigated throughout the work including the passive cable equation, Hodgkin Huxley model, leaky integrate and fire model, Baer and Rinzel model and the spike-diffuse-spike model. We include their mathematical formulation and a brief description of their deterministic behaviour. We then discuss the concept of 'noise' and how stochastic behaviour can be mathematically represented in the form of SDE and SPDE's. Then we describe how to evaluate a stochastic integral in the Itô framework and what it means to have a solution to SDE and SPDE's. We briefly consider the differences between Itô and Stratonovich calculus and how to convert between the two interpretations. The construction of a temporally correlated noise as an Ornstein-Uhlenbeck process is discussed as is the construction of a short-ranged spatially correlated noise. There is a section outlining the numerical methods employed throughout the subsequent chapters to solve both deterministic and stochastic systems. The numerical algorithms are given in a general form here and the full algorithm is given in each chapter for the exact equations being solved. Finally Chapter 3 gives an overview of various stochastic phenomena observed in neural systems throughout the literature; this includes coherence and stochastic resonance and synchronised/coupled oscillators.

We consider the numerical solution of the equations related to the spike-diffuse-

spike model of the dendrite in Chapter 4. Here we consider the effect of different types of noise, white, temporally and spatially correlated, included in either the equations governing spine or cable voltage evolution. We measure the effect in two ways, the speed of a propagating wave and the distance travelled along the length of the cable as the noise intensity increases. In the case of a correlated noise we also investigate the effect of the correlation scale of the noise. We show that in general large noise is destructive to the propagation of a wave but that the system is robust to small levels of noise, albeit the wave travels with a reduced speed. We treat the Baer and Rinzel model in the same way in Chapter 5, where we consider the model driven by white, temporally and spatially correlated noise in the spine heads and in the cable. We also use a small noise expansion to derive a deterministic equation which is altered by a term arising from the drift correction that occurs when changing from a Stratonovich to an Itô interpretation. This new system of deterministic equations describing the BR model under the influence of small spatially correlated noise, is transformed into the travelling wave frame to investigate the effect of the noise on the existence of travelling waves in parameter space. This is carried out using the continuation software AUTO-07P which allows the user to search for bifurcations, limit points and to choose the system parameters of interest for continuation of existing solutions. Chapter 6 investigates the behaviour of the BR model with a spatially dependent spine density that can, in the limiting cases, be thought of as the original BR model and the SDS model with HH dynamics in place of the IF process. Here we consider these two limiting cases under the influence of noise and also the behaviour of the system as the parameter, which controls the shape of the spine density, changes from one limit to the other. We look to this model to reconcile some conflicting results which we obtain when looking at the behaviour of the SDS and BR model. In order to investigate the behaviour of the dendrite models when forced by noise then we must simulate the system a number of times to get a mean behaviour and this can be costly in terms of computing time so in Chapter 7 we look at a probabilistic representation of the SDS model in the hope of capturing the behaviour of the system without the time constraints of simulating the full model. We show that information about the speed of waves in the SDS model with noise in the spine heads can be captured using a reduced simulation of the SDS model. Finally Chapter 8 investigates some of the signal processing capabilities of the SDS model and its robustness to noisy input signals as well as its ability to function with intrinsic noise but a clean signal. We consider the SDS model's ability to act as a low pass filter and how much noise may be present in the signal or the system before this capability breaks down. We also briefly show how the SDS model of a length of spiny dendrite can, with the correctly chosen parameter values, act as a high pass filter and how the branched SDS structure described in Chapter 4 can be used as either an OR or AND logic gate. The BR model with

spatially dependent spine density also shows the ability to act as a low pass filter.

Chapter 2

Neural Models

2.1 Introduction

This chapter, and the following Chapter 3, serves to provide background information required in all subsequent chapters. We outline the basic features of each of the models we study and give the full set of differential equations in each case. We also discuss the importance of noise in neural systems and how to mathematically describe a noisy system. We start in Section 2.2.1 with a general discussion of the difficulties of modelling a realistic dendritic tree and then outline in detail the simplest description of the dendrite, the passive cable equation, see [33] and [98] for derivations. The passive cable equation describes the evolution of the membrane potential of the cable which diffuses, in space and time. Passive refers to the membrane resistance being independent of the potential in the cable.

In Section 2.3 we consider a model of nerve membrane with active properties, the Hodgkin Huxley (HH) model. This set of four ordinary differential equations, along with experimentally derived constants and parameters, introduces the active properties of a nerve membrane through a series of ionic channels. The production of action potentials in model neurons, using the basic ionic mechanisms, was made possible by Hodgkin and Huxley [44] through their observations and measurements during experiments using the squid giant axon.

A much simplified model capturing aspects of the HH model without the need for empirical data is the leaky integrate and fire model (IF), explained in Section 2.4. The model is described by one ordinary differential equation and allows the voltage to increase to a chosen threshold at which point the model neuron is said to fire, although an action potential is not explicitly described. After this 'firing event' the voltage is reset to a chosen start value and a refractory time can be imposed before the neuron can start to increase the voltage again, through the mechanism of the IF equation. Both the IF and HH models are employed to describe the voltage dynamics in the spine heads of the dendrite models we consider throughout this work.

We then discuss the Baer-Rinzel model, Section 2.7, for a spiny dendrite [6]. This model combines the passive cable and the HH model to provide a description of a length of dendrite with active spines. The spines are attached to the cable with a chosen density, which was taken to be a constant in the original paper by Baer and Rinzel, [6]. We also outline the Spike-Diffuse-Spike (SDS) model in Section 2.8 ([15], [16]) which also describes a length of spiny dendrite. The SDS model again uses the passive cable equation to model the dendrite, but the spines are described by the leaky Integrate and Fire (IF) model. The IF model captures the basic properties of the HH equations without the details of the ionic currents. The spine density is no longer a constant but modelled more realistically by considering spines attached at discrete points along the cable with spine stems of a chosen resistance. Finally we look at a combination of the SDS and BR models where we use the full HH dynamics as a description of the spine head but now have a spine density with spatial dependence.

2.2 Dendritic trees

The structure of individual axons and dendrites is very complex and the membrane properties are active, meaning that the membrane resistance can be changed by voltage sensitive ionic channels to generate action potentials. The dendritic tree as a whole is even more complex and can display a wide range of morphologies from the relatively simple structure of the apical dendrites in the pyramidal cell to the intricate and dense branching patterns observed in Purkinjie neurons. As a consequence of this complex branching patterns, it is very difficult to mathematically model a real dendritic tree, even with passive properties on the branches. Each branch may have different biological parameters such as membrane resistance, capacitance and diameter, and the diameter may not be constant on any one branch due to tapering and varicosities. The structure and properties of each neuron depends on its role in the central nervous system (CNS) and is determined during development. A lot of work in mathematical neuroscience looks at the fully developed CNS, as we do here, but there is a growing interest in the developmental stages. The book, [112], on developmental models gives a comprehensive overview of the biology and models of different stages of development. This book covers very early development, gene networks and the growth of the neural tube (which becomes the brain and spinal cord in the adult vertebrate system), the growth of neurites (the precursor to dendrites and axons), network organisation and refinement. A more specific neurite review is set out in [36] where the authors review the mathematical models of neurite initiation, growth and the formation of branching patterns, and compare the models to experimental results. Attempts to model realistic dendritic trees have involved various simplifica-

tions, for example, a reconstruction of passive Purkinjie cells in [92] and the inclusion of single active gating variable to these reconstructed cells in the same paper. Similarly, active properties were uniformly distributed throughout a fully reconstructed morphology in [115], and modelled using two, sodium and potassium, active gating channels. Both [92] and [115] models are implemented using NEURON simulation environment. Others have focused on improving the computational efficiency of algorithms that describe the behaviour of action potentials in branched structures. In [11] the authors find an algorithm which uses Green's function, Section 2.2.3, over the reconstructed dendritic tree to find the response to current injected at different points on the tree. They use a sum over trips approach, with an imposed maximum trip length, to construct the voltage spread through the tree. This maximum trip length means that in some simulations the contribution from distal branches in the tree will be neglected, in favour of shorter computation times. Another example of improving computational efficiency is given in [43] where the author simulates the voltage evolution in an arbitrarily branched tree with Hodgkin-Huxley dynamics for each cable using a Crank-Nicholson method. By the correct labelling of the nodes in the tree the resultant coefficient matrix for the tree structure lends itself to upper triangularisation and so eliminates any off diagonal elements which then allows the efficient solving of the equations describing the branched, active tree. The paper also evaluates the HH membrane conductances in such a way that the $O(\Delta t^2)$ is maintained with no extra steps and constructs a table of values for the coefficients that appear in some of the integrals such that these values can be looked up rather than computed at each time step and so increase the computational efficiency. These three improvements increases the speed of computation without losing the $O(\Delta t^2)$ accuracy of the numerical method. A different class of model for investigating the function of dendritic trees is the equivalent cylinder or more recently the equivalent cable model. The main idea behind this type of construction is to reduce the whole branching structure to one simple, electrically equivalent unbranched structure. The first to do this was [87], see [48], [84] and [98] for an overview of Rall's work, with his equivalent cylinder model. Rall's model makes four major assumptions and therefore is only a realistic representation for a small class of dendritic trees. The first assumption is the $\frac{3}{2}$ power law which comes from impedance matching at the branch point i.e. minimising the reflection at the branch point. To do so the characteristic conductance seen on entering and leaving the branch point must be equal. When the system is at rest the characteristic conductance $G_0 \equiv \sqrt{\frac{g_{rest}}{r}}$, where g_{rest} is the shunt conductance and r is the series resistance. Since $g_{rest} \propto d$ and $r \propto \frac{1}{d^2}$, (here d is the diameter of the branch), then

$$G_0 \propto d^{\frac{3}{2}} \ . \tag{2.1}$$

Therefore if we have a length of dendrite, labelled 1, which branches into two daughter dendrites, labelled 11 and 12 respectively, the diameters must satisfy:

$$d_1^{\frac{3}{2}} = d_{11}^{\frac{3}{2}} + d_{12}^{\frac{3}{2}} \ . \tag{2.2}$$

The second assumption is that each path from the soma end of the dendrite to the distal terminal of the tree is of equivalent electronic length. If we start with the same branching structure as before and each of the daughter dendrites branch into two more branches each, labelled 111, 112, 121 and 122 respectively, then the length of each segment is l_i and electronic space constant is $\lambda_i^2 = \frac{r_{m_i} d_i}{4 r_{a_i}}$ with $i = \{1, 11, \ldots, 122\}$. We can then express the second assumption as:

$$\Lambda = \frac{l_1}{\lambda_1} + \frac{l_{11}}{\lambda_{11}} + \frac{l_{111}}{\lambda_{111}} = \frac{l_1}{\lambda_1} + \frac{l_{11}}{\lambda_{11}} + \frac{l_{112}}{\lambda_{112}} = \frac{l_1}{\lambda_1} + \frac{l_{12}}{\lambda_{12}} + \frac{l_{121}}{\lambda_{121}} = \frac{l_1}{\lambda_1} + \frac{l_{12}}{\lambda_{12}} + \frac{l_{122}}{\lambda_{122}} \ . \tag{2.3}$$

The third requirement that the dendritic tree must satisfy is that the cytoplasmic resistivity and the specific membrane conductivity are the same throughout the tree. Finally the boundary conditions on the original structure and the new equivalent structure must be the same. If the electronic time constant $\tau = c_m r_m$ is the same throughout the whole tree then the previous assumptions hold for a tree with time dependent voltage and current and so the voltage measured at one end of the equivalent cylinder is the response to an injected current at the other. This voltage/current relationship holds due to the reciprocity theorem from linear network theory. There is a slightly more general $\frac{3}{2}$ power law which exists for a non-uniform membrane resistance, shown in [48], yet due to the other assumptions this equivalent cylinder approach is still restrictive in its application to the wide range of real dendritic trees. An improvement on the equivalent cylinder, the exponentially tapering cylinder was introduced by Rall [87] and developed in Goldstein and Rall [35]. This paper also investigated the speed and maximum height of the action potential travelling in, not only the tapered cable, but in cables with varicosities and those with sealed end boundary conditions. They show that the speed of the action potential is proportional to the changing space constant and derived a formula to predict how the proportionality constant depends on the taper of the cylinder. The class of dendrites which can be described by a tapered equivalent cable was extended in [85]. In this paper the conditions on number of branches and on the radii of these branches are given as well as a set of exactly solvable geometries e.g. sine hyperbolic, exponential, quadratic and sinusoidal. Therefore the voltage evolution for these specific classes of dendrites is known exactly and so can be represented by an equivalent cable. This may increase the size of class of dendritic trees that is described but still there is no direct mapping between the input on the dendritic tree and a point on the equivalent cable. A method to map exactly from the dendritic tree to a certain point on the equivalent cable, which has a non-uniform

diameter, was first developed by Whitehead and Rosenberg in 1993 and is described in [79] in more detail with an example of the application of the Lanczos method to reduce a simple tree to an equivalent cable. The equivalent cylinder developed here is effectively many small cylinders appropriately joined together, depending on the branching conditions, with each cylinder having different diameters. Each cylinder is modelled by the passive cable equation and the conditions for joining the sections together are Kirchoff's current conservation laws, and appropriate boundary conditions at the terminal branches. With appropriate numbering the nodes on the tree the discretised voltage produces a matrix representation of the dendritic tree. The rest of the method follows the Lanczos procedure, which involves three matrix transformations that result in an equivalent cable. The new matrix still has entries corresponding to coefficients for the node voltages, but this time related to nodes on the equivalent cable. There is also a separate matrix which is a result of the method that describes the mapping from the nodes on the tree to the nodes on the cylinder. The above method for the reduction to an equivalent cable is improved in [68] and is used to reconstruct real neurons: the cholinergic interneurons in Laminae III and IV of dorsal horn of the spinal cord. Each synaptic contact in the real tree was mapped to the nearest node of the discretised equivalent cable and so the response of the whole tree to any synaptic input could be predicted from the new equivalent cable. The difference in the two methods is in the matrix transformation from the tree matrix to the cable matrix; instead of the Lanczos method Lindsay uses the Householder method.

Another aspect of dendritic function which has been studied experimentally but not fully explored mathematically is the concept of dendritic democracy. Since dendrites are effectively leaky electrical cables any input which has to travel a long distance (e.g. from end of distal dendrite, through tree to soma) will be much attenuated at long distances from its source. This is not observed in vitro and a distal input has similar efficacy at the soma as a proximal input; [39] is a brief review. The author of [39] suggests three possible mechanisms for the democracy seen experimentally: (1) distal input is amplified by voltage gated channels, (2) the strength of the synapse is increased by more neurotransmitter release/post-synaptic receptor sites or (3) distal synaptic contacts could be more active, i.e. receive more input. Experimental evidence ruled out the first option but showed that it is possible that an increase in the synaptic conductance is responsible. Paper [108] investigates mathematically how the conductance could be scaled on a dendritic branch to create dendritic democracy. The authors derive analytical expressions for the conductance as a function of its position relative to the soma, which ensure that e.g. the peak voltage response and width of response pulse at the soma is the same for distal and proximal inputs. These analytical solutions agree with full simulation of the model. Close to the soma the scaling is linear, then it becomes faster than linear as the distance increases until a

critical distance after which no scaling can create democracy. Clearly increasing conductance alone cannot account for dendritic democracy and the authors suggest that a possible [Ca^{2+}] current, introduction of subthreshold dynamics or a tapered cable could help. The question of how a synapse knows its position in the dendritic tree is addressed in [103] for a model of CA1 neurons. They suggest that perhaps some sort of concentration gradient exists that tells the synapse where it is but they show that all that is needed to maintain democracy is a back propagating action potential.

2.2.1 Passive cable theory

Cable theory was first developed, in the mid-18th century by Lord Kelvin, to describe the spread of electric potential along the telegraph cable which linked the U.K. and the U.S.A. (See [56] for some historical background.) This theory was later used to describe the current flow in nerve fibres such as the axon and dendrites (see [57] for a brief historical description), where the charge carriers are sodium and potassium ions instead of, in the case of a wire, electrons.

However the general long, thin nature of individual dendrites allows the use of linear passive cable theory to give a nice simplification of their behaviour. This is perhaps the most simple model of the axon/dendrite and it can be (and has been) further developed to introduce ever more complex dynamics. As discussed in Section 2.2 there are many considerations in reproducing a realistic tree structure and its active properties and this poses a difficult mathematical problem which many have tried to simplify. We however consider a general single length of dendrite (or a very simple branched structure with one branch point and three branches), not a real dendrite, and so can use a general model, the passive cable equation. We subsequently add complexities onto the basic cable by introducing active spines, by BR and SDS models, and noise to the system.

This section gives a derivation of a straight and a tapered passive cable equation using Ohm's Laws and Kirchoff's Laws. In the case of a straight cable the equation derived allows the analytical derivation of a Green's function as the solution to the cable equation with a Dirac delta input. The Green's function is a convenient and useful way to construct the response of the cable to any other input without having to solve the whole system again with the new input. To do this Green's function is convolved with the new input to find the new output. The tapered cable, however, has nonlinear membrane properties, such as resistance and capacitance, which gives rise to a nonlinear cable equation and therefore no analytical solution is possible.

2.2.2 Deriving the passive cable equation

We first derive the passive cable equation for a general cable where the radius is dependent on x, the axial distance, $x \in [0, L]$, L is the length of the cable. Then the associated Green's function for a straight cable. The derivation of the passive cable equation can be found in much of the literature [98], [56], [33], [48]. From the circuit

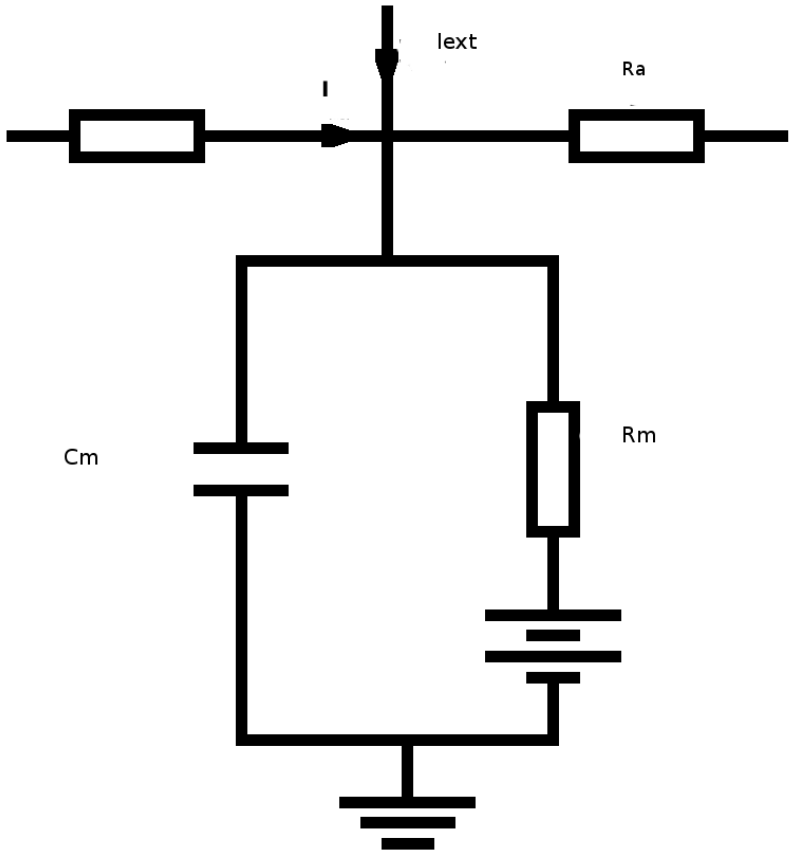

Figure 2.1: Circuit diagram for a section of cable describing a passive dendrite, with length dx. It also shows the associated resistances, capacitances and currents.

diagram in Figure 2.1, the longitudinal resistance, $R_a(x)$, and the transmembrane capacitance and resistance, $C_m(x)$ and $R_m(x)$ respectively will all change with the diameter of the cable and so are functions of x. They can all be expressed in terms of quantities per unit length, dx: $R_a = r_a(x)dx$, $C_m = c_m(x)dx$ and $R_m = r_m(x)dx$ where r_a is called the intracellular resistance, c_m is called the specific capacitance, r_m is called the passive membrane resistivity and $I_{ext}(x)$ is the external current. See the list of parameters for a further description and a range of biologically realistic values for these variables.

The following steps make use of Ohm's law, $V = IR$, and Kirchhoff's laws for current at a node in a circuit. These are fundamental laws used commonly in circuit theory and can be found in many physics texts, for example [38] is a good basic text.

Using Ohm's law across the resistor $R_a(x)$ gives the following expression:

$$V(x+dx,t) - V(x,t) = I(x,t) r_a(x) dx \ . \tag{2.4}$$

Here $V(x,t)$ is the voltage at point (x,t) and I is the axial current. Next dividing by dx and letting $dx \to 0$ gives:

$$\frac{\partial V}{\partial x} = I(x,t) r_a(x) \ . \tag{2.5}$$

Using Kirchoff's law for currents at a node, "The sum of currents entering a node is equal to the sum of currents leaving the node", we obtain:

$$I(x+dx,t) - I(x,t) = c_m(x)\frac{\partial V}{\partial t}dx + \frac{V}{r_m(x)}dx - I_{ext}(x)dx \ , \tag{2.6}$$

again dividing by dx and letting $dx \to 0$ gives:

$$\frac{\partial I}{\partial x} = c_m(x)\frac{\partial V}{\partial t} + \frac{V}{r_m(x)} - I_{ext}(x) \ . \tag{2.7}$$

Take the derivative of Equation (2.5) with respect to x to get:

$$\frac{\partial^2 V}{\partial x^2} = r_a(x)\frac{\partial I}{\partial x} + I(x,t)\frac{\partial r_a(x)}{\partial x} \ . \tag{2.8}$$

Substituting for $\frac{\partial I}{\partial x}$ gives the passive cable equation for a tapered cable:

$$\frac{\partial^2 V}{\partial x^2} = c_m(x) r_a(x)\frac{\partial V}{\partial t} + \frac{r_a(x)}{r_m(x)}V(x) - r_a(x) I_{ext}(x) + I(x,t)\frac{\partial r_a(x)}{\partial x} \ . \tag{2.9}$$

Finally by multiplying the equation by the electronic scale length $\lambda^2 = \frac{r_m(x)}{r_a(x)}$, and introducing the membrane time constant $\tau = c_m(x) r_m(x)$, we obtain the following form of the cable equation:

$$\lambda^2(x)\frac{\partial^2 V(t,x)}{\partial x^2} = \tau(x)\frac{\partial V(t,x)}{\partial t} + V(t,x) - r_m(x) i_{ext}(x) + \lambda^2(x) I(x,t)\frac{\partial r_a(x)}{\partial x} \ , \tag{2.10}$$

for $x \in [0, L]$. If we want to consider a straight cable, as we do, then the equation reduces to:

$$\lambda^2\frac{\partial^2 V(x,t)}{\partial x^2} = \tau\frac{\partial V(x,t)}{\partial t} + V(x,t) - R_m I_{ext} \ . \tag{2.11}$$

The term $r_m(x) i_{ext}(x)$ changes to $R_m I_{ext}$ since the resistance and external currents are no longer space dependent. We can use the capitalised version to indicate that these quantities are constant.

2.2.3 Green's function for the straight passive cable equation

Green's function is an integral kernel which allows one to solve inhomogeneous differential equation with some associated boundary conditions. For a general inhomogeneous equation $L(x)u(x) = f(x)$, where $L(x)$ is a differential operator (linear and self-adjoint), $u(x)$ the unknown solution to the equation and $f(x)$ is the known inhomogeneous term, we can write the Green's function, $G(x)$, satisfies: $L(x)G(x, x') = \delta(x - x')$. We can find Green's function here by looking for the solution to a linear partial differential equation with a Dirac delta function as its input current, I_{ext}. Then the solution for any input can be constructed using Green's functions. [33] shows a derivation of Green's function for the passive cable equation which we reproduce here. First we rescale the cable equation to obtain a dimensionless form, then derive Green's function by solving the dimensionless cable equation with the Dirac delta function as the input current. To solve the PDE we make use of Fourier transforms to convert the PDE to an ODE and find a solution to the simpler equation.

Rescaling Equation (2.11), to obtain a dimensionless form of the cable equation, with the following new variables: $x^* = \frac{x}{\lambda}$, $t^* = \frac{t}{\tau}$ and $I^*_{ext} = R_m I_{ext}$. This gives a unit free version of Equation (2.11) that looks like:

$$\frac{\partial V(x,t)}{\partial t} - \frac{\partial^2 V(x,t)}{\partial x^2} + V(x,t) = I_{ext}(x,t) \ , \tag{2.12}$$

where the stars have been dropped from the new variables simply to make the notation neater. Next replace $I_{ext}(x,t)$ by a Dirac delta function at $t = x = 0$, i.e. $\delta(t)\delta(x)$, to give:

$$\frac{\partial V(x,t)}{\partial t} - \frac{\partial^2 V(x,t)}{\partial x^2} + V(x,t) = \delta(t)\delta(x) \ . \tag{2.13}$$

Using a Fourier transform, see [59], with respect to the spatial variable reduces Equation (2.13) to an ODE. The transform, F, is performed on given functions of $x \in \mathbb{R}$ to give a new function of a new variable $k \in \mathbb{C}$, as shown in Equation (2.14). When applied to the PDE the hope is that the resulting transformed equation can be easily solved. The Fourier transform is given by Equation (2.14):

$$F[f(x)] = \hat{f}(k) = \frac{1}{\sqrt{2\pi}} \int_{-\infty}^{\infty} f(x) e^{-ikx} dx \ . \tag{2.14}$$

Similarly the inverse Fourier transform is defined in Equation (2.15):

$$F^{-1}[\hat{f}(k)] = f(x) = \frac{1}{\sqrt{2\pi}} \int_{-\infty}^{\infty} f(k) e^{ikx} dk \ . \tag{2.15}$$

When the Fourier transform is applied to the first and second differential of $f(x)$ we obtain $F[\frac{df(x)}{dx}] = ik\hat{f}(k)$ and $F[\frac{d^2 f(x)}{dx^2}] = -k^2\hat{f}(k)$. When this is applied to Equation

(2.13) we find the resulting ODE, Equation (2.16).

$$\frac{d\hat{V}(k,t)}{dt} + k^2\hat{V}(k,t) + \hat{V}(k,t) = \frac{1}{\sqrt{2\pi}}\delta(t) \ , \tag{2.16}$$

where $\hat{V}(k,t)$ is the Fourier transform of the original voltage $V(x,t)$. This ODE, Equation (2.16), can be solved using an integrating factor, $e^{(1+k^2)t}$. Using this and the fact that the integral of a Dirac delta function is the Heaviside function, denoted by $\Theta(t)$, the solution to Equation (2.16) is:

$$\hat{V}(k,t) = \frac{\Theta(t)}{\sqrt{2\pi}}e^{-(1+k^2)t} \ . \tag{2.17}$$

We must next perform an inverse Fourier transform to obtain an equation for the potential in terms of x and t.

$$V(x,t) = \frac{1}{\sqrt{2\pi}}\int_{-\infty}^{\infty}\hat{V}(k,t)e^{ikx}dk = \frac{\Theta(t)e^{-t}}{2\pi}\int_{-\infty}^{\infty}e^{(ikx-k^2t)}dk \ .$$

Completing the square for the exponential gives:

$$V(x,t) = \frac{\Theta(t)e^{-t}}{2\pi}\int_{-\infty}^{\infty}\exp[-(k\sqrt{t} - \frac{ix}{2\sqrt{t}})^2 - \frac{x^2}{4t}]dk. \tag{2.18}$$

Let Int $= \int_{-\infty}^{\infty}\exp[-(k\sqrt{t} - \frac{ix}{2\sqrt{t}})^2]dk$ and $m = k\sqrt{t} - \frac{ix}{2\sqrt{t}}$. Taking the square of Int gives:

$$[\text{Int}]^2 = \frac{1}{t}\int_{-\infty}^{\infty}e^{-m^2}dm\int_{-\infty}^{\infty}e^{-n^2}dn \ . \tag{2.19}$$

Next, changing to polar coordinates and changing the integration limits accordingly gives:

$$[\text{Int}]^2 = \frac{1}{t}\int_0^{2\pi}\int_0^{\infty}e^{-r^2}rdrd\theta \ . \tag{2.20}$$

Finally integrating this and taking the square root gives Int $= \sqrt{\frac{\pi}{t}}$, so on substituting this into Equation (2.18) and simplifying, we have the following expression for $V(x,t)$:

$$V(x,t) = \frac{\Theta(t)}{\sqrt{4\pi t}}e^{-t-\frac{x^2}{4t}} \ . \tag{2.21}$$

This expression for $V(x,t)$ is the solution for the infinite passive cable equation with a Dirac delta function as its input, therefore this is also Green's function. When the original variables are replaced ($x^* = \frac{x}{\lambda}$ and $t^* = \frac{t}{\tau}$) we have the following Green's function:

$$G_\infty(x,t) = \frac{\Theta(t)}{\sqrt{4\pi\frac{t}{\tau}}}e^{-\frac{t}{\tau}-\frac{x^2}{4Dt}} \ , \tag{2.22}$$

where $D = \frac{\lambda^2}{\tau}$. This form of the Green's function will be used in Chapter 7, to construct a solution for the voltage evolution in a length of spiny dendrite modelled by the SDS model, Section 2.8. Since the solution of the passive cable equation with any input current, I_{ext}, can be obtained using the convolution of the Green's function with the input of interest we can use this to find the voltage evolution when the input comes from action potentials generated in the spines.

2.3 Hodgkin Huxley model

The Hodgkin Huxley (HH) model was developed in 1952 to describe the ionic mechanisms which drive the initiation and propagation of action potentials in the squid giant axon. The model uses experimentally obtained data to describe the evolution of an action potential in a membrane with active potassium and sodium channels. Hodgkin and Huxley used voltage and space clamp techniques to control the potential difference across the membrane of a squid giant axon, and so were able to observe ionic currents flowing across the membrane in response to voltage and ionic concentration changes. In doing this, Hodgkin and Huxley found the maximum membrane conductances associated with sodium and potassium ions and the voltages at which the sodium and potassium currents are zero. They were also able to model the dynamics of the sodium and potassium conductances, which change in order to depolarise/hyperpolarise the membrane potential at the appropriate times of action potential generation. For a more detailed description of the experiments see the original paper [44] and a brief description in [98]. This model is important in neuroscience (descriptions of the HH model can be found throughout the literature, e.g. [98], [48], [56], [83]); providing the basis for many single cell neural models. The HH model is also important due to the way in which it combines experimental work with mathematical modelling to describe the role of ionic currents in action potential generation.

2.3.1 The Hodgkin Huxley equations

The HH model is a system of four ODEs describing the time evolution of the membrane voltage, $U(t)$ and the conductance variables m, n, h which are probabilities relating to the sodium and potassium ionic gates that lend the HH model its active properties. By 'active' we mean that the membrane is capable of generating its own action potential through changes in the conductance/resistance by changing the concentration of certain ions across the membrane. The following description of the HH

equations is for a point in space.

$$\begin{aligned} C_m \frac{dU(t)}{dt} &= G_{Na} m^3(U) h(U)(V_{Na} - U) + G_K n^4(U)(V_K - U) \\ &+ G_L(V_L - U) + I_{inj}(t) \ , \end{aligned} \tag{2.23}$$

where C_m is specific capacitance per unit area, U is the membrane potential, I_{inj} is an input current, G_{Na}, G_K and G_L are the maximum sodium, potassium and leakage conductances and V_{Na}, V_K and V_L are the respective ionic and leakage reversal potentials. The m, n and h dynamics are described by:

$$\frac{dX(U)}{dt} = \alpha_X(U)(1 - X) - \beta_X(U)X, \text{ with } X \in [m, n, h]. \tag{2.24}$$

The α's and β's are empirically derived formulae given by Equation (2.25) to Equation (2.30).

$$\alpha_m(U) = \frac{0.1(U + 40)}{1 - e^{-0.1(U+40)}} \tag{2.25}$$

$$\alpha_n(U) = \frac{0.01(U + 55)}{1 - e^{-0.1(U+55)}} \tag{2.26}$$

$$\alpha_h(U) = 0.07e^{-0.05(U+65)} \tag{2.27}$$

$$\beta_m(U) = 4e^{-0.0556(U+65)} \tag{2.28}$$

$$\beta_n(U) = 0.125e^{-0.0125(U+65)} \tag{2.29}$$

$$\beta_h(U) = \frac{1}{1 + e^{-0.1(U+35)}}. \tag{2.30}$$

The variable m is the probability of finding one of the sodium activation particles in its open state, h is the probability of finding one of the sodium inactivation particles in its non-inactivating state and n is the probability of finding one of the potassium activation particles in its open state. The α_X, $X \in [m, n, h]$ is the rate constant counting the transitions from the closed to open state for each X and β_X, $X \in [m, n, h]$ is the rate constant counting the transitions from the open to closed state for each X. The parameters G_{Na}, G_K and G_L are the maximum sodium, potassium and leakage conductances, these have standard values which have been determined experimentally and V_{Na}, V_K and V_L are the respective ionic and leakage reversal potentials, these values can be scaled to allow the resting potential of the system to be at zero but otherwise the resting potential of the system is -65mV. To understand why we need the variables m, n and h we look at how the ionic concentrations change in the different

phases of the action potential generation, see Figure 2.2. During the initial resting

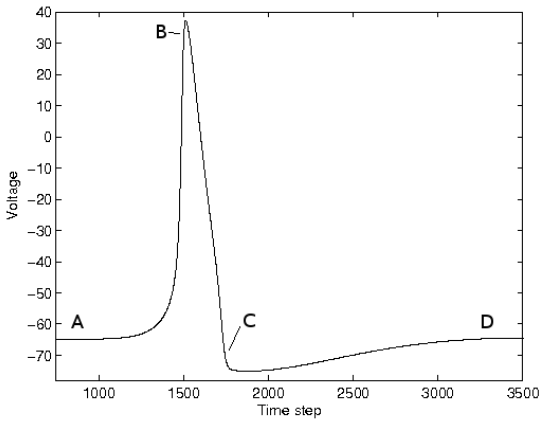

Figure 2.2: An Action Potential generated by the HH equations, this shows the different phases in the evolution of the action potential as governed by the HH equations, labelled by A, B, C, D and described in the main text. The AP is generated by solving Equation (2.23) with an input voltage of $V_{inj}(0) = 10$, $V_{inj}(t > 0) = 0$, temporal discretisation $\Delta t = 0.01$ and initial conditions $V(0) = -65$.

phase (up to label A on Figure 2.2), the membrane voltage is at its resting value of -65mV. At this stage the sodium m-gate is closed and the h-gate is open so no sodium ions are flowing while the potassium n-gate is also closed and so no potassium is flowing through the membrane. Following a stimulus input which happens at a point just before A the action potential enters the next phase. In the rising or depolarisation stage (from label A to label B on Figure 2.2) the sodium m-gates open and since there is a negative potential gradient the sodium ions flow through the membrane and, since they are positive ions, they start to raise the potential across the membrane. When the voltage reaches its peak and the falling or depolarisation phase (from label B to label C on Figure 2.2) occurs the m-gate stays open but the h-gate closes so sodium ions can no longer flow, and the n-gate opens so that the potassium can escape and so decrease the potential difference once again. The n-gate stays open longer than is needed to reach the resting potential and so we observe the undershoot phase (from label C to label D on Figure 2.2), the m-gate also closes at this point. Finally the gates revert to the initial resting state (just after label D on Figure 2.2) of m-gate closed, h-gate open and n-gate closed.

The Hodgkin-Huxley equations can be solved with different types of injected current, I_{inj}, and can be shown to give single spike and repetitive spiking responses. If the input current is constant and high enough (above threshold levels) to induce spiking the frequency of the output spiking pattern is only limited by the refractory time, see Figure 2.3. This refractory time arises from the inactivation of sodium channels, which has a time dependence, i.e. after firing there is a length of time during which

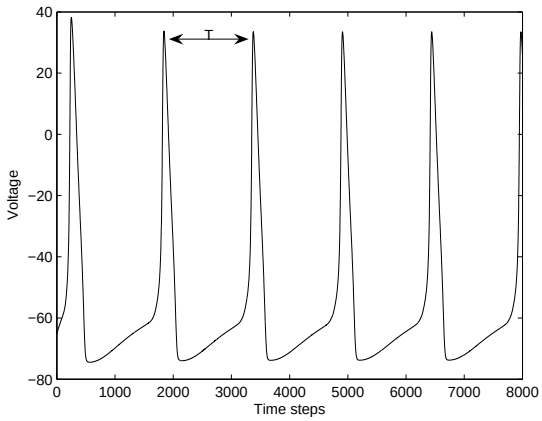

Figure 2.3: HH equations with constant injected current. The injected current is high enough to raise the voltage to a high enough level for continuous spiking. This is generated by solving Equation (2.23) with an input voltage of $V_{inj}(t) = 10$, temporal discretisation $\Delta t = 0.01$ and initial conditions $V(0) = -65$.

the sodium channels are unable to open and so the depolarisation process cannot begin. See Chapter 3 for a discussion of the Hodgkin Huxley model with noise, and which noise induced phenomena have been observed in the HH model.

Fitzhugh-Nagumo model

The Fitzhugh-Nagumo (FHN) model is a reduction of the full HH dynamics to a two variable model which captures the excitation of the membrane voltage and its subsequent recovery without the ion channel dynamics m, n and h. The FHN model is described throughout the literature and books [98] and [33] have small sections describing derivation and some properties of the model. The reduction is possible due to the difference in the kinetics of the n and h variables, which are slow, and the m variable, which is fast. The equations in general, dimensionless, form are:

$$\begin{aligned} \frac{dV}{dt} &= f(V) - W + I \\ \frac{dW}{dt} &= a(bV - cW), \end{aligned}$$

where V is the fast variable (voltage), W is the slow variable (m) and $a \ll 1$ and b, $c \in [0, 1]$ are constants. $f(V) = V(V - a)(1 - V)$ is the usual function used for a neural model. The FHN model is not used throughout this work but is referred to when reviewing other work e.g. noisy travelling waves.

2.4 Integrate and fire model

The integrate and fire model is a very simple firing single neuron model which captures the behaviour of the HH model without the complicated ionic dependence. We consider a leaky integrate and fire model and this is the model used throughout this work. The IF model can however be altered slightly to be either quadratic or exponential, although these are not considered here. This change means the voltage path up to threshold takes a different form to that of the leaky IF model. To make the IF model quadratic the $-U$ term in Equation (2.31), below, becomes: $(U-U_{rest})(U-h)$ where U_{rest} is the resting potential of the model and h is the firing threshold. For an exponential form of the model replace the $-U$ term with e^{U-h}. Figure 2.4 shows

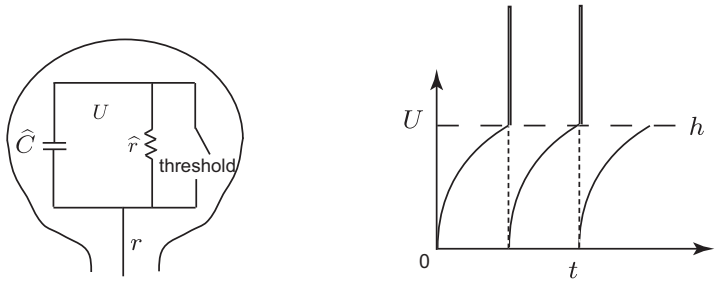

Figure 2.4: Left: Circuit diagram representation of a spine head, modelled by the IF model. Right: Schematic of the voltage, U increasing to threshold level, h, spiking and resetting to zero again. The sharp increases at $U = h$ are the spikes of the system, shown here as step functions, but they can be chosen to be any function.

the circuit representation of the leaky integrate and fire model which is a resistor $\hat{r}$ in parallel with a capacitor $\hat{C}$, driving the overall current I, [33], [98] and [83] all describe the IF model. We use again Ohm's law and Kirchhoff's law along with the relation between voltage and current through a capacitor $I_C = C\frac{dU}{dt}$ ([38]), which is simply called an integrator, to obtain the expression, Equation (2.31) for the current in the circuit representation.

$$\frac{dU}{dt} = \frac{1}{\hat{C}}I(t) - \frac{U}{\hat{r}\hat{C}} \ . \tag{2.31}$$

Term $\frac{U}{\hat{r}}$ is the leak term and is representative of a general loss of current from ionic sources that are not explicitly modelled. Given sufficient input current the voltage $U(t)$ will increase to a chosen threshold, call it h, and will be said to fire: $T^m_{fire} = \{t > T^{m-1}_{fire} | U(t) \geq h\}$. This equation says that the mth firing time occurs when at some time after the $(m-1)$th firing time when the voltage is greater than or equal to the chosen threshold. The model does not produce an action potential so at the time, T^m_{fire} one can choose the form of the action potential generated, in Figure 2.4 it is shown as a step function since this is the form used in the Spike Diffuse Spike

model, how it is generated will be shown in Section 2.8. At the threshold crossing the voltage in the model is reset to a chosen value and the model can start to integrate again, given sufficient input, increasing the voltage back towards h. The IF model can be improved by including a refractory time, τ_R, during which the model cannot fire again, this would alter the firing equation thus: $T^m_{fire} = \{t > T^{m-1}_{fire} + \tau_R | U(t) \geq h\}$.

2.5 Synchronisation and coupled oscillators

Most single neuron models, e.g. the HH or IF models described above (Section 2.3 and Section 2.4 respectively) can be described as oscillators, that is, with sufficient input the deterministic model spikes at regular times. In Section 2.7 and Section 2.8 we discuss the Baer-Rinzel and Spike-diffuse-spike models of spiny dendrites which can be thought of as chains of diffusively coupled oscillators. Each spine is modelled using either HH or IF dynamics and is coupled to its neighbours through the diffusive, passive cable. In this section we first look at the properties of single oscillators and then of a coupled system. The time between spiking events is the period of the neural system, T, and is due to the solution of the system, $\frac{dX}{dt} = F(X(t))$, being a limit cycle with an associated phase, ϕ. It is convention in neural oscillators to call the spiking event 0 phase, therefore the spiking times are $t_s = \{0, T, 2T, 3T, \dots\}$, see the HH example Figure 2.5 plot (a). If the system is perturbed slightly, by an injection of extra current say, then the timing of the next spike will change, see Figure 2.5 plot (b). Let the period of the perturbed system be $\hat{T}$, then the phase resetting curve (PRC) is defined to be the change in the spiking times divided by the period: $\Delta(\phi) = \frac{T-\hat{T}}{T}$. Note that $\Delta(\phi) \in [0, 1]$, due to the scaling with respect to the period, but it is sometimes scaled such that $\Delta(\phi) \in [0, 2\pi]$. The PRCs have different forms depending on the type of bifurcation which leads to the oscillatory behaviour of the system, [22]. We have two classes of neural models: class I come from a saddle-node bifurcation, an example of this is the quadratic IF model, and the class II is from a Hopf bifurcation, e.g. HH model. So if we introduce a small perturbation into a general ODE for the system (where X is the oscillating quantity of interest, e.g. voltage for neural systems), we obtain:

$$\frac{dX}{dt} = F(X(t)) + \epsilon G(X(t), t) \ , \tag{2.32}$$

ϵ is a small value, F is the function which describes the oscillating system and G is the perturbation . This perturbation can be due to some input, noisy or otherwise, or due to the coupling of the oscillator to another. Following the working from [60], then introducing a phase variable $\theta(t)$, the Equation (2.32) can be reduced to the phase

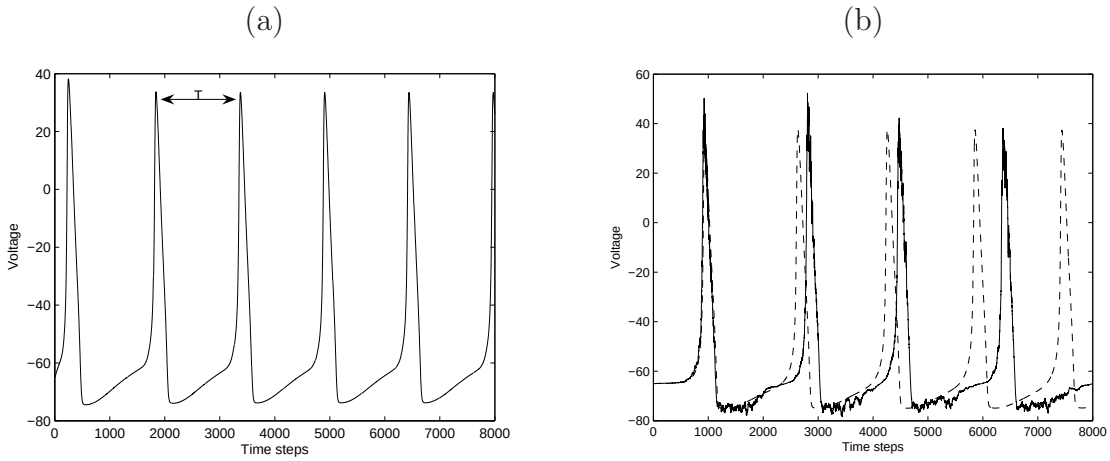

Figure 2.5: Plot (a) is an example of the regular spiking in the deterministic Hodgkin Huxley model. Time between the peaks is the period of the system T. Plot (b) is an example of noise induced phase shifting in the Hodgkin Huxley model. Noise is introduced to the model by using a white noise to drive Equation (2.23), i.e. $I_{inj} = I_{determ} + I_{noise}$ with I_{determ} the current used for plot (a) and I_{noise} is a temporal multiplicative white noise (generation of this type of noise is described in Chapter 3). The deterministic voltage trace is also shown to compare the period of the deterministic system to that of the noisy period. It can be seen that the spike time shifts forward and backwards with respect to the deterministic spike times. These are generated by solving Equation (2.23) with an input voltage of $V_{inj}(t) = 10$, temporal discretisation $\Delta t = 0.01$ and initial conditions $V(0) = -65$.

model:

$$\theta' = 1 + \epsilon\Delta(\theta)g(\theta, t) \tag{2.33}$$

where $g(\theta, t)$ is the component of G which relates to the membrane voltage. If the perturbation was due to coupling of oscillators then the function $g(\theta, t)$ would represent the coupling. The coupling in neural systems is due to synaptic connections, either electrical or chemical, and are usually pulse coupling or gap junction coupling(diffusive coupling). Once coupled Equation (2.33) will become a system of equations, for example for two mutually coupled oscillators we will have the equations:

$$\begin{aligned} \frac{d\theta_1}{dt} &= 1 + \epsilon\delta(\theta_2)\Delta(\theta_1) \\ \frac{d\theta_2}{dt} &= 1 + \epsilon\delta(\theta_1)\Delta(\theta_2). \end{aligned}$$

Once coupled we can look at the behaviour of the coupled system and in turn look for the synchrony/asynchrony of the system, that is $\theta_2 - \theta_1 = 0$ in the former case and $\theta_2 - \theta_1 \neq 0$ for the latter. Here we showed the very simple example of two mutually coupled oscillators but we can consider the case of a network of all-to-all symmetrically coupled neurons, chains of coupled neurons, rings of coupled neurons and even randomly connected networks. Geol and Ermentrout, [34], look at waves and synchrony on coupled chains and rings as well as 2-D arrays of oscillators. The paper [22] gives a general overview of neural oscillators and weak and strong coupling as well as briefly discussing the coupling of leaky integrate and fire neurons. It is shown in [13] that a pair of electrically coupled (gap junction) integrate and fire neurons can achieve synchrony or asynchrony depending on the coupling strength and the size of the spikes emitted by the neurons. Similarly in [104] the conditions on the coupling strength for networks of diffusively coupled HH neurons are derived to show stability of synchronous solutions. Bressloff and Coombes, [9], consider chains of pulse coupled integrate and fire neurons and the travelling waves which they support, this is similar to the SDS model, Section 2.8 which can also support travelling waves, see Section 2.9.

2.6 Synaptic plasticity and motility

In the following sections we discuss a dendrite model with active spines, BR model Section 2.7 and SDS model Section 2.8, where the spines are modelled by the HH or IF equations respectively. We mentioned that spines are important in learning and memory in Chapter 2, and here we discuss a mechanism by which the brain may learn and memorise: synaptic plasticity. Although we consider fixed distributions of spines in this work, the models can be easily altered to have changing spine densities or

irregular distributions of spines. Synaptic plasticity is a mechanism which allows the brain to learn and store memories. It is the term given to the changing strengths of connections between neurons as the brain learns and processes new information. The spines onto which synaptic connections are made can physically change in size and shape or the spines can appear or disappear, known as spine motility. This plasticity has been observed experimentally, [120] is a good review of experimental evidence for morphological changes in spines of the rodent hippocampus. Some of the earlier experiments reviewed seem contradictory and that the changes depend very much on the experimental setup e.g. one study reviewed in this paper showed that LTP caused shortening of spine stems where as several others showed no change under the same circumstances. However the advent of two-photon confocal microscopy has allowed improved observation of the changes in real time and better experimental results. The changes in spine morphology changes the calcium compartmentalisation in the dendrite so it is thought that the concentration of calcium ions, $[Ca^{2+}]$ is an important factor in spine plasticity. The presence of calcium can result in long term potentiation, LTP, or long term depression, LTD depending on the amount of calcium present in the spine. LTP gives sufficient conditions for a synapse to grow in strength and is typically activated by periods of high frequency pre-synaptic stimulation. LTD is the opposite, where the synapse will decrease in strength and is typically invoked by low frequency pre-synaptic stimulation, [33] has a description of LTP/LTD. In a further review, [8], the authors consider spine motility, which can be considered a form of plasticity since the spines move on the dendritic shaft in response to activity. They discuss the role of calcium in the movement of spines. For spines to grow they require actin-cytoskeleton which is activated by calcium in the correct measure as well as other neurotransmitters. If $[Ca^{2+}]$ is small or large this results in spine death, however if there is a moderate presence of $[Ca^{2+}]$ then spines can grow. The morphology of the spine stem is very important in controlling the quantity of $[Ca^{2+}]$ since the length of the stem directly controls the calcium time constant and so the rate of diffusion in the spine, which relates back to the growth/death of spines. The growth/death of spines can facilitate/destroy synaptic connections and so can be related to learning. The role of spines is discussed in [52] and suggests different roles for different types of spines in the cerebral cortex; they also review supporting experimental evidence. They suggest that large headed spines are stable and so have strong synaptic connections so can therefore be thought of as "memory spines". Conversely small headed spines are not stable and have weak connections. Their instability allows them to move or grow into the large headed variety and so can be labelled "learning spines". In the paper [113] the authors suggest a mathematical model for a length of spiny dendritic tissue that has space and time dependent spine density and spine stem resistance. The model uses the Baer Rinzel model, Section 2.7, as the spiny dendrite and introduces

an ODE to describe the activity dependent spine resistance and an expression for the density which depends on the resistance. As they stimulate the model with a high level of electrical activity they induce LTP which results in an increase in the spine density localised around the activity site. The draw back in this model is that although the density may increase near to activation sites the density elsewhere cannot decrease below the initial value. This model is extended in [114] by adding a dynamic calcium concentration to the already space-time dependent density. Therefore this new model has the BR equations as before, but now has three additional coupled ODEs modelling density, $[Ca^{2+}]$ and stem resistance respectively. The density and $[Ca^{2+}]$ both depend on the synaptic input and the stem resistance (which is related to stem length) depends on calcium concentration, when $[Ca^{2+}]$ is moderate the stem lengthens and when $[Ca^{2+}]$ is high the stem shortens. The authors consider how the density and resistance change with activity and how the new configuration of spines (both passive and active) affects the output of the whole branch. As the activity increases the spine density also increases, as expected. When the spines are passive, the increased density makes little difference to the output of the branch whereas the active spines can induce action potential propagation when the density reaches a critical value. Also as the frequency of the stimulation increases the $[Ca^{2+}]$ increases and the stems lengthen. When the spines are active this morphology change allows the spines to produce action potentials and so the output of the branch is enhanced. Finally when the $[Ca^{2+}]$ is high spines die and so high stimulation results in no output.

Instead of LTP or LTD as discussed until this point, there is another mechanism which can result in morphological changes and so learning; it is called spike timing dependent plasticity (STDP), [19]. As already discussed the frequency of pre-synaptic stimulation determines if the spine experiences LTP or LTD and therefore if the synaptic strength increase or decreases. In STDP the increase/decrease in synaptic strength depends not on the frequency of stimulation but on the time between a pre and post-synaptic spike, Δt, although repeated spike pairs does matter. If Δt is too large then no change will take place, however as the size of Δt gets smaller then the larger the change in synaptic strength; the sign of Δt determines whether this change is to make the synapse stronger or weaker i.e. if the order of spiking is pre-post then the strength will increase and if the order is post-pre then the connection will become weaker. STDP is also a type of Hebbian learning, that is as a cell is repetitively stimulated then the connection between the stimulating and stimulated cell is strengthened. While [19] discusses the experimental evidence of STDP, an example of a simple mathematical model of STDP can be found in [33]. A model which shows LTP, LTD and STDP is given in [119]. The authors calculate the changes in calcium concentration in spines as a result of different stimulation frequencies and as a function of the pre-post spike timing and they introduce a back propagating

action potential. The back propagating action potential is shown to alter the pre-post interactions in such a way as to allow STDP learning, which is not possible without it. Without the back propagating action potential the model can show changes in $[Ca^{2+}]$ that are consistent with LTP/LTD, and this allows the investigation of how the calcium changes affects the length of time that LTP/LTD exists. It appears from the experimental and mathematical investigations into synaptic plasticity that calcium plays an important role and that the shape and movement of dendritic spines does indeed play an important part in learning and memory.

2.7 Baer-Rinzel model

The Baer-Rinzel (BR) model [6] describes the voltage evolution of a spiny dendrite. The voltage in the spines is modelled using the HH, Section 2.3, equations and they are coupled, with a certain density, to a uniform passive cable, whose voltage, V, is modelled by the passive cable equation, by a spine stem resistance.
The density of spines can be any function of space, but the original BR model, of the three considered in this work, assumes this to be a constant. So combining the HH and passive cable models by coupling the equations together through the spine stem resistance r we obtain the equations of the BR model, Equation (2.34). Where $U(x,t)$ is the voltage in the spines and $V(x,t)$ is the voltage in the cable. The coupling of the HH model to the spatially extended cable equation is done through the last terms in both Equation (2.34) and Equation (2.38), so now the original HH equations are driven by a current from the cable and the cable diffuses the action potential along the length of the cable.

$$\begin{aligned} C_m\frac{dU}{dt} &= G_{Na}m^3(U)h(U)(V_{Na}-U)+G_Kn^4(U)(V_K-U) \\ &+ G_L(V_L-U)-\frac{U-V}{r} \end{aligned} \tag{2.34}$$

$$\frac{dm(U)}{dt} = \alpha_m(U)(1-m)-\beta_m(U)m \tag{2.35}$$

$$\frac{dh(U)}{dt} = \alpha_h(U)(1-h)-\beta_h(U)h \tag{2.36}$$

$$\frac{dn(U)}{dt} = \alpha_n(U)(1-n)-\beta_n(U)n \tag{2.37}$$

$$C\frac{\partial V}{\partial t} = -G_L(V-V_L)+\frac{1}{r_a\pi a}\frac{\partial^2 V}{\partial x^2}+\rho(x)\frac{U-V}{r}. \tag{2.38}$$

The parameters in Equation (2.34) have the same meaning as before (Section 2.3), and are listed in the Nomenclature at the start of the thesis. $\rho(x)$ is the density of the spines along the cable, the larger $\rho(x)$ is the stronger the coupling between the spines and the cable. In the original BR model the density is taken to be a constant. Here we extend the model to include $\rho(x)$ as a function of x, we investigate the behaviour of the system when the spines are attached at discrete points along the cable, as we will see in the SDS model Section 2.8, and when we have something in between these two extremes, see Chapter 6.

Although there is now a spatial extension in the HH equations which describe the spines, they can only interact with each other through the cable.

The BR model has been shown to support travelling waves, solitary, multi-bump and periodic waves, in the appropriate parameter ranges, see Section 2.9 for a description of travelling wave solutions to the BR model. One example is shown in Figure 2.6 where the region of existence for a travelling wave is shown as ρ changes with all other parameters fixed. There are two regimes shown in the figure, when the density is too small there is no propagation of a travelling wave but when the density increases to the limit point and beyond then the system supports travelling wave solutions. This type of figure could be reproduced for a different set of parameters e.g. we could fix all the parameters except the resistance and so on. For each value of the density there are two wave speeds associated with it, except at the limit point, marked on Figure 2.6, where there is only one. The faster speed represents the stable waves which can be seen in any direct simulation of the BR equations. So for each of the parameters there would be a different curve showing the existence of the wave for that particular regime, see Chapter 5. For further details see [70], the analysis in this paper can be followed in the case of small noise in the system.

2.8 SDS model

The SDS model [15], [16] and [109] describes a length of spiny dendritic cable, as represented in the schematic in Figure 2.7. This model is similar to the BR model in its coupling of a passive dendrite and active spines, although the SDS model does not use the HH equations, the spines are still coupled to the cable through a spine stem resistance r and a density $\rho(x)$, which could be any suitable spatially dependent function we choose. The SDS model, as described in [16], chooses a more physically realistic function for $\rho(x)$ that ensures the spines are separate entities along the cable instead of a constant as in the BR model. Some of the biological detail of action potential generation is lost by not using the HH equations.

The cable is modelled by the passive cable equation, and the spine head dynamics by the leaky integrate and fire model with a refractory time τ_R. The spines are attached

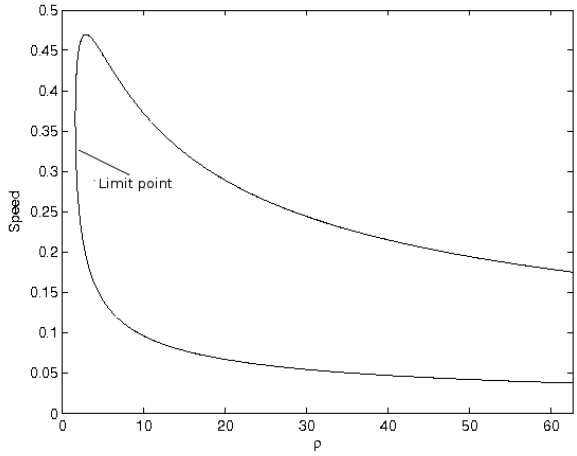

Figure 2.6: Bifurcation diagram for the Baer-Rinzel model, showing where in parameter space, for ρ, the travelling wave exists, the speed of this wave is shown on the y-axis. This is the existence for one set of parameter values, with only the density changing. The limit point shows where the system switches from the regime which supports travelling waves to one where no travelling waves exist (at small ρ). This figure was generated using the bifurcation package AUTO-07P to continue a travelling wave solution of the BR model in the two parameters ρ and c to show where in parameter space these travelling waves exist.

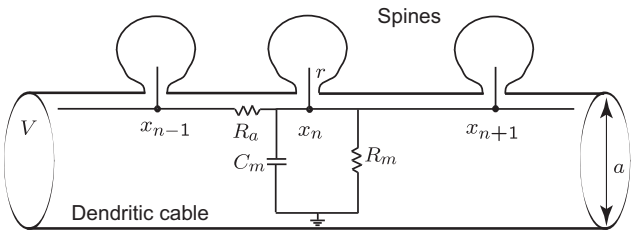

Figure 2.7: Diagram of a length of spiny dendritic tissue showing the circuit diagram representation of one compartment of the cable.

at discrete points along the cable by a spine stem with resistance, r. The points at which the spines are attached can be spaced with any spatial distribution but here we have chosen equally spaced points.
The membrane potential in the cable, V(x, t), is given by:

$$\frac{\partial V}{\partial t} = D\frac{\partial^2 V}{\partial x^2} - \frac{V}{\tau} + Dr_a I_{ext} \ . \tag{2.39}$$

$D = \frac{\lambda^2}{\tau}$ is the diffusion coefficient, $\tau = r_m c_m$ is the membrane time constant, $\lambda = \sqrt{\frac{dr_m}{4r_a}}$ is the electronic space constant, r_a is the intracellular resistance per unit length and I_{ext} is any external current with $x \in [0, L]$ and $t \in [0, T]$, L is the length of the cable and T is the end time. If we replace I_{ext} with the current coming from the spines, we get:

$$\frac{\partial V}{\partial t} = D\frac{\partial^2 V}{\partial x^2} - \frac{V}{\tau} + Dr_a\rho(x)\frac{\hat{V} - V}{r} \ . \tag{2.40}$$

Where $\rho(x) = \sum_{n\in\Gamma}\delta(x - x_n)$ which is the density of spines, attached at discrete points x_n, $\hat{V}(x_n, t)$ is the action potential produced by the spine at the point x_n, the form of the action potential is free to be chosen, and r is the spine stem resistance. The spine head dynamics are modelled by the leaky integrate and fire (IF) model, see Section 2.4. From the circuit representation of the spine head, Figure 2.8, the leaky

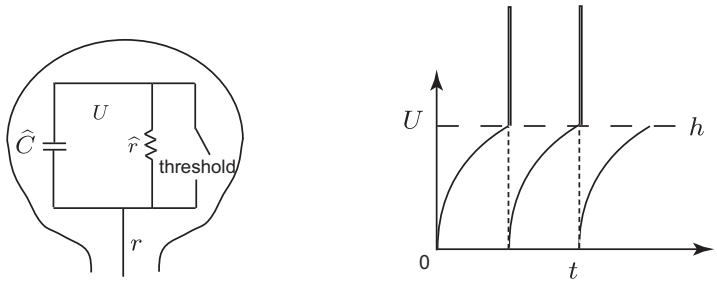

Figure 2.8: Left: Circuit diagram representation of a spine head. Right: Schematic of the voltage, U increasing to threshold level, h, spiking and resetting to zero again.

IF model takes the following form.
The action potential, $U_n(t)$, in the nth Spine evolves as:

$$\hat{C}\frac{dU_n}{dt} = -\frac{U_n}{\hat{r}} + \frac{V_n - U_n}{r} - \underbrace{\hat{C}h\sum_m \delta(t - T_n^m)}_{\text{Reset}} \ . \tag{2.41}$$

The $I(t)$ in Equation (2.31) has been replaced with the coupling term $\frac{V_n - U_n}{r}$, which attaches the spines to the cable. The m-th firing time of the nth spine, T_n^m, is governed by the integrate and fire process:

$$T_n^m = \inf\{t | U_n(t) \geq h, t > T_n^{m-1} + \tau_R\} \ , \tag{2.42}$$

where τ_R is the refractory time period, during which the spine is unable to fire. This refractory time is introduced to mimic the dynamics of the HH model, which has a natural refractory time. At $U_n = h$ an action potential is injected into the cable; the form of this injected potential can be chosen to be a suitable function, in the SDS model described here, the function was chosen to be a rectangular pulse, given by:

$$\eta(t) = \eta_0 \Theta(t)\Theta(\tau_s - t) \tag{2.43}$$

Where $\Theta(t)$ is the Heaviside function, τ_s is the length of time the pulse lasts for and η_0 is the strength (magnitude) of the pulse.

These equations describing the dynamics of spiny dendritic tissue can be solved using a combination of analytical and numerical techniques. Here we provide a brief description of how this is implemented, see [109] for a fuller description of the methodology. Explicit solutions can be obtained for both $V(x,t)$ and $U(t)$. $V(x,t)$ has a Neumann series solution involving the Green's function for the passive cable, described in Section 2.2.1, and up to threshold $U(t)$ can be solved by directly integrating Equation (2.41) and substituting for $V(x,t)$. The firing times, however, have to be numerically determined using the threshold condition $U_n(t) = h$. After finding the latest firing time $V(x,t)$ can be recalculated and so $U_n(t)$ recalculated, the threshold condition checked and so on, building up a complete picture of the cable throughout the time interval. Although in most instances throughout this work the SDS equations are solved by a fully numerical technique, we use this method in Chapter 7.

The solution of this problem shows that the SDS model supports the propagation of saltatory travelling waves along the length of the cable ([16], [109]). The success or failure of propagation depends on many biological parameters, e.g. spine spacing, spine stem resistance and membrane properties. The parameter we are particularly interested in is the spine spacing, since it is easily altered and is a parameter which in the real biological system varies depending on the type of neuron the dendrite belongs to; Figure 2.9 shows the area of parameter space where the travelling wave exists for varying d.

Figure 2.9 is analogous to Figure 2.6 in that it shows the area of existance of a travelling wave for changing spine spacing d. As the spine spacing increases the speed of the wave slows and at the limit point the system cannot support travelling waves; therefore there are two distinct regimes where the wave exists and where it does not. Figure 2.6 was generated using the continuation software AUTO-07P and thus shows the stable, faster branch and the slower, unstable branch.

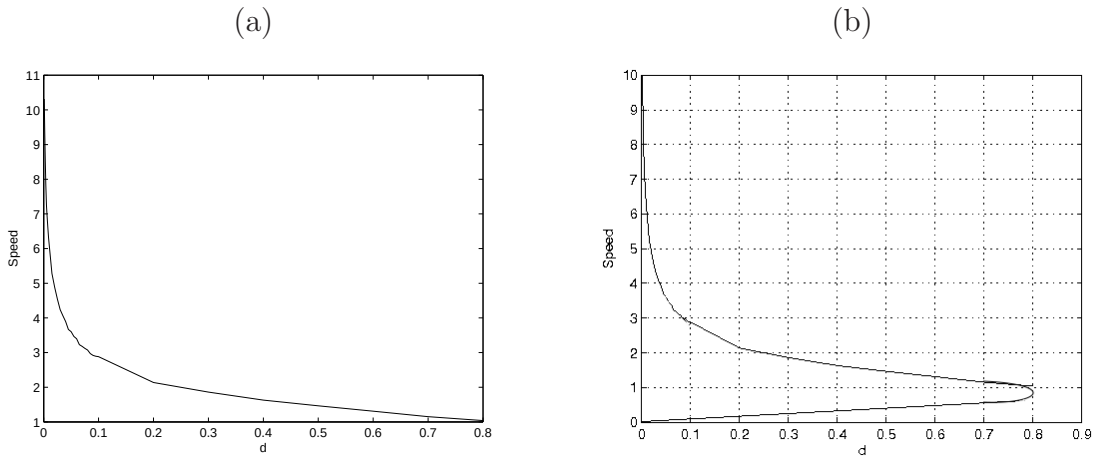

Figure 2.9: Speed of a travelling wave in the SDS model as a function of spine spacing, d. Plot (a) shows the direct simulation of the SDS model to find speed as a function of spine spacing. Plot (b) shows the top, fast branch again obtained from direct simulation and shows the speed of the stable wave in the SDS model. The bottom, slow branch has been drawn on to represent the unstable solution, which can not be observed directly. This figure is a reproduction of a figure in [109] and is given as an illustrative aid to emphasise that there are two regimes for the deterministic SDS model. All other parameters are as described in the parameter list at the start of the thesis. We solve Equation (2.40) along with Equation (2.31) with temporal discretisation $\Delta t = 0.1$, $t \in [0, 70] and$ spatial discretisation $\Delta x = 0.08$, $x \in [0, 96]$. The boundary conditions used are Dirichlet and initial conditions $V(x, 0) = 0$, $U_1(0) = U_2(0) = 0.04$ and $U_{n>2} = 0$.

2.9 Travelling waves in neural models

Throughout this work we are concerned with the behaviour of travelling waves under the influence of noise, primarily how the speed of any travelling wave changes as the noise intensity increases. A travelling wave is, in general terms, a transference of energy through the movement of a medium from one point to another e.g. a water wave or sound wave. The energy and so the signal is transmitted through the perturbation of water molecules or air particles in the two examples given; each molecule is perturbed from its initial state by the passing of the wave and so perturbs its neighbouring molecule and so on. Despite the fact that not one molecule/object makes the journey from the initial point of the wave to the final point, the energy has been transported from one point to another, distant point, [38]. In neural models the signal can be chemical or electrical and we are concerned with the propagation of action potentials, therefore consider electrical signals which concern the movement of charged particles, usually electrons.

Travelling waves have been observed by experimentalists in the course of *in vivo* or *in vitro* experiments with either whole cell recordings or axo-dendritic recordings. Examples include waves associated with epileptic seizure [102], waves seen in sleep cycles [102] and along axons or dendrites, [99] is a review of theoretical and experi-

mental action potential propagation in dendrites. An interesting example which is of particular relevance to the models considered in this work is described in [26] where the authors grow cultured hippocampal neurons along a 1-D mould to produce a linear network of neurons. They observe travelling packets of activity as well as synchronous behaviour along the whole length of the sample. They are able to measure wave speeds of around 100mm/s which is in agreement to an order of magnitude with measured speeds in slice preparations taken from unmylenated rat hippocampal axons. The authors also compare their experimental results to a theoretical model by Osan and Ermentrout [81], which models a linear network of neurons with IF dynamics connected synaptically (that support travelling wave solutions) and find good agreement. As briefly discussed here there are many types of waves in neural systems and travelling waves are just one of the experimentally and theoretically observed solutions. As dendritic models go the Baer and Rinzel model was the first to couple active spines to a passive cable and show travelling wave solutions. The original BR paper, [6] showed numerically smooth and saltatory travelling waves; saltatory means that the wave appears to jump from one active spine to the next and this has been observed in the nervous system in dendrites and on an axon where the mylenated sheath is broken by nodes of Ranvier. A more recent paper, [110], summarises, briefly, this result and shows how the change in parameters can enhance the propagation or cease propagation. No analytical results for the travelling waves or their stability in the BR model have been found and J. Rinzel extended the work on the travelling waves in the BR model by considering a simplified version using dynamics similar to the Fitzhugh Nagumo model for the spine heads instead of the HH model, [89]. This new system has only two free parameters and so makes the solution and stability analysis available by analytical means. To do this the authors transform the two coupled ODE system into the travelling wave frame using the standard anzatz and so find existence of the wave solutions as the parameters change. They use a linear stability analysis to show that the fast solutions are the stable branch of solutions. A full numerical study of the travelling wave solutions in the BR model has been carried out in [70] using the travelling wave frame and a dynamical systems approach. The existence of the waves in parameter space was explored and further multi-bump solutions were found to exist as were bursting packets. Using a similar approach, [15], show the existence of travelling wave solutions and their stability in another simplification of the BR model. The authors exploit the fast nature of the m-dynamics in the BR model to reduce the spine head dynamics to an all or nothing response modelled by the IF model. They again use the standard travelling wave anzatz to convert to a co-moving frame and can analytically find the travelling wave solutions and their stability; they arrive at an explicit value for the wave speed depending on the system parameters. The authors continue to extend their own work in a later paper, [16], to find the existence and

stability of saltatory waves in a similar SDS model where the spines are no longer a constant density as in the BR model but are in fact attached at discrete points physically separated by equal distances. Once again the authors derive an expression for the waves speed as a function of the system parameters. Travelling wave solutions have also been explored in a neural network environment; [17] uses a firing rate model on a spatially extended domain to model a network of synaptically connected neurons. The integro-differential equation is converted to a PDE and then to a delayed ODE through the conversion to the travelling wave frame and exact expressions for the wave speed can be obtained when the firing rate function is a Heaviside function and if the firing rate threshold is too large then propagation fails. The numerical solution is obtained for different forms of the synaptic footprint. The model is then extended to include a passive dendritic tree and for specific firing rate functions the exact form of the speed of the wave can be determined.

Apart from the travelling wave solution where an action potential propagates with some speed there are other forms of waves that exist in neural systems. The paper [65] discusses the existence of rotational waves in a ring of diffusively, symmetrically coupled oscillators; this type of system is seen in the motor control of animal leg motion. The dynamics of the oscillator are not explicitly described but the results hold for a general class of oscillators and the stability of one branch of oscillations is found. The phase difference between each oscillator is either zero, showing synchronous behaviour or at a maximum which shows asynchronous behaviour. All of the analysis is done using Hopf bifurcation theory. A recent paper [74] shows analysis of spiral waves in a network of coupled oscillators using a Gaussian kernel which allows the analytical solution using perturbation theory to find the spiral waves and the speed of the rotating arms.

Chapter 3

Stochastic forcing and numerical methods

This chapter is also for background information and covers the concept of 'noise' and how to introduce it to ordinary and partial differential equations. also investigate how to correctly interpret the stochastic integral and how to generate different types of noise, i.e. white or correlated. We then cover the numerical methods used to simulate the new stochastic differential equations and the techniques devised to measure the effect of the noise on the dendritic models which were described in Chapter 2.

3.1 Noise

In a broad sense, noise is often considered to be any 'unwanted', meaningless data, for example, the crackling noise heard on an untuned radio but not all noise is destructive and can be, in some cases, useful.
In neural circuitry there are many potential sources of noise: the proximity of other neurons and axons, synaptic connections from other neurons, the nature of the gating of ion channels in the cell membrane can give rise to random effects and as with all physical systems, thermal noise, which arises from random molecular movement due to thermal energy. There is a comprehensive review of noise sources at all levels of the central nervous system (CNS) in [24]; the paper also looks at the effects of the noise and ways in which the CNS compensates for the noise. All sensory information which the brain receives, from sight, smell etc, is noisy and so is one source of external noise. Internal noise sources, already mentioned e.g. ion channels, place a limit on the size of structures within the brain since the smaller the structure (axon/dendrite) then the bigger the affect of the internal noise. So the size of axons are limited as is the density of the wiring in the brain to reduce noise from what the authors term 'cross-talk' (electrical interference). The CNS can deal with noise by averaging behaviour e.g. visual input is averaged over photoreceptors which share a visual field, and so

some of the fluctuations due to noise are smoothed. The presence of noise in real neurons has been observed *in vivo*, e.g. [61] reviews synaptic noise and shows large fluctuations in the membrane voltage of feline cortical networks. [27] also discusses the presence of noise in *in vivo* experiments with the rat cortex. The reproduction of these real fluctuations is often investigated *in vitro* using a stochastic conductance model to simulate the synaptic noise and a dynamics clamp technique to force the prepared slices of neurons, thereby merging the computational and experimental techniques, [61], [27] and [50]. The models which force the real neurons, in the papers mentioned, use a multiplicative white noise to create the fluctuations but the actual intensities used is not explicitly given. The results are in agreement with *in vivo* observations; in [27] the noise allows the cell to detect sub-threshold signals and in [50] the presence of noise is shown to be necessary to facilitate the behaviour that characterises stellate neurons.

This section looks at how noise can be described mathematically and how it can be numerically simulated. Noise can take many forms, correlated in space and/or time or uncorrelated; we will consider temporally correlated noise as an Ornstein-Uhlenbeck process and uncorrelated noise as a simple Brownian motion or Wiener process.

3.1.1 Some basic probability theory

We start by briefly looking at some basic probability theory and definitions which will help us to define the stochastic integral in Equation (3.11) and understand the solution of an SDE. There are many good introductory texts on probability theory such as [47] and [49] but several books that use or discuss more general stochastic problems have very good, concise introductions to probability theory, such as [32], [80], [5], [31] and [55], all of which deal with SDEs. [62] discusses stochastics in the neurosciences and gives a brief introduction to some of the probability theory required and [88] is a text book for physicists and engineers which has a probability section that discusses the concept of random variables and their associated distribution functions. First we introduce a probability space, $(\Omega, \mathcal{U}, P)$ in order to define a random variable. The probability triple includes Ω, which is any nonempty set called a sample space, $\mathcal{U}$ is a σ-algebra, a collection of events, and P is a probability measure which gives the probability of an event in the σ-algebra happening. If we consider flipping a fair coin then we can define the triple for this simple experiment: $\Omega = \{heads, tails\}$, $\mathcal{U} = \{\emptyset, \{\text{heads}\}, \{\text{tails}\}, \{\text{heads, tails}\}\}$ and $P = \{0, \frac{1}{2}, \frac{1}{2}, 1\}$.

Definition 3.1.1 *A σ-algebra is a collection, $\mathcal{U}$, of sub-sets of Ω with the following properties:*

- $\emptyset$, $\Omega \in \mathcal{U}$.

- *If* $A \in \mathcal{U}$ *then the complement* $A^C \in \mathcal{U}$.
- *If* $A_1, A_2, \ldots \in \mathcal{U}$, *then* $\bigcup_{k=1}^{\infty} A_k \in \mathcal{U}$ *and* $\bigcap_{k=1}^{\infty} A_k \in \mathcal{U}$.

Definition 3.1.2 $P : \mathcal{U} \to [0,1]$ *is defined as a probability measure if the following hold:*

- $P(\emptyset) = 0$, $P(\mathcal{U}) = 1$.
- *If* $A_1, A_2, \ldots \in \mathcal{U}$, *then* $P(\bigcup_{k=1}^{\infty} A_k) \leq \sum_{k=1}^{\infty} P(A_k)$.
- *If* $A_1, A_2, \ldots$ *are disjoint sets in* $\mathcal{U}$, *then* $P(\bigcup_{k=1}^{\infty} A_k) = \sum_{k=1}^{\infty} P(A_k)$.

The probability space defined by the triple $(\Omega, \mathcal{U}, P)$ is not observable, so we must define a quantity which we can observe in the real world $\mathbb{R}^n$, this is a random variable.

Definition 3.1.3 $X : \Omega \to \mathbb{R}^n$ *is called an n-dimensional random variable if for each* $B \in \mathcal{B}$ *we have* $X^{-1}(B) \in \mathcal{U}$.

Here $\mathcal{B}$ is a collection of Borel subsets of $\mathbb{R}^n$ which is the smallest σ-algebra (of $\mathbb{R}^n$) containing all open sets.

If a random variable, $X(t)$ is dependent on time we can define a stochastic process and sample path as follows:

Definition 3.1.4 *The collection* $X(t)|t \geq 0$ *is a stochastic process and* $\forall \omega \in \Omega$, $t \mapsto X(t, \omega)$.

Now that we have a definition for a random variable we can continue to define a few more useful quantities such as the expected value/mean and the variance. We use the probability density function, which holds all information about its associated random variable, to find, for example, the expected value, variance or some other property of interest. A useful example which will be used frequently is the normally distributed (or Gaussian) random variable, for 1-D case, with mean μ and variation σ^2 has the probability distribution $p(x) = \frac{1}{\sqrt{2\pi\sigma^2}} e^{-\frac{(x-\mu)^2}{2\sigma^2}}$. More generally:

Definition 3.1.5 *If* $X : \Omega \to \mathbb{R}^n$ *has the density function:*

$$p(x) = \frac{1}{\sqrt{(2\pi)^n \det \mathbf{C}}} e^{-\frac{1}{2}(x-\mu)\mathbf{C}^{-1}(x-\mu)} \tag{3.1}$$

$x, \mu \in \mathbb{R}^n$ *and* $\mathbf{C}$ *is a positive definite, symmetric matrix, then* X *is said to have a Gaussian (or normal) distribution with mean* μ *and covariance matrix* $\mathbf{C}$.

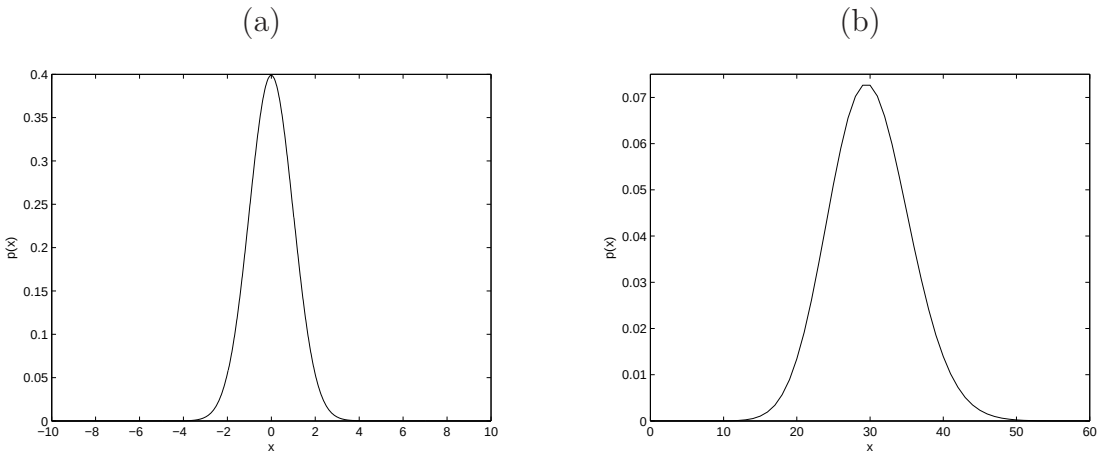

Figure 3.1: Plot (a) shows the normal distribution $\mathcal{N}(0,1)$ and plot (b) shows an example of the Poisson distribution, $\alpha = 30$.

Another useful distribution is the Poisson distribution, since it can be used for spike rate models for a single neuron, [33]. The Poisson distribution is given by:

$$p(x) = \frac{(x)^{\alpha}}{\alpha!} e^{-x} \ , \tag{3.2}$$

where x is the number of events, α is the average rate at which the events occur in a specified region. Figure 3.1 plot (b) shows an example of a Poisson distribution where $\alpha = 30$.

If we have the probability density associated with a random variable, X, then we can find the probability of X occurring within a certain range $x = [a, b]$ by $Pr(X \in [a, b]) = \int_a^b p(x)dx$. The expected value (or mean) of X is the most likely value of X and is given by Equation (3.3):

$$\mu = \mathbb{E}(X) = \int_{-\infty}^{\infty} xp(x)dx \ . \tag{3.3}$$

The variance is a measure of how the random variable deviates from its mean value and is given by $\sigma^2 = \mathbb{V}(X) = \mathbb{E}(X^2) - (\mathbb{E}(X))^2$. We have shown two of the common notations for mean (μ and $\mathbb{E}$) and variance (σ^2 and $\mathbb{V}$). A similar measure is the co-variance, which measures how a random variable, X, changes with respect to another random variable, Y, and is given by $F_c(X, Y) = \mathbb{E}(XY) - \mathbb{E}(X)\mathbb{E}(Y)$. We also define the auto-correlation, Equation (3.4), of a random variable, which is a measure of how quickly a random variable changes in time.

$$C(X(t)) = \mathbb{E}(X(t_1)X(t_2)) \ , \tag{3.4}$$

where t_1 and t_2 are two points in time.

3.1.2 Brownian motion

We will require the definition of the random variable $W(t)$, which is considered to be a standard Brownian motion or standard Wiener process. Brownian motion is perhaps the most well known stochastic process and was first discovered by R.Brown in 1826 when he observed the apparently random movement of pollen particles in water. The process was first mathematically described by T.N.Theile in 1880 and later consolidated by a paper by A.Einstein in 1905. The derivation of Brownian motion using a random walk argument, i.e. a particle moving on a 2 dimensional lattice and implementing the Laplace-De Moivre theorem, gives the normal distribution, [23].

Definition 3.1.6 *A one dimensional Wiener process, $W(t)$, defined on the time interval $[0,T]$ depends continuously on $t \in [0,T]$. To be classified as a Wiener process $W(t)$ must satisfy the following conditions ([62], [41], [86]):*

- *$W(t=0) = 0$, with probability 1.*
- *For $0 \leq s < t \leq T$, a Brownian increment $W(t) - W(s) \sim \sqrt{t-s}N(0,1)$, where $\mathcal{N}(0,1)$ is a normally distributed random variable with zero mean and unit variance.*
- *For $0 \leq s < t < u < v \leq T$, $W(t) - W(s)$ and $W(v) - W(u)$ are independent paths.*

We now have enough information to generate a Brownian path on a time interval $[0,T]$ and using N increments of Δt such that $\mathrm{N}\Delta t = T$. The independent Brownian increments ΔW can be generated using Definition (3.1.6), starting at $W(t=0) = 0$ we can find the next point $W(\Delta t) = W(\Delta t) - W(0) \sim \mathcal{N}(0, \Delta t)$ then $W(2\Delta t) = W(2\Delta t) - W(\Delta t) \sim \mathcal{N}(0, \Delta t)$ and so on until $W(T) = W(T) - W((\mathrm{N}-1)\Delta t)$. Therefore each step can be generated using a normally distributed random variable, scaled correctly by the time step, which can be easily generated in Matlab. Figure 3.2 shows an example of a Brownian path generated by this method.

Definition 3.1.7 *A function $f : [0,T] \mapsto \mathbb{R}$ is termed uniformly Hölder continuous with exponent $\gamma > 0$ if there is a constant K such that $|f(t) - f(s)| \leq K|t-s|^{\gamma}$.*

A Brownian motion is termed "nowhere differentiable" since it is not Hölder continuous for exponents greater than $\frac{1}{2}$.

Theorem 3.1.1 *For all $\frac{1}{2} < \gamma \leq 1$, $t \mapsto W(t,\omega)$ is nowhere Hölder continuous for exponent γ, is nowhere differentiable and is of infinite variation on each subinterval.*

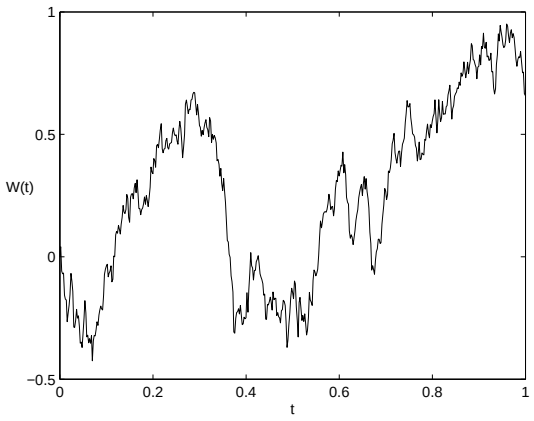

Figure 3.2: An example of a Brownian path generated in Matlab.

The proof of this theorem, by Dvoretzky, Erdös, Kakutani, is outlined in [23].

We can think of $\frac{dW(t)}{dt} = \xi(t)$ as a white noise path although formally a continuous time random process, $X(t)$, is only termed white noise if:

- The mean is equal to zero, i.e. $\mathbb{E}[X(t)] = 0$
- The autocorrelation function satisfies: $\mathbb{E}[X(t_1)X(t_2)] = \sigma^2\delta(t_1 - t_2)$,

where σ^2 is the variance as before.

3.1.3 Stochastic integrals

In this subsection we briefly review how to understand and evaluate a stochastic integral. We also look at the definition of an Itô and Stratonovich integral and how we can convert between an SDE evaluated in the Itô sense and in the Stratonovich sense. There are many books that cover this topic, [55], [5] are two examples and [23] is a good set of lecture notes that defines the Itô integral and discusses the Stratonovich integral. So we consider the integral form of our standard SDE Equation (3.11).

Definition 3.1.8 *A partition of* $[0, T]$ *is a finite collection of points* $P = \{0 = t_0 < t_1 < \cdots < t_m = T\}$ *with step size* $|P| = \max_{0 \le k \le m-1} |t_{k+1} - t_k|$.

Recall the Riemann approximation for a general deterministic integral $\int_a^b f(x)dx$, where $f(x) : \mathbb{R} \to \mathbb{R}$ and $a, b \in \mathbb{R}$. As defined above, the interval $[a, b]$ can be split into the partition $\{a = x_0 < \ldots < x_m = b\}$ which can then be used to define the Riemann sum: $S = \sum_i 1^m f(y_i)(x_i - x_{i-1})$, where $x_{i-1} \le y_i \le x_i$. The smaller the increment $x_i - x_{i-1}$ then the more accurate the approximation will be and the arbitrary choice of y_i will not affect the outcome of the sum.

We consider, as an example, the integral $\int_0^T W dW$ with W a 1-dimensional Brownian motion, as defined in Section 3.1.2. Although a Brownian motion is nowhere differentiable, we will follow a Riemann sum type approximation of the integral and then pass appropriate limits. If we set $\tau_k = (1-\phi)t_k + \phi t_{k+1}$, with $\phi \in [0,1]$ we can then define the Riemann type approximation for the stochastic integral:

$$\int_0^T W dW \approx R_m = \sum_{k=0}^{m-1} W(\tau_k)(W(t_{k+1}) - W(t_k)) \ . \tag{3.5}$$

It can be shown that given a sequence of partitions P_n (where t_m^n is the mth point in the nth partition and $(t_m^n - t_{m-1}^n) \to 0$ as $n \to \infty$), [23], [80], that for $R_n = \sum_{k=0}^{m_n-1} W(\tau_k^n)(W(t_{k+1}^n) - W(t_k^n))$ and with the limit in $L^2(\Omega)$:

$$\lim_{n\to\infty} R_n = \frac{W(T)^2}{2} + (\phi - \frac{1}{2})T \ . \tag{3.6}$$

The limit obviously depends on the choice of ϕ. If $\phi = 0$ we have the Itô definition of the stochastic integral, where the integrand is evaluated at the left hand end point and $\phi = \frac{1}{2}$ gives the Stratonovich definition, where we evaluate at the midpoint. These two cases clearly differ and can give rise to different values of the stochastic integral. It is clear that in the Itô sense the integral does not follow the normal rules of calculus since for this case $\lim_{n\to\infty} R_n = \frac{W(T)^2}{2} - \frac{T}{2}$ which has an extra term, $-\frac{T}{2}$, that would not appear under the normal rules of calculus. The Stratonovich integral does follow the normal rules since, $\lim_{n\to\infty} R_n = \frac{W(T)^2}{2}$ when $\phi = \frac{1}{2}$, however this requires some future knowledge of the process to evaluate at the midpoint. The Itô and Stratonovich definitions of the stochastic integral are the most famous and widely used but there are infinitely many approximations for the integral since $\phi \in [0,1]$ will give rise to a different approximation with each choice of ϕ. In order to make it clear which of the stochastic integrals is being used, we employ the following notation: $\int W dW$ denotes the Itô interpretation and $\int W \circ dW$ denotes that the Stratonovich interpretation is being used.

We now consider the integral $\int_0^T G(t) dW$ for some non-anticipating functions $G(t)$. A function is non-anticipating if it is $\mathcal{F}$ measurable, with $\mathcal{F}$ a filtration. This means that the function G only depends on prior information. We now define a filtration but first we need $\mathcal{W}(t) = \mathcal{U}(W(s)|0 \le s \le t)$, the σ-algebra known as the history of the Brownian motion up to time t and the future of the Brownian motion is the σ-algebra $\mathcal{W}^+(t) = \mathcal{U}(W(s) - W(t)|s \ge t)$.

Definition 3.1.9 *$\mathcal{F} \subseteq \mathcal{U}$ is a family of σ-algebras called non-anticipating if:*

- $\mathcal{F}(t) \supseteq \mathcal{F}(s) \ \forall \ t \ge s \ge 0$
- $\mathcal{F}(t) \supseteq \mathcal{W}(t) \ \forall \ t \ge 0$

- $\mathcal{F}(t)$ *is independent of* $\mathcal{W}^+(t)$ $\forall t \geq 0$.

We will approximate the function G by a step-process, define the Riemann sum and then pass limits which will then define the Itô integral.

Definition 3.1.10 *A process is called a step-process if for a partition* $P = \{0 = t_0 \leq t_1 \leq \cdots \leq t_m = T\}$ *then* $G(t) \equiv G_k$ *for* $t_k \leq t < t_{k+1}$, $k = 0, \ldots, m-1$.

Then we can define the Itô integral of G (a step-process) as:

$$\int_0^T G dW = \sum_{k=0}^{m-1} G_k(W(t_{k+1}) - W(t_k)) = \sum_{k=0}^{m-1} G_k \Delta W_k, \tag{3.7}$$

with the increment ΔW_k. If we have a general function $G \in \mathbb{L}^2[0,T]$ then there exists a sequence of bounded step-processes $G^n \in \mathbb{L}^2[0,T]$ such that $\mathbb{E}\left(\int_0^T |G - G^n|^2 dt\right) \to 0$, see [23]. $\mathbb{L}^2$ is the set of square integrable functions, or $\mathbb{L}2$ functions, it is the set of all measurable functions whose absolute values squared have a finite integral with respect to some measure μ: $||f||_p := \left(\int |f|^2 d\mu\right)^{\frac{1}{2}} < \infty$. It can then be shown that for the step processes G^n:

$$\mathbb{E}\left[(\int_0^T G^n - G dW)^2\right] = \mathbb{E}\left[\int_0^T (G^n - G)^2 dt\right] \to 0 \text{ as } n \to \infty \ . \tag{3.8}$$

Therefore in this mean square limit, as the partition mesh gets smaller, the step-process approximates the general function G and as such we can define the Itô integral as:

$$\int_0^T G dW = \lim_{n\to\infty} \int_0^T G^n dW \ . \tag{3.9}$$

And so Equation (3.7) is a valid approximation of the integral: $\int_0^T G dW$, and we have the following properties for the Itô integral, [80], [23]:

- $\mathbb{E}(\int_0^T G dW) = 0$ is the Martingale property
- $\mathbb{E}((\int_0^T G dW)^2) = \mathbb{E}(\int_0^T G^2 dt)$ is called the Itô isometry.

3.1.4 Stochastic differential equations

A deterministic system is one which can be described by Ordinary Differential Equations (ODEs) or Partial Differential Equations (PDEs) which contain all information of how properties of the system evolve in time and/or space. Given the set of equations and the initial conditions of a system the future state of the system can be determined without any ambiguity in the final outcome, i.e. given the same initial conditions the final outcome will always be the same, (provided the description of the system is correct and the method used to solve the system is correctly chosen and

implemented).

Stochastic Differential Equations (SDEs) describe the evolution of a system which has a degree of randomness associated with it, e.g. the stock market fluctuations. This randomness is time dependent rather than any random initial conditions or random parameters in the differential equation. In this case, given a set of SDEs describing the system and the initial state of the system, there is not any one outcome for the future state of the system, there is instead a probability distribution associated with the outcome.

In an SDE, one or more of the terms is a stochastic process which can also be described as a random function defined over a time interval or space region. Here we look in more detail at SDEs. There are many books describing SDEs and probability theory, but [23] is a good set of lecture notes available on the Internet, [80] is an introduction to SDEs and [32] is geared towards applications of SDEs.

If we think of adding a white noise to a deterministic ODE then we could write: $\frac{dX}{dt} = f(X(t)) + g(X(t))\xi(t)$, where $\xi(t)$ is white noise. We cannot directly deal with this white noise $\xi(t)$ mathematically since it is not continuous but we can think of $\xi(t) = \frac{dW(t)}{dt}$ (or $dW = \xi dt$). Then we can rewrite the our 'noisy' ODE as a general Itô SDE of the form:

$$dX(t) = f(X(t))dt + g(X(t))dW(t) \ , \tag{3.10}$$

which can be more easily and properly understood in integral form:

$$X(T) = X_0 + \int_0^T f(X(t))dt + \int_0^T g(X(t))dW(t) \tag{3.11}$$

here $f(X(t))$ and $g(X(t))$ are functions, which have specific properties, of the random variable $X(t)$ and $W(t)$ is a Wiener process which is integrated in the Itô sense. Since we have just discussed in Section 3.1.3, the Itô integral we can then attempt to find a solution to this SDE. In the following section we give sufficient conditions on $f(X)$ and $g(X)$ such that there exists a solution to Equation (3.10), $X(t)$.

3.1.5 Existence of solutions to an Itô SDE

For the general SDE given before:

$$dX(t) = f(X(t))dt + g(X(t))dW(t) \tag{3.12}$$

$$X(0) = X_0 \ , \tag{3.13}$$

where we have the unique solution $X \in \mathbb{R}^n$ given certain conditions on $f : \mathbb{R}^n \times [0,T] \to \mathbb{R}^n$ and $g : \mathbb{R}^n \times [0,T] \to \mathbb{M}^{m\times n}$, see [23], [86], [55] and [5]. If the functions f and g satisfy the following Lipschitz conditions then we will have a solution to the SDE Equation (3.12):

- $|f(x,t) - f(\hat{x},t)| \leq L|x - \hat{x}| \ \forall \ 0 \leq t \leq T,\ x,\ \hat{x} \in \mathbb{R}^n$
- $|g(x,t) - g(\hat{x},t)| \leq L|x - \hat{x}| \ \forall \ 0 \leq t \leq T,\ x,\ \hat{x} \in \mathbb{R}^n$
- $|f(x,t)| \leq L(1 + |x|) \ \forall \ 0 \leq t \leq T,\ x \in \mathbb{R}^n$
- $|g(x,t)| \leq L(1 + |x|) \ \forall \ 0 \leq t \leq T,\ x \in \mathbb{R}^n$

with L some constant. Also let X_0 be any $\mathbb{R}^n$ valued random variable such that $\mathbb{E}(|X_0|^2) < \infty$ and X_0 is independent of $\mathcal{W}^+(0)$ (the future of the Brownian path). The solution of an SDE can be found exactly if the SDE is linear. An SDE is linear if the coefficients $f(X(t))$ and $g(X(t))$ satisfy the following:

$$f(X(t)) = a(t) + B(t)X \tag{3.14}$$

$$g(X(t)) = c(t) + D(t)X \tag{3.15}$$

for $a : [0,T] \to \mathbb{R}^n$, $B : [0,T] \to \mathbb{M}^{n\times m}$, $c : [0,T] \to \mathbb{M}^{n\times m}$ and $D : [0,T] \to L(\mathbb{R}^n, \mathbb{M}^{n\times m})$, the space of bounded linear mappings from $\mathbb{R}^n$ to $\mathbb{M}^{n\times m}$.
The exact solutions to many standard SDEs can be easily found in the literature, for example see [55] and [23]. The solution to Equation (3.12) with the linear coefficients given by Equation (3.14) and Equation (3.15) is given by:

$$\begin{aligned} X(t) &= e^{\int_0^t (B(s) - \frac{1}{2}D^2(s))ds + \int_0^t D(s)dW} \times \\ &\quad [\quad X_0 + \int_0^t (a(s) - c(s)D(s)) e^{-\int_0^s (B(r) - \frac{1}{2}D^2(r))dr - \int_0^s D(r)dW} ds \\ &\quad + \quad \int_0^t (c(s) e^{-\int_0^s (B(r) - \frac{1}{2}D^2(r))dr - \int_0^s D(r)dW}) dW] \ . \end{aligned} \tag{3.16}$$

As an example, consider the SDE that describes geometric Brownian motion $dX = \mu X dt + \sigma X dW$, with initial condition $X(0) = X_0$. We use Equation (3.16) to find the exact solution for geometric Brownian motion, so by equating coefficients: $B(t) = \mu$, $D(t) = \sigma$ and substituting into Equation (3.16) we obtain:

$$X(t) = X_0 e^{(\mu - \frac{1}{2}\sigma^2)t + \sigma W}. \tag{3.17}$$

Solutions can also be obtained using numerical algorithms described in Section 3.3.

3.1.6 Itô and Stratonovich SDEs

The above section on the existence of solutions to SDEs has been shown for the Itô interpretation of the stochastic integral. It can also be shown for the Stratonovich interpretation but here we are only going to show how to convert an SDE of one type to the other. The Itô integral is denoted $\int_0^t g(s)dW(s)$, and the Stratonovich $\int_0^t g(s) \circ dW(s)$, this notation is to distinguish between the two interpretations. One difference between the two integrals is the value of the mean and so this can be exploited in converting from one calculus to the other: $\mathbb{E}\left(\int_0^t g(s)dW(s)\right) = 0$ and $\mathbb{E}\left(\int_0^t g(s) \circ dW(s)\right) \neq 0$, when the drift term is adjusted to convert a Stratonovich integral to an Itô integral it is simply adjusting the mean such that it will now be zero.

$$dX(t) = \left(f(X) - \frac{1}{2}g(t)g'(t)\right)dt + g(t) \circ dW(t) \ . \tag{3.18}$$

Equation (3.18) is equivalent to the familiar Itô SDE $dX(t) = f(X)dt + g(t)dW(t)$, and the extra term in the drift is called the drift correction or noise induced drift. Similarly $dX(t) = f(X)dt + g(t) \circ dW(t)$ is the same as the corrected Itô version: $dX(t) = \left(f(X) + \frac{1}{2}g(t)g'(t)\right)dt + g(t)dW(t)$.

In this way we can switch between the two interpretations and compare the effect of evaluating the SDE at different points in the interval. The Stratonovich interpretation is often used in cases where the noise is fluctuating on a much faster scale than the system dynamics since the mid-point interpretation can be thought of as averaging this fast behaviour in some way. However if the time-scales are much closer and the system responds to the noise on a similar time-scale then the Itô interpretation is more appropriate since it is non-anticipating, evaluating at the left hand end point.

3.1.7 Temporally correlated noise

A stochastic differential equation can also be forced by a non-white noise, i.e. the $dW(t)$ term does not have to be a Brownian motion. Here we consider noise that is temporally correlated.

To generate a temporally correlated noise we use an Ornstein-Uhlenbeck process (sometimes called a mean-reverting process) which is given by the following SDE:

$$dK(t) = \beta(\theta - K(t))dt + \sigma dW(t) \ , \tag{3.19}$$

where $K(t)$ is a stochastic process called the Ornstein-Uhlenbeck process, β is a parameter which can adjust the time scale of the correlation, called the mean reversion rate, θ is the mean to which the process will revert to if given enough time, σ is another parameter which is called the volatility and W is a Brownian motion, as before. The variance of the solution is given by $\mathbb{V}(K) = \frac{\sigma^2}{2\beta}$.

Unlike the Wiener process, increments of the OU process are not independent although it is still a Gaussian process. If the mean is zero, $\theta = 0$, then we write the OU process as:

$$dK(t) = -\beta K(t)dt + dW(t) \ , \tag{3.20}$$

here β is called the reversion rate, and has units of s^{-1} and so can be related to a time by taking the reciprocal $\frac{1}{\beta}$. The OU process is an example of a Gaussian process which means that if we take a linear combination of the variables $K(t)$ then that combination will be normally distributed. The fact that it is a mean-reverting model means that in the long term (how long depends upon the parameter β), $K(t)$ will revert to the mean θ. We can then introduce this process, with zero mean, to our SDE, in the form of Equation (3.20):

$$dX(t) = f(X(t))dt + g(X(t))dK(t) \ . \tag{3.21}$$

Now there are two coupled SDEs, Equation (3.20) and Equation (3.21) which can be solved simultaneously to give the random variable $X(t)$.

3.1.8 Stochastic partial differential equations

We consider a parabolic stochastic differential equation of the form:

$$\frac{\partial X}{\partial t} = \frac{\partial^2 X}{\partial x^2} + f(X) + g(X)\frac{\partial W(x,t)}{\partial t}, \tag{3.22}$$

with initial condition $X(0) = X_0$ and $x \in [0, L]$, $t \in [0, T]$.The process $W(x, t)$ is a Q-Wiener process, we will go on to define what this is. We saw in Section 2.2.1, that the passive cable equation is a parabolic PDE and so when extended to the noisy cable equation will be a parabolic SPDE. [14], [86], [18] and [30] deal with the solution and existence of SPDEs.

Hilbert spaces, covariance operators and Q-Wiener processes.

We require there to be a separable Hilbert space H, with the appropriate inner-product and norm, on which a covariance operator, Q, will act. This operator is analogous to the covariance matrix we saw in the finite dimensional Brownian motion case, Section 3.1.2. Briefly, a Hilbert space, H, is a vector space with an inner product $\langle f, g\rangle$, $f, g \in H$ such that the norm can be defined as $|f| = \sqrt{\langle f, f\rangle}$. Now we look at the definition of a covariance operator.

Definition 3.1.11 *If an operator $Q : H \to H$ is a covariance operator it satisfies the following properties:*

- *Q is non-negative,*

- *Q is symmetric.*

This covariance operator can be likened to the covariance we saw in Section 3.1.2, for a finite dimensional Brownian motion: $\text{Cov}(W(s)W(t)) = \min\{s, t\}$.

We can consider Q to be trace class: $trQ = \sum_{j=1}^{\infty} \langle Qe_j, e_j \rangle < \infty$, where e_j are the eigenfunctions of the operator Q. If Q is in trace class then it can be shown by the Hilbert-Schmidt theorem (see [86]):

$$Qe_j = \lambda_j e_j,\ \lambda \geq 0,\ j \in \mathbb{N} \tag{3.23}$$

i.e. there is a complete orthonormal basis for the space H, e_j are eigenvectors with corresponding eigenvalues λ_j. Assuming that we have an appropriate operator Q, and the orthonormal basis e_j for the Hilbert space H then we can define, as shown in [18] and [86]:

Definition 3.1.12 *The Q-Wiener process can be represented by the sum:*

$$W(x,t) = \sum_{j=1}^{\infty} \lambda_j^{\frac{1}{2}}(x) e_j(x) b_j(t) \tag{3.24}$$

with λ_j are the eigenvalues of $Q : H \to H$ and $b_j(t)$ are standard Brownian motions.

We can liken Equation (3.24) to a Fourier series, and the choice of the coefficients λ_j will determine the correlation of the noise path in space. Since Q is trace class it is easier to show that the Q-Wiener process defined in Equation (3.24) has the correct expectation ($\mathbb{E}(W) = 0$), covariance and has independent increments (just as for a 1-D Wiener process in Section 3.1.2) and so it is a Gaussian process in H.

When we have $Q = I$, the identity matrix, which is not trace class, then W is white noise since $\lambda_j = 1,\ \forall\ j$. Incidentally this is the reason white noise has its name, as all the frequencies are equally weighted as in white light all the colours (and so light frequencies) are equal. In this case the sum reduces to $W(x,t) = \sum_{j=1}^{\infty} e_j(x) b_j(t)$ and the process is termed a cylindrical Wiener process.

Stochastic integral in infinite dimensions

We are now in a position to define the stochastic integral with respect to the Q-Wiener process, described above: $I(t) = \int_0^t g(s) dW(s)$. It can be shown that the sum of the finite dimensional stochastic integrals in the limit defines the infinite dimensional case, [86], [18], [14].

$$\sum_{j=1}^{J} \lambda_j^{\frac{1}{2}} \left(\int_0^t e_j(x) g(s) db_j(s) \right) \to \int_0^t g(s) dW(s)\ \text{, as } J \to \infty\ . \tag{3.25}$$

This limit holds for Q being trace class and for the following condition on the function $g(s)$: $\mathbb{E}\left[\int_0^T \sup_{x\in D} |g(x,t)|^2 dt\right] < \infty$. Similarly the infinite dimension Stratonovich integral is given by ([14]):

$$\sum_{j=1}^{J} \lambda_j^{\frac{1}{2}} \frac{1}{2} \left(\int_0^t e_j(x)(g_j + g_{j-1}) db_j(s) \right) \to \int_0^t g(s) \circ dW(s) \text{ , as } J \to \infty \text{ .} \tag{3.26}$$

Existence of solutions to an SPDE

We can look at three types of solution to our general parabolic SPDE, Equation (3.22); strong, weak and mild solutions.

- $X(t)$ is a strong solution if:

$$X(t) = X(0) + \int_0^t (\Delta X(s) + f(X(s)))ds + \int_0^t g(X(s))dW(s).$$

- $X(t)$ is a weak solution if:

$$\langle X(t), \psi \rangle = \langle X(0), \psi \rangle + \int_0^t \langle \Delta X(s), \psi \rangle + \langle f(X(s)), \psi \rangle ds + \int_0^t \langle \psi, g(X(s))dW(s) \rangle.$$

- $X(t)$ is a mild solution if:

$$X(t) = e^{t\Delta}X(0) + \int_0^t e^{(t-s)\Delta} f(X(s))ds + \int_0^t e^{(t-s)\Delta} g(X(s))dW(s).$$

Here all the integrals are well defined. There are then conditions on the combination of eigenvalues of Δ and Q that define a strong solution, and conditions on the smoothness of solutions that define a weak and mild solution, see [18].

3.1.9 Itô and Stratonovich interpretation of SPDEs

Just as we had for the SDE case, we can choose the way in which we interpret the stochastic integral. Here we give the Itô /Stratonovich drift conversion for SPDEs:

$$\frac{\partial X}{\partial t} = \frac{\partial^2 X}{\partial x^2} + f(X) + g(X)\frac{\partial W(x,t)}{\partial t} \text{ , } X_0 = X(x,0), \tag{3.27}$$

is the same as the Stratonovich interpretation:

$$\frac{\partial X}{\partial t} = \frac{\partial^2 X}{\partial x^2} + f(X) - \frac{1}{2}F_c(0)g(X)\frac{\partial g(X)}{\partial x} + g(X) \circ \frac{\partial W(x,t)}{\partial t} \text{ , } X_0 = X(x,0), \tag{3.28}$$

where $F_c(0)$ is the covariance of the noise term, [14].

3.1.10 Spatially correlated noise

A spatial correlation can also be introduced by exploiting the form of the sum Equation (3.24). As described previously, when the coefficients $\lambda_j = 1$ then the process $W(x,t)$ is a white noise process, therefore the correct choice of λ_j (eigenvalues of the operator Q in trace class) will impart a correlation to the process $W(x,t)$. In the numerical section Section 3.3.4 we use the eigenfunctions of the Laplacian to derive a set of coefficients that satisfy a specific form of correlation.

3.2 Noise induced phenomena

When a neural model includes some source of noise one might expect a destructive effect since noise, in a very general sense, is an unwanted signal but this is not always the case. This section describes some noise induced phenomena which enhance the response of a neural model to a given input, e.g. stochastic resonance (SR), Section 3.2.2, occurs in a regime where deterministically the neuron model shows no spiking response but the inclusion of noise elicits firing events. In addition to SR we look at coherence resonance (CR) and noise induced synchronisation, in which noise can synchronise coupled and un-coupled neural oscillators.

3.2.1 Coherence Resonance (CR)

In a neural context coherence resonance (CR) is the improvement of the regularity of firing due to the presence of noise. This response of the neuron tends to be an inherent oscillation of the system and can be related to periodic limit cycles in some neural models. Noise can kick a system near bifurcation from a fixed point onto a limit cycle thereby displaying enhanced firing. CR has been shown in several neuronal models e.g. FitzHugh-Nagumo, Quadratic Integrate and Fire [63], Leaky Integrate and Fire [67], [82] and the Hodgkin-Huxley model [71], [66]. CR has also been shown in experimental set-ups [72]. There are two ways in which to measure the CR in a system, first by looking at the coefficient of variation (CV), which is the ratio of the variation in the interspike interval (ISI), the time between firing events, and the mean of the ISI. CR minimises this ratio for some optimal value of noise intensity.

$$CV = \frac{\sqrt{\langle \mathrm{ISI}^2 \rangle - \langle \mathrm{ISI} \rangle^2}}{\langle \mathrm{ISI} \rangle} \tag{3.29}$$

where ISI is the time between firing events. The second way to measure the CR is using the power spectral density, [82], [67], which uses the Fourier transform of the autocorrelation function of the spike train, $x(t) = \sum_{t_i} = \delta(t - t_i)$, where t_i are the

times of the spikes. Then the power spectral density is given by:

$$S(\omega) = \int_{-\infty}^{\infty} \langle x(t)x(t+\tau)\rangle e^{i\omega\tau} d\tau \ . \tag{3.30}$$

The degree of coherence can also be measured using the power spectral density as defined by:

$$\mathrm{B} = \frac{S(\omega_{max})}{\Delta\omega/\omega_{max}} \ , \tag{3.31}$$

where ω_{max} is the frequency of the first peak and $\Delta\omega$ is the difference in frequency between the peak and a point at which its height has decreased by a chosen amount. In [67] the authors derive an exact expression for the power spectral density for the leaky integrate and fire model driven by additive white Gaussian noise. This is of interest to us since in the SDS model we consider the spine head dynamics to be modelled by the leaky integrate and fire dynamics, albeit diffusively coupled by the cable.

3.2.2 Stochastic Resonance (SR)

Stochastic resonance (SR) occurs when noise enhances a subthreshold signal to induce a neural response, i.e. create a spike/firing event. In the deterministic regime of a neural model a subthreshold signal is one which will not illicit a response from the cell, no firing, therefore any temporally encoded information in this subthreshold signal will be lost. The SR phenomena induces spikes from the system and does so at an optimal level of the noise. SR can be seen in many applications and has been studied in neural models. SR has been observed in the FitzHugh-Nagumo model ([63], [106], [66]), Quadratic integrate and fire and the leaky integrate and fire model, [63], [66], [29]. The optimal noise value is usually obtained by finding the peak in the signal to noise ratio (SNR) as the noise intensity changes, a typical input would be: $I_{in} = A\sin(\Omega t) + \mu\xi(t)$, where A is the amplitude of the input, Ω is the frequency, μ is the strength of the noise and ξ is a Gaussian noise. This uses the power spectral density that we saw in the measurement of CR Equation (3.30), evaluated at the input frequency, $S_S(\Omega)$, scaled by the power spectral density, S_N, of the equivalent Poisson process, i.e. the Poisson process that matches the output spike train. This definition of SNR is from [33]:

$$\mathrm{SNR} = \frac{S_S(\Omega)}{S_N} \ . \tag{3.32}$$

There are other similar definitions given by [29], [101] but all are of the basic form which is $\mathrm{SNR} = \frac{\text{signal power}}{\text{noise power}}$. There is another form of SR which can be observed when the input signal is suprathreshold, suprathreshold stochastic resonance (SSR). SSR

was first reported in multithreshold networks, [105], where each device in the summing network was subjected to the same input signal but independent Gaussian noise, and they are represented by a Heaviside function. Therefore their output is one if the input plus noise is above some threshold. It is shown that even when the input signal is above threshold the output of the network can be maximised by an optimal amount of noise. This result was extended to a network of Fitzhugh-Nagumo models, [106]. In the paper [94] SR was shown to exist in a spatially extended neural model, i.e. one where the spatial extent of the dendritic tree is modelled by the cable equation and the action potentials were generated by the Hodgkin Huxley model. In this type of model the noise sources can be distributed throughout the tree and induce a classical SR type response.

3.2.3 Noise induced synchrony

Noise can be shown to induce synchrony in coupled and non-coupled oscillators. Two oscillators which are driven with a common noise, but not coupled, show a synchronised response when the noise input strength is sufficient. Paper [37] shows this phenomenon in four different systems and [60], [122] and [1] show examples of neural systems with common noise induced synchronisation. The paper [122] also considers weakly coupled non-identical thermally sensitive Hodgkin-Huxley neurons and shows that noise induces synchronisation in this case, although there is an interplay between the coupling strength and the noise intensity and only the right combination of these two variables will result in synchronisation. [122] also shows that this behaviour is not particular to the HH model but that in general a system with a saddle-node bifurcation can exhibit noise induced synchrony. Noise induced synchronisation is also observed in [116], where the Hodgkin-Huxley neurons are not thermally sensitive and are strongly coupled. Again the synchronisation relies on the correct combination of coupling strength and noise intensity. In both these examples the noise used is temporally correlated although there is no comment on the effect of the correlation time-scale on the existence of the synchrony and only one value of the correlation time is given in each paper. Conversely asynchrony can be induced by noise and [46] shows the use of noise induced asynchrony to optimise performance in the vestibulo-ocular reflex (where the eyes respond to a head movement). Mid levels of noise in the model system optimises the response which is observed *in vivo* experiments with monkeys.

3.2.4 Noisy travelling waves

When noise is present in a system which supports travelling waves, in the deterministic case, then the effect of the noise can be harmful or helpful. The type of noise, noise intensity and properties of the model all play a part in determining the behaviour of

the system under the influence of noise e.g. a change in the speed of propagation and stability of travelling waves where there are none in the deterministic case. A computational study of the spatially extended Hodgkin-Huxley model, in [45], investigates the effect of additive white noise on the propagation of spikes. Although the noise can kill propagation of spikes this paper investigates the effect of smaller noise intensities, in the membrane current, where there are successful travelling spikes. The spike timing experiences large variation with noise intensity and the variation grows with distance along the cable. The paper also shows that noise in the ion channels can induce random or noise induced spiking. In a more general setting the effect of noise on propagating fronts is investigated in models which appear in, not only neural dynamics, but non-linear physics and chemistry. Paper [4] investigates the effect of spatially correlated, white in time noise on a 1-D model of front propagation. The noise term in the SPDE is interpreted in the Stratonovich sense and so has non-zero mean; the authors exploit this fact to rescale the equation to give a new zero mean noise term. Then a small noise approximation is used to obtain an altered deterministic equation which has a term dependent on properties of the noise but with no explicit noise term. It is shown that the presence of noise can stabilise fronts which are not observed in the deterministic case and that when the noise is multiplicative the speed of the fronts increases, whereas additive noise does not affect the speed. [91] also investigates propagating fronts, under the influence of noise. This paper does not investigate the speed of the fronts but rather how the noise changes the diffusion coefficient. The noise is once again spatially correlated, white in time and again the SPDE is rescaled to give a non-zero mean noise term. Then the noisy front is decomposed into a mean profile with fluctuations. The effective diffusion is dependent on the properties of the noise e.g. noise intensity, but not the noise itself. Another paper which investigates the effects of noise on propagating fronts with the noise rescaling is [96]. A reaction diffusion system was subjected to noise which is correlated in both space and time and after the rescaling of the noise term a deterministic expression was obtained for the speed of the wave fronts. The speed reduces as the temporal correlation scale increases and the speed increases with increasing spatial correlation length.

The method of rescaling the noise term to have zero mean and using a small noise approximation is a popular way of extracting information about the effect of small noise on travelling waves. Papers [2] and [7] employ this approach to investigate the wave propagation in excitable media. The theory in [2] applies to a general type of Fitzhugh-Nagumo model (Section 2.3) and numerically investigates one particular case, called the Barkley model. The authors show that when the noise is white the model supports noise induced waves which increase in speed as the noise intensity increases. The noise can also support spiral waves which are not present in the

deterministic case. For correlated noise both the temporal and spatial correlation scales reduce the speed as the scale increases. Similarly [66] investigates the Barkley model and also shows an increase in wave speed as the noise intensity increases. It also shows that additive noise does not change the speed of a travelling wave but it does induce pulse propagation where there are none in the deterministic case. [7] shows a speed decrease as noise intensity increases in a chemical reaction model but also shows that the noise can support waves not present in the deterministic model. In the same chemical model, [51], shows that noise can enhance weak signals upto an optimal value of the intensity (SR), before the noise then overwhelms the signal and destroys the wave.

Although the models investigated in the papers discussed in this section have different forms, the treatment of the noise follows the same method. To give any analytical results the noise term must be rescaled to have zero mean and then the noise intensity taken to be small in order to obtain some expressions for the speed of waves. It seems that in all cases the inclusion of noise also helps to promote travelling waves which do not appear in the deterministic regime and multiplicative noise will change the speed of any travelling wave/front.

3.3 Overview of numerical methods

Here we outline the algorithms that we will use throughout the rest of this body of work. These methods were chosen because they were simple, but effective and relatively quick to simulate using Matlab, [75] ([42] is a good book on the use of Matlab). We also show how a spatially correlated noise can be constructed using a fast Fourier transform to satisfy a correlation function chosen to suit our requirements. There are references given for each subsection, but [58] discusses numerical methods of neural models and also covers (albeit briefly) solution to ODEs/PDEs and branching structures.

3.3.1 Solving ODEs

For the following work we use an Euler algorithm for solving any ODEs encountered. In most cases we use a semi-implicit Euler method, but the exact numerical algorithm is written out for each case throughout. There are many standard texts on ODEs and numerical methods e.g. [90] for an introduction to ODEs, [59] and [88] are texts geared towards engineers which have sections on ODEs and a small section on numerical methods and [97] and [10] are two numerical analysis texts which cover numerical solutions to ODEs. Here we aim to describe both the explicit and implicit Euler algorithms for the ODE:

$$\frac{dX(t)}{dt} = f(X(t)) \ , \ X(0) = X_0 \ . \tag{3.33}$$

We also assume that $f(X(t))$ is sufficiently smooth. We can derive the Euler algorithm by looking at the Taylor series expansion of $X(t + \Delta t)$:

$$X(t + \Delta t) = X(t) + \Delta t \frac{dX(t)}{dt} + \frac{\Delta t^2}{2!} \frac{d^2X(t)}{dt^2} + \ldots , \tag{3.34}$$

where Δt is a small increment of time. If we truncate the series after the $O(\Delta t)$ term and rearrange we get the approximation:

$$\frac{dX(t)}{dt} \approx \frac{X(t + \Delta t) - X(t)}{\Delta t} \ . \tag{3.35}$$

Due to the truncation of this expansion we can say that the remaining terms form the error in this approximation and is of order $O(\Delta t)$. If we want to find our solution $X(t)$ for $t \in [0, T]$, we can split our domain into N small steps of size Δt such that $t^n = n\Delta t$, $n = 0, 1, 2, \ldots$, $t^0 = 0$ and $t^N = N\Delta t = T$, and using the Equation (3.35) we can find the solution to $\frac{dX(t^n)}{dt} = f(X(t^n))$ as:

$$X(t^{n+1}) = X^{n+1} \simeq X(t^n) + \Delta t f(X(t^n)). \tag{3.36}$$

We can then build up a solution for all time $t \in [0, T]$ by repeated application of Equation (3.36). To obtain the implicit Euler method we can simply use a backwards step when deriving the approximation to the derivative from the Taylor series to get:

$$\frac{dX(t)}{dt} \approx \frac{X(t) - X(t - \Delta t)}{\Delta t} \ , \tag{3.37}$$

and so using the same discretisation of the time interval:

$$X(t^{n+1}) \simeq X^{n+1} = X(t^n) + \Delta t f(X^{n+1}) \ . \tag{3.38}$$

We can combine the explicit and implicit methods to obtain a semi-implicit method, by evaluating some of the terms that make up $f(X(t))$ at time step n and some at step $n + 1$. The implicit or semi-implicit method tends to be chosen over the explicit method since it is more stable, with respect to the step size chosen, and so if a larger step size is used then the computation time is reduced while there is little trade off with the error (as with the explicit method).

3.3.2 Solving PDEs

There are many texts covering the subject of PDEs, again [59] and [88] contain chapters on PDEs and a bit on their numerical solution, and the numerical analysis text [10] has numerical schemes for the solution of PDEs. Consider a simple PDE of form:

$$\frac{\partial X(x,t)}{\partial t} = \frac{\partial^2 X(x,t)}{\partial x^2} + f(X(x,t)) \ , \tag{3.39}$$

with initial conditions $X(x,0) = X^0$, $x \in [0,L]$ and appropriate boundary conditions (either Dirichlet or Neumann). The temporal solution of the PDE is simple, we can use any of the Euler methods outlined in the previous section, we use a semi-implicit version. Before we apply the temporal integration however we must take care of the spatial differential $\frac{\partial^2 X(x,t)}{\partial x^2}$. To do this we also use a finite differences approximation. Here we look at the central difference approximation which is a combination of the forward and backward approximations we have seen so far:

$$X(x \pm \Delta x, t) = X(x,t) \pm \Delta x \frac{X(x,t)}{dx} + \frac{\Delta x^2}{2!}\frac{d^2X(x,t)}{dx^2} \pm \frac{\Delta x^3}{3!}\frac{d^3X(x,t)}{dx^3} + \dots$$

Then subtracting the backwards difference series from the forward difference series:

$$X(x+\Delta x, t) - X(x-\Delta x, t) = 2\Delta x \frac{dX(x,t)}{dx} + 2\frac{\Delta x^3}{3!}\frac{d^3X(x,t)}{dx^3} + \dots$$

Truncating the series at the Δx^2 term gives:

$$\frac{dX(x,t)}{dx} \approx \frac{X(x+\Delta x,t) - X(x-\Delta x,t)}{2\Delta x} \ . \tag{3.40}$$

This only gives us the approximation to the first derivative but we can apply the same steps again to get an approximation for the second order derivative (of order $O(\Delta x^2)$) as:

$$\frac{d^2X(x,t)}{dx^2} \approx \frac{X(x+\Delta x,t) - 2X(x,t) + X(x-\Delta x,t)}{\Delta x^2} \ . \tag{3.41}$$

Using the second-order central difference method and writing in a neater notation i.e. we write X as a vector with components x_j i.e. $\underline{X}(t) = \begin{pmatrix} X_0 \\ X_1 \\ \vdots \\ X_J \end{pmatrix}$, where $X_j = X(x_j,t)$. We have used the spatial mesh $x_0, x_1, \dots, x_J$ with step size Δx, i.e. $j = 1,2,\dots,J$, $J = \frac{L}{\Delta x}$, where $x \in [0,L]$. So here the subscript j's correspond to the value of the

function $X(x,t)$ at spatial point x_j.

$$\frac{\partial^2 X(x,t)}{\partial x^2}|_{x_j} \approx \frac{X_{j+1}(t) - 2X_j(t) + X_{j-1}(t)}{\Delta x^2} + f(X_j(t)) \tag{3.42}$$

$$\approx \frac{A}{\Delta x^2}\underline{X}(t) + \underline{b}\ . \tag{3.43}$$

The matrix A is given by:

$$\begin{pmatrix} -2 & 1 & 0 & 0 & \dots & 0 \\ 1 & -2 & 1 & 0 & \dots & 0 \\ 0 & 1 & -2 & 1 & \dots & 0 \\ \vdots & \vdots & \vdots & \vdots & \ddots & \vdots \\ 0 & 0 & 0 & 0 & 1 & -2 \end{pmatrix}.$$

The vector, $\underline{b}$, is used to incorporate Dirichlet boundary conditions (BCs), if chosen, and Neumann boundary conditions can be incorporated into the matrix A itself. Dirichlet BCs enforce chosen values of the solution on the boundary; therefore we have $X(0,t) = \alpha_1$ and $X(L,t) = \alpha_2$, where α_1 and α_2 are the values chosen at either end of the spatial domain. Neumann boundary conditions enforce a chosen value of the normal derivative of the solution on the boundary. We have:

$$\frac{\partial X}{\partial \hat{n}}(0,t) = \nabla X \cdot \hat{n}(0,t) = \frac{\partial X}{\partial x} \cdot \hat{n}(0,t) = \gamma_1, \tag{3.44}$$

$\hat{n}$ is the normal direction at either end of the domain $x \in [0, L]$, which is an outwards direction. There is also an equation like Equation (3.44) for $x = L$, enforcing a value of the derivative there. If we choose the derivative to be of unit value, in an outward direction then the following entries of A must be changed: a_{11} from -2 to $a_{11} = -1$ and the very last, a_{JJ} from -2 to $a_{JJ} = -1$.

After applying the second order central difference approximation we have effectively obtained a set of j ODEs which are expressed together by the use of the vector notation and the use of matrix A. If we then apply the explicit Euler method, we could equally choose the implicit, for the temporal integration we can write, for one spatial point j, one line of the algorithm as:

$$X_j^{n+1} = X_j^n + \Delta t \left(\frac{X_{j+1}^n - 2X_j^n + X_{j-1}^n}{\Delta x^2} + f(X_j^n) \right)\ . \tag{3.45}$$

The discretisation can be written in matrix form as:

$$\underline{X}^{n+1} = \underline{X}^n + \Delta t \left(\frac{A}{\Delta x^2}\underline{X}^n + F(\underline{X}^n) \right), \tag{3.46}$$

and for the implicit method:

$$\left(\mathrm{I} + \Delta t(\frac{A}{\Delta x^2} + F)\right) \underline{X}^{n+1} = \underline{X}^n, \tag{3.47}$$

and finally for a semi-implicit method:

$$\left(\mathrm{I} + \frac{\Delta t}{\Delta x^2} A)\right) \underline{X}^{n+1} = \underline{X}^n + F(\underline{X}^n). \tag{3.48}$$

These discretisations will be used in the simulation of the voltage in the passive cable as used in the SDS and BR models in subsequent chapters.

3.3.3 Numerically simulating a branched passive cable structure

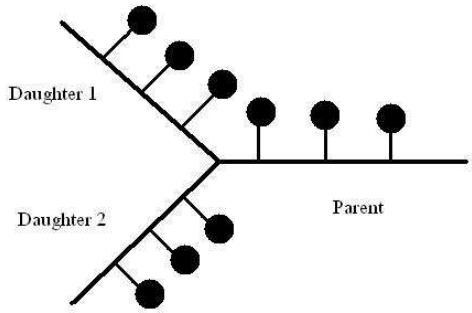

Figure 3.3: Diagram of the branched SDS model. The straight lines resemble the cable (modelled by the passive cable equation) and the protruding structures represent the discretely attached spines on each branch. Each individual branch is modelled by the standard SDS model as in Section 2.8.

We now show how to numerically solve the problem of a branched structure. A branch point is the intersection of 3 lengths of electric cable, here the cable is modelled using the passive cable equation see Section 2.2.1. We consider a branched structure in Chapter 8 when we consider how the voltage spreads throughout a 3 branched SDS model, Figure 3.3. Each of the branches can be solved with the numerical methods described in Section 3.3, up to the penultimate discretisation point before the branch point, which is itself a discretisation point. We will develop this algorithm, by following [93] using a notation that can be applied to any point on any of the branches. We now label the points in space: $x_{j-1} + \Delta x = x_j = x_{j+1} - \Delta x$, with Δx as before is the spatial step size. In the final algorithm we will number the nodes, after deriving the necessary approximations at the branch point.

We use this notation and central finite differences to approximate the spatial derivatives of the voltage in the cable $V(x,t)$, Equation (3.49).

$$\frac{\partial V_j}{\partial x_j} = \frac{V_{j+1} - V_{j-1}}{2\Delta x} + \frac{\Delta x^2}{6}\frac{\partial^3 V_j}{\partial x_j^3} + O(\Delta x^2) \tag{3.49}$$

$$\frac{\partial^2 V_j}{\partial x_j^2} = \frac{V_{j+1} - 2V_j + V_{j-1}}{\Delta x^2} + \frac{\Delta x^2}{12}\frac{\partial^4 V_j}{\partial x_j^4} + O(\Delta x^2) \tag{3.50}$$

When we consider the branch point, point 6 in Figure 3.4, we need to solve each of the branches at the final point before branching, and this leads us to the problem that either one of x_{j-1} or x_{j+1}, depending on which side of the branch point you are on, will be missing. We can use the identity: $V(x,t) - V_j(t) = \int_{x_j}^{x} \frac{\partial V(s,t)}{\partial s} ds$ and repeated integration by parts to get:

$$V(x,t) = V_j + \sum_{k=1}^{\infty} \frac{(x - x_j)^k}{k!}\frac{\partial^k V_j}{\partial x^k} \tag{3.51}$$

If we use $x = x_j + \Delta x$ and $x = x_j - \Delta x$ and rearrange Equation (3.51) for an expression to $O(\Delta x^2)$ accuracy we obtain, for a branch to the left (Equation (3.52)) of the branch point and a branch to the right (Equation (3.53)) of the branch point respectively:

$$\frac{\partial^2 V_j}{\partial x_j^2} = \frac{8V_{j+1} - V_{j+2} - 7V_j}{2\Delta x^2} - \frac{3}{\Delta x}\frac{\partial V_j}{\partial x_j} + O(\Delta x^2) \tag{3.52}$$

$$\frac{\partial^2 V_j}{\partial x_j^2} = \frac{3}{\Delta x}\frac{\partial V_j}{\partial x_j} - \frac{7V_j - 8V_{j-1} + V_{j-2}}{2\Delta x^2} + O(\Delta x^2)\ . \tag{3.53}$$

If we re-write the cable equation, Equation (2.12): $\frac{\partial V}{\partial t} = D\frac{\partial^2 V}{\partial x^2} - I$, with $I = \frac{V}{\tau} - \frac{Dr_a\rho}{r}(\hat{V} - V)$, so at a point away from the ends of the branches we can use the same discretisation as before Equation (3.45). However when we are at the branch point we must use a boundary condition that incorporates all the contributions from all the branches. If we consider a branch point which has one branch to the left and 2 branches to the right then we can obtain the voltage evolution by using Kirchoff's current at a node law: $I_{j-1} + \sum_{k=1}^{2} I_{j+1}^k = 0$. Using all our discretisation so far we get expressions for:

$$I_{j-1} = \frac{\partial V_j}{\partial t} + I_j - \frac{D}{2\Delta x^2}(8V_{j+1} - 7V_j - V_{j+2}) \tag{3.54}$$

and

$$I_j = \frac{\partial V_j}{\partial t} + I_j - \frac{D}{2\Delta x^2}(7V_j - 8V_{j-1} + V_{j-2})\ . \tag{3.55}$$

Using this form of the discretisation we obtain a new matrix of discretisation A, as in

Equation (3.43). As an example, consider the branched structure in Figure 3.4 which has 3 nodes on each branch. The resulting matrix for this structure is:

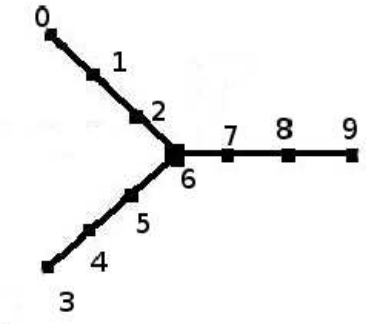

Figure 3.4: Diagram of a branched cable structure with one parent, which is obviously to the right of the branch point, and two daughter branches each to the left of the branch point. Each of the branches has three nodes and a shared node at the branch point.

$$\begin{pmatrix}
-D_1/2 & D_1 & -D_1/2 & 0 & 0 & 0 & 0 & 0 & 0 & 0 \\
D_1 & -2D_1 & D_1 & 0 & 0 & 0 & 0 & 0 & 0 & 0 \\
0 & D_1 & -2D_1 & 0 & 0 & 0 & D_1 & 0 & 0 & 0 \\
0 & 0 & 0 & -D_2/2 & D_2 & -D_2/2 & 0 & 0 & 0 & 0 \\
0 & 0 & 0 & D_2 & -2D_2 & D_2 & 0 & 0 & 0 & 0 \\
0 & 0 & 0 & 0 & D_2 & -2D_2 & D_2 & 0 & 0 & 0 \\
0 & -D_1/3 & 8D_1/3 & 0 & -D_2/3 & 8D_2/3 & B & -8D_p/3 & D_p/3 & 0 \\
0 & 0 & 0 & 0 & 0 & 0 & D_p & -2D_p & D_p & 0 \\
0 & 0 & 0 & 0 & 0 & 0 & 0 & D_p & -2D_p & D_p \\
0 & 0 & 0 & 0 & 0 & 0 & 0 & -D_p/2 & D_p & -D_p/2
\end{pmatrix},$$

where D_1, D_2 and D_p are the diffusion constants for the 1st daughter, 2nd daughter and parent branches respectively and $B = 7D_p/3 - 7D_1/3 - 7D_2/3$. It can been seen that the 1, -2, 1 structure is still there on the lines of the matrix that represent the parts of the cable away from any sort of boundary, terminal or branching.

3.3.4 Solving stochastic systems

Here we outline the numerical schemes implemented to solve the SDEs and SPDEs that we obtain when looking at the stochastic versions of the dendrite models. We make simple extensions of the numerical schemes used for the ODEs and PDEs, [41], [30].

Euler-Maruyama method

The Euler-Maruyama method is a simple numerical method for solving SDEs that is an extension of the Euler method for ODEs Section 3.3.1. When the noise is white then the EM method is of $O(\Delta t^{\frac{1}{2}})$. We consider a general Itô SDE of the form:

$$\begin{aligned} dX(t) &= f(X(t))dt + g(X(t))dW(t) \\ X(t) &= X_0 + \int_0^T f(X(t))dt + \int_0^T g(X(t))dW(t) \end{aligned}$$

Just as the Euler method uses the truncated Taylor expansion the EM algorithm also uses this for the deterministic part of the SDE and uses the definition of the stochastic integral for the stochastic part. It can be implemented as follows:

$$X^{n+1} = X^n + f(X^n)\Delta t + g(X^n)\Delta W^n. \tag{3.56}$$

With discretised interval:$\Delta t = T/N$ and $\Delta W^n = W(t^{n+1}) - W(t^n)$ is a random variable with mean $= 0$, and variance $= t^{n+1} - t^n = \Delta t$. The first two terms on the right hand side of the approximation are clearly the same as for the standard Euler method Equation (3.36) and the last term is the stochastic integral and is approximated by the Riemann type step as was described in Section 3.1.3, since we have shown that the sum $\sum_{n=0}^{\infty} g(X^n)(W^{n+1} - W^n)$ is the definition of the Itô stochastic integral. When the Brownian increment $(W(t^{n+1}) - W(t^n))$ is simulated in Matlab we use the inbuilt pseudo-random number generator function 'randn' and in order to ensure the correct variance of the increment we scale the numbers produced by 'randn' by $\sqrt{\Delta t}$ since 'randn' produces numbers from a normal distribution $\mathcal{N}(0, 1)$.

Stochastic Heun method

The Heun algorithm is a second order Runge-Kutta method and uses the Euler algorithm as a predictor step, and therefore is sometimes called the improved Euler method. The traditional Heun method can be easily extended to solve a Stratonovich SDE to $O(\Delta t)$ (for white noise). Consider the simple SDE:

$$dX(t) = f(X(t))dt + g(X(t)) \circ dW(t) \tag{3.57}$$

Where the variables are as before and the integral this time is obviously interpreted in the Stratonovich sense, i.e. we need to evaluate the integral at the mid point of the interval $t_j - t_{j-1}$. First we need the predictor step given simply by the Euler-

Maruyama method above:

$$\tilde{X}^{n+1} = X^n + f(X^n)\Delta t + g(X^n)\Delta W^n \ , \tag{3.58}$$

this gives us the solution to $dX(t) = f(X(t))dt + g(X(t))dW(t)$ in the Itô sense, which can then be used to find the Stratonovich integral, since it requires some prior knowledge of the functions $f(X)$ and $g(X)$.

And so the solution is given by:

$$X^{n+1} = X^n + \frac{\Delta t}{2}(f(X^n) + f(\tilde{X^n})) + \frac{1}{2}(g(X^n) + g(\tilde{X^n}))\Delta W^n. \tag{3.59}$$

This clearly relates back to the definition of the Stratonovich integral, where the midpoint (of the time interval) is used to evaluate the function $g(X)$, instead of the left hand end point as in the Itô case. The Equation (3.6) shows that the point chosen will effect the outcome of the integral and for the Stratonovich integral we have $\frac{g(X(t))+g(X(t+\Delta t))}{2}$. Again the Brownian increment is generated using Matlab's 'randn' function and the scaling $\sqrt{\Delta t}$ to ensure the correct variance.

Solving SPDEs

When we come to solve an SPDE, then we use a combination of the methods seen so far. We first use part of the method described in Section 3.3.2, which uses the central finite difference method to approximate the spatial derivative and gives us a set of coupled ODEs (one for each spatial point). These ODEs can be solved using one of the methods for stochastic temporal integration described above, either EM or Heun. We use the second-order central difference method, as before, and write X as a vector with components x_j i.e. $\underline{X}(t) = \begin{pmatrix} X_0 \\ X_1 \\ \vdots \\ X_J \end{pmatrix}$, where $X_j = X(x_j, t)$. We have used the spatial mesh $x_0, x_1, \ldots, x_J$ with step size Δx, i.e. $j = 1, 2, \ldots, J$, $J = \frac{L}{\Delta x}$. We can again write the spatial differential term as: $\frac{\partial^2 X}{\partial x^2} \approx \frac{A}{\Delta x^2}\underline{X}$, where A is the following matrix:

$$\begin{pmatrix} -2 & 1 & 0 & 0 & \ldots & 0 \\ 1 & -2 & 1 & 0 & \ldots & 0 \\ 0 & 1 & -2 & 1 & \ldots & 0 \\ \vdots & \vdots & \vdots & \vdots & \ddots & \vdots \\ 0 & 0 & 0 & 0 & 1 & -2 \end{pmatrix}.$$

Choosing Neumann boundary conditions enforces a chosen value of the normal derivative of the solution on the boundary. We have:

$$\frac{\partial X}{\partial \hat{n}}(0,t) = \nabla X \cdot \hat{n}(0,t) = \frac{\partial X}{\partial x} \cdot \hat{n}(0,t) = \beta_1, \tag{3.60}$$

$\hat{n}$ is the normal direction at either end of the domain $x \in [0, L]$, which is an outwards direction. There is also an equation like Equation (3.60) for $x = L$, enforcing a value of the derivative there. If we choose the derivative to be of unit value, in an outward direction then the following entries of A must be changed: a_{11} from -2 to $a_{11} = -1$ and the very last, a_{JJ} from -2 to $a_{JJ} = -1$. Therefore we have in matrix form the set of J coupled ordinary differential equations (in Itô integral form):

$$\underline{X} \approx \underline{X}_0 + \int_0^T \left(\frac{A}{\Delta x^2} \underline{X} + f(\underline{X}) \right) + \int_0^T g(\underline{X}) dW. \tag{3.61}$$

Next we must approximate the temporal integration with either the EM method (or the Heun method if using the Stratonovich interpretation):

$$X_j^{n+1} = X_j^n + \Delta t \left(\frac{X_{j+1}^n - 2X_j^n + X_{j-1}^n}{\Delta x^2} + f(X_j^n) \right) + g(X_j^n) \Delta W_j^n \ , \tag{3.62}$$

where we have shown the temporal integration for one point in space and used the temporal mesh: $t \in [0, T]$, split into N small steps of size Δt such that $t^n = n\Delta t$, $n = 0, 1, 2, \ldots$, $t^0 = 0$ and $t^N = N\Delta t = T$. $\Delta W_j^n = W_j(t^{n+1}) - W_j(t^n)$ is a Wiener increment and its form depends on the type of noise we consider. If the noise we are considering is white in space and time then again we can use the 'randn' function in Matlab but the scaling of the variance will be slightly different, we must use $\sqrt{\frac{\Delta t}{\Delta x}}$, [30]. To generate a noise which is temporally correlated but white in space then we use the OU process at each point in space:

$$dK_j(t) = -\beta K_j(t) dt + dW_j(t) \ . \tag{3.63}$$

In Equation (3.62) ΔW_j^n is replaced by $\Delta K_j = K_j^{n+1} - K_j^n = -\Delta t \beta K_j + \Delta W_j^n$. Again the Wiener increment is generated (for each point in space) by the 'randn' function in Matlab and scaled by $\sqrt{\frac{\Delta t}{\Delta x}}$.

The generation of a spatial correlated noise is slightly more complicated and is introduced by a process described in e.g. [100], [30]. This form of the spatially correlated noise is constructed such that it is easy to simulate and so that it satisfies chosen properties of the correlation length and the following working follows [100]. If

we recall that when we defined a Q-Wiener process, Equation (3.24) we had the sum:

$$W(x,t) = \sum_{j\geq 0} \lambda_j^{\frac{1}{2}}(x)\mathbf{e_j}(x)b_j(t) \ . \tag{3.64}$$

Assuming that Q has the same eigenfunctions as the Laplacian (and assuming Neumann boundary conditions), Δ, $\mathbf{e_j}(x) = \sqrt{\frac{2}{L}}\cos(\frac{\pi jx}{L})$ where $j = 1, 2, 3, \ldots$ and $\mathbf{e_0}(x) = \sqrt{\frac{1}{L}}$ are orthonormal eigenfunctions of the Laplacian on $[0, L]$, $b_j(t)$ are standard Brownian motions and λ_j are coefficients chosen to satisfy a form of spatial correlation. We choose a correlation such that the noise is white in time and with a short range correlation in space, correlation length ζ. The covariance and correlation function are given by Equation (3.65) and Equation (3.66):

$$\mathbb{E}(W(x,t)W(x',t')) = F_c(x-x')\min\{t,t'\} \tag{3.65}$$

$$F_c(x) = \frac{1}{2\zeta}\exp(-\frac{\pi x^2}{4\zeta^2}) \ . \tag{3.66}$$

$F_c(x)$ is the correlation function, and has been chosen to have an exponential form to satisfy the short range condition, [100]. Note that the correlation function can take any form required. We now show how to compute the coefficients. We start with the covariance Equation (3.65), which can also be written as:

$$\mathbb{E}\left(W(x,t)W(x',t')\right) = \min\{t,t'\}\sum_{j\geq 0}\lambda_j\mathbf{e}_j(x)\mathbf{e}_j(x') \tag{3.67}$$

Setting $x' = 0$, $t = t'$, substituting, Equation (3.66) and equating, Equation (3.65) and Equation (3.67) become:

$$t\frac{1}{2\zeta}\exp(-\frac{\pi x^2}{4\zeta^2}) = t\sum_{j\geq 0}\lambda_j\mathbf{e}_j(x)\mathbf{e}_j(0) = t\frac{1}{\sqrt{L}}\sum_{j\geq 0}\lambda_j\mathbf{e}_j$$

Then multiplying both sides by $\mathbf{e}_j = \sqrt{\frac{2}{L}}\cos(\frac{\pi jx}{L})$, and integrating over x we obtain:

$$\frac{1}{2\zeta}\int_{-\infty}^{\infty}\mathbf{e}_j\exp(-\frac{\pi x^2}{4\zeta^2})dx = \sqrt{L}\lambda_j\int_{-\infty}^{\infty}\mathbf{e}_j\mathbf{e}_j dx, \tag{3.68}$$

using the orthonormal properties of the eigenfunctions:

$$\frac{1}{2\zeta}\sqrt{\frac{2}{L}}\int_{-\infty}^{\infty}\cos(\frac{\pi jx}{L})\exp(-\frac{\pi x^2}{4\zeta^2})dx = \frac{1}{\sqrt{L}}\lambda_j \ . \tag{3.69}$$

Finally using the fact that $\int_{-\infty}^{\infty}\exp(-ax^2)\cos(bx)dx = \sqrt{\frac{\pi}{a}}\exp(-\frac{b^2}{4a})$ we can rearrange

to obtain:

$$\lambda_j = \exp(-\frac{\pi j^2 \zeta^2}{2L^2}) \ , \tag{3.70}$$

for the coefficients. Now that we have computed the coefficients then we can use this noise in Equation (3.62) and take the increment, as a vector in space, $\Delta\underline{W} = \sum_{j=1}^{N} \lambda_j^{\frac{1}{2}}(x)\mathbf{e_j}(x)(b_j(t^{n+1}) - b_j(t^n))$. The sum is truncated to the number of spatial points N. This can implemented in Matlab by generating the Brownian increments as before with the 'randn' function and then using a discrete cosine transform, 'idct', to generate the full sum with the correct basis functions.

And so we can write the general discretised Itô SPDE in vector form as:

$$\underline{X}^{n+1} = \underline{X}^n + \Delta t \left(\frac{A}{\Delta x^2}\underline{X}^n + f(\underline{X}^n) \right) + g(\underline{X}^n)\Delta\underline{W}^n, \tag{3.71}$$

where $\Delta\underline{W}$ can be chosen according to the type of noise required.

If we wish to consider a Stratonovich integral then we can implement the Heun method for the temporal integration as for SDEs. So using, as the predictor step (in vector notation):

$$\underline{\tilde{X}}^{n+1} = \underline{X}^n + \Delta t \left(\frac{A}{\Delta x^2}\underline{X}^n + f(\underline{X}^n) \right) + g(\underline{X}^n)\Delta\underline{W}^n, \tag{3.72}$$

we can then apply the Heun step, to get the following discretised Stratonovich SPDE:

$$\begin{aligned} \underline{X}^{n+1} &= \underline{X}^n + \frac{\Delta t}{2} \left(\frac{A}{\Delta x^2}\underline{X}^n + f(\underline{X}^n) + \frac{A}{\Delta x^2}\underline{\tilde{X}^n} + f(\underline{\tilde{X}^n}) \right) \\ &+ \left(g(\underline{X}^n) + g(\underline{\tilde{X}^n}) \right) \Delta\underline{W}^n. \end{aligned} \tag{3.73}$$

3.4 Measuring the effect of the noise on travelling waves in a dendrite model

We now look at ways in which to investigate how the presence of noise effects the model of a spiny dendrite. We look at how the different types of noise effect the travelling wave in the SDS and BR models in Chapter 4 and Chapter 5/Chapter 6 but here we discuss the methods used to measure the effect of the noise on the travelling wave in general. When we simulate the models of the dendrites, with some noise, we initiate a wave at one end of the cable and record the voltage in the cable, $V(x,t)$ and in the spines $U(x,t)$ for all points in space and time defined by our discretisation. We therefore have two matrices $\mathbf{V} \in \mathbb{R}^{J\times N}$ and $\mathbf{U}$, one each for $V(x,t)$ and $U(x,t)$ which will be of the size $J \times N$, where J is the number of spatial points and N is the number of temporal points. In the case of the SDS model we only record $U(x_n,t)$ at

the position of the spines x_n, n spines, since the matrix would be zero at points in between the spines. In the SDS case the matrix $\mathbf{U}$, J will be the number of spines rather that of all spatial points.

3.4.1 Mean voltage plots

Using the voltage matrix $\mathbf{V}$ for the voltage in the cable at all points in space and time of our chosen domain. This means that we have a matrix, $\mathbf{V} \in \mathbb{R}^{J\times N}$, where J is the length of space vector and N is the length of time vector, so the entry at $\mathbf{V}_{jn}$ is the voltage in the cable at x_j at time t^n. For any given strength of noise the simulation is repeated many times, to give a large number of realisations, N_{sample}, and for each realisation the matrix voltage $\mathbf{V}$ is saved. The mean voltage is then simply given by $\mathbb{E}(\mathbf{V}) = \frac{\sum_{i=1}^{N_{sample}} \mathbf{V}_i}{N_{sample}}$, where N_{sample} is the total number of realisations considered.

3.4.2 Distance travelled by a stochastic wave in the SDS model

One measure of the effect of the noise in the system is the distance travelled along the cable by a wave. In the deterministic case we have two simple regimes which depend on the system parameters either any wave initiated will travel along to the end of the cable or any wave initiated will fail to travel the full length of the cable. As an example, see Figure 2.9, which shows the range of spine spacing d for which the SDS system supports a travelling wave. When we include noise in the system we no longer have these two simple cases. Instead, for a chosen parameter, when there is noise present we have a certain probability that the wave will travel the full length of the cable, will fail to propagate at all and a certain probability that it will fail somewhere in between these two extremes.

To measure the distance travelled we do not need to look directly at the voltage in the cable, for the SDS model. We can simply consider the firing times of the spines since it is the sequential firing that will determine if the wave has failed at any point. During the simulation of a single realisation we can record the firing times of each spine as a matrix of size 'number of spines $\times$ time steps' and so can easily see at which spine the propagation fails. The matrix of firing times, call it $\mathbf{F} \in \mathbb{R}^{M\times N}$, where M is the number of spines and N the number of time steps. Each entry is either t_n if the spine is firing at that time or 0 if not. We sum the matrix, $\mathbf{F}$, along each row to obtain a new vector, of the same size as the number of spines, and so each entry is associated with one spine. If any of these entries in the new vector are zero then the corresponding spine has not fired and the propagation has failed. From this we can determine the distance travelled (measured in spine number). As for the mean voltage we save this distance for each realisation and then average over the number of samples

to obtain an expected extent of propagation for a given level of noise intensity. We can also check if the spines are firing sequentially by looking at the first time recorded for each spine in $\mathbf{F}$. If these times are increasing as the spine number increases then the spines are firing in order.

3.4.3 Speed of propagation of stochastic wave

We determine the speed of propagation in two ways. The first is to use the simple definition of speed: $c = \frac{d}{t}$, where c is the speed, d is the distance travelled and t the time taken to travel distance d. This method gives only the average speed over the time t. The second method introduces an instantaneous speed as well as a time averaged speed. This second method uses a scaled convection term added to the cable equation to measure the movement of the saltatory travelling wave with respect to a fixed template function, at each time step. This method follows the work in [69], which uses a template function to freeze a stochastic travelling wave and so measure its speed. In this work the wave is not actually frozen but allowed to travel whilst still measuring the instantaneous speed by the same template comparison method as [69].

For all measures of speed the final computed values, for all levels of noise, are scaled by the deterministic speed, c_{det}. This rescaling allows comparison of the different models which have different absolute values for the speed; it also makes it easy to see in the graphs if the wave is speeding up ($c > 1$) or slowing down ($c < 1$), with respect to the deterministic wave.

Measuring speed by equation of motion

In order to find the speed of any wave propagating on the cable we simply find the times, t_1 and t_2, at which the wave crosses two points, x_1 and x_2, along the cable and use:

$$c = \frac{x_2 - x_1}{t_2 - t_1}. \tag{3.74}$$

The way in which we define 'crossing' a point is outlined below. To use this equation for speed we must first choose the two points x_1 and x_2; the further apart these two points are, the more accurate the average speed will be. Note that the speed will be an average over the distance travelled, $x_2 - x_1$, and not an instantaneous speed. We take our two points, x_1, x_2, to be close to the point at which the wave is initiated $x = 0$ and end of the cable, $x = L$ respectively. If the wave fails to reach x_2 then we say that the wave has failed to propagate. Failure is determined by the size of the voltage in the cable at point x_2; if $V(x_2, t) \geq \theta$, θ is a threshold value chosen from the voltage values in the deterministic case, then it is still propagating. The threshold value must be large enough that the voltage will only reach this level if the voltage is close to that

of the deterministic system and so we avoid the case where the propagation is noise induced, i.e. we are not measuring small fluctuations induced by noise only but we do see the underlying signal too. To determine the time at which the wave crosses point

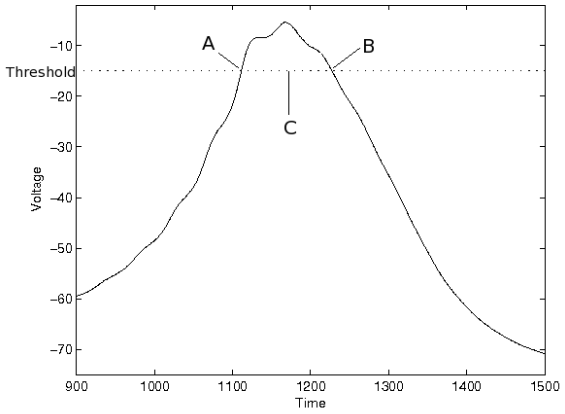

Figure 3.5: Schematic of voltage, $V(t)$ at a point in space, x_j for all time above threshold with interpolation points shown.

x_j, $j \in [1, 2]$, we first find all the points in time where the voltage is above threshold, see Figure 3.5. We then find the first point at which $V(x_j, t) = \theta$, point A and the last point at which $V(x_j, t) = \theta$, point B. We then take the point in the middle (as defined below), point C, as our time, t_n that the 'wave' crosses point x_j.

$$A = \min\{t|V(x_j, t) = \theta\} \tag{3.75}$$

$$B = \max\{t|V(x_j, t) = \theta\} \ . \tag{3.76}$$

We need to find the times corresponding to points A and B before we can find the time corresponding to point C. Unfortunately the voltage will rarely be exactly θ therefore we cannot get A and B directly from our saved matrix of voltage data, so we need to interpolate to find points A and B. To do this we need to find the last point at which the voltage is known before A or B and the first point at which the voltage is known after A or B. We will call these four new points $V(A^-)$, $V(A^+)$, $V(B^-)$ and $V(B^+)$.

$$A^- = \sup\{t|V(x_j, t) \leq \theta, t < A\} \tag{3.77}$$

$$A^+ = \inf\{t|V(x_j, t) \geq \theta, A < t < B\} \tag{3.78}$$

$$B^- = \sup\{t|V(x_j, t) \geq \theta, A < t < B\} \tag{3.79}$$

$$B^+ = \inf\{t|V(x_j, t) \leq \theta, t > B\} \tag{3.80}$$

Note that $t(A^-) \leq t(A^+) \leq t(B^-) \leq t(B^+)$. If $t(A^-) = t(A^+)$, $t(B^-) = t(B^+)$, then we have already found the time t_n that the wave passes point x_j. If they are not equal then the differences $t(A^+) - t(A^-) = t(B^+) - t(B^-) = \Delta t$ and we can find these points using the 'find' command in Matlab. Since our points $t(A^-)$, $t(A^+)$, $t(B^-)$ and $t(B^+)$ are only Δt apart we use interpolation to find the times $t(A)$ and $t(B)$. We use linear interpolation to create a straight line between our sets of known points $V(A^-)$ and $V(A^+)$ with $t(A^-)$ and $t(A^+)$ and $V(B^-)$ and $V(B^+)$ with $t(B^-)$ and $t(B^+)$ e.g. $V - V(A^+) = \frac{V(A^+)-V(A^-)}{t(A^+)-t(A^-)}(t - t(A^+))$. Now that we have an equation for the line, we can use it to find the time at which $V = \theta$. To implement this interpolation technique we use the Matlab function 'interp1' which uses a linear interpolation to find $t(A)$ and $t(B)$. For each of the points we either have a time that the 'wave' reaches that point or no data if the 'wave' fails before the point. We then use the two points to evaluate the speed:

$$c = \frac{x_2 - x_1}{t_2 - t_1} \ . \tag{3.81}$$

Again the final step is to find the speed over a number of realisations at each level of noise intensity then find the average value.

Measuring speed by template comparison

In this method we assume we can measure the speed of the pulse at each point in time. For a general PDE of the form:

$$\frac{\partial V}{\partial t} = B\frac{\partial^2 V}{\partial x^2} + f(V) \ , \tag{3.82}$$

we can use a travelling wave anzatz: $\xi = x + \gamma(t)$, where $\gamma(t)$ is the unknown position of the wave at each point in time (note that $\gamma = ct$, when the speed, c, of the wave is known and constant).
Inserting this anzatz to the PDE (and replacing ξ by x) we obtain:

$$\frac{\partial V}{\partial t} = B\frac{\partial^2 V}{\partial x^2} + f(V) + \lambda(t)\frac{\partial V}{\partial x} \tag{3.83}$$

where $\lambda(t) = \frac{\partial \gamma}{\partial t}$. We must also introduce a phase fixing condition to compensate for the extra variable $\lambda(t)$: $\psi(V, \lambda) = 0$. We choose to match the travelling wave with a template function, $\tilde{V} : \mathbb{R} \to \mathbb{R}$, to satisfy the phase condition. To do this we choose to minimise the L^2 norm: $||V - \tilde{V}||_{L^2}$, with respect to the distance between the solution, V and the template, $\tilde{V}$:

$$\langle \frac{d\tilde{V}}{dx}, V - \tilde{V} \rangle = 0 \ . \tag{3.84}$$

The function $\tilde{V}$ can be chosen to be a range of different shapes, and this choice will effect the value of speed obtained, but not the behaviour of the system. We can use a

Gaussian function that is similar in amplitude and width to the voltage profile $V(t)$ at one point in space x_j, and we position this template at the start of a cable before the spines begin. (Note that the travelling pulse changes profile depending on its position along the cable). Alternatively we can run a simulation of the deterministic SDS model on the domain we are interested in to obtain $V_{determ}(x,t)$ then use this as the template solution, i.e. at each time step we compare the stochastic travelling wave to the deterministic wave at the same time step, only the deterministic wave is shifted backwards so that it 'runs' behind the stochastic wave. This means that, especially for small noise when the difference in speed of the deterministic and stochastic waves is small, the template and the travelling wave both change profile at approximately the same time. We can use Equation (3.84) along with our chosen $\tilde{V}$ and the discretised solution:

$$\begin{aligned} V_j^{n+1} &= V_j^n + \Delta t \frac{V_{j+1}^n - 2V_j^n + V_{j-1}^n}{\Delta x^2} + \frac{Dr_a\rho}{r}(\hat{V}^n - V_j^{n+1}) - \frac{V_j^{n+1}}{\tau} \\ &+ \lambda^n \frac{V_{j+1}^n - V_{j-1}^n}{2\Delta x}) \end{aligned} \tag{3.85}$$

to obtain a value for the speed, λ at each time step of the simulation.
The difference we have to that of the examples in [69] is that we do not actually freeze the travelling wave. So while we use Equation (3.85) to measure the speed we use Equation (4.6) to evolve the dynamics ahead at each time step. In doing this the wave is free to travel the length of the cable but we obtain a vector of speeds at the end of the simulation. If we say $\lambda(t) = (\lambda(t_0), \lambda(t_1), \ldots, \lambda(t_N))$, then we can get a time averaged speed for the wave:

$$\Lambda = \frac{1}{T}\int_0^T \lambda(t)dt \ . \tag{3.86}$$

In order to obtain an average wave speed when we consider noise in the system, we apply the above method to measure a time averaged speed for each realisation of the noise and take an average over the number of realisations and so obtain an expected value of the speed for a certain value of the noise strength.

Chapter 4

Noise in the Spike diffuse spike model

4.1 Introduction

The motivation for looking at this model with noise comes from the paper [109] by Timofeeva, Lord and Coombes, which builds on earlier work by Coombes and Bresslof [15], [16]. The neuron's environment is inherently noisy, and so it is important to consider noise in any realistic model of the neuron and the paper [109] briefly looks at some of the effects of noise in the spine head dynamics of the SDS model for spiny dendritic tissue. The aim of this chapter is to investigate more fully the SDS model with noise included in various forms. The noise is added to the spine head dynamics and to the cable equation to represent the different sources of stochastic behaviour in a real neuron. The noise in the spine head can be thought to arise from the stochastic nature of the synaptic gating process. In a real dendrite the cable is not passive and the inclusion of noise in the cable can again arise from the stochastic gating in ion channels. We also consider the type of the noise used; it may be simply space/time white noise or a noise with either a spatial or temporal correlation. In this chapter we first state the stochastic equations required to describe the noisy SDS model, in Section 4.2, and give the fully discretised version of these equations in Section 4.3. We continue with the outline of the algorithm used to solve these equations numerically and build up the solution for the spine head and cable voltage over the whole space and time domain. We also look at the ways in which we measure the effect of the noise; through mean voltage plots, average distance travelled along the cable and the speed of propagation, Section 3.4. Finally we look at the results, Section 4.4, of the simulation of the SDS model with the different types of noise and how the voltage, distance and speed measures change as the noise intensity and correlation scale changes.

4.2 Constructing a stochastic SDS model

Here we set out the full system of stochastic differential equations and stochastic partial differential equations that describe the noisy spiny dendrite, for white, temporally and spatially correlated noise. All the basic deterministic equations from which we construct the SDEs and SPDEs from are outlined fully in Chapter 2.

4.2.1 Noise in the spine heads

We first introduce noise to the spine heads by the addition of temporal white noise to the IF model, Equation (2.31). This noise can be thought of arising from the stochastic gating process at the synapse. To do this we have to construct an SDE from the ODE, by adding a noise term, that describes the IF process. We rearrange Equation (2.41) in a neater form and added the noise term to get, for spine n:

$$\begin{aligned} dU_n(t) &= \left(\frac{V_n(t)}{\hat{C}r} - \epsilon U_n(t)\right) dt + (\mu + \nu g(U_n(t)))dW_n(t) \\ &- \left(h\sum_m \delta(t - T_n^m)\right) dt \ . \end{aligned} \tag{4.1}$$

The parameters are the same as in Chapter 2, with the addition of $\epsilon = \frac{1}{\hat{C}}(\frac{1}{\hat{r}} + \frac{1}{r})$, μ is the strength of additive noise, ν the strength of multiplicative noise and $W_n(t)$ is a Wiener process, as before, for the nth spine. From here on we will not explicitly write out the reset term in any IF equation to make reading easier. Also the reset term is not necessary for the consideration of the noisy path to threshold. The function $g(U_n(t))$ is a function of the voltage, and the form of this function will be specified for each case considered in all subsequent sections of this chapter. If $\nu = 0, \mu \neq 0$ then the noise is purely additive, but $\nu \neq 0, \mu = 0$ then the noise is said to be multiplicative. For multiplicative noise it is assumed that the amount of noise in the system is related to the amount of activity in the system since if there is more activity then there will be more synaptic events and so more channel noise. Both additive and multiplicative noise could be considered together since the additive could be considered a general 'background' noise, arising from surrounding neurons, and the multiplicative a specific activity related noise originating, for example, in the stochastic nature of the ion channels at the synapse of the neuron in question.

We may also consider the noise in the spine heads to be temporally correlated with the Ornstein-Uhlenbeck process, Section 3.1.7 in Chapter 3, describing this type of

correlation. This gives the following system:

$$\begin{aligned} dU_n(t) &= \left(\frac{V_n(t)}{\hat{C}r} - \epsilon U_n(t)\right) dt + (\mu + \nu g(U_n(t)))dK_n(t) \qquad (4.2) \\ dK_n(t) &= -\beta K_n(t)dt + dW_n(t) \ . \end{aligned}$$

The variables here are the same as for Equation (4.1) with the following additions: $K_n(t)$ and β are the same parameters described in Section 3.1.7, and as β increases it should be noted that the temporal correlation scale gets shorter.

Finally we consider spatially correlated noise in the spine heads where the noise is white in time but there is some correlation between the noise received by each spine (at any particular moment in time), which depends on the correlation scale chosen and the distance between the spines. As outlined in Section 3.1.10 we have chosen a form of spatially correlated noise which has a short range and so nearby spines will experience a more strongly correlated noise than spines which are further apart on the cable. Now the SDE describing the spine head dynamics is:

$$dU_n(t) = \left(\frac{V_n(t)}{\hat{C}r} - \epsilon U_n(t)\right) dt + (\mu + \nu g(U_n(t)))dW_n(x_n, t) \ , \qquad (4.3)$$

where $W_n(x_n, t)$ is the spatially correlated noise given by Equation (3.64) and Equation (3.70) and evaluated at point x_n which is the position of the nth spine. Note that this noise is white in time and that the correlation is between points in space which, in the deterministic case, are diffusively coupled through the cable.

4.2.2 Noise in the cable

We can introduce noise into the system in the form of a space-time white noise in the cable Equation (2.40) to obtain a stochastic partial differential equation (SPDE):

$$\frac{\partial V}{\partial t} = D\frac{\partial^2 V}{\partial x^2} - \frac{V}{\tau} + Dr_a\rho(x)\frac{\hat{V} - V}{r} + (\mu + \nu g(V))\frac{\partial W(x,t)}{\partial t} \ . \qquad (4.4)$$

The parameters are as in Equation (2.40), with μ, ν the strength of additive and multiplicative noise respectively and $g(V)$ is a function specified in each subsequent section. $W(x,t)$ is a space-time Wiener process, see Section 3.1, which can be white or correlated in time or space. The noise in the cable may also be temporally correlated, as in the spine heads, using the OU process to generate the temporal correlation but

maintain the white property in space. The cable equation then becomes:

$$\begin{aligned} \partial V &= \left(D\frac{\partial^2 V}{\partial x^2} - \frac{V}{\tau} + Dr_a\rho(x)\frac{\hat{V}-V}{r} \right)\partial t + (\mu + \nu g(V))\partial K(x,t) \quad (4.5) \\ dK(x,t) &= -\beta K(x,t)dt + dW(x,t)\ . \end{aligned}$$

Finally in the cable we also consider a noise which is white in time but correlated in space, as outlined in Section 3.1.10, where $W(x,t)$ is constructed as before in Equation (3.64).

4.3 Solving the stochastic SDS model

Here we implement the numerical methods set out in Section 3.3 in Chapter 3 for the equations describing the stochastic SDS model. We conclude by using the discretised equations in a loop that solves the stochastic SDS model over the whole space and time domain chosen. We will write out explicitly the discretised equations used in the simulations, the parameters used and the boundary conditions employed.

4.3.1 The discretised SDS model

All stochastic integrals in this chapter are considered in the Itô sense and the equations, for the SDS model, are evaluated on the domain, $x \in [0, L]$ and $t \in [0, T]$, where L is the length of the cable and T the time over which the system is solved. We employ the same discretisation as in Chapter 3: x_j is a point on the spatial mesh $x_0, x_1, \ldots, x_J$ with step size Δx, i.e. $j = 1, 2, \ldots, J$ $J = \frac{L}{\Delta x}$ and t_n is a point on the temporal mesh $t_0, t_1, \ldots t_N$ of step size Δt, $n = [1, 2, \ldots, N]$, and $N = \frac{T}{\Delta t}$, so for example $V_j^{n+1} = V(x_j, t_{n+1})$.

The stochastic cable equation, given by Equation (4.4), is solved with a central finite difference method, Equation (3.43), to approximate the second derivative of $V(x,t)$ and with a semi-implicit Euler-Maruyama method, Equation (3.56), to integrate over time.

$$\begin{aligned} V_j^{n+1} &= V_j^n + \Delta t \left(\frac{V_{j+1}^n - 2V_j^n + V_{j-1}^n}{\Delta x^2} + \frac{Dr_a\rho}{r}(\hat{V}^n - V_j^{n+1}) - \frac{V_j^{n+1}}{\tau} \right) \\ &+ (\mu_c + \nu_c g(V_j^n))\Delta W_j^n \quad (4.6) \end{aligned}$$

The Wiener process, $W(x,t)$ can be a spatio-temporal white noise or the spatially correlated, white in time noise given by Equation (3.64), and $\Delta W_j^n = (W_j^n - W_j^{n-1})$. If the noise is generated using an OU process then the final discretisation has an extra

term:

$$V_j^{n+1} = V_j^n + \Delta t \left(\frac{V_{j+1}^n - 2V_j^n + V_{j-1}^n}{\Delta x^2} + \frac{Dr_a\rho}{r}(\hat{V}^n - V_j^{n+1}) - \frac{V_j^{n+1}}{\tau} \right) - \beta K_j^n(\mu + \nu g(V_j^n)))\Delta t + (\mu + \nu g(V_j^n))\Delta W_j^n. \quad (4.7)$$

We obtain K_j^n by solving the OU SDE with an explicit Euler-Maruyama method, the noise is white in space since the Brownian increment is generated independently for all points in space (i.e. there is a different OU path for each point in space):

$$K_j^{n+1} = K_j^n - \Delta t(\beta K_j^n) + \Delta W_j^n. \quad (4.8)$$

We must also solve the spine head dynamics up to threshold (h), Equation (4.1) and we do so using an explicit Euler, see Section 3.3.1 ,or Euler-Maruyama method, Equation (3.56), for the deterministic and stochastic cases respectively. So for the mth spine, with temporal white noise, or spatially correlated noise, the discretised IF equation is:

$$U_m^{n+1} = U_m^n + \Delta t \left(\frac{V_m^n}{\hat{C}r} - \epsilon U_m^n \right) + (\mu + \nu g(U_m^n))\Delta W_m^n. \quad (4.9)$$

Here V_m^n is the voltage in the cable evaluated at the position of the mth spine, and W_m is the Wiener process for the mth spine. Each W_m are independent Brownian paths if the noise is white but are correlated according to Equation (3.64) if we consider a spatially correlated noise. In the case of temporally correlated noise we have the extra term from the OU dynamics:

$$U_m^{n+1} = U_m^n + \Delta t \left(\frac{V_m^n}{\hat{C}r} - \epsilon U_m^n) - (\beta K_m^n(\mu + \nu g(U_m^n)) \right) + (\mu + \nu g(U_m^n))\Delta W_m^n \ , \quad (4.10)$$

where again we have independent W_m's and where K_m^n is obtained using Equation (4.8).

When considering an SDE with white noise we can find an exact solution to Equation (4.1), as outlined in Section 3.1.5. As long as we choose the function $g(U)$ to satisfy the linear conditions, Equation (3.14) and Equation (3.15), which we can do with the simple function $g(U) = U$. We can equate from Equation (4.1) the appropriate terms, $a(t) = \frac{V}{\hat{C}r}$, $B(t) = -\epsilon$, $c(t) = \mu$ and $D(t) = \nu$, and obtain the

following solutions for a purely additive or purely multiplicative noise respectively:

$$U_m(t) = e^{-\epsilon t}\left[U_m(0) + \frac{1}{\hat{C}r}\int_0^t (V_m(s)e^{\epsilon s})ds + \mu\int_0^t e^{\epsilon s}dW_m(s)\right], \tag{4.11}$$

$$U_m(t) = e^{-(\epsilon+\frac{1}{2}\nu^2)t+\nu W_m(t)}\left[U_m(0) + \frac{1}{\hat{C}r}\int_0^t V(s)e^{(\epsilon+\frac{1}{2}\nu^2)s-\nu W_m(s)}ds\right]. \tag{4.12}$$

Observe that in Equation (4.11) there remains a stochastic integral to evaluate and so it may be of no computational advantage to use the exact solution as opposed to the original discretised SDE, Equation (4.9). However in the case of purely multiplicative noise the exact solution negates the need for a stochastic integral to be evaluated and so may help the computational efficiency.

Now that we have a numerical framework for solving for the voltage in both the cable and the spine heads we must combine them to get a solution for the full system. We run a loop in time, solving for all points in space at each time step, to do this we follow this set of steps:

1 Set all parameters of the system;

2 Initial conditions, $V(x,t^0) = 0$, $U_1(x_{Spine1},t^0) = U_2(x_{Spine2},t^0) = h + 0.01$, where h is the threshold for firing, i.e. set the first two spines above threshold to initiate a wave;

3 Evolve all spine head dynamics forward one step by Equation (4.9) or Equation (4.10);

4 Check which spines are above threshold and out with the refractory time, to determine which spines can fire $U_m(t^n) \geq h, t^n > T_m^{n-1} + \tau_R$, where T_m^{n-1} is the last firing time of the mth spine. Also need to check which spines have already fired and are still firing i.e. $t^n < T_m^{n-1} + \tau_s$, τ_s is length of time the spine is firing;

5 Keep track of the firing spines, in a firing matrix, of zeros and ones for not firing and firing respectively, $\mathbb{F}$ of size: no. spines M×N no.time steps;

6 Construct the injected voltage, $\hat{V}(x,t^n)$, this will be η_0 (strength of injected pulse) at x_m corresponding to a firing spine, the mth spine, and zero everywhere else;

7 Now evolve cable voltage forward one time step, using Equation (4.6);

8 Save $U(t^n)$ and $V(x,t^n)$ in matrices;

9 Go back to step 3 and repeat until $t^n = t^N = T$;

Finally we have a full picture of the voltage in the cable and spine heads at each point in space and time saved in the two matrices $\mathbb{U}$ and $\mathbb{V}$, size $M \times N$ and $J \times N$ respectively, we also have all the firing times saved in the matrix $\mathbb{F}$. For each noise intensity we choose, we can simulate the stochastic SDS model many times, N_{sample}, and obtain an average value for the voltages. We may also measure the effect of the noise on the distance travelled and speed of propagation of any travelling waves, by the methods explained in Section 3.4. The reliability of this scheme was checked by looking at the convergence of the solution of the spine head voltage U and can show strong convergence as the step size decreases. Since we can find an exact solution to the stochastic integrate and fire model, as outlined in Chapter 3, we can use this as our true solution and look for convergence to this true solution as the step size used in the EM method reduces. To this end we found that the EM method does converge with strong order $\frac{1}{2}$, the condition for strong convergence is: $\mathbb{E}|U^n - U(n\Delta t)| \leq C\Delta t^{\frac{1}{2}}$ (C is some constant) and weak order 1: $|\mathbb{E}p(U^n) - \mathbb{E}p(U(n\Delta t))| \leq C\Delta t^1$, again C is some constant and p is a set of functions which satisfy some conditions of smoothness.

4.4 Results

In this section we look at the results of our simulations as measured by the methods outlined in Section 3.4, distance travelled by waves, speed of propagation and the mean voltage in the cable. Throughout this section the parameters of the system stay the same with the exception of the spine spacing d and all of the noise intensity parameters μ and ν which we change to observe the effect of noise intensity on the behaviour of the system, we also alter the correlation scale, β for the OU noise and ζ for the spatially correlated noise. The spacing d is either $d = 0.8$ or $d = 1$ and these values are chosen since they represent two different regimes in the deterministic system, as can be shown in Figure 4.2: $d = 0.8$ allows a wave to propagate and $d = 1$ cannot support a travelling wave. Although the results here are only for two values of d, all other values in the two regimes show the same behaviour i.e. $d < 0.8$ supports travelling waves which show the same behaviour under the influence of noise and for all regimes with $d > 1$ never supports travelling waves. Figure 4.2 was computed by simulating the deterministic SDS model, Equation (4.4), for spine spacing $d \in [0, 1]$. Figure 4.1 shows an example of the voltage in the cable for the two spine spacings: plot (a) shows $d = 0.8$ and plot (b) $d = 1$.

Unless otherwise stated, each result that follows is computed by taking 100 realisations of the stochastic SDS model to compute average values. We scale the mean speeds and distances by the deterministic values for ease of comparison and show the variation by means of error bars on all plots which represent the standard deviation, $\pm$S.D.(X) $= \sqrt{\mathbb{E}(X^2) - (\mathbb{E}(X))^2}$. We show that for all forms of multiplicative noise

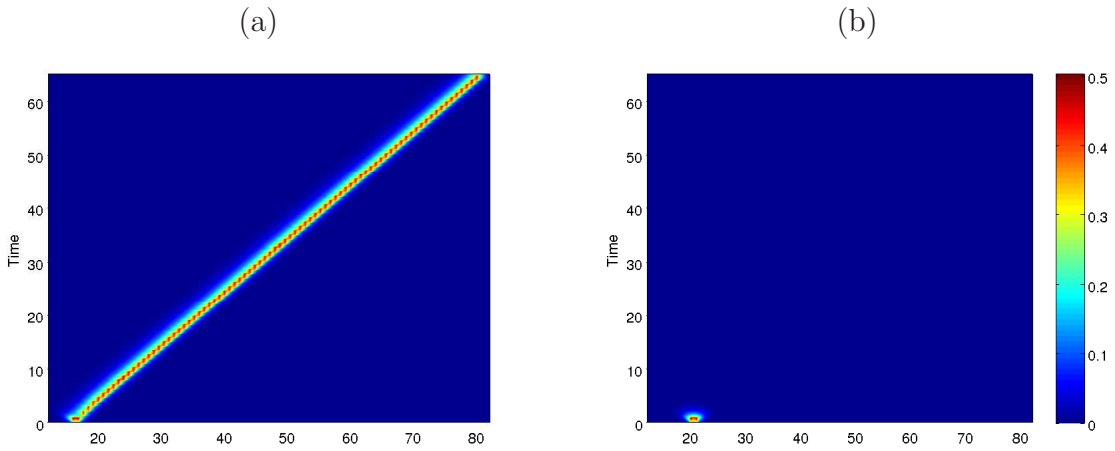

Figure 4.1: This figure shows the, mean voltage in the cable for the two regimes considered (spine spacing $d = 0.8$ and $d = 1$), the colour bar shows the scale for the voltage. Plot (a) has spine spacing $d = 0.8$ shows a saltatory travelling wave. The dark blue background is the resting state of the system 0 volts and as the colour changes through green, to yellow and to a strong red, the voltage is increasing; the bright horizontal red patch seen at approximately (16, 0) is the voltage produced from the first two spines firing together due to the initial condition that they both start with a voltage slightly above the firing threshold h. The wave then moves in a saltatory fashion from one spine to the next, bringing each one successively to threshold and that results in a pulse being injected to the cable which is seen on the plot as a bright red 'dot'. Each 'dot' is slightly further ahead in space, centred on the position of the spines, and in time since there is a delay as the wave diffuses along the cable to the next spine. The final result is a chain of 'dots' sloping upwards on the plot; the steeper the gradient the slower speed of the wave, likewise the shallower the gradient the faster the speed of the wave. Plot (b) has $d = 1$ and shows the initial conditions (first two spines above threshold) by two bright patches at $t = 0$. The larger value of the spine spacing cannot support a travelling wave therefore there are no other bright spots of voltage. All other parameters are as described in the parameter list at the start of the thesis. We solve Equation (2.40) along with Equation (2.31) with temporal discretisation $\Delta t = 0.1$, $t \in [0, 70]$ and spatial discretisation $\Delta x = 0.08$, $x \in [0, 96]$ (measured in non-dimensional electronic length units) with 81 spines attached along this length. The boundary conditions used are Dirichlet and initial conditions $V(x, 0) = 0$, $U_1(0) = U_2(0) = 0.04$ and $U_{n>2} = 0$.

in either the spine heads or in the cable, the speed of propagation is reduced (from the speed of a deterministic wave) as the noise intensity is increased. As the level of noise in the system increases the number of out of order waves increases i.e. the spines start to fire non-sequentially and so defy our condition for travelling waves to be present, therefore the waves are robust to only low levels of noise intensity. In the case of additive noise the spines not only fire out of order but as the noise intensity increases we see synchronised firing of the spines along the full length of the cable. This effect can be reversed to some extent by introducing a spatially correlated noise to the spine heads, where a longer correlation length will, for the same noise intensity, promote sequential firing once again.

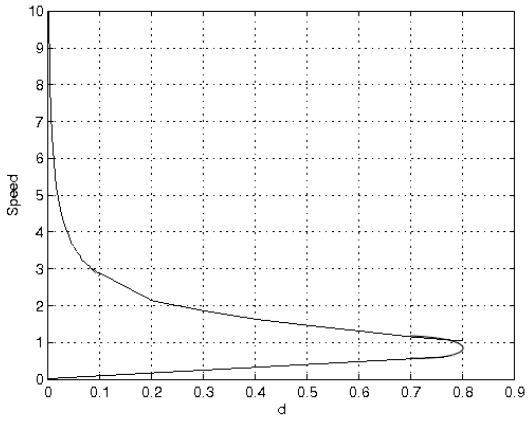

Figure 4.2: Speed of a travelling wave in the SDS model as a function of spine spacing, d. The top, fast branch of this diagram is obtained from direct simulation and shows the speed of the stable wave in the SDS model. The bottom, slow branch has been drawn on to represent the unstable solution, which can not be observed directly. This figure is a reproduction of a figure in [109] and is given as an illustrative aid to emphasise that there are two regimes for the deterministic SDS model. All other parameters are as described in the parameter list at the start of the thesis. We solve Equation (2.40) along with Equation (2.31) with temporal discretisation $\Delta t = 0.1$, $t \in [0, 70]$ and spatial discretisation $\Delta x = 0.08$, $x \in [0, 96]$ (measured in non-dimensional electronic length units) with 81 spines attached along this length. The boundary conditions used are Dirichlet and initial conditions $V(x, 0) = 0$, $U_1(0) = U_2(0) = 0.04$ and $U_{n>2} = 0$.

4.4.1 Noise in the spine head dynamics

White multiplicative noise

We first look at the effects of multiplicative white noise in the spine heads. There is a choice over what form the noise will take; $g(U(t))$ can be any function we wish. We consider four forms of the function $g(U)$ and we discover that the form of the multiplicative noise term has little effect on the behaviour of the system with respect to noise. The forms of the multiplicative term investigated are: the simplest linear

form $g(U) = U$, the positive definite $g(U) = U^2$, $g(U) = \sqrt{U}$ and a form chosen to preserve the range of the voltage in the spine heads, $g(U) = U(1-U)$ while $U \in [0,1]$ and zero otherwise. This final form is taken from [21] and requires that the noise is 'switched off' in the simulation while $U \notin [0,1]$. We implement this by checking the voltage in each of the spine heads at each time step in the numerical algorithm and if any $U_n \notin [0,1]$ then the noise intensity at that spine is set to zero, $\nu_n = 0$, until the voltage returns to the correct range, then the noise is switched back on. Figure 4.3 shows the speed of a travelling wave over a small range of noise intensities for the three forms of $g(U)$. The small noise range for each form is chosen to show only the successful waves, i.e. those that travel to the end of the cable and by sequential firing of the spines. It is clear that although the ranges of ν are different, the behaviour of the system is the same in each case, the higher the noise intensity the slower the wave, therefore the noise is in some way destructive to the travelling wave. At small levels of noise the error bars are small and so the variation from trial to trial is small but as the noise intensity increases so does the uncertainty/variation in the mean value.

The most realistic of these forms of noise is $g(U) = U(1-U)$ since it preserves the range of $U \in [0,1]$, also the 'switching on/off' of the noise means that the voltage does not blow up to huge values like it can for the other forms of multiplicative noise terms. We see the effect of the voltage 'blow up' in Figure 4.4, where it seems that high intensities of noise promote travelling waves. Figure 4.4 shows the distance travelled along the cable, measured by spine number as the noise intensity for multiplicative white noise increases. We can see, in Figure 4.4, that for plots (a) and (b), where $g(U) = U^2$ and there are 37 spines, there seems to be three 'levels' of noise that each have a different behaviour. At low levels of noise intensity, the system behaves as it would in the deterministic case, in the mid-range noise seems only to stifle the propagation, and at high levels the noise can promote or induce (in the $d = 1$ case plot (b)) some propagation. At these high levels of noise intensity the voltage in the spine heads has become un-realistically large ($U > 1$) and only increases further as the noise intensity increases to the point where all spines are always above threshold and can fire without real propagation (i.e. no sequential firing). Plots (c) and (d) of Figure 4.4, where $g(U) = U(1-U)$ and there are 81 spines, shows that as noise intensity increases the propagation is killed by the noise and cannot recover as intensity is increased further. In the case of $d = 1$, plot(d) there is a slight increase in the distance travelled along the cable, from 2 spines (which always fire due to the initial conditions) to approximately 8 spines distance but the error bars grow since there is some random firing associated with higher noise levels which will increase the variation in the measured distance.

Since $g(U) = U(1-U)$ is the most realistic form of the noise it is the form that was used in obtaining most of the following results. If another form is used it will

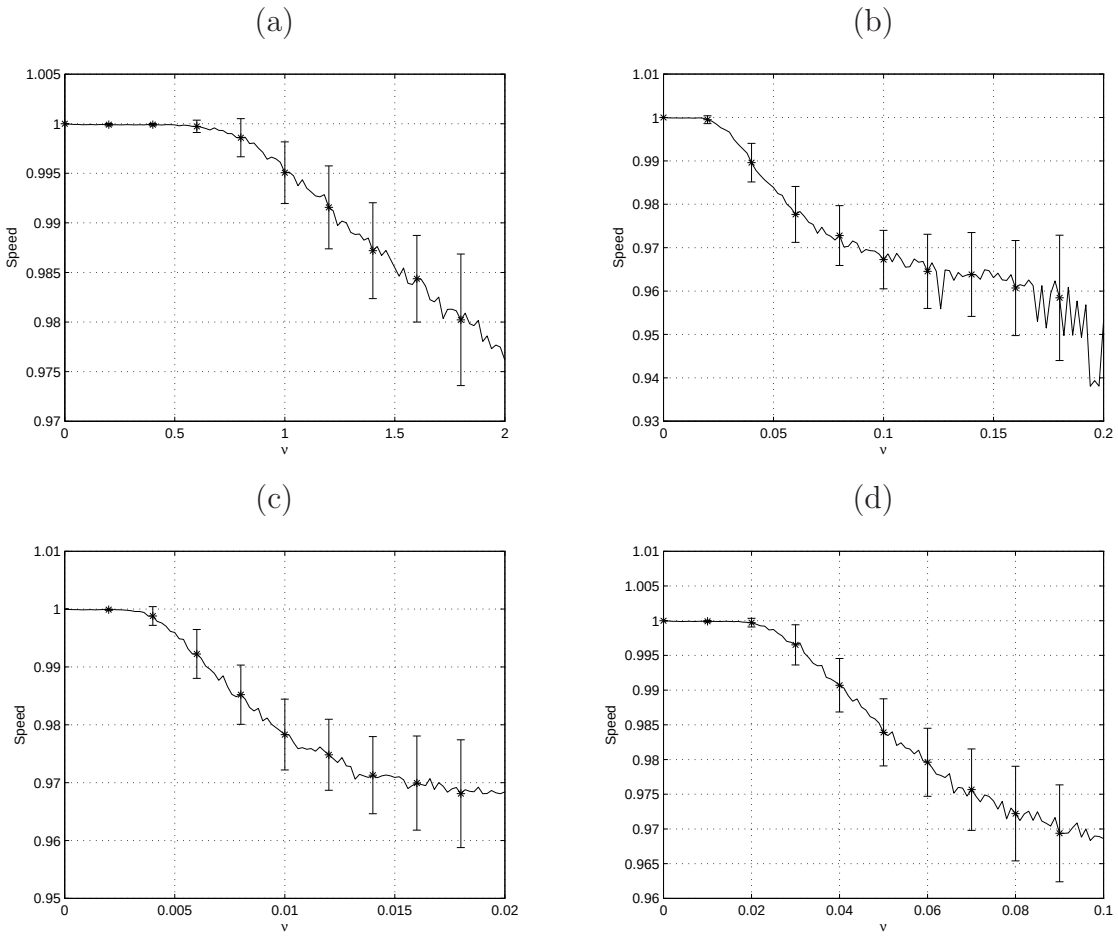

Figure 4.3: This figure shows the similarity in the response of the speed of a wave in the SDS model to different forms of the multiplicative temporal white noise in the spine heads. (a) shows $g(U) = U^2$, (b) is $g(U) = U$, (c) has $g(U) = \sqrt{U}$ and (d) is $g(U) = U(1-U)$ while $U \in [0, 1]$ and zero otherwise. All other parameters are as described in the parameter list at the start of the thesis. We solve Equation (4.4) along with Equation (4.1) with temporal discretisation $\Delta t = 0.1$, $t \in [0, 70]$ and spatial discretisation $\Delta x = 0.08$, $x \in [0, 96]$ (measured in non-dimensional electronic length units) with 81 spines attached along this length. The boundary conditions used are Dirichlet and initial conditions $V(x, 0) = 0$, $U_1(0) = U_2(0) = 0.04$ and $U_{n>2} = 0$.

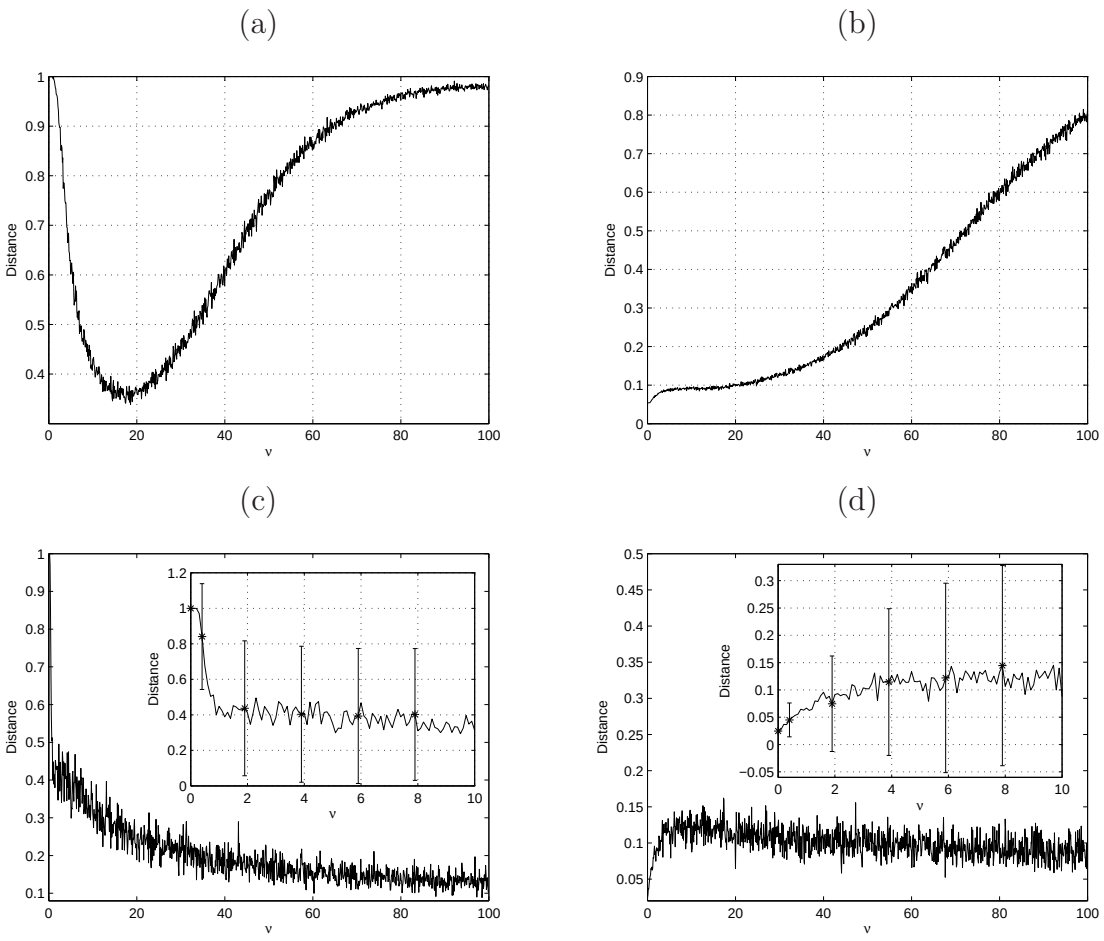

Figure 4.4: Mean distance travelled along the cable as a function of the noise intensity. Noise is multiplicative and white in the spine heads for all plots. In (a) $g(U) = U^2$ and the cable has 37 spines with spine spacing $d = 0.8$. At low noise intensity any wave still reaches the end of the cable, as the intensity increases the wave is suppressed and fails to propagate very far until at high noise intensities the voltage is pushed much higher than is realistic and all spines fire so it seems the wave reaches the end of the cable. (b) also has $g(U) = U^2$ and 37 spines, with spine spacing $d = 1$. Here, as the noise intensity increases, the voltage again increases beyond realistic values and induces firing along the cable. (c) and (d) have $g(U) = U(1 - U)$, 81 spines spaced $d = 0.8$ and $d = 1$ respectively. Due to the form of the noise the voltage is contained in the correct range $U \in [0, 1]$ and although at small noise intensities the deterministic behaviour is observed for all higher intensities propagation is killed. The inset plots show a close up of the main plot and also show the error bars. All other parameters are as described in the parameter list at the start of the thesis. We solve Equation (4.4) along with Equation (2.31) with temporal discretisation $\Delta t = 0.1$, $t \in [0, 70]$ spatial discretisation $\Delta x = 0.08$, $x \in [0, 96]$ (measured in non-dimensional electronic length units) with 81 spines attached along this length. The boundary conditions used are Dirichlet and initial conditions $V(x, 0) = 0$, $U_1(0) = U_2(0) = 0.04$ and $U_{n>2} = 0$.

be clearly stated in the text and in the figure captions. We now look at the range of noise intensities for which we have sequential travelling waves, we do this by simply checking the firing times are always increasing as the spines get further along the cable. Figure 4.5, plot (a), shows a close up of plot (c) in Figure 4.4 and plot (b) show the number of waves, in the 100 realisations, that had spines fire out of order somewhere along the cable, as the noise intensity increases. We can see that only a small range of noise intensities, $\nu \in [0, 0.1]$, support sequential travelling waves and that the waves travel most of the length of the cable.

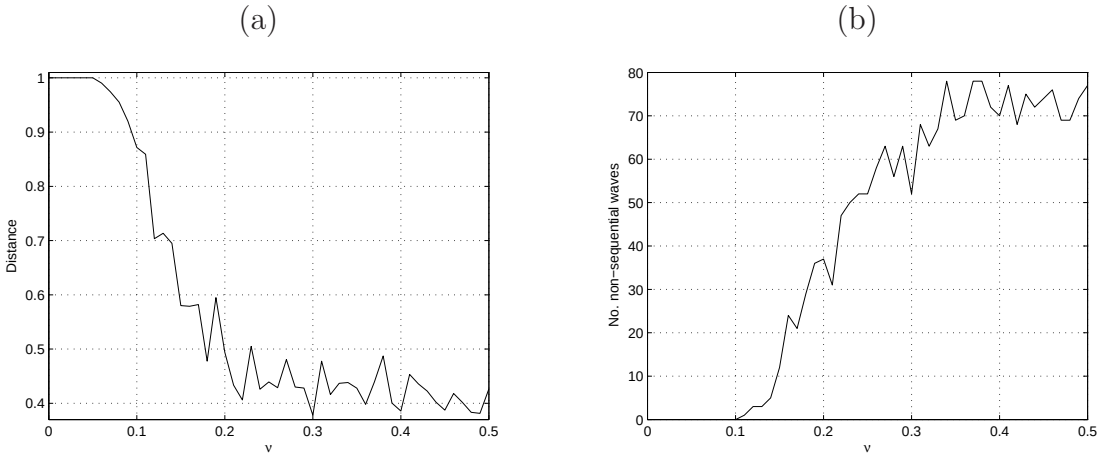

Figure 4.5: This figure shows the close up, of Figure 4.4 plot (c), and shows distance travelled along the length of the cable, in spine number, and the number of non-sequential waves, as the noise intensity increases. The form of the noise is $g(U) = U(1-U)$, $d = 0.8$ and there are 81 spines all with multiplicative white noise in the dynamics. Plot (a) shows the distance travelled and plot (b) shows the number of non-sequential waves. All other parameters are as described in the parameter list at the start of the thesis. We solve Equation (4.4) along with Equation (2.31) with temporal discretisation $\Delta t = 0.1$, $t \in [0, 70]$ and spatial discretisation $\Delta x = 0.08$, $x \in [0, 96]$ (measured in non-dimensional electronic length units) with 81 spines attached along this length. The boundary conditions used are Dirichlet and initial conditions $V(x, 0) = 0$, $U_1(0) = U_2(0) = 0.04$ and $U_{n>2} = 0$.

We now look again at the speed of the travelling waves for a small range of multiplicative noise values. As seen in Figure 4.3, plot(d) the speed of the wave reduces as the noise intensity increases. We look at the speed measured in two different lengths of cable to show that the physical size of the model dendrite does not affect this behaviour. The short cable is 48 units long and has 37 spines and the long cable is 96 units long with 81 spines and as can be seen in Figure 4.6 there is no difference in the behaviour. The error bars in the short cable case are larger that in the long cable, since the longer the structure the less it is affected by noise, [24].

Finally in the white noise in the spine heads section we look at the speed recorded for different noise intensities when the voltage in the spine heads is calculated with the exact solution given in Equation (4.12) instead of a purely numerical solution

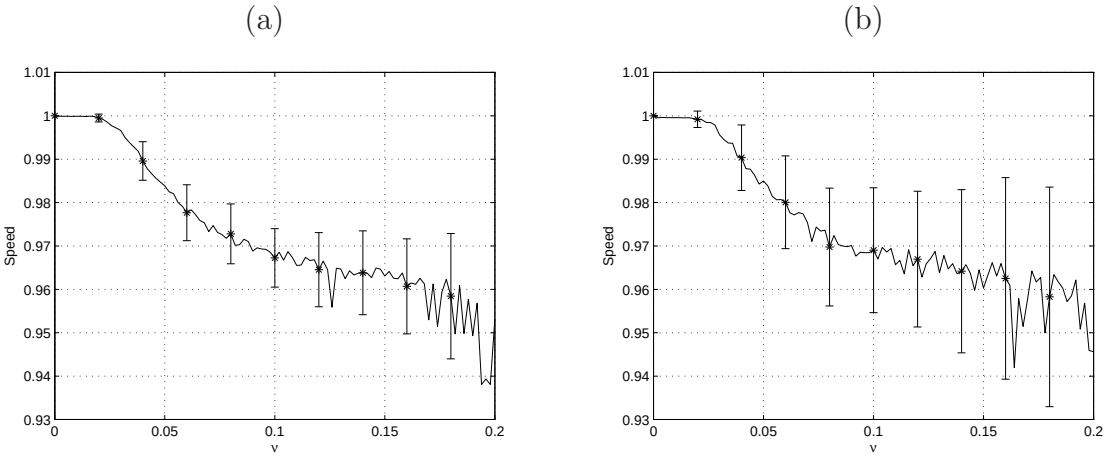

Figure 4.6: Speed of propagation, measured by level set method, as a function of multiplicative white noise strength in the spines for two cables of different length. Plot (a) shows the long cable is 96 units long and has 81 spines along its length and Plot (b) shows the short cable has length 48 units and has 37 spines along its length. It is clear that the length of the cable makes little difference in the behaviour of the travelling waves and the values of the normalised speed are very similar. The long cable however does reduce the variance as can be seen by the length of the error bars, the bars on plot (a) are shorter than those in plot (b). All other parameters are as described in the parameter list at the start of the thesis. We solve Equation (4.4) along with Equation (4.1) with temporal discretisation $\Delta t = 0.1$, $t \in [0, 70]$ and spatial discretisation $\Delta x = 0.08$. The boundary conditions used are Dirichlet and initial conditions $V(x, 0) = 0$, $U_1(0) = U_2(0) = 0.04$ and $U_{n>2} = 0$.

given by the EM method employed thus far. We can see that again the behaviour of the speed reducing from the deterministic value as the noise intensity increases is the same as for all other forms of the noise. The exact solution may be desirable since we do not have to compute a stochastic integral for this purely multiplicative case but the form that the noise must take, $g(U) = U$, to allow the exact solution to be computed is not ideal. The figure, Figure 4.7, does show, however, that the EM method is a suitable method for computing the SDE that describes the stochastic IF dynamics.

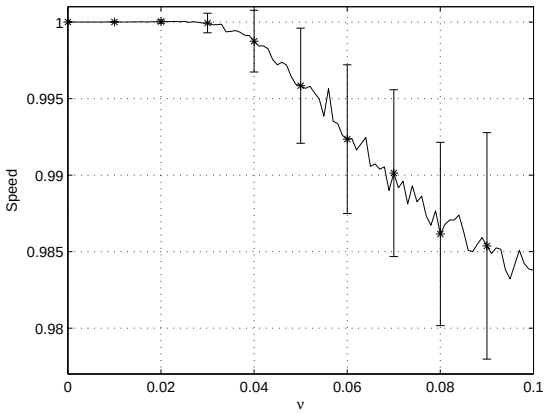

Figure 4.7: Speed of propagation, measured by level set method, as a function of multiplicative white noise strength in the spines when $g(U) = U$ and the SDE describing the stochastic IF dynamics is solved with the exact form. It is clear that this agrees with the behaviour observed in previous simulations with a purely numerical method, therefore we can conclude that the EM method is a suitable method for solving the SDE. All other parameters are as described in the parameter list at the start of the thesis. We solve Equation (4.4) along with Equation (4.12) with temporal discretisation $\Delta t = 0.1$, $t \in [0, 70]$ and spatial discretisation $\Delta x = 0.08$, $x \in [0, 96]$ (measured in non-dimensional electronic length units) with 81 spines attached along this length. The boundary conditions used are Dirichlet and initial conditions $V(x, 0) = 0$, $U_1(0) = U_2(0) = 0.04$ and $U_{n>2} = 0$.

We also use the template comparison method to measure the speed of the waves, described in Section 3.4.3. Figure 4.8 shows the speed as measured by the two different methods, plot (a) is the level set method and plot (b) is the template comparison method. The difference in the actual number recorded for the speed is due to the difference in the methods and in fact the numbers for the template comparison speed will differ for different template functions. The difference in speed measured arises from a slight difference in the level set method used in each case. The increase in speed shown here in Figure 4.8 occurs due to the boundary conditions and so is an artificial artifact of the computation. If the first point in the level set method is at the start of the cable (around the 3rd spine) then the boundary effects the speed measures, however if the speed is measured over the middle portion of the cable when the wave is established and away from the boundary, then we get results as in all the

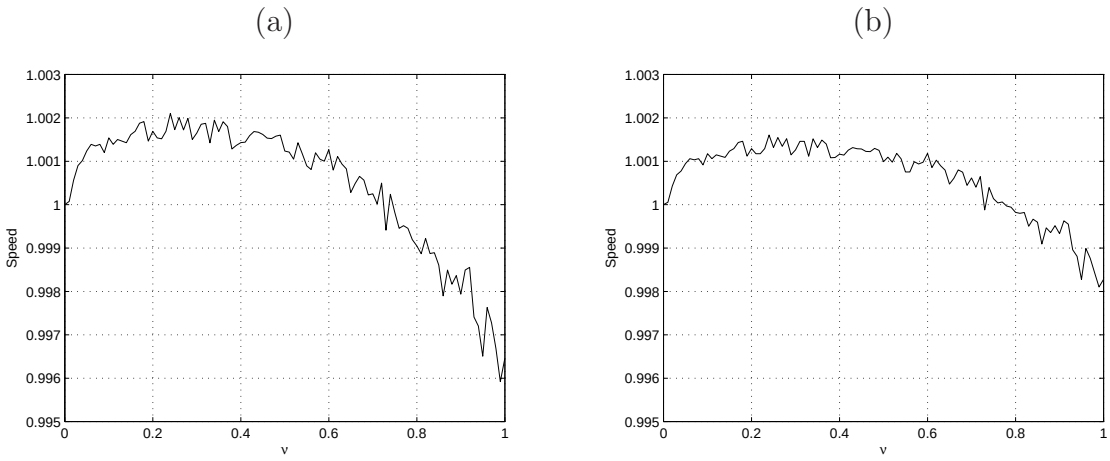

Figure 4.8: Both these figures show the speed of a travelling wave in the SDS model with multiplicative white noise of the form: $g(U(t)) = U^2$, as a function of the noise intensity, $d = 0.8$. (a): Speed measured by the level set method as function of noise intensity. (b): Speed measured by the template comparison method. All other parameters are as described in the parameter list at the start of the thesis. We solve Equation (4.4) along with Equation (4.1) with temporal discretisation $\Delta t = 0.1$, $t \in [0, 70]$ and spatial discretisation $\Delta x = 0.08$, $x \in [0, 96]$ (measured in non-dimensional electronic length units) with 81 spines attached along this length. The boundary conditions used are Dirichlet and initial conditions $V(x, 0) = 0$, $U_1(0) = U_2(0) = 0.04$ and $U_{n>2} = 0$.

previous figures. The reason that we must use the first section of the cable here is to give an accurate comparison between the level set and the template comparison methods, since the template comparison method uses the instantaneous speed over the whole length of the cable for all time, making it difficult to neglect this false effect from boundary. Consequently in all level set simulations except the one relating to Figure 4.8 the first point used in the level set method is some distance away from the end of the cable. The template comparison method also requires significantly longer computing time than the level set method, since the speed must be calculated at each step in time, unlike the level set method which requires only one calculation of the speed. Therefore we used the level set method since it is in agreement with the more sophisticated template comparison method but requires less computing time.

Multiplicative temporally correlated noise

We look at the effect of temporally correlated noise in the spine heads. Here we have an extra variable to investigate, β, which controls the correlation time scale of the noise. We expect to obtain some different results from the white noise case since we can choose the value of β to be close to the natural timescale in the system which is the refractory time τ_R.

We look at the distance travelled by a wave as the noise intensity increases and we fix a value of ν for different values of β, to investigate the effect of the correlation

scale. We once again use the form $g(U) = U(1-U)$ for the multiplicative noise and we conclude that the system behaves in much the same way as it did when the noise was white, therefore the temporal correlation is of no major significance.

First we look at the distance travelled along the cable, measured in spine number, for a large range of noise intensities, the spine spacing is $d = 0.8$ and the form of the noise is again $g(U) = U(1-U)$ and $\beta = 2$. We see in Figure 4.9, plot (a) that as noise intensity increases the propagation is suppressed and plot (b) that the number of non-sequential firing waves rapidly increases with the noise intensity.

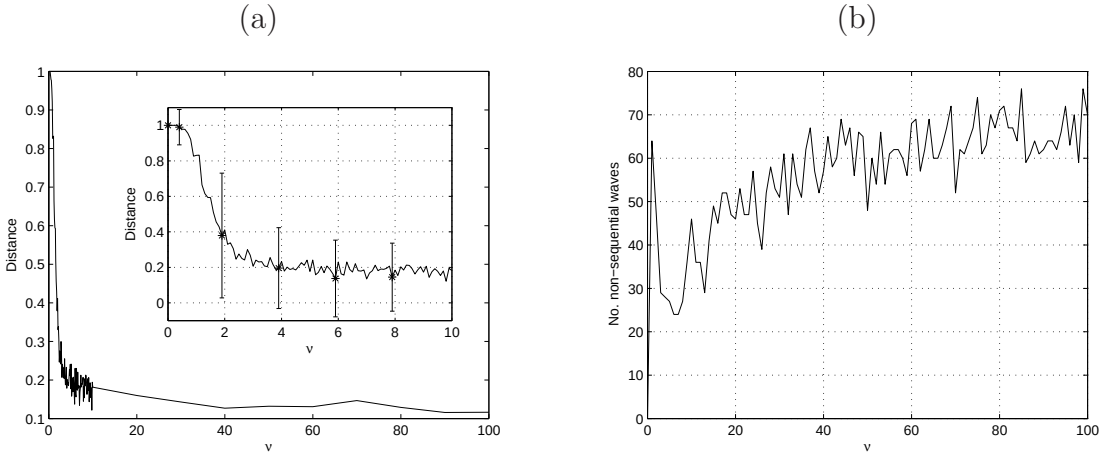

Figure 4.9: Plot (a) shows the distance travelled, measured in spine number, as the noise intensity increases for temporally correlated, $\beta = 2$, multiplicative noise in the cable. There are 81 spines along the length of the cable. Plot (b) shows how many of the 100 realisations, for each noise intensity, did not have the spines firing in order. All other parameters are as described in the parameter list at the start of the thesis. We solve Equation (4.4) along with Equation (4.2) with temporal discretisation $\Delta t = 0.1$, $t \in [0, 70]$ and spatial discretisation $\Delta x = 0.08$, $x \in [0, 96]$ (measured in non-dimensional electronic length units) with 81 spines attached along this length. The boundary conditions used are Dirichlet and initial conditions $V(x, 0) = 0$, $U_1(0) = U_2(0) = 0.04$ and $U_{n>2} = 0$.

We now look at the speed of the waves over the small range of noise intensities $\nu \in [0, 1]$, where the waves are sequential. We see, in Figure 4.10, that the temporally correlated noise also reduces the wave speed with respect to the deterministic speed as the noise intensity increases. We now look at the effect of the correlation scale β on the speed of the wave to see if there may be a 'special' value that drastically changes the behaviour observed so far. Figure 4.11 shows the speed of the wave as a function of the correlation scale, for a fixed value of ν. As β increases the speed also increases slightly, although the increase is so small that the waves are still slower than the deterministic speed. Therefore we can conclude that there is no 'special' value of β.

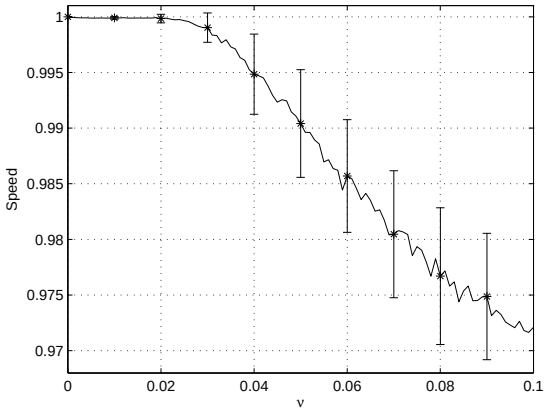

Figure 4.10: Speed of propagation as a function of multiplicative temporally correlated noise strength, $\beta = 2$, $d = 0.8$. The speed decreases with respect to the deterministic wave speed as the noise intensity increases. All other parameters are as described in the parameter list at the start of the thesis. We solve Equation (4.4) along with Equation (4.2) with temporal discretisation $\Delta t = 0.1$, $t \in [0, 70]$ and spatial discretisation $\Delta x = 0.08$, $x \in [0, 96]$ (measured in non-dimensional electronic length units) with 81 spines attached along this length. The boundary conditions used are Dirichlet and initial conditions $V(x, 0) = 0$, $U_1(0) = U_2(0) = 0.04$ and $U_{n>2} = 0$.

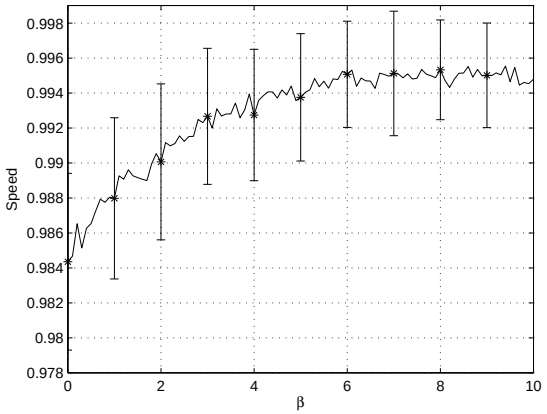

Figure 4.11: Speed of propagation as a function of the temporal correlation scale. The speed increases as the β increases but is still smaller than the deterministic wave speed. All other parameters are as described in the parameter list at the start of the thesis. We solve Equation (4.4) along with Equation (4.2) with temporal discretisation $\Delta t = 0.1$, $t \in [0, 70]$ and spatial discretisation $\Delta x = 0.08$, $x \in [0, 96]$ (measured in non-dimensional electronic length units) with 81 spines attached along this length. The boundary conditions used are Dirichlet and initial conditions $V(x, 0) = 0$, $U_1(0) = U_2(0) = 0.04$ and $U_{n>2} = 0$.

Multiplicative spatially correlated noise

We generate spatially correlated noise, white in time, and include this in the spine-head dynamics as in Equation (4.1), replacing the white noise with the spatially correlated noise. The spatial correlation scale was chosen such that it equated to a distance of approximately three spines. The distance and speed of the travelling waves under the influence of this spatial noise behaves just as the white noise case as shown in Figure 4.12. The speed of the waves, plot (b) in Figure 4.12, start to slow down at a higher noise intensity than for the white noise case, therefore the system is more robust to this spatially correlated noise than the white noise. As the correlation scale,

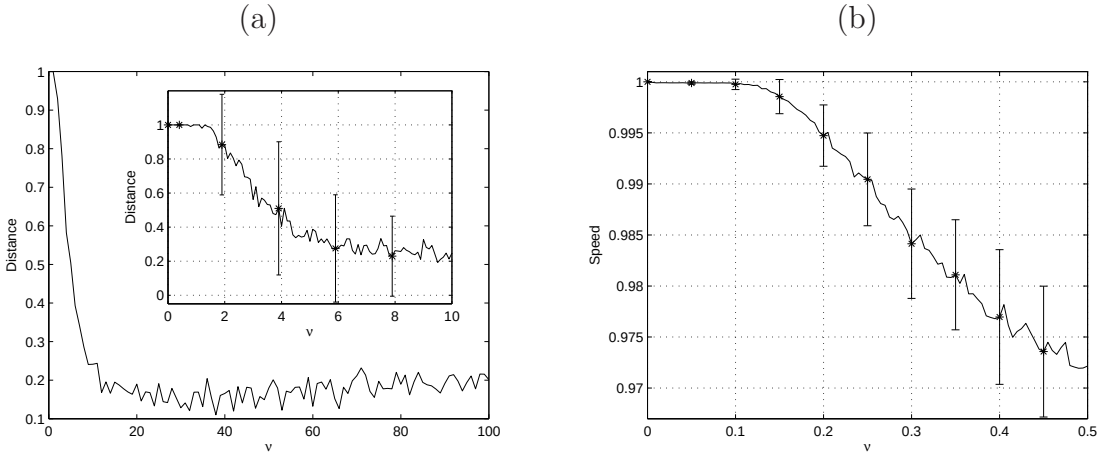

Figure 4.12: Plot (a) shows the distance travelled, measured in spine number, as the noise intensity increases for spatially correlated, $\zeta = 1.25$, multiplicative noise in the spine heads. There are 81 spines along the length of the cable. Plot (b) shows the speed of the waves travelling with spatially correlated noise in the spine heads, the waves start to slow down at a slightly higher level of noise intensity as compared to the white noise. All other parameters are as described in the parameter list at the start of the thesis. We solve Equation (4.4) along with Equation (4.3) with temporal discretisation $\Delta t = 0.1$, $t \in [0, 70]$ and spatial discretisation $\Delta x = 0.08$, $x \in [0, 96]$ (measured in non-dimensional electronic length units) with 81 spines attached along this length. The boundary conditions used are Dirichlet and initial conditions $V(x, 0) = 0$, $U_1(0) = U_2(0) = 0.04$ and $U_{n>2} = 0$.

ζ, of the noise is increased the distance travelled by the wave for a set value of the noise intensity also increases. Figure 4.13 plot (a) shows the distance as the correlation scale increases for noise intensity $\nu = 0.2$ and plot (b) shows the number of non-sequential waves as the noise intensity increases. The distance travelled increases as the noise increases and also the number of non-sequential waves decreases. Therefore the longer correlation scale appears to help the travelling waves.

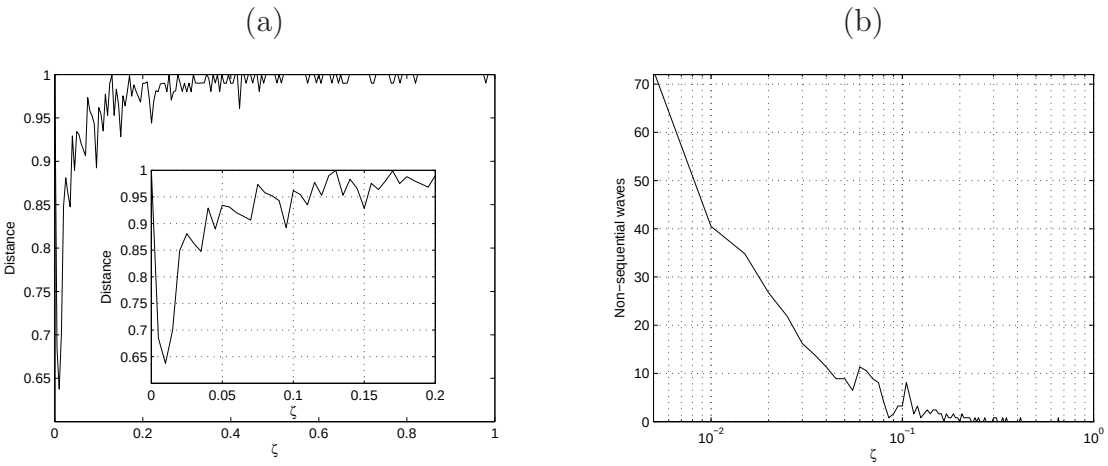

Figure 4.13: Plot (a) shows the distance travelled, measured in spine number, for noise intensity, $\nu = 0.2$, as the correlation length, ζ increases, for multiplicative spatially correlated noise in the spine heads. There are 81 spines along the length of the cable. Plot (b) shows the number of non-sequential waves as a function of the correlation scale. All other parameters are as described in the parameter list at the start of the thesis. We solve Equation (4.4) along with Equation (4.3) with temporal discretisation $\Delta t = 0.1$, $t \in [0, 70]$ and spatial discretisation $\Delta x = 0.08$, $x \in [0, 96]$ (measured in non-dimensional electronic length units) with 81 spines attached along this length. The boundary conditions used are Dirichlet and initial conditions $V(x, 0) = 0$, $U_1(0) = U_2(0) = 0.04$ and $U_{n>2} = 0$.

Additive noise in the spine heads

Here we consider additive noise in the spine heads; white, temporally and spatially correlated. We find for all forms of the additive noise, when very small, the system behaves like the deterministic case but as we increase the additive noise intensity the resulting wave defies our definition of a sequential travelling wave and we see simultaneous firing of all the spines which is reminiscent of noise induced synchrony.

We look at the mean voltage of the stochastic SDS model, with additive noise, in two regimes; first where waves travel in the deterministic case (spine spacing $d = 0.8$) and secondly where waves do not travel in the deterministic system (spine spacing $d = 1$). In Figure 4.14 noise is additive, white and added to the spine head dynamics. Each of the plots shows the average voltage for 100 realisations in space and time for a cable of length 48 units studded with 37 spines, plot (a) has $d = 0.8$ and noise intensity $\mu = 0.001$, plot (b) $d = 0.8$, $\mu = 0.01$, plot (c) $d = 0.8$, $\mu = 0.1$ and plot (d) $d = 1$ and $\mu = 0.1$. The x-axis shows the space domain, the y-axis the time domain and the colour of the plot shows how strong the voltage is at each point in time and space. The dark blue background is the resting state of the system 0 volts and as the colour changes through green, to yellow and to a strong red, the voltage is increasing; for example in plot (a) of Figure 4.14 the bright horizontal red patch seen at approximately $(2, 0)$ is the voltage produced from the first two spines firing together

due to the initial condition that they both start with a voltage slightly above the firing threshold h. The wave then moves in a saltatory fashion from one spine to the next, bringing each one successively to threshold and that results in a pulse being injected to the cable which is seen on the plot as a bright red 'dot'. Each 'dot' is slightly further ahead in space, centred on the position of the spines, and in time since there is a delay as the wave diffuses along the cable to the next spine. The final result is a chain of 'dots' sloping upwards on the plot; the steeper the gradient the slower speed of the wave, likewise the shallower the gradient the faster the speed of the wave. As can be seen in the plot (a) of Figure 4.14, a small intensity of additive noise ($\mu = 0.001$) does not change the behaviour, to the eye, from that of the deterministic case, we still get full propagation of the travelling waves. As we increase the noise as in in plot (b), $\mu = 0.01$, we see that the mean voltage at the end of the cable is lower than plot (a), as shown by the colour bar, and so we can deduce that fewer than all 100 waves are successful, i.e. some of the realisations do not reach the end of the cable. Therefore the increase in noise halts the propagation of the travelling wave. Increasing the noise to $\mu = 0.1$, as in plot (c), only leads to the spines firing simultaneously, shown by the near horizontal 'wave' and now the average 'wave' shown holds no meaning, i.e. the propagation becomes instantaneous and so the spines at the end of the cable are not reacting to the input (the firing is noise induced). This defies our definition of a propagating wave which requires sequential firing. Finally plot (d) shows the mean voltage in the regime which has no propagation in the deterministic case, and we see purely noise induced phenomena where again the 'wave' travels instantly. In Figure 4.14 the simultaneous firing in plot (c) and (d) can be thought of as noise induced synchronisation since the noise brings the spine to threshold simultaneously, see [77] and [76] which shows the same effect, also called synchronisation, in a network of IF neurons. Although we do not investigate this behaviour here, it is an interesting effect.

For a small range of noise intensities, $\mu \in [0, 0.01]$, we look at the speed of the waves, see Figure 4.15. We look only at this small range since at higher values of μ the noise induces synchrony in the spine head firing. The speed obtained may be very large $c \to \infty$, or negative if the spines near the end of the cable fire before the spines at the beginning of the cable, which is possible at higher noise intensities when the firing is purely noise induced. Figure 4.15 shows that as the noise intensity increases the waves slow down but that they travel non-sequentially for a noise intensity $\mu \geq 0.0016$. There is only a small range of noise intensities, for white additive noise, over which travelling waves exist, so it seems that this type of noise is detrimental to the waves in the SDS model.

The behaviour of the SDS model with additive temporally correlated noise in the spine heads is the same as for the white noise case. The sequential travelling waves

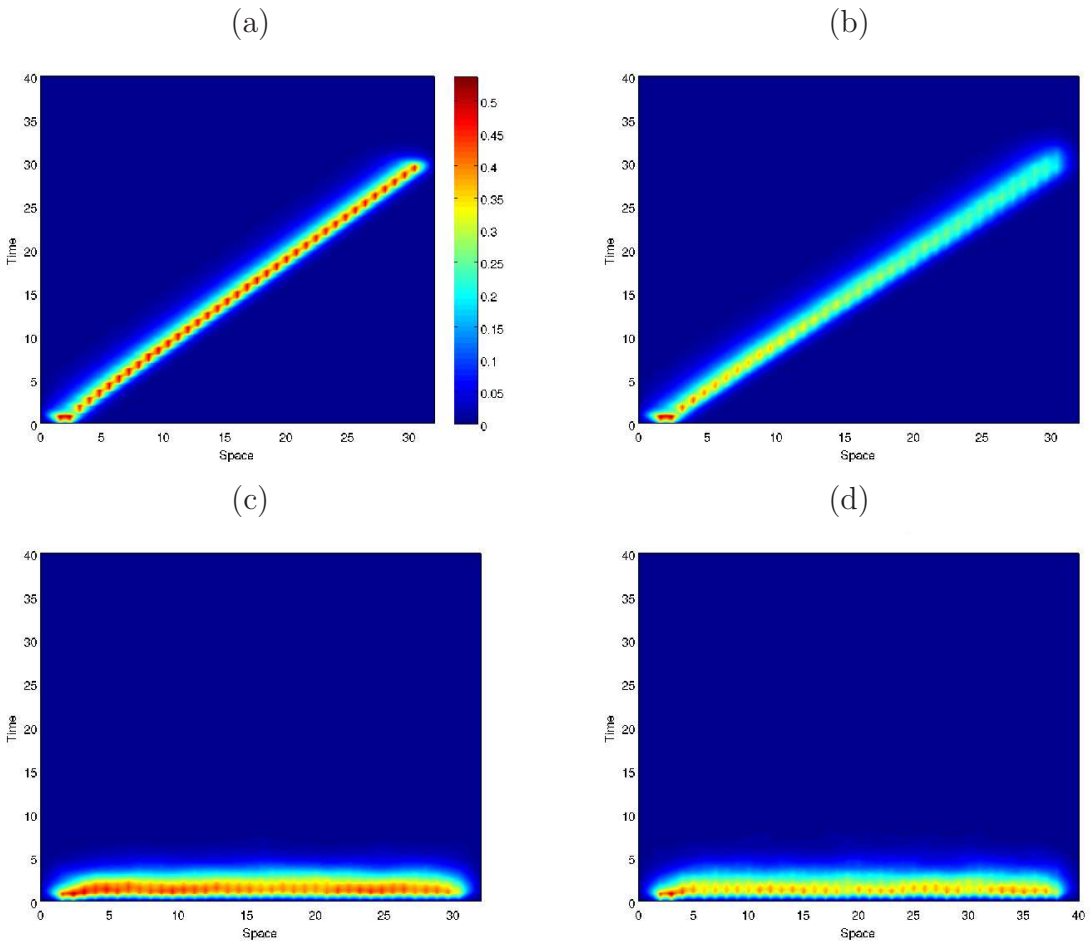

Figure 4.14: This figure shows the, mean voltage in the cable for different strengths of white additive noise in the spine heads, the colour bar shows the scale for the voltage. Plot (a) has spine spacing $d = 0.8$, noise intensity $\mu = 0.001$ and shows a strong travelling wave. Plot (b) has $d = 0.8$, $\mu = 0.01$ and the colour (and so the voltage) is weaker towards the end of the cable which means that not all of the 100 waves travel to the end of the cable, the noise inhibits propagation. Plot (c) has spine spacing $d = 0.8$, $\mu = 0.1$ and the wave is now showing simultaneous firing of all the spines or noise induced synchronisation. Plot (d) has spine spacing $d = 1$ and $\mu = 0.1$ and again the spines fire simultaneously, but here the phenomena is entirely noise induced since without the noise no wave exists. This shows that when the additive noise intensity increases, the voltage in all the spines simultaneously reach threshold and fire almost instantly, giving the impression that the wave speed is infinite.All other parameters are as described in the parameter list at the start of the thesis. We solve Equation (4.4) along with Equation (4.1) with temporal discretisation $\Delta t = 0.1$, $t \in [0, 70]$ and spatial discretisation $\Delta x = 0.08$, $x \in [0, 48]$ (measured in non-dimensional electronic length units) with 37 spines attached along this length. The boundary conditions used are Dirichlet and initial conditions $V(x, 0) = 0$, $U_1(0) = U_2(0) = 0.04$ and $U_{n>2} = 0$.

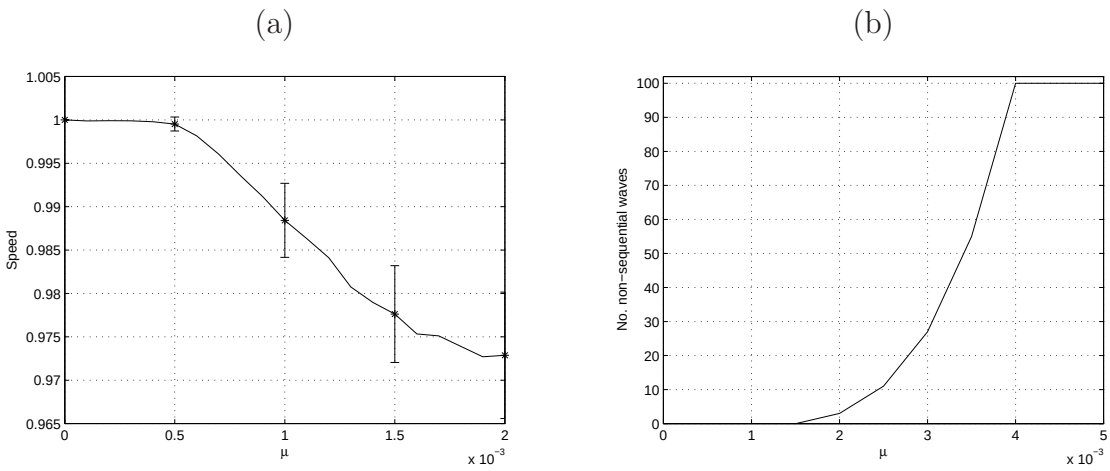

Figure 4.15: Plot (a): Speed of successful waves measured using the level-set method with white additive noise in the spine heads, $d = 0.8$. Plot (b): Number of waves that fail, i.e. number of waves where the spines fire out of order. It can been seen that the noise slows the wave and that very small levels of noise intensities lead to non-sequential waves. All other parameters are as described in the parameter list at the start of the thesis. We solve Equation (4.4) along with Equation (4.1) with temporal discretisation $\Delta t = 0.1$, $t \in [0, 70]$ and spatial discretisation $\Delta x = 0.08$, $x \in [0, 96]$ (measured in non-dimensional electronic length units) with 81 spines attached along this length. The boundary conditions used are Dirichlet and initial conditions $V(x, 0) = 0$, $U_1(0) = U_2(0) = 0.04$ and $U_{n>2} = 0$.

only exist over a short range of noise intensities since the noise induces synchrony and the speed is reduced, just as in the white noise case. When the noise is spatially correlated the speed also decreases with increasing noise intensity but the correlation scale can promote sequential firing at a noise intensity where the spines fire out of order under the influence of white or temporally correlated noise. Figure 4.16 shows the voltage in the cable when there is spatially correlated noise in the spine heads at the same level of noise intensity, $\mu = 0.02$, but two different correlation lengths. Plot (a) has a correlation scale of $\zeta = 0.01$ and shows disordered firing of the spines since there is no coherent travelling wave. The higher voltage at the top of the plot is purely noise induced since there is no further external input, after the initial condition of the first two spines being above threshold. Plot (b) has a correlation scale of $\zeta = 3$ and shows a travelling wave with sequentially firing spines, it would seem that the longer correlation scale helps the system support travelling waves at higher noise levels then can be supported when the noise in the system is white. The spatially correlated noise has a positive effect on the stochastic SDS model, restoring sequential firing at a noise intensity where the white noise destroys the travelling wave. As the noise intensity continues to increases, no increase in correlation scale can restore the sequential firing and the synchronously firing behaviour dominates.

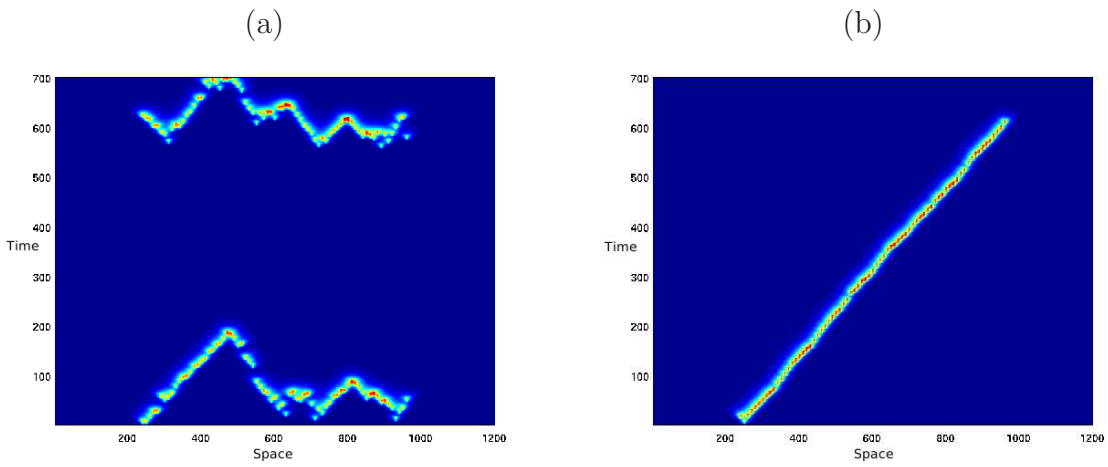

Figure 4.16: The plots above show the voltage in the cable for a spatially correlated noise in the spine heads with intensity of $\mu = 0.02$. Plot (a) has a correlation scale of $\zeta = 0.01$ and shows disordered waves with the spines firing out of order. Plot (b) has a correlation scale of $\zeta = 3$ and shows a travelling wave that has sequential spine firing. The longer correlation scale restores the sequential firing that the higher noise intensity destroys. All other parameters are as described in the parameter list at the start of the thesis. We solve Equation (4.4) along with Equation (4.3) with temporal discretisation $\Delta t = 0.1$, $t \in [0, 70]$ and spatial discretisation $\Delta x = 0.08$, $x \in [0, 96]$ (measured in non-dimensional electronic length units) with 81 spines attached along this length. The boundary conditions used are Dirichlet and initial conditions $V(x, 0) = 0$, $U_1(0) = U_2(0) = 0.04$ and $U_{n>2} = 0$.

4.4.2 Noise in the cable equation

As in Section 4.4.1 we look at the distance travelled and speed of travelling waves in the SDS model but now we will consider noise in the cable equation and deterministic integrate and fire dynamics in the spine heads. We find that the behaviour of the system under the influence of noise in the cable has the same behaviour as the system with noise in the spine heads. We see the decrease in wave speed with an increase in multiplicative noise strength and random firing of the spines when the noise is additive. The only difference to the cases where the noise is in the spine heads is that there seems to be no noise induced synchrony, as the additive noise intensity increases the voltage seems to have no pattern, i.e. no synchronised firing, only random fluctuations as the intensity becomes large enough to overcome the deterministic behaviour. The type of noise (white, temporally/spatially correlated) has no effect on the overall behaviour observed, although the correlation scales in the temporally and spatially correlated noise can affect the exact value of the speed of the waves .

Multiplicative noise

The voltage in the cable should be in the range $V \in [0, 1]$, as for the spine head voltage, so once again we use the form of the multiplicative noise which will preserve

this range of values, $g(V) = V(1-V)$ when $V \in [0,1]$ and zero otherwise. We can see from Figure 4.17 that as the intensity of white noise in the cable increases the distance travelled along the cable (measured in spine number) decreases. The type of noise

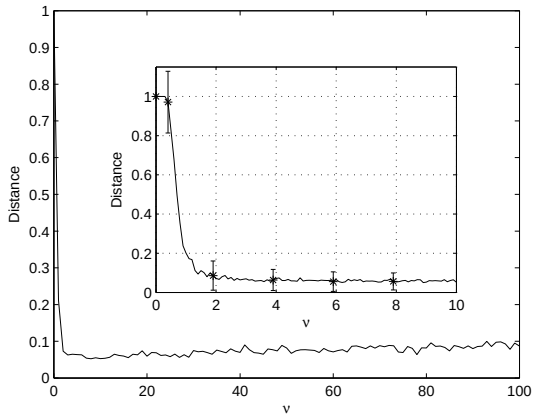

Figure 4.17: This figure shows the distance travelled, measured in spine number, as the noise intensity increases for white multiplicative noise in the cable. There are 81 spines along the length of the cable. All other parameters are as described in the parameter list at the start of the thesis. We solve Equation (4.4) along with Equation (4.1) with temporal discretisation $\Delta t = 0.1$, $t \in [0, 70]$ and spatial discretisation $\Delta x = 0.08$, $x \in [0, 96]$ (measured in non-dimensional electronic length units) with 81 spines attached along this length. The boundary conditions used are Dirichlet and initial conditions $V(x, 0) = 0$, $U_1(0) = U_2(0) = 0.04$ and $U_{n>2} = 0$.

does not effect this behaviour, see Figure 4.18 which shows that as noise intensity increases the distance travelled by the wave decreases for both temporally correlated, plot (a), and spatially correlated, plot (b), noise. The error bars on these plots are large at mid range noise since there is a large trial-to-trial variability in the distance travelled but at higher noise levels the variation is smaller since the higher noise kills nearly all propagation. The speed of the travelling waves that exist when there is a small amount of noise in the cable slow down as the noise intensity increases. Again this happens for all types of noise, as can be seen in Figure 4.19; plot (a) shows the speed as a function of noise intensity for space time white noise, plot (b) shows the speed of the waves for temporally correlated noise and finally plot (c) shows the speed as a function of the noise intensity of spatially correlated noise. In plot (c) the range of noise intensities is larger since the spatially correlated noise, at the correlation scale chosen, $\zeta = 1.25$, sustains sequential travelling waves for a larger intensity than the white noise case. We look at the speed of the waves for a fixed level of noise but with a changing correlation scale, in both the temporally and spatially correlated cases. When the cable is effected by the temporally correlated noise we chose the noise intensity to be $\nu = 0.4$ and varied the correlation time scale, $\beta \in [0, 10]$. As β increases the speed of the wave increases just as was observed when the noise was in

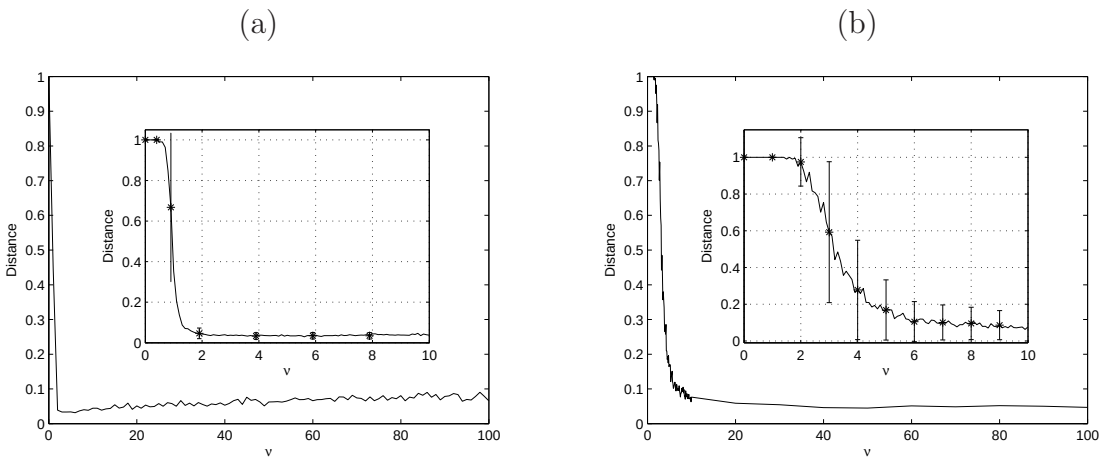

Figure 4.18: Plot (a) shows the distance travelled, measured in spine number, as the noise intensity increases for temporally correlated, $\beta = 2$, multiplicative noise in the spine heads and plot (b) shows the mean distance travelled by a wave when the noise is spatially correlated, $\zeta = 1.25$. All other parameters are as described in the parameter list at the start of the thesis. We solve Equation (4.4) along with Equation (4.2) (plot (a)) and Equation (4.3) (plot(b)) with temporal discretisation $\Delta t = 0.1$, $t \in [0, 70]$ and spatial discretisation $\Delta x = 0.08$, $x \in [0, 96]$ (measured in non-dimensional electronic length units) with 81 spines attached along this length. The boundary conditions used are Dirichlet and initial conditions $V(x, 0) = 0$, $U_1(0) = U_2(0) = 0.04$ and $U_{n>2} = 0$.

the spine heads, see plot (a) in Figure 4.20. Plot (b) of Figure 4.20 shows that the speed of the wave stays almost constant as the spatial correlation increases, although the increase in correlation scale does reduce the variability.

4.5 Conclusions

We have considered the effects of different types of noise on the propagation of a saltatory travelling wave along a length of spiny dendritic tissue modelled by the SDS model. To compare the effects of the white, temporally correlated and spatially correlated noise we looked at the distance that a wave travels along the cable, the speed of any travelling wave and the number of non-sequential firing of the spines at different levels of noise intensity. We find that the SDS model of dendrites is robust to small levels of noise.

We have shown that in the regime where the deterministic system supports travelling waves, spine spacing $d = 0.8$, all multiplicative noise, in either the spine heads or the cable, reduces the speed of any travelling wave: Figure 4.3 shows the speed with white noise in the spine heads, Figure 4.10 temporally correlated noise in spine heads, Figure 4.12 plot (b) shows speed with spatially correlated noise in spine heads and Figure 4.19 shows all types of noise in the cable. In addition the form of the multiplicative noise does not affect this behaviour, we used four forms of $g(U)$ which all

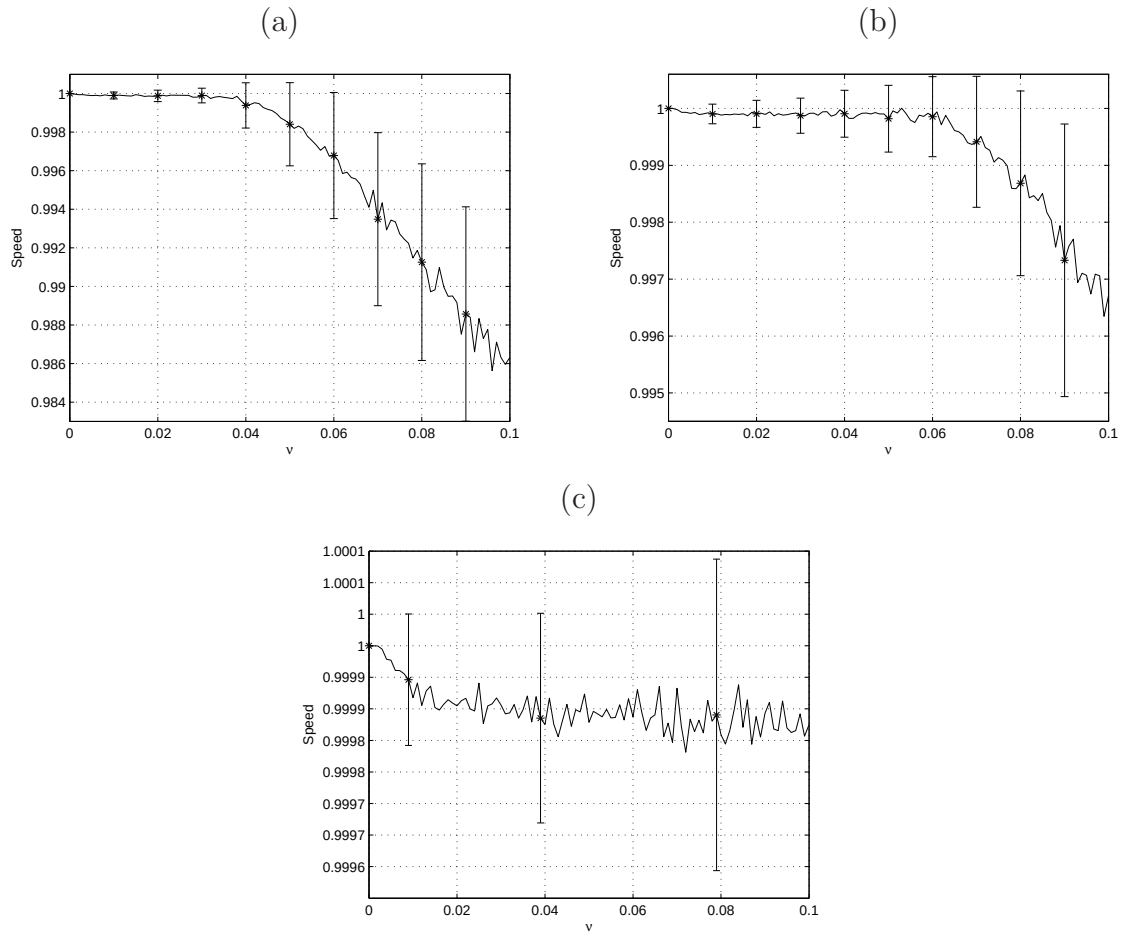

Figure 4.19: Plot (a) shows the mean speed of a wave travelling in the cable with white noise present, as the noise intensity increases the speed reduces. Plot (b) shows the speed of the wave decreasing as the noise intensity increases for temporally correlated noise with $\beta = 2$ and finally plot (c) shows the wave speed decreasing as the intensity of the spatially correlated noise increases, $\zeta = 1.25$. All other parameters are as described in the parameter list at the start of the thesis. We solve Equation (4.4) along with Equation (4.1) (plot (a)), Equation (4.2) (plot (b)), and Equation (4.3) (plot (c)) with temporal discretisation $\Delta t = 0.1$, $t \in [0, 70]$ and spatial discretisation $\Delta x = 0.08$, $x \in [0, 96]$ (measured in non-dimensional electronic length units) with 81 spines attached along this length. The boundary conditions used are Dirichlet and initial conditions $V(x, 0) = 0$, $U_1(0) = U_2(0) = 0.04$ and $U_{n>2} = 0$.

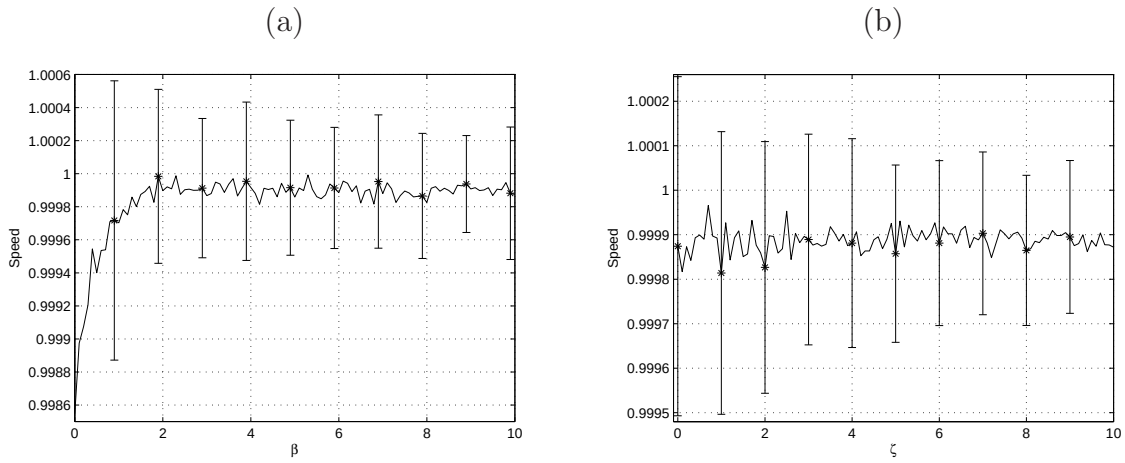

Figure 4.20: Plot (a) shows the mean speed of a wave travelling in the cable as the temporal correlation scale increases, this slows the wave down. Plot (b) shows the speed of the wave is constant as the spatial correlation length increases. All other parameters are as described in the parameter list at the start of the thesis. We solve Equation (4.4) along with Equation (4.2) (plot (a)) and Equation (4.3) (plot (b)) with temporal discretisation $\Delta t = 0.1$, $t \in [0, 70]$ and spatial discretisation $\Delta x = 0.08$, $x \in [0, 96]$ (measured in non-dimensional electronic length units) with 81 spines attached along this length. The boundary conditions used are Dirichlet and initial conditions $V(x, 0) = 0$, $U_1(0) = U_2(0) = 0.04$ and $U_{n>2} = 0$.

reduced the speed of the travelling wave as the intensity of the noise increased. Figure 4.3 plot (a) shows the speed for $g(U) = U^2$, plot (b) $g(U) = U$, plot (c) $g(U) = \sqrt{U}$ and plot (d) $g(u) = U(1 - U)$ when $U \in [0, 1]$ and zero otherwise. All of these plots show the decrease in speed as intensity increases albeit over slightly different ranges of intensities. The correlation scales of the OU noise and the spatially correlated noise have little effect on the behaviour of the speed of the travelling wave. We expected 'special' values of the the temporal scale β and spatial scale ζ since the system has natural scales in the refractory time, τ_R, and the spine spacing d. We find however that there is no one value of either β or ζ that stands out. In the spine heads as the temporal correlation scale, Figure 4.11, increases the speed of the wave, for a fixed level of noise intensity, also increases although the speed levels off as β increases but never reaches the value of the deterministic wave speed. The spatial correlation ζ makes no difference to the speed of the waves. In the cable (Figure 4.20), as β increases the speed again increases and the increase in spatial correlation ζ, makes little difference to the speed of the wave.

The spatial correlation has a very interesting affect on the behaviour of the noisy SDS model when the noise is additive in the spine heads. Although there is not one 'special' value it does seem that longer correlation lengths do produce some special behaviour. Figure 4.16 shows two plots of the voltage in cable of the SDS model under the influence of spatially correlated additive noise in the spine heads with the same

intensity. Plot (a) shows that at a short correlation length $\zeta = 0.1$ the spines fire in a random fashion but as the correlation scale increases in plot (b) $\zeta = 3$ the wave is restored. This effect of increasing the correlation scale will only restore the wave for certain levels of noise, at a certain point the strength of the noise will overcome the effect of the correlation scale and the spines will once again fire randomly. This effect could be of interest in dendritic democracy since the noise can be thought of as a correlated input to the spines and as the correlation scale increases the signal which starts at the distal end of the dendrite is successful in reaching the proximal end; when the correlation scale is small or non-existent (white noise) then input at a distal spine does not reach the proximal end.

All additive noise in the system in the spines can induce synchrony (see [77] and [76] for other examples of this phenomena in IF neurons). At very small levels of additive noise the spines fire sequentially and the speed of the wave decreases with the increase in intensity, Figure 4.15 plot (a) shows the speed as the intensity increases and plot (b) shows the number of waves that have spines firing out of order. Figure 4.14 shows the voltage in the cable which indicates that the spines fire simultaneously as the additive noise intensity increases. This behaviour occurs in both the regime where a deterministic wave travels $d = 0.8$ and when the deterministic system does not support waves $d = 1$, in this case the system is showing some noise induced synchrony. The distance travelled by the waves decreases as the noise intensity increases; Figure 4.4 shows that the noise kills propagation as multiplicative noise intensity increases. Plots (a) and (b) shows the distance travelled for noise of the form $g(U) = U^2$ in $d = 0.8$ and $d = 1$ regimes respectively, for this form of the noise mid levels of noise kill the propagation and high levels of noise appear to induce propagation again. At high levels however these 'waves' are really synchronous firing so the distance measured is that of full propagation. Plots (c) and (d) are for $g(U) = U(1-U)$ again in the two regimes $d = 0.8$ and $d = 1$, here noise kills the propagation for $d = 0.8$ and again appears to induce some firing in the $d = 1$ case, although this firing is random. Figure 4.5 shows the distance travelled over a small range of multiplicative white noise intensities $\nu \in [0, 0.5]$ and shows that waves are only sequential over a small range $\nu \in [0, 0.1]$ and by $\nu = 0.5$ almost all the waves are out of order. This is also the case for the different forms of noise.

The SDS model is robust to small ranges of both additive and multiplicative noise intensities of all forms. In this small range of noise intensities the waves that travel along the model dendrite make it to the end of the cable and they do so by sequential firing of all the spines. As the intensity of the noise increases the speed of the waves decreases. As the noise intensity increases beyond this small range the spines start to fire out of order and eventually fire synchronously. Correlated noise makes no difference to this overall behaviour except in the case of small additive spatially

correlated noise where the correlation scale can restore sequential firing where white noise produces random behaviour.

Chapter 5

Noise in the Baer and Rinzel model

5.1 Introduction

The Baer and Rinzel model of spiny dendritic tissue couples an active continuum of spines to a diffusive cable as described in Equation (2.34) to Equation (2.38) in Section 2.7. The spine dynamics are modelled by the Hodgkin-Huxley equations and the diffusive cable by the passive cable equation, both described in Chapter 2. In this chapter we investigate the inclusion of noise to the system and how it effects the propagation of travelling waves; we do this by looking at the distance travelled by the travelling wave, the number of failed waves and at the speed of propagation. In direct simulation of the system we use both the Itô and Stratonovich interpretations of the stochastic integral and investigate the differences in the observed dynamics that these two interpretations bring about. In the Stratonovich interpretation the multiplicative noise term gives rise to an extra contribution to the systematic dynamics of the model (due to the non zero mean) and so in the small noise limit gives behaviour which differs from the deterministic behaviour. In this small noise case we use AUTO-07P, [20], to explore the existence of travelling waves in parameter space and see how noise changes the regions of parameter space where these waves exist.

5.2 The stochastic model

To introduce the noise in the BR model we can look at adding a noise term into the HH current equation, the m, n, h evolution equations or into the cable equation. This noise term can the be additive or multiplicative and the noise itself may be white in time and space or correlated temporally or spatially (as we saw in the SDS model, Chapter 4). We add noise to the basic BR equations, Equation (2.34) to Equation

(2.38), to obtain the stochastic BR equations as follows:

$$C\frac{\partial V}{\partial t} = -g_L(V-V_L) + \frac{1}{r_a \pi d}\frac{\partial^2 V}{\partial x^2} + \rho\frac{U-V}{r} + (\mu_c + \nu_c g_c(V))\frac{\partial W(x,t)}{\partial t} \quad (5.1)$$

$$\hat{C}\frac{\partial U}{\partial t} = g_K n^4(V_K - U) + g_{Na}hm^3(V_{Na}-U) + g_L(v_L - U) - \frac{U-V}{r} + (\mu_H + \nu_H g_H(U))\frac{dW(x,t)}{dt} \quad (5.2)$$

$$\frac{dX}{dt} = \alpha_X(1-X) - \beta_X X + (\mu_X + \nu_X g_X(X))\frac{dW(x,t)}{dt}\ , \quad (5.3)$$

where $X \in [m,n,h]$, the μ's give the strength of additive noise and the ν's the strength of the multiplicative noise and W is a Wiener process chosen to satisfy the form of noise we require, i.e. white or correlated. Note that the equations for $X \in [m,n,h]$ and U are coupled together, at each point in space, by the cable or by the noise if it is spatially correlated. If we choose to have multiplicative noise the form of the function g, in each of the equations must be chosen properly to ensure the fluctuations are added correctly to the resting state of V, U and X ,$X \in [m,n,h]$. The functions, g_c and g_H, for both the voltage in the cable and in the HH current equation, preserve the resting voltage and so $g_c(V)$ and $g_H(U)$ are chosen such that the fluctuations are around the rest state of -65 V. As for the m, n, h equations we need to ensure the values remain in the range $[0,1]$ since they are probabilities. With these considerations in mind we choose the functions of the multiplicative noise to be:

$$g_c(V) = -(65+V)$$

$$g_H(U) = -(65+U)$$

$$g_X(X) = X(1-X)\ .$$

We can consider $dW(x,t)$ as either white, temporally correlated (through the OU process) or spatially correlated as in Section 3.1. We also need to decide if we wish to interpret the stochastic integral in the Itô or Stratonovich fashion. After choosing our form of noise we need to then numerically solve the resulting stochastic system using either the Euler-Maruyama or Heun algorithms, see Section 3.3, to give us the results of Itô and Stratonovich calculus respectively.

5.2.1 Small noise in the BR model

We can use a small noise expansion of the stochastic BR model, Equation (5.1) to Equation (5.3), to evaluate the behaviour of the system without having to simulate

or solve any stochastic integrals. This approach follows the working of [30] and [32]. The expansion is a standard perturbation approach, using Taylor's theorem; consider the working for a simple SDE:

$$dx = a(x)dt + \epsilon b(x)dW \ . \tag{5.4}$$

We will assume that the solution can be written as follows:

$$\begin{aligned} x(t) &= x_0(t) + \epsilon x_1(t) + \epsilon^2 x_2(t) + ... \\ &= x_0(t) + \sum_{m=1}^{\infty} \epsilon^m x_m \ . \end{aligned}$$

We also can write the coefficients:

$$\begin{aligned} a(x) &= a_0(x_0) + \epsilon a_1(x_0, x_1) + \epsilon^2 a_2(x_0, x_1, x_2) + ... \\ &= a\left(x_0(t) + \sum_{m=1}^{\infty} \epsilon^m x_m\right) \text{ using Taylor's expansion,} \\ &= \sum_{p=0}^{\infty} \frac{1}{p!} \frac{d^p a(x_0)}{dx_0^p} (\sum_{m=1}^{\infty} \epsilon^m x_m)^p \\ &= a(x_0) + \frac{da(x_0)}{dx_0} (\sum_{m=1}^{\infty} \epsilon^m x_m) + \frac{1}{2} \frac{d^2 a(x_0)}{dx_0^2} (\sum_{m=1}^{\infty} \epsilon^m x_m)^2 + ... \ . \end{aligned}$$

We do the same for $b(x)$, then substitute all these expansions into the original SDE, Equation (5.4), and equate terms with like powers of ϵ, to get to the zeroth order approximation of the SDE:

$$dx_0 = a(x_0)dt \ ,$$

and to the first order:

$$dx_1 = -\frac{da(x_0)}{dx_0} x_1 dt + b(x_0)dW \ .$$

Clearly the zeroth order gives us the deterministic part of Equation (5.4) and the first order gives us another SDE and so it would be just as easy to numerically solve the original SDE if this new SDE is no simpler. This expansion is only valid if $b(x)$ is a constant, i.e. additive noise, since the mean of an additive noise term is zero. This expansion is consistent with results we found in the SDS model Section 4.4, where a small amount of additive noise proved to have no/little effect and therefore the model behaved as the deterministic model. Likewise later in this chapter we will see that

small additive noise in the system does not change the behaviour from that of the deterministic BR model.

In the Stratonovich interpretation, for multiplicative noise we have a non-zero mean and so need to adjust the mean of the noise term before we can apply a similar approach. In the case of a noise which is multiplicative, white in time and correlated in space, we can evaluate the mean of the noise term and re-write the SPDE with a zero-mean noise term. For the following, general Stratonovich SPDE (as in Section 3.1):

$$\partial X = \left(\frac{\partial^2 X}{\partial x^2} + f(X) \right) \partial t + \nu g(X) \circ dW \ , \tag{5.5}$$

we can evaluate the mean of the noise term using Novikov's theorem ([78]) and follow the working set out is [30] to get: $\langle g(X) dW(x,t) \rangle = \nu F_c(0) \langle g(X) g'(X) \rangle$. Where $F_c(0)$ is the correlation function (see Section 3.1.1) evaluated at 0, (F_c is used here since the symbol C is already in use for the capacitance). We can then use this mean to re-write Equation (5.5) thus:

$$\partial X = \left(\frac{\partial^2 X}{\partial x^2} + f(X) + \nu S \right) \partial t + \nu (g(X) \circ dW(x,t) - S \partial t) \ ,$$

where, $S = \nu F_c(0) g'(X) g(X)$. Now we can apply the perturbation expansion as above to get the zeroth order approximation:

$$\frac{\partial X_0}{\partial t} = \frac{\partial^2 X_0}{\partial x^2} + f(X_0) + \nu^2 F_c(0) g'(X) g(X) \ .$$

In this instance instead of obtaining the deterministic equation we retrieve an altered equation, of the zeroth order, which has no stochastic term in it but which has some dependence on the noise strength and correlation function, [30]. Using these techniques on the BR equations, Equation (5.1), with the form of multiplicative noise given we can find the following zeroth order approximations:

$$C \frac{\partial V}{\partial t} = -g_L (V - V_L) + \frac{1}{r_a \pi a} \frac{\partial^2 V}{\partial x^2} + \rho \frac{U - V}{r} - \nu_c^2 F_c(0)(65 + V) \ , \tag{5.6}$$

$$\begin{aligned} \hat{C} \frac{\partial U}{\partial t} &= g_K n^4 (V_K - U) + g_{Na} h m^3 (V_{Na} - U) + g_L (V_L - U) - \frac{U - V}{r} \\ &- \nu_H^2 F_c(0)(65 + U) \ , \end{aligned} \tag{5.7}$$

$$\frac{dX}{dt} = \alpha_X (1 - X) - \beta_X X + \nu_X^2 F_c(0) X (1 - 3X + 2X^2) \ . \tag{5.8}$$

The use of Novikov's theorem to adjust the mean of the Stratonovich SPDE can be described as a drift correction which results in an Itô SPDE, where the mean is zero,

and the small noise expansion yields the mean behaviour in X_0.

5.3 Simulation

This section looks at the simulations carried out on either the full system, in Matlab, or on the reduced small noise system, in AUTO-07P. We describe here how the simulation was carried out and how we measured the effects of the noise.

5.3.1 Discretisation in space and time for stochastic BR model

We follow the numerical methods in Chapter 3, to simulate the stochastic BR model in both the Itô and Stratonovich interpretations of the stochastic integral. Here we give the discretised versions of Equation (5.1) to Equation (5.3). Implementing a semi-implicit Euler-Maruyama scheme we get the following equations for the discretised BR model. Here the subscript j's correspond to the value of the voltages, V, U and m, n, h variables at spatial point x_j if there is a spatial mesh $x_0, x_1, \ldots, x_J$ with step size Δx, i.e. $j = 1, 2, \ldots, J$ $J = \frac{L}{\Delta x}$, where L is the length of the cable. Also the superscript n relates to V, U and m, n, h variables being evaluated at time t_n with a temporal mesh $t_0, t_1, \ldots t_N$ of step size Δt, $n = [1, 2, \ldots, N]$, T is the final time and $N = \frac{N}{\Delta t}$, so $V_j^{n+1} = V(x_j, t_{n+1})$. First the cable equation:

$$\begin{aligned} V_j^{n+1} &= V_j^n + \Delta t f(V_j^n) + (\mu_c + \nu_c g(V_j^n))\Delta W_j^n \qquad (5.9) \\ f(V_j^n) &= \frac{1}{C}\left(\frac{V_{j+1}^n - 2V_j^n + V_{j-1}^n}{r_a \pi a \Delta x^2} + \frac{\rho}{r}(U_j^{n+1} - V_j^{n+1}) + (G_L(V_L - V_j^{n+1}))\right) . \end{aligned}$$

The discretised m, n, h equations, with $X \in [m, n, h]$:

$$\begin{aligned} X_j^{n+1} &= X_j^n + \Delta t \left(\alpha_X(U_j^n) - \alpha_X(U_j^n)X_j^{n+1} - \beta_X(U_j^n)X_j^{n+1}\right) \\ &+ (\mu_X + \nu_X g(X_j^n))\Delta W_j^n. \qquad (5.10) \end{aligned}$$

And finally the discretised equation for the voltage in the spine heads:

$$\begin{aligned} U_j^{n+1} &= U_j^n + \frac{\Delta t}{\hat{C}}(G_K(n_j^{n+1})^4(V_K - U_j^{n+1}) + G_{Na}h_j^{n+1}(m_j^{n+1})^3(V_{Na} - U_j^{n+1}) \\ &+ G_L(V_L - U_j^{n+1})) + \frac{V_j^n - U_j^{n+1}}{r}) + (\mu_H + \nu_H g(U_j^n))\Delta W_j^n . \qquad (5.11) \end{aligned}$$

When we use the Heun method to evaluate the voltage in the cable, we must have an extra discretised equation. In the Heun method we have a predictor step, for which we can use Equation (5.9). Therefore we call this step $\tilde{V}_j^{n+1}$ and for ease of reading

call $f(V_j^n) = \left(\frac{V_{j+1}^n - 2V_j^n + V_{j-1}^n}{\Delta x^2} + \frac{\rho}{Cr}(U_j^{n+1} - V_j^{n+1} + \frac{1}{c}(G_L(V_L - V_j^{n+1})))\right)$ and use it in the Heun step of the numerical integration as such:

$$V_j^{n+1} = V_j^n + \frac{\Delta t}{2}\left(f(V_j^n) + f(\tilde{V_j^n})\right) + \mu_c dW_j^n + \frac{1}{2}(\nu_c g(V_j^n) + \nu_c g(\tilde{V_j^n}))\Delta W_j^n. \quad (5.12)$$

Equation (5.12) is one of the Heun steps and there will be one for each of X, $X \in [m, n, h]$ and U with Equation (5.10) and Equation (5.11) as the predictor steps respectively. We now have a discretised system which can be used to evaluate the voltage in the cable, the spines and the values of the m, n, h variables, for all of our space and time domains and we can choose the method of evaluating the noisy term. The voltage can then be used as outlined in Chapter 3 to measure the speed using the level set method, of a travelling wave and get an average speed, over a number of realisations, of stochastic waves. The only difference in using the level-set method here, compared with the SDS case, is that the 'level' that the wave must cross has a different value since the voltage is on a different scale. We then investigate how the noise intensity and noise type effect the value of the speed of any propagating waves.

5.3.2 Zeroth order approximation of stochastic BR model in the travelling wave frame

As well as the simulation of the full system we can look at the behaviour of the reduced, small noise system. We wish to look at the existence of the travelling waves and so we convert Equation (5.6) to Equation (5.8), into the travelling wave frame, using the standard anzatz $\xi = ct - x$, where c is the wave speed. The resulting equations are:

$$V_\xi = \hat{W} \quad (5.13)$$

$$CcV_\xi = -g_L(V - V_L) + \frac{1}{r_a \pi d}V_\xi + \rho\frac{U - V}{r} - \nu_c^2 F_c(0)(65 + V) \quad (5.14)$$

$$c\hat{C}U_\xi = g_K n^4(V_K - U) + g_{Na}hm^3(V_{Na} - U) + g_L(V_L - U) - \frac{U - V}{r} - \nu_H^2 F_c(0)(65 + U) \quad (5.15)$$

$$cX_\xi = \alpha_X(1 - X) - \beta_X X + \nu_X^2 F_c(0)X(1 - 3X + 2X^2), \quad (5.16)$$

where $X \in [m, n, h]$.

We now have six coupled ODEs, instead of a PDE and four ODEs, and we have new parameters, wave speed c and noise intensity ν. We now want to investigate how these parameters effect the travelling wave and also how the speed changes with noise

intensity, to allow a comparison with the full system.

The continuation package AUTO-07P was used to investigate the 'new' system of equations in the travelling wave frame, similar to the work in [70] for the deterministic BR model. We use the fixed point, or resting state, of the deterministic system as a starting point for the numerical continuations and search for a Hopf bifurcation (HB) in one of the many parameters in the deterministic system (for the time being the noise parameters are kept at zero). A Hopf bifurcation would lead us to a family of periodic solutions of the system. After some investigation of the parameters of the system we found a HB whilst varying the value of V_L, although this was at an unrealistic value for V_L. From this point we used a two parameter continuation with V_L and the period T of the new orbit, to track back to the correct biological value for V_L. We now have a periodic orbit for our system and the correct value of all the parameters. We can follow this new point, in ρ and T, to large period periodic orbit which is a good approximation for a homoclinic orbit. This homoclinic orbit corresponds to some of the travelling wave solutions of our original problem.

5.4 Results

Here we look at the results of the measuring the speed of the waves in the noisy BR model. First we look at the direct simulation results for all types of noise in the m-dynamics and in the cable equation. We then proceed to look at the small noise results obtained from the AUTO-07P package simulations for spatially correlated noise in the m-dynamics and the cable. We do not look at noise in the n-dynamics or the h-dynamics since the system does not seem to be very robust to noise in these equations i.e. for very small quantities of noise the BR model exhibits noise induced behaviour and random firing of the spines along the length of cable. During AUTO-07P simulation of the BR model with small noise the package was unable to perform a continuation when one of the continuation parameter was either ν_n or ν_h, even for a very small step size. Direct simulation of the system with noise in the n or h-dynamics resulted in broken, or out of order waves. Figure 5.1 shows the results of direct simulation in the n and h-dynamics and it can be seen that for a small intensity of noise the wave is out of order and eventually will fire simultaneously as the noise intensity increases. In the h-dynamics the level of noise is higher but the wave is broken up and it was also observed that no matter how strong the noise in the h-dynamics there was never any noise induced synchronous firing, or repetitive firing.

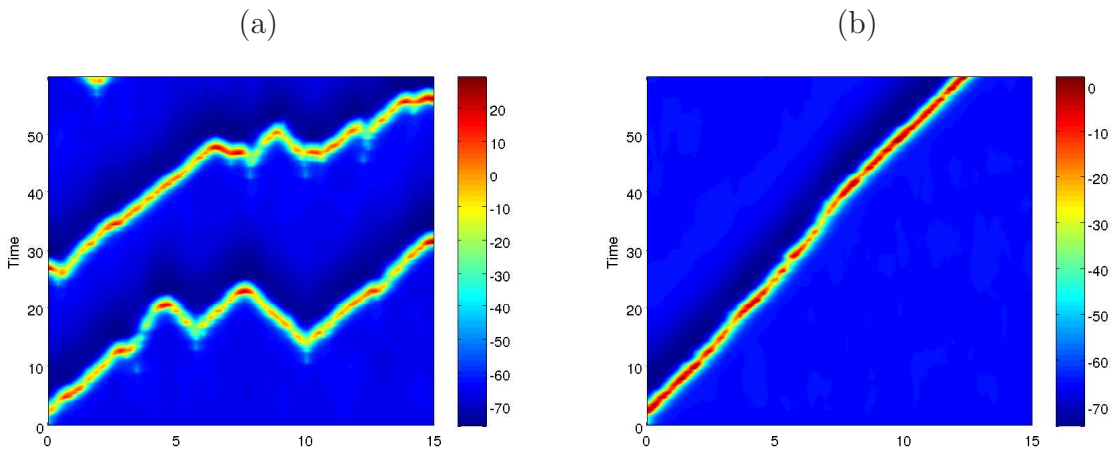

Figure 5.1: Shown here are the voltages for the cable when there is white multiplicative noise in the n dynamics, $\nu_n = 0.03$ (plot (a)) and h-dynamics $\nu_h = 0.1$(plot (b)). The waves in plot (a) show the out of order firing of the spines and plot (b) shows the broken wave. All other parameters are as described in the parameter list at the start of the thesis. We solve Equation (5.1) to Equation (5.3) with temporal discretisation $\Delta t = 0.01$, $t \in [0, 80]$ and spatial discretisation $\Delta x = 0.05$, $x \in [0, 15]$. The boundary conditions used are Dirichlet and initial conditions $V(x, 0) = -65$, $U(x_1, 0) = 10$, $U(x_{n>1}, 0) = -65$, m, n, h are initially at their rest values.

5.4.1 Direct simulation

We show the results of measuring the speed of travelling waves as the noise intensity increases, with the different types of noise considered i.e. white, temporally correlated and spatially correlated. The noise in the spines was added to the m-dynamics only since trying to use continuation of the noise parameters in AUTO-07P with noise in n, and h dynamics was unsuccessful, as mentioned. We also consider noise in the cable equation. All the simulations were generated using the Itô interpretation of the stochastic integral and so the EM method was employed, unless otherwise stated. As for the SDS model, we scale the mean speeds by the deterministic value for ease of comparison and show the variation by means of error bars on all plots which represent the standard deviation, $\pm$S.D.(X) $= \sqrt{\mathbb{E}(X^2) - (\mathbb{E}(X))^2}$.

The Figure 5.2 shows the behaviour of the speed of a travelling wave affected by white noise either in the cable or the spines. The white additive noise in the top left of the figure shows an increase in speed over a small range of noise intensities. As the noise intensity increases above $\mu_m = 0.04$ the spines start to fire randomly and out of spatial order, eventually all synchronising and so firing simultaneously. When this occurs the measured wave can approach infinite speed, or travel with negative speed if a section of spines at the end of the cable fire before the beginning of the cable. An example of this out of order firing is shown in Figure 5.3. The same effect is observed in the multiplicative case at a higher level of noise intensity. The wave begins to travel

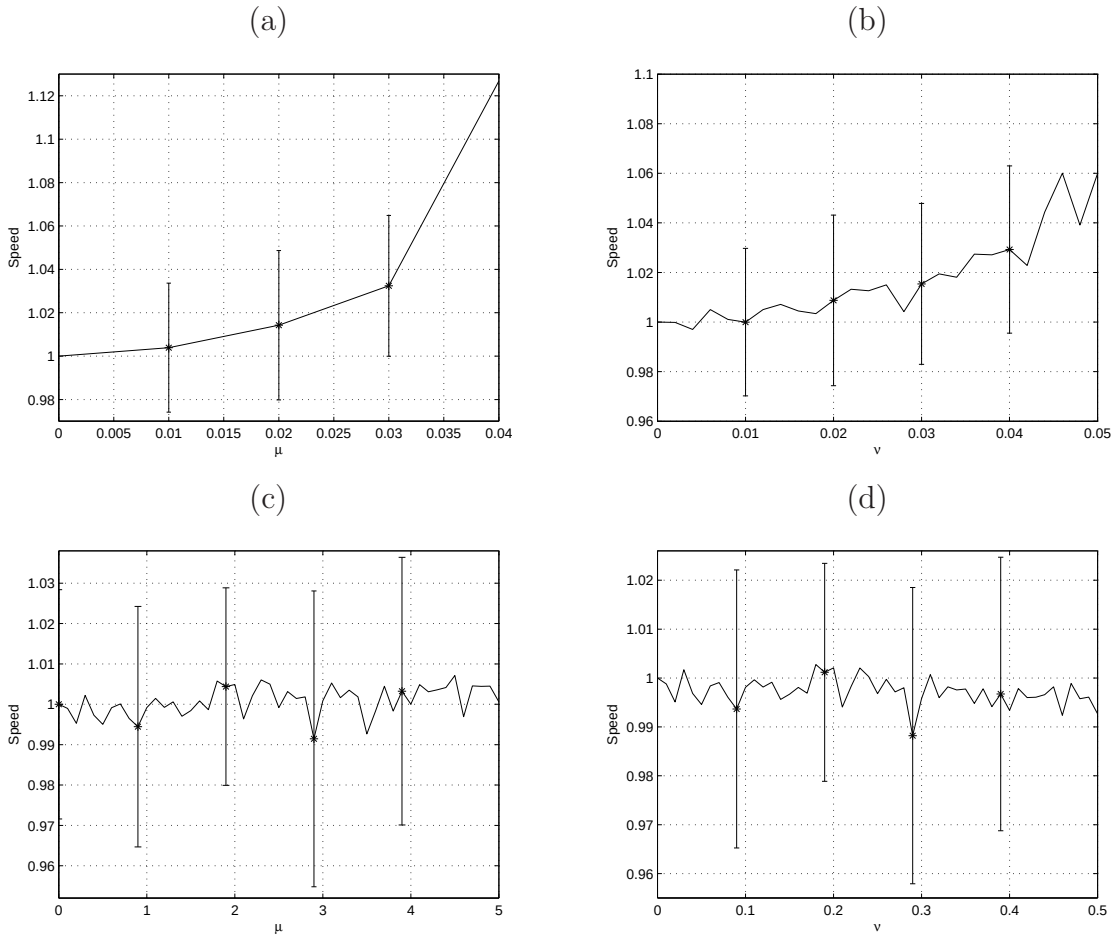

Figure 5.2: This figure shows the speed of the travelling wave in the BR model with white noise in the m-dynamicsl. Plot (a) shows that additive white noise in the spines increases the speed of the wave over a very small range of noise intensities. The sharp increase occurs as the system becomes synchronised. Plot (b) shows that multiplicative white noise in the spines also increases the speed of the wave, but over a more substantial range of noise intensities. Plot (c) shows the speed variation with additive white noise in the cable and shows very little change in the speed of the wave. Plot (d) shows multiplicative white noise in the cable and the speed stays almost constant as intensity increases. All other parameters are as described in the parameter list at the start of the thesis. We solve Equation (5.1) to Equation (5.3) with temporal discretisation $\Delta t = 0.01$, $t \in [0, 80]$ and spatial discretisation $\Delta x = 0.05$, $x \in [0, 15]$. The boundary conditions used are Dirichlet and initial conditions $V(x, 0) = -65$, $U(x_1, 0) = 10$, $U(x_{n>1}, 0) = -65$, m, n, h are initially at their rest values.

out of order and so can no longer be classified as a travelling wave, by our definition. The multiplicative noise in the spine heads also increases the speed of the wave as the noise intensity increases and the noise in the cable makes little difference to the speed of the waves. For all plots as the noise intensity increases so does the variation and so the size of the error bars. Next we look at the travelling waves as they are

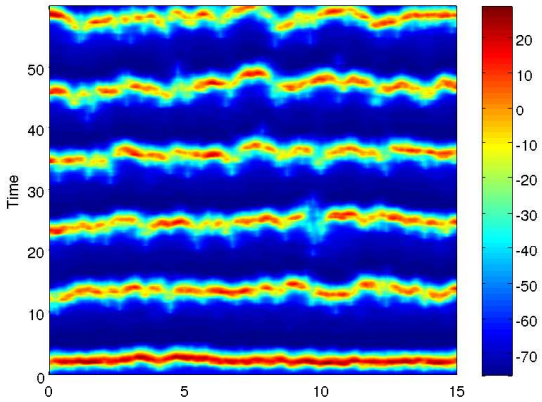

Figure 5.3: Sample of the voltage in the cable as the additive white noise in the spines increases. The spines fire in a random fashion and so defy our definition of a travelling wave, sequential firing in the spines. Here the 'wave' travels out of order and almost horizontally which implies that the speed if it were to be measured would be infinite. The presence of multiple waves is due to the natural refractory time and the random firing allowing spines to fire repetitively. The noise intensity is $\mu = 0.1$. All other parameters are as described in the parameter list at the start of the thesis. We solve Equation (5.1) to Equation (5.3) with temporal discretisation $\Delta t = 0.01$, $t \in [0, 80]$ and spatial discretisation $\Delta x = 0.05$, $x \in [0, 15]$. The boundary conditions used are Dirichlet and initial conditions $V(x, 0) = -65$, $U(x_1, 0) = 10$, $U(x_{n>1}, 0) = -65$, m, n, h are initially at their rest values.

affected by temporally correlated noise. We can see in Figure 5.4 that the presence of temporally correlated noise does make a difference to the behaviour when the noise is multiplicative in the cable; the speed decreases while the error bars continue to grow.

The temporally correlated noise in the m-dynamics helps to stabilise waves which were out of order in the white noise case. Figure 5.5 plots (a) and (b) show the voltage in the cable with additive noise in the m-dynamics, $\mu = 0.01$, for white and temporally correlated noise respectively. It is clear that the temporal correlation of $\beta = 2$ promotes a travelling wave; it could do this by matching some internal time scale in the BR model. Plots (c) and (d) show the voltage in the cable when the noise is multiplicative in the m-dynamics, $\nu = 0.1$, for white and $\beta = 2$ correlated noise; again the correlation promotes a sequential travelling wave.

Finally in this section we look at the effect of spatially correlated noise in the BR model, again we look at the noise added to the m-dynamics and in the cable voltage dynamics. Figure 5.6 shows that the spatially correlated multiplicative noise in the

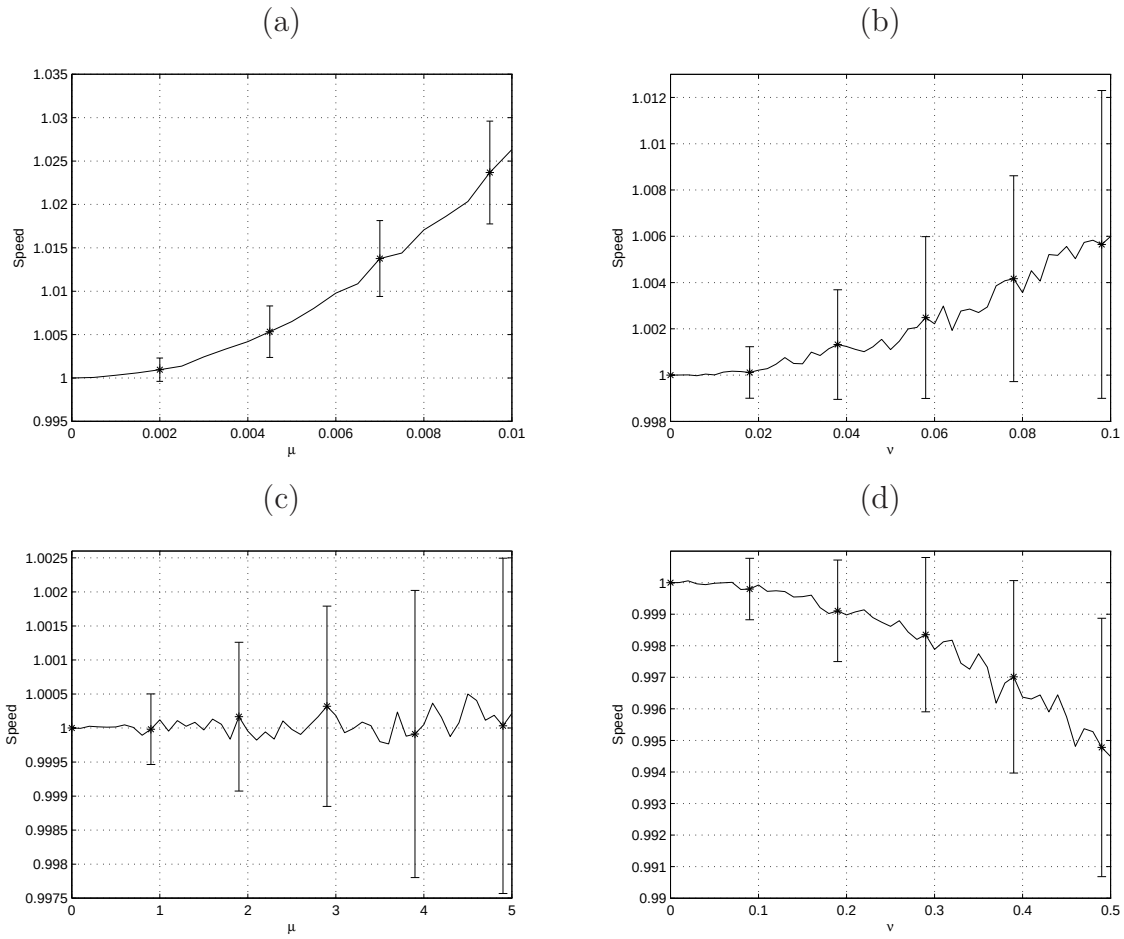

Figure 5.4: This figure shows the speed of the travelling wave in the BR model with temporally correlated noise in the spines and in the cable as the noise intensity increases. Plot (a): additive temporally correlated noise in the spines. Plot (b): multiplicative temporally correlated noise in the spines. Plot (c): additive temporally correlated noise in the cable. Plot (d): multiplicative temporally correlated noise in the cable. It can be seen from these figures that there is little difference from the white noise cases. All other parameters are as described in the parameter list at the start of the thesis. We solve Equation (5.1) to Equation (5.3) with temporal discretisation $\Delta t = 0.01$, $t \in [0, 80]$ and spatial discretisation $\Delta x = 0.05$, $x \in [0, 15]$. The boundary conditions used are Dirichlet and initial conditions $V(x, 0) = -65$, $U(x_1, 0) = 10$, $U(x_{n>1}, 0) = -65$, m, n, h are initially at their rest values.

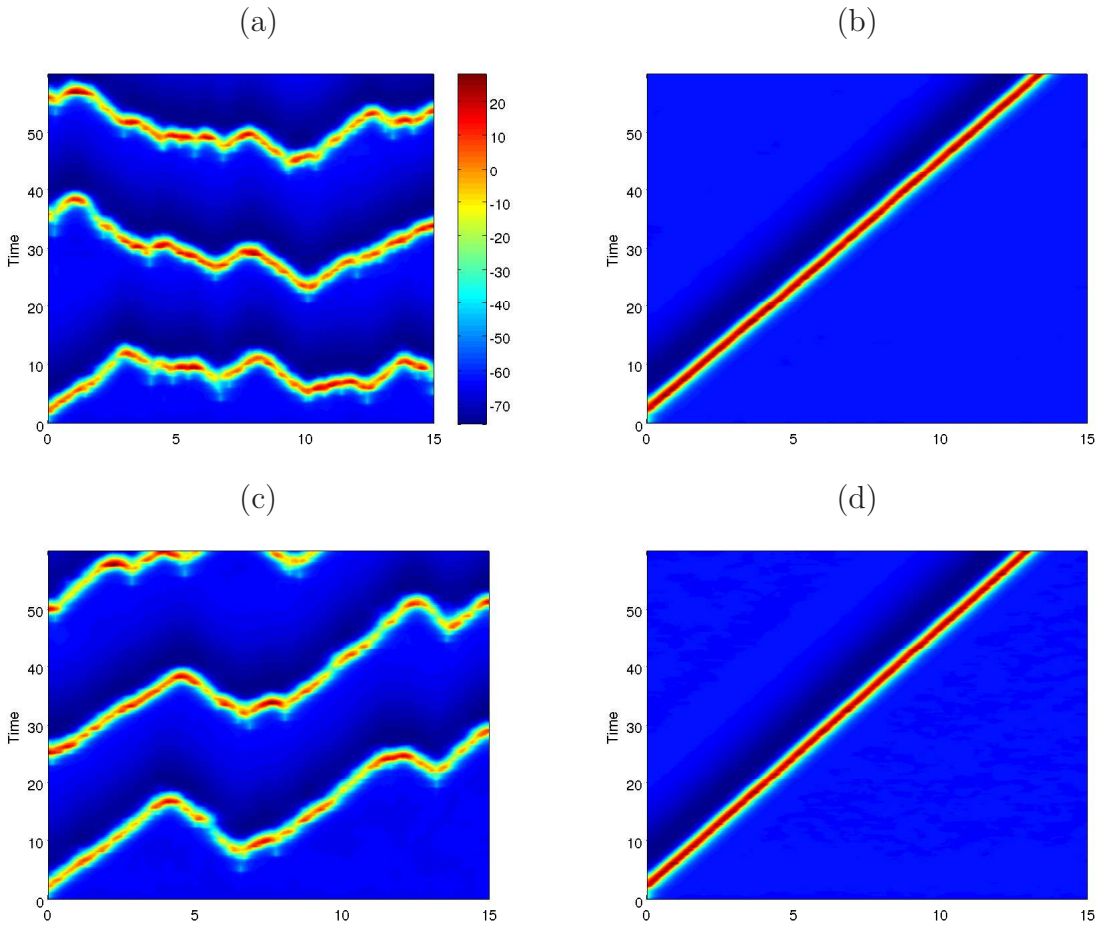

Figure 5.5: This figure shows a sample of the voltage in the cable when there is noise present in the spine head m-dynamics. Plot (a) has additive white noise of strength $\mu = 0.01$, plot (b) has additive OU noise strength $\mu = 0.01$ and $\beta = 2$, plot (c) has multiplicative white noise of strength $\nu = 0.1$ and plot (d) has multiplicative OU noise of strength $\nu = 0.1$ and $\beta = 2$. It can be seen that the waves travel out of order when the noise is white but when a temporal correlation is added the waves regain their sequential travel. All other parameters are as described in the parameter list at the start of the thesis. We solve Equation (5.1) to Equation (5.3) with temporal discretisation $\Delta t = 0.01$, $t \in [0, 80]$ and spatial discretisation $\Delta x = 0.05$, $x \in [0, 15]$. The boundary conditions used are Dirichlet and initial conditions $V(x, 0) = -65$, $U(x_1, 0) = 10$, $U(x_{n>1}, 0) = -65$, m, n, h are initially at their rest values.

BR model, in both the spines and the cable, increases the speed of the travelling wave. We have used both an Itô and Stratonovich interpretation since we require the Stratonovich interpretation to compare with the small noise analysis and continuation results. It is clear that there is a difference between the two interpretations; noise in the Itô sense does not alter the speed as the intensity increases whereas the Stratonovich case shows a clear increase in speed.

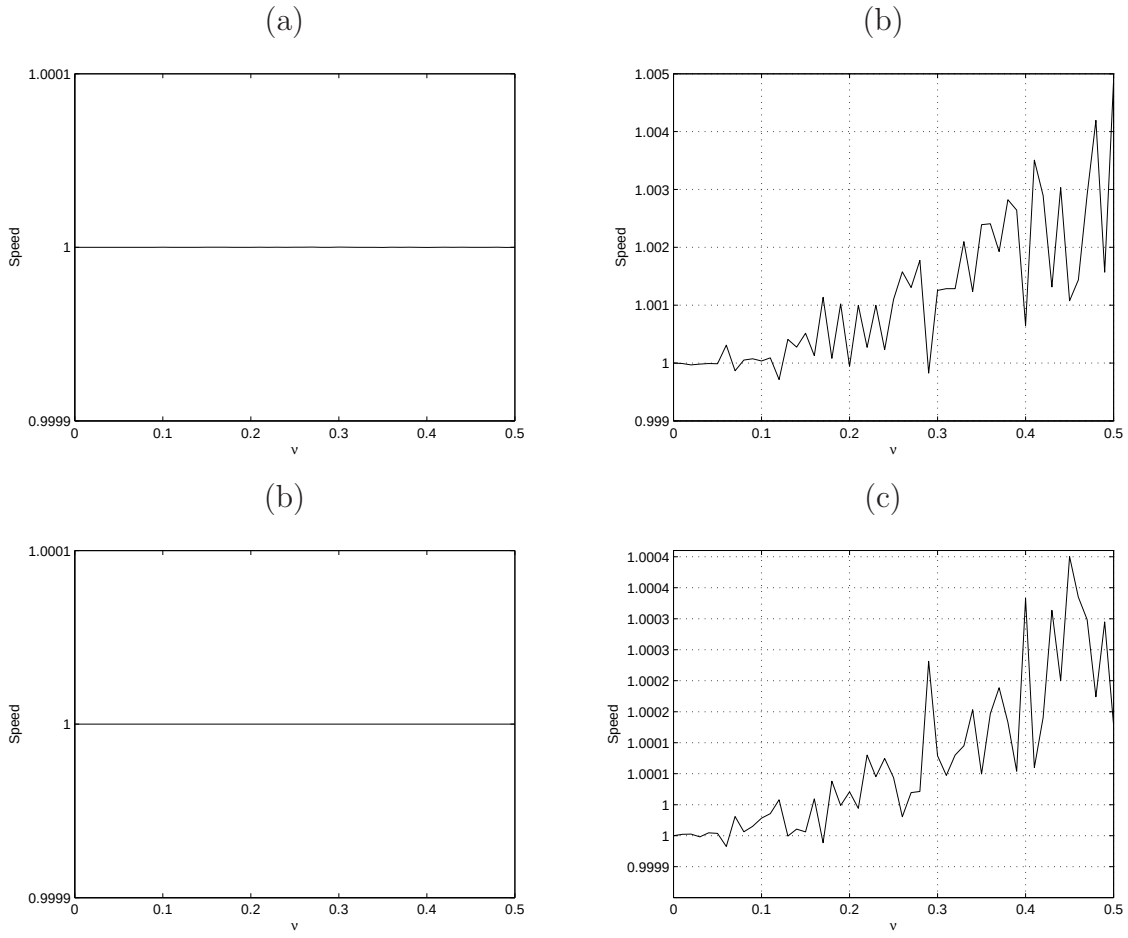

Figure 5.6: This figure shows the speed of the travelling wave in the BR model with spatially correlated multiplicative noise in the cable, $\zeta = 1.25$. Plot (a) and (b) shows the speed when the noise is in the spine heads, m-dynamics, in the Itô and Stratonovich cases respectively. Plot (c) and (d) shows the speed when the noise is in the cable, in the Itô and Stratonovich cases respectively. The Itô interpretation does not alter the speed of the wave but the Stratonovich interpretation increases the speed as noise intensity increases. All other parameters are as described in the parameter list at the start of the thesis. We solve Equation (5.1) to Equation (5.3) with temporal discretisation $\Delta t = 0.01$, $t \in [0, 80]$ and spatial discretisation $\Delta x = 0.05$, $x \in [0, 15]$. The boundary conditions used are Dirichlet and initial conditions $V(x, 0) = -65$, $U(x_1, 0) = 10$, $U(x_{n>1}, 0) = -65$, m, n, h are initially at their rest values.

Figure 5.6 shows in plots (b) and (d) that the speed of the wave increases as the noise intensity increases, this is in agreement with our small noise approximation and

results from AUTO-07P, see Section 5.4.2.

5.4.2 Continuation results

With the large period fixed, we can then continue in various combinations of parameters to find the regions of the parameter space where the travelling waves exist. We are interested in ρ the spine density, r the spine stem resistance, and c the wave speed. To find limits for existence we investigate the effect of the noise intensity. In Figure 5.8 we show the areas of existence of the travelling wave in the ρ-r parameter space, plot (a), and the limit point diagram for ρ and the speed of the waves c in plot (b); finally plot (c) shows the existence of travelling waves in r, c parameter space. The fast branch of this figure (plot (b)) is the stable branch and shows the waves we observe in the direct simulations. From the point on the fast branch of plot (b) which corresponds to the ρ used in the direct simulations we can look at the solution of the cable voltage V, and see, in Figure 5.7, that the profile qualitatively agrees with that of the direct simulations; plot (a) is the AUTO-07P result and plot (b) is a voltage profile from direct simulation.

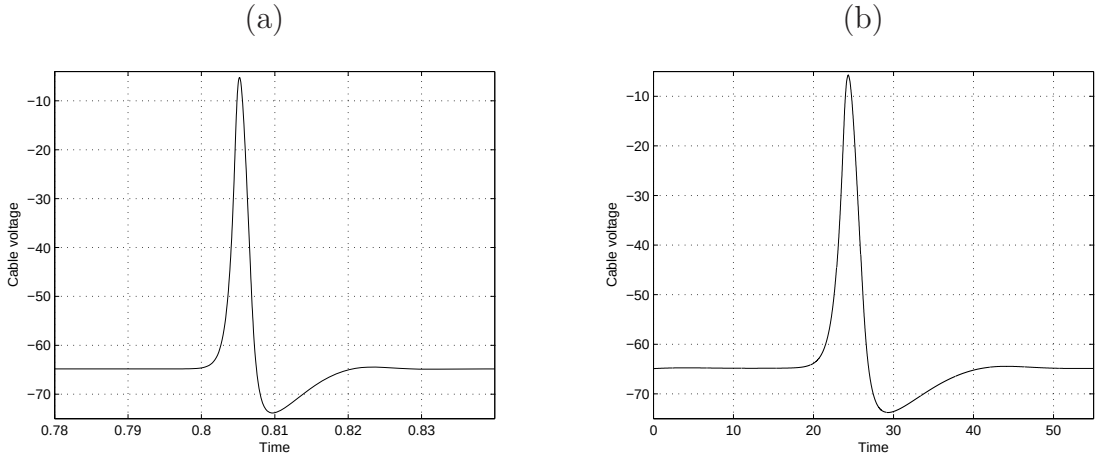

Figure 5.7: This figure shows the voltage profile in the cable as obtained from the AUTO-07P simulation of the BR system in the travelling wave frame, plot (a) and plot (b) also shows the voltage profile as obtained from the direct simulation of the BR model.

In Figure 5.8 the type of line in each plot corresponds to different levels of noise in the system, the solid line corresponds to $\nu_m = 0$, the deterministic case, dot-dashed line depicts $\nu_m = 0.1$ and $\nu_m = 0.5$ is represented by the dashed line. In all three plots the area in which the waves exist in parameter space increases as the noise intensity increases. The solutions exist on the lines plotted, i.e. for fixed values of all other parameters a solution exists at each corresponding set of values on the line. For example in plot (a), solid line, of Figure 5.8 for the particular fixed value of the speed there exists a solution at approximately $(\rho, r) = (1, 0.4)$ and $(20, 0.4)$ so for each fixed

value of speed there is a line similar to the one plotted in Figure 5.8 and the lines shown are taken at arbitrary fixed values to show as examples.

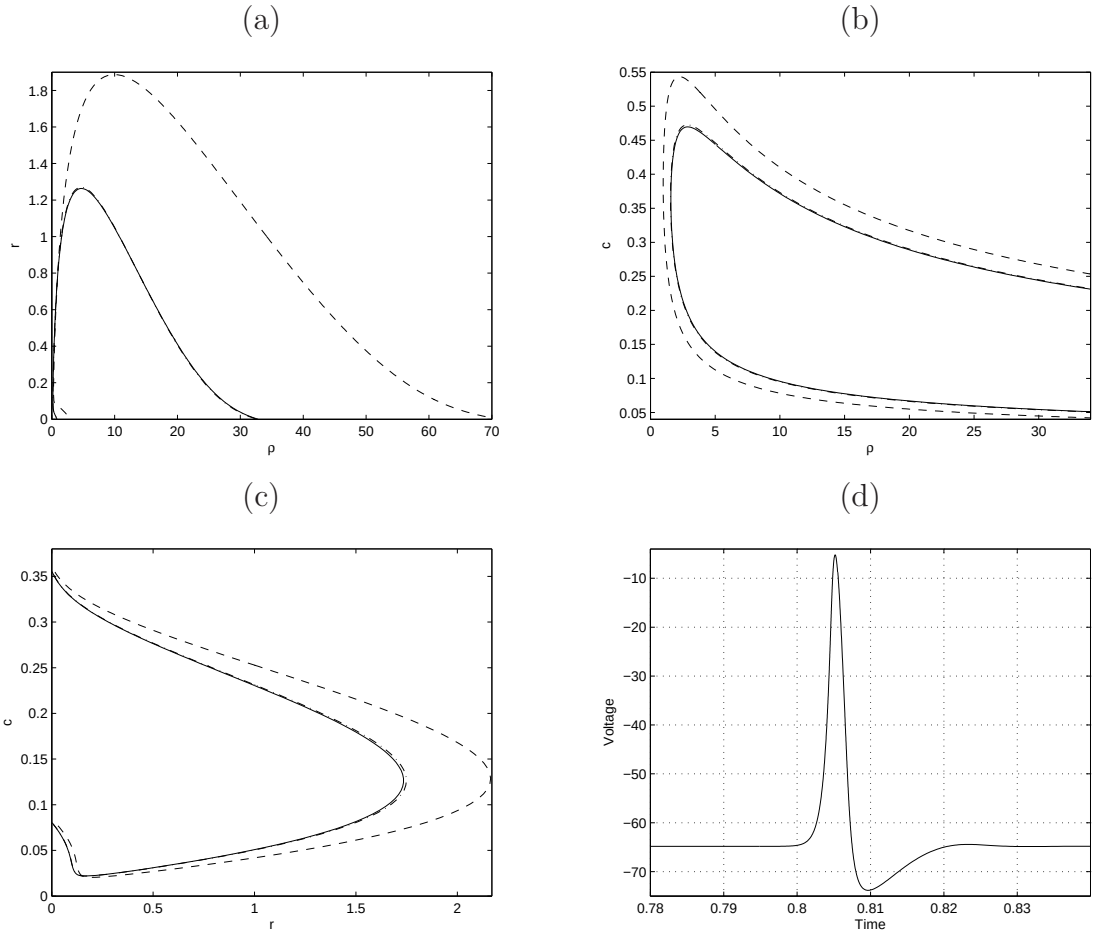

Figure 5.8: Examples of limit point diagrams for the deterministic and small noise case. In all plots the solid line is $\nu = 0$, dot dashed line $\nu = 0.1$ and dashed line $\nu = 0.5$. Plot (a) is the spine density against the spine stem resistance, plot (b) shows spine density against the speed of the wave and plot (c) shows the spine stem resistance against the speed of the wave. Each plot show an increase in the area of existence in parameter space for the travelling waves as the noise intensity increases. Plot (d) shows the voltage in the cable profile when there is a small amount of noise in the cable-dynamics; the plot does not show any fluctuations since there is not actually any explicit noise term in the rescaled equations, only some of the noise properties.

To see the effect of the noise on the existence of these waves in parameter space, we choose a point on the fast branch of the deterministic ρ-c curve and continue from there in two parameters, for example ν_m (spatially correlated noise intensity in the m-dynamics) and c. We choose ρ equal to that used in the Matlab simulations to provide a comparison. We can then see how the wave speed changes as noise is added into the equations, Figure 5.9. This figure, plot (a), shows the speed of the wave increasing as the noise intensity in the m-dynamics is increased. We fix a noise intensity by choosing a point on this new curve, and from this point we can repeat

the two parameter continuations to get the plots in Figure 5.8. Figure 5.9 shows that as the intensity of the spatially correlated noise in the cable increases the speed also increases, although it is a small increase for both the noise in the m-dynamics and in the cable equation, plot (b).

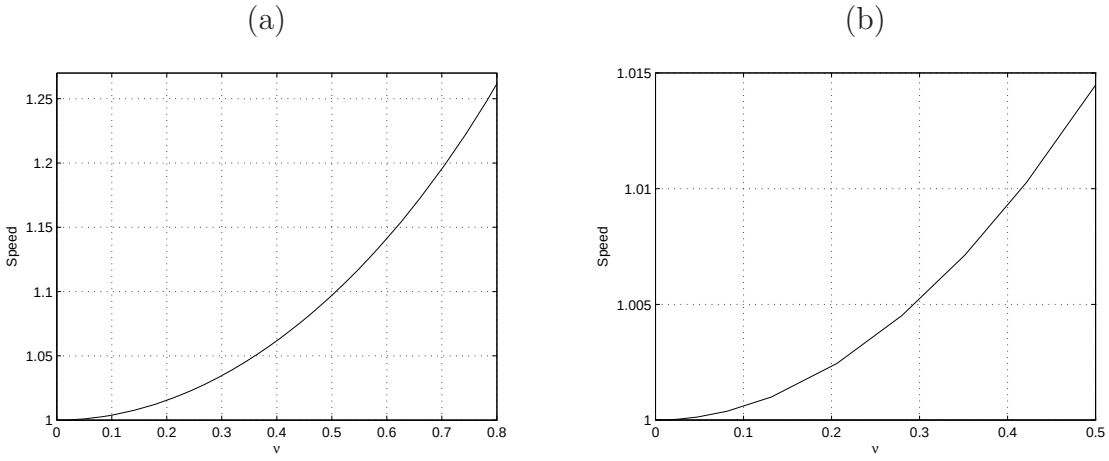

Figure 5.9: Speed of propagation as a function of noise strength, from AUTO-07P simulation of the noisy BR system. The speed increases with noise intensity of the spatially correlated noise in the m-dynamics, plot (a) and when the noise is in the cable equation, plot (b).

From the original homoclinic orbit we can look for period doubling (PD) bifurcations to find 2 pulse solutions of the BR model. We can repeat the preceding steps to get existence of the 2 pulse solutions in the parameter space for the deterministic and noisy cases. As for the single pulse solutions as the noise intensity increases so does the area of existence of the 2 pulse solutions. From the 2 pulse branch from the PD bifurcation we can look for another PD bifurcation to get 4 pulse solutions and so on. We show the cable voltage solution of the 2 pulse wave in Figure 5.10 and can show how the parameter regions for existence of a travelling 2 pulse solution exist as noise increases in Figure 5.11, plot (a). Plot (b) of Figure 5.11 shows how the speed increases with noise intensity.

5.5 Conclusions

In this chapter we investigated the effects of different types of noise on the behaviour of the BR model of spiny dendrites and found some interesting results which conflict with the results we found in the SDS model. We looked at the speed of travelling waves in the BR model as the noise intensity increases over a small range. When the noise is multiplicative in the spine head m-dynamics, of any form (white, temporally or spatially correlated), the speed of the wave increases as the noise intensity increases.

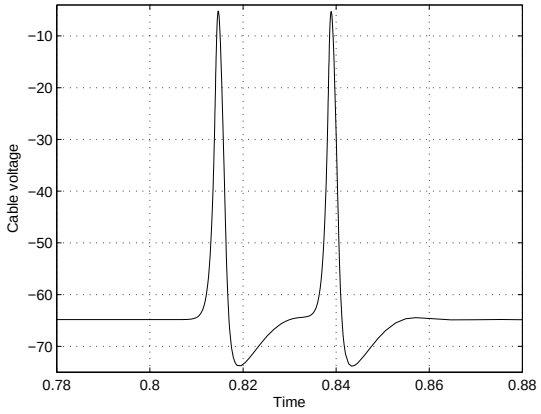

Figure 5.10: This figure shows the voltage profile obtained by AUTO-07P simulation for a 2 pulse solution to the BR model without noise.

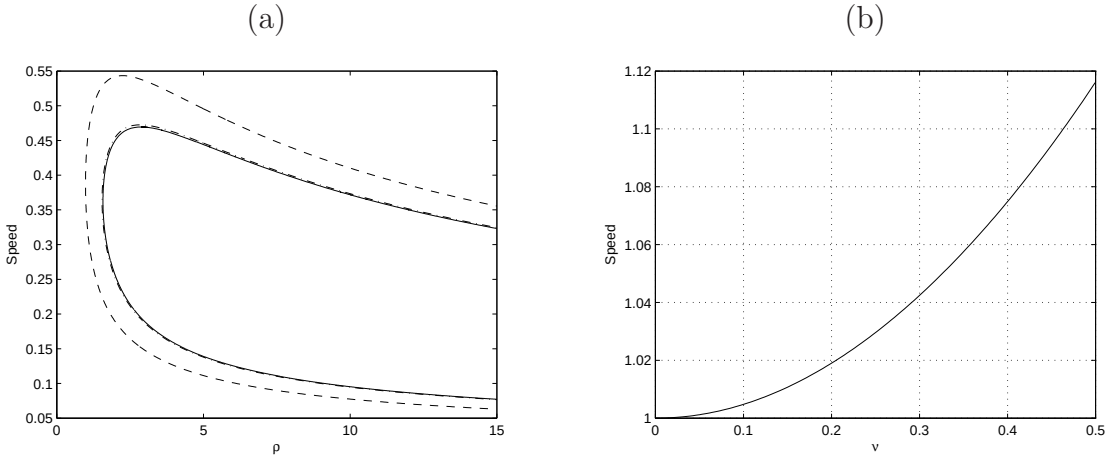

Figure 5.11: This figure shows the existence of 2 pulse solutions in parameter space and the speed of the w pulse solution as a function of noise intensity. Plot (a) shows how the area in parameter space for the parameters ρ and c increase as the noise intensity increases. The solid line is $\nu = 0$, dot dashed line $\nu = 0.1$ and $\nu = 0.5$ for the dashed line. As the noise increases the fast, stable branch gets faster and the slow unstable branch gets slower. Plot (b) shows the increase in speed as the noise intensity increases.

When the noise is in the cable dynamics the speed decreases if the noise is white or temporally correlated but increases in the spatially correlated case. In the SDS model it was simple to check if the wave was travelling along the cable by sequential firing of the spines by checking the times at which the spines fired; the BR model however uses the HH dynamics in the spine heads and so has no threshold condition to check firing making it harder to record firing times. The waves measured in the BR model appear to be sequential for noise levels up to approximately $\nu = 0.1$, and as the intensity continues to increase beyond this level the system starts to fire synchronously, and so the wave speed continues to increase further. So although the increase is small, the

waves definitely increase in speed over the range $\nu \in [0, 0.1]$. The effect of a temporal correlation is very interesting and an increase in the correlation time scale acts to stabilise the travelling waves and encourages sequential travel in a regime where the white noise induces an out of order wave.

Due to this behaviour at small levels of noise we looked at a small noise expansion of the noisy BR model with spatially correlated noise in the m-dynamics and the cable equation. We derived a deterministic approximation of the noisy system which included an extra, deterministic, term which included the noise intensity and correlation function of the noise but not the noise itself. These modified deterministic equations were transformed in to the travelling wave frame and the parameter space was searched for existence of the travelling waves using the AUTO-07P package. We included the noise intensity as a continuation parameter so that we could investigate how the speed of the waves was altered by increasing noise intensity. Figure 5.9 shows the speed of the waves as the noise intensity increases as obtained by the AUTO-07P simulations and it is clear that this agrees with the direct simulations as the speed increases over a small range of increasing noise intensities. This method is a very quick way to explore the behaviour as a function of different parameters and showed that as the noise intensity increases the travelling waves exist over larger areas of parameter space. We showed in Figure 5.8, that this was the case for three different pairs of important parameters: spine density ρ, spine stem resistance r and the wave speed c. So not only is the BR model robust to small levels of noise, the noise actually helps the model to support waves in parameter regimes where the deterministic system cannot. We could also use the AUTO-07P package to search for more complicated travelling solutions, such as 2-pulse waves. We found that repeating the continuations in noise for the 2-pulse solution also increases the region of existence in parameter space and that the 2-pulse solution also travelled faster with an increase in noise intensity.

Chapter 6

Baer Rinzel model - Non-constant spine density

6.1 Introduction

We have produced results in Chapter 4 and Chapter 5 that are conflicting i.e. the speed of travelling waves in each of these spiny dendrite models behaves differently in the presence of noise. In the case of the SDS model, when noise is introduced to either the spine head or cable dynamics the speed of any resulting wave is reduced, contrary to the results of the BR model, where the speed increases in the presence of noise in the spine heads, and spatially correlated noise in the cable. In a bid to reconcile these differences we introduce a modified Spike-Diffuse-Spike model in the hope that it will shed some light on the inconsistencies.

Although both the SDS and the BR models represent a length of spiny dendrite there are two main differences between; that is the spine head dynamics are represented by two different models and the way in which the spines are coupled to the cable is different. In the SDS model, Section 2.8, the spines are attached at discrete, equally space points along the cable and the dynamics are modelled by the IF model. In the BR model, Section 2.7, the spines are a continuum and the dynamics are modelled by the HH model. The BR model has more realistic dynamics than the SDS model but the SDS model has a more realistic physical representation of the spine stem morphology. This chapter will examine the Baer Rinzel model with a non-constant spine density, $\rho(x)$, that can be chosen to give spines that have an area of attachment to the cable, rather that either a continuum or a discrete stem. The model can also behave like the traditional BR model or like the SDS model, i.e. discrete spine attachment, with HH dynamics. This model has the BR model equations, Equation (2.34), but with a spatially dependent density of spines, $\rho(x)$.

6.2 The modified dendrite model

6.2.1 The model equations

We introduce the stochastic BR model with non-constant spine density. The only difference to the stochastic BR equations, Equation (5.1), is the introduction of the spatially dependent density of the spines $\rho(x)$.

$$C\frac{\partial V}{\partial t} = -g_L(V - V_L) + \frac{1}{r_a \pi d}\frac{\partial^2 V}{\partial x^2} + \rho(x)\frac{\hat{V} - V}{r} + (\mu_c + \nu_c g_c(V))\frac{\partial W}{\partial t} \quad (6.1)$$

$$\begin{aligned}\hat{C}\frac{\partial \hat{V}}{\partial t} &= g_K n^4(V_K - \hat{V}) + g_{Na} h m^3(V_{Na} - \hat{V}) \\ &+ g_L(v_L - \hat{V}) - \frac{\hat{V} - V}{r} + (\mu_H + \nu_H g_H(\hat{V}))\frac{dW}{dt} \quad (6.2)\end{aligned}$$

$$\frac{dX}{dt} = \alpha_X(1 - X) - \beta_X X + +(\mu_X + \nu_X g_X(X))\frac{dW}{dt}\ . \quad (6.3)$$

All the parameters are as before with the exception of $\rho(x)$, which we now choose to be either a linear sum of delta functions, such that the spines are attached at discrete points, as in the SDS model, or we choose a function which gives us a density somewhere between the discrete and continuous cases. We can use the following function, Equation (6.4), as the new spatially dependent density, which has a parameter to control the area of the spine stem attached to the cable:

$$\rho(x) = \sum_n \rho_{max}\xi_n \exp(-\kappa(x - x_n)^2)\ . \quad (6.4)$$

Here we have ρ_{max} is the maximum value of the density, taken to be the value used for the original BR model, and

$$\xi_n = \begin{cases} 1 & \text{if } x_n - \frac{d}{2} < x \leq x_n + \frac{d}{2} \\ 0 & \text{otherwise,} \end{cases}$$

where d is the spine spacing (as before) and $\kappa \in \mathbb{R}^+$ controls the width of the spine stem. As $\kappa \to 0$, $\rho(x) \to \rho_{max}$ and as $\kappa \to \infty$, $\rho(x) \to \sum_n \rho_{max}\delta(x - x_n)$. Therefore at the $\kappa \to 0$ limit the model resembles the BR model and at $\kappa \to \infty$ limit the model resembles the SDS model with HH dynamics (instead of IF) in the spine heads.

6.2.2 Simulation

The discretisation of the new model is exactly the same for the BR model, since the governing equations are exactly the same and the only difference occurs in the value of

$\rho(x)$ at each point but since $\rho(x)$ does not change in time we can simply generate $\rho(x)$ before the time loop in the simulation and run the algorithm as before, Section 5.3.1. If x_j is a point on the spatial mesh $x_0, x_1, \ldots, x_J$ with step size Δx, i.e. $j = 1, 2, \ldots, J$ $J = \frac{L}{\Delta x}$, then the density can be discretised thus:

$$\rho_j = \rho_{max} \sum_n \exp(-\kappa(x_j - x_n)^2) \ .$$

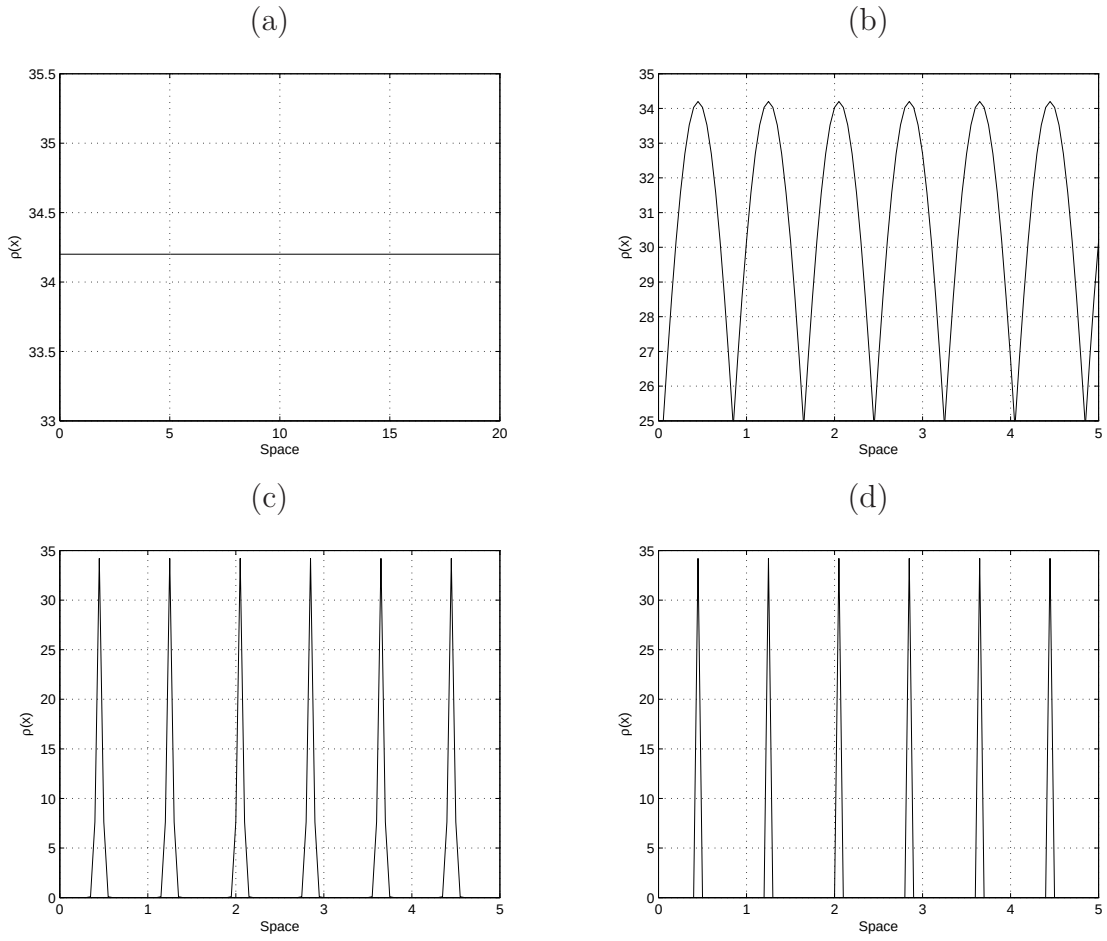

Figure 6.1: Examples of the space dependent density as κ changes with $d = 0.8$ the spine spacing (distance between peaks). Plot (a) BR limit, plot (b) $\kappa = 2$, plot (c) $\kappa = 600$ and plot (d) $\kappa = 10000$. All other parameters are as described in the parameter list at the start of the thesis. We solve Equation (6.1) and Equation (6.4) with temporal discretisation $\Delta t = 0.01$, $t \in [0, 80]$ and spatial discretisation $\Delta x = 0.05$, $x \in [0, 20]$. The boundary conditions used are Dirichlet and initial conditions $V(x, 0) = -65$, $U(x_1, 0) = 10$, $U(x_{n>1}, 0) = -65$, m, n and h are initially at their rest values.

Figure 6.1 is an example of $\rho(x)$ with various values of κ and a spine spacing of $d = 0.8$. As the value of κ increases from plot (a) to plot (d) the model is moving from the BR limit to the SDS-HH limit.

The discretised BR equations are as before:

$$V_j^{n+1} = V_j^n + \Delta t \left(\frac{V_{j+1}^n - 2V_j^n + V_{j-1}^n}{\Delta x^2} + \frac{\rho_j}{Cr}(U_j^{n+1} - V_j^{n+1} + \frac{1}{c}(G_L(V_L - V_j^{n+1}))) \right)$$
$$+ (\mu_c + \nu_c g(V_j^n))\Delta W_j^n) \ .$$

The discretised m, n, h equations, with $X \in [m, n, h]$:

$$X_j^{n+1} = X_j^n + \Delta t \left(\alpha_X(U_j^n) - \alpha_X(U_j^n)X_j^{n+1} - \beta_X(U_j^n)X_j^{n+1} \right)$$
$$+ (\mu_X + \nu_X g(X_j^n))\Delta W_j^n \ . \tag{6.5}$$

And finally the discretised equation for the voltage in the spine heads:

$$U_j^{n+1} = U_j^n + \frac{\Delta t}{\hat{C}}(G_K(n_j^{n+1})^4(V_K - U_j^{n+1}) + G_{Na}h_j^{n+1}(m_j^{n+1})^3(V_{Na} - U_j^{n+1})$$
$$+ G_L(V_L - U_j^{n+1})) + \frac{V_j^n - U_j^{n+1}}{r}) + (\mu_H + \nu_H g(U_j^n))\Delta W_j^n \ .$$

Again we want to know the effect of noise on the system and so use the level set method to measure the speed of the travelling waves in the stochastic system to compare to the results obtained for both the original SDS and original BR models. We then wanted to investigate the behaviour of the stochastic system when we changed the size of the spine stem, i.e. changes the value of κ in Equation (6.4), we can therefore compare the original BR, the SDS-HH model in the two limits and cases in between the two extremes.

6.3 Results

The SDS model with HH dynamics behaves as the SDS model with IF dynamics; the speed of the waves in the system decrease as noise increases. Shown in Figure 6.2 are a few examples of the speed as a function of the noise intensity. As in the original SDS model the speed of the waves decreases as the noise intensity increases. The results of these simulations, Figure 6.2, tell us that the type of dynamics used in the spiny dendritic model have not caused the discrepancies between the models since using the HH dynamics instead of the IF in the SDS model does not change the overall behaviour of the speed of the travelling wave as noise intensity increases.

We look to the spine density function $\rho(x)$ for an explanation. First we look at some voltage plots for different values of κ to see how the cable voltage looks as the width of the spine stem changes. Each plot in Figure 6.3 shows the voltage strength (indicated by colour) in the whole space-time domain. The value of the voltage is in

the same range as the original BR model since the basic equations are the same and only the form of the density $\rho(x)$ changes. The top left figure is the BR-SDS model in the BR limit $\kappa = 0$, the top right is the voltage plot when $\kappa = 2$, bottom left is for $\kappa = 600$ and finally the bottom right is the SDS limit when $\kappa = 10000$.

We now look at the speed of a noisy wave as the parameter κ changes, and so as the spine stem width changes. From the behaviour we have observed so far we expect as κ increases and so the model changes from a BR type, $\kappa = 0$, to an SDS type, $\kappa = 1000$, then the plot of the noisy wave speed should cross the plot of the deterministic wave speed, since the BR model speeds up with the inclusion of noise and the SDS-HH slows down, just as the SDS model, with the inclusion of noise. Figure 6.4 shows the speed of a deterministic wave in the modified BR model as κ changes and so the spine stem changes from a continuum like the original BR model to a discrete distribution of spines as in the SDS-HH model. There is an optimal value of κ which maximises the deterministic wave speed, this occurs at $\kappa = 670$. The spatial discretisation used will have an impact on the accuracy of the density, $\rho(x)$, when κ is large, and this will in turn effect the measured value of the speed. The size of the spatial step, Δx, does not have such an impact where κ is small and at large values of κ the speed of the measured wave will converge as the step size decreases. Figure 6.5 shows that at small κ the speed of the wave with different step sizes is very close but as Δx increases there is a small difference in the measured speed; although the exact value of the speed differs slightly the overall qualitative behaviour is the same.

It is difficult to see in Figure 6.6 the point at which the curves cross and the values of the three curves at the limiting cases $\kappa = 0$ and $\kappa = 1000$. The best fit lines in Figure 6.6 are found using a least squares method which minimises the sum of the squares of the errors between each data point and the fitted line. We implement this by using the MATLAB function 'dtrend'. Since the changes in the speed are small and we look at the table shown below, Figure 6.7, the values of the speed at each end of the noisy curves is shown for the three types of noise in the spines.

6.4 Conclusion

In this chapter we have tried to reconcile the difference in the behaviour of the speed of waves in the SDS and BR models when noise is present. As previously discussed, in Chapter 4 we showed that as noise intensity increases the speed of the travelling waves in the SDS model decreases but in Chapter 5 the BR shows an increase in speed of travelling waves under the influence of small noise intensities. We first looked at the SDS model with HH dynamics in the spine heads instead of the IF dynamics.

We did this using the modified BR model with spatially dependent spine density in the limit where the spines are attached at discrete points, as in the original SDS model. We included noise in this SDS-HH model in the m-dynamics and in the cable equation, as before, and found that the model behaved just as the original SDS model did under the influence of noise. Figure 6.2 shows a few examples of the wave speed as noise intensity increases: plot (a) shows multiplicative white noise in the cable, plot (b) is additive temporally correlated noise in the spine heads, plot (c) has multiplicative temporally correlated noise in the spine heads and plot (d) shows multiplicative spatially correlated noise in the spine heads. In each of these plots the speed of the wave decreases, so it seems that the type of dynamics (and so the form of the pulse injected to the cable from the spine) does not account for the difference in behaviour from the SDS to the BR models. This is interesting since the more realistic dynamics included in the SDS-HH model do not provide any extra information or influence the behaviour of the model dendrite but it does vastly increase the computing time and so proves to be an inefficient complication. We looked at the spine stem resistance as a function of space in between the two extremes of the SDS-HH model and the original BR model; so a Gaussian type function was chosen with a parameter, κ, included that could change the density from one limit to the other. In the deterministic case the value of κ can maximise the speed of the wave so it seems that the extent of spine stem attachment to the cable is important and can alter the speed of the wave without the influence of noise. When we include noise in the system we expect, from the BR model and the SDS-HH models, that the wave speed should increase as noise is included at the $\kappa = 0$ limit and decrease at the opposite extreme $\kappa \to \infty$. Figure 6.6 shows this for the white noise in the m-dynamics case; the changes in speed are very small and so we plotted the difference between the deterministic speed and the 'noisy' speed as a function of κ. Although the plots fluctuate, the mean trend of the dotted lines in both plot (a), where $\nu = 0.02$ and plot (b) where $\nu = 0.15$ is to cross the $y = 0$ line which indicates that the noisy wave is slowing down, with respect to the deterministic wave, as κ increases. The values of the noise at each limit of the modified model for different types of noise in the m-dynamics and cable were shown in the table, Figure 6.7, it agrees with the plots in Figure 6.6, and it shows that the waves speeds at the limits do speed up and slow down in agreement with previous results. Therefore it seems that the extent of the spine stem is an important factor in determining the behaviour of the model with respect to noise.

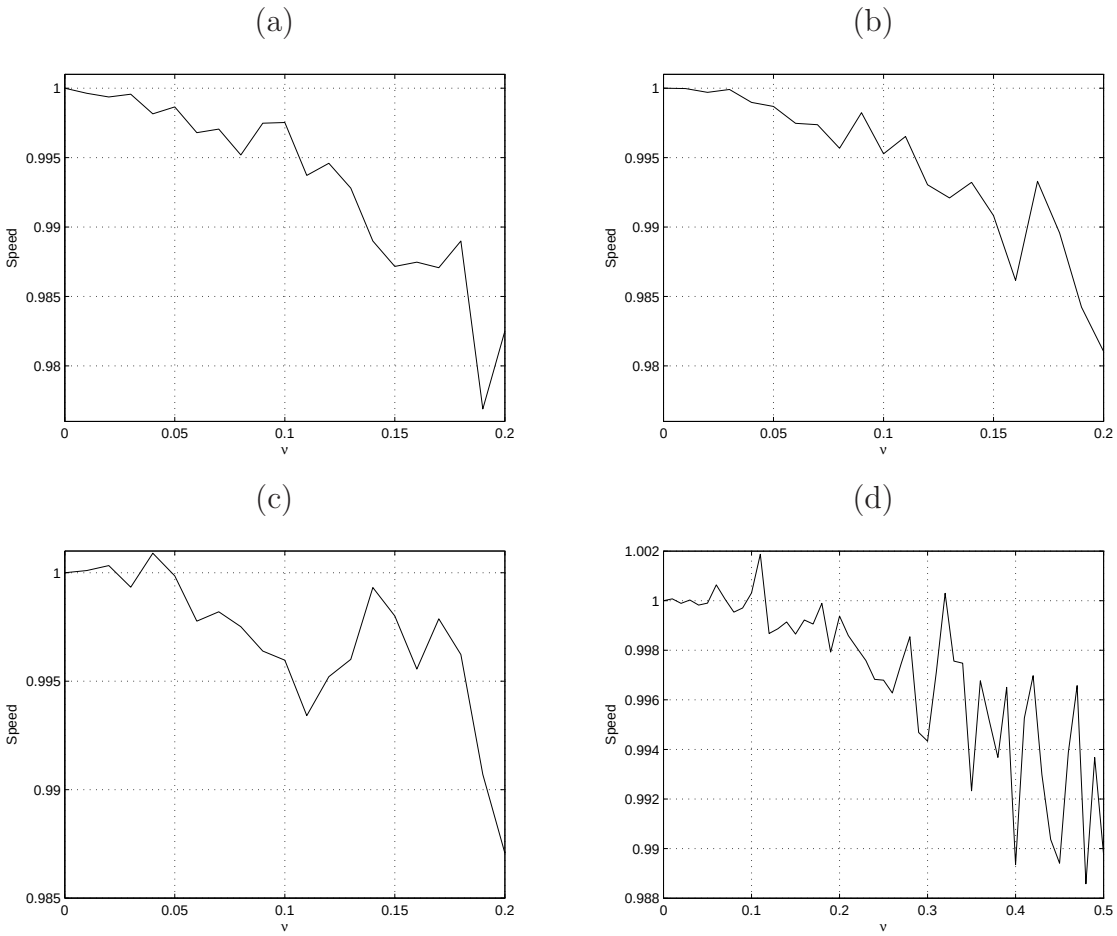

Figure 6.2: This figure shows the speed of the travelling wave in the SDS-HH model with different types of noise as the noise intensity increases, in each case the noise slows the wave speed. For each plot $\kappa = 10000$ and $d = 0.8$. Plot (a) shows the effect of multiplicative white noise in the cable. Plot (b) shows the effect of multiplicative OU noise in the cable. Plot (c) is multiplicative OU noise in the spines. Plot (d) shows multiplicative spatially correlated noise in the cable. All other parameters are as described in the parameter list at the start of the thesis. We solve Equation (6.1) and Equation (6.4) with temporal discretisation $\Delta t = 0.01$, $t \in [0, 80]$ and spatial discretisation $\Delta x = 0.05$, $x \in [0, 20]$. The boundary conditions used are Dirichlet and initial conditions $V(x, 0) = -65$, $U(x_1, 0) = 10$, $U(x_{n>1}, 0) = -65$, m, n and h are initially at their rest values.

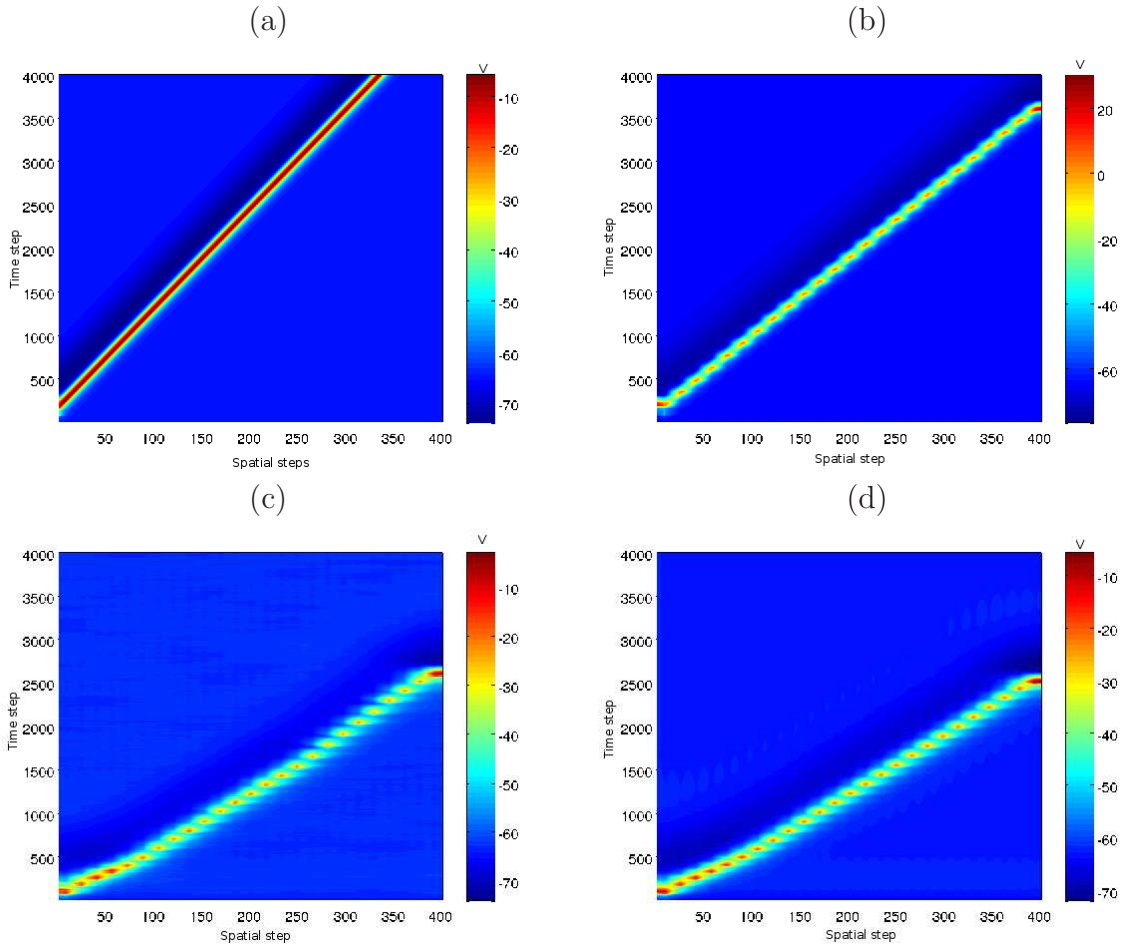

Figure 6.3: Voltage in the cable is indicated by the colour bar on each plot over the space-time (x/y axis) domain. Plot (a) shows the cable voltage for the SDS-HH model in the BR limit $\kappa = 0$, plot (b) shows the cable voltage when $\kappa = 2$. Plot (c) is the cable voltage for the SDS-HH model when $\kappa = 600$ and plot (d) shows cable voltage for the SDS-HH model with $\kappa = 10000$. All other parameters are as described in the parameter list at the start of the thesis. We solve Equation (6.1) and Equation (6.4) with temporal discretisation $\Delta t = 0.01$, $t \in [0, 80]$ and spatial discretisation $\Delta x = 0.05$, $x \in [0, 20]$. The boundary conditions used are Dirichlet and initial conditions $V(x, 0) = -65$, $U(x_1, 0) = 10$, $U(x_{n>1}, 0) = -65$, m, n and h are initially at their rest values.

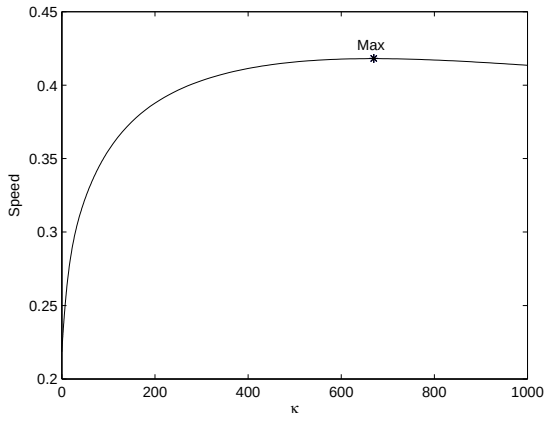

Figure 6.4: This figure shows the deterministic speed of waves in the modified BR model as the parameter κ increases from the BR limit to the SDS limit. There is an optimal value of κ which maximises the speed of the wave, this occurs at $\kappa = 670$. All other parameters are as described in the parameter list at the start of the thesis. We solve Equation (6.1) and Equation (6.4) with temporal discretisation $\Delta t = 0.01$, $t \in [0, 80]$ and spatial discretisation $\Delta x = 0.05$, $x \in [0, 20]$. The boundary conditions used are Dirichlet and initial conditions $V(x, 0) = -65$, $U(x_1, 0) = 10$, $U(x_{n>1}, 0) = -65$, m, n and h are initially at their rest values.

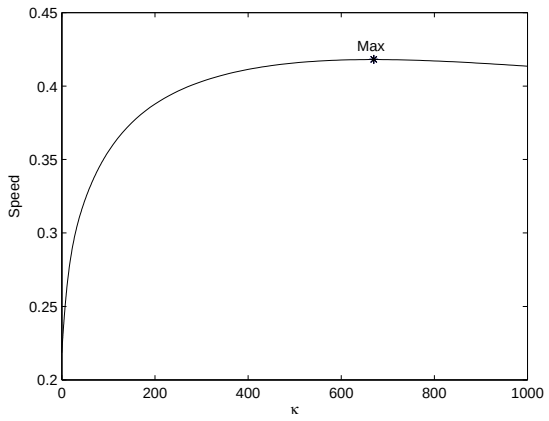

Figure 6.5: This figure shows the deterministic speed of waves in the modified BR model as the parameter κ increases from the BR limit to the SDS limit. The different lines show three values of dx. All other parameters are as described in the parameter list at the start of the thesis. We solve Equation (6.1) and Equation (6.4) with temporal discretisation $\Delta t = 0.01$, $t \in [0, 80]$ and spatial discretisation as in the legend, $x \in [0, 20]$. The boundary conditions used are Dirichlet and initial conditions $V(x, 0) = -65$, $U(x_1, 0) = 10$, $U(x_{n>1}, 0) = -65$, m, n and h are initially at their rest values.

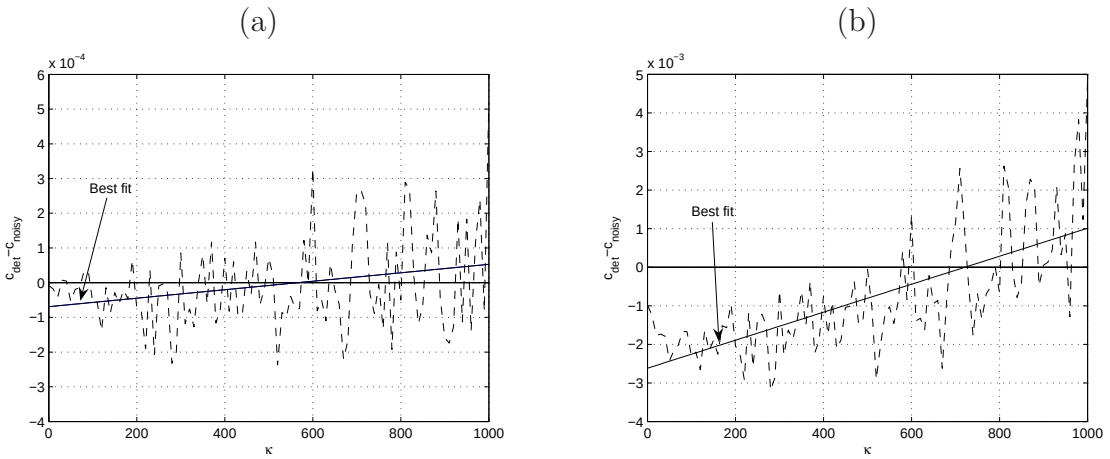

Figure 6.6: This figure shows the difference between the deterministic speed and the speed of the noisy wave as κ increases. Plot (a) shows $c_{determ} - c_{noisy}$, as κ increases, where the noise intensity is $\nu = 0.02$ and plot (b) has noise intensity $\nu = 0.15$. The dotted lines show the difference in the speed, starting negative as the noisy speed is faster than the deterministic wave speed and becoming positive as the noisy wave becomes slower than the deterministic wave. In plot (a) the difference in wave speed is very small but as the noise intensity increases, plot (b), the difference increases and the dotted line is above the line $y = 0$ for a larger range of κ. The best fit line is found by using a least square fit. All other parameters are as described in the parameter list at the start of the thesis. We solve Equation (6.1) and Equation (6.4) with temporal discretisation $\Delta t = 0.01$, $t \in [0, 80]$ and spatial discretisation $\Delta x = 0.05$, $x \in [0, 20]$. The boundary conditions used are Dirichlet and initial conditions $V(x, 0) = -65$, $U(x_1, 0) = 10$, $U(x_{n>1}, 0) = -65$, m, n and h are initially at their rest values.

	White		OU		Spatial	
ν	SDS lim	BR lim	SDS lim	BR lim	SDS lim	BR lim
0.02	0.9988	1.0005	1.0000	1.0000	1.0000	1.0005
0.15	0.9884	1.0046	0.9995	1.0023	1.0007	1.0005
0.3	0.9855	1.0059	0.9865	1.0037	0.9819	1.0096

Figure 6.7: This table shows the speed of the travelling wave, scaled by the deterministic speed, for three levels of noise intensity ν in the BR model with spatially dependent spine density $\rho(x)$ at the two limits. The SDS limit has $\kappa \to \infty$ and the BR limit has $\kappa = 0$. It can be seen that as the noise increases the speed in the SDS limit for each type of noise slows and in the BR limit the speed increases.

Chapter 7

Probabilistic representation of SDS model

This chapter aims to provide a probabilistic description of the SDS model in an attempt to give a quick method of simulating the noisy SDS model and so predict behaviour of the system under the influence of multiplicative noise in the spine head dynamics. Following the analysis in the paper by Keener, [54], for a model which describes calcium waves, we aim to predict the extent and speed of propagation of the saltatory travelling wave in the stochastic SDS model. Initially we show that the probabilistic model proposed in [54] is suitable for capturing the behaviour of the stochastic SDS model. To do this we use the expected values of, e.g. voltage in the cable and spine heads, and firing times of all spines, that were obtained using the simulation method described in Section 3.4 of Chapter 3. We then use the methodology in [54] to extract, for different levels of noise, the probability density functions for each spine, expected firing times of each spine and the extent of propagation of a wave from the simulated data. Although the expected firing times etc can be directly obtained from the data we are using this to check that the probabilistic model is accurate for the SDS model. We then show a quick method of obtaining the general behaviour of the system e.g. the probability of wave failure and speed of successful waves without having to simulate the full system of equations for the SDS model many times, thus saving computing time.

7.1 Probabilistic analysis of SDS model

The subsequent analysis is done following the paper by Keener, [54]. We look at the probability of each spine firing given the occurrence of previous firing events and at the expected time of firing for each spine, again depending on the previous firing events. In summary we construct a probability density function (PDF) for each spine, dependent on the voltage in the cable at each spine and the voltage in each spine head.

We can then extract from the PDF, the cumulative probability of firing for each spine and then expected firing time and speed of propagation. This is repeated for different combinations of noise intensity, ν, and input strength, η_0.

7.1.1 Cumulative probability and probability density functions

The process of reaching threshold in a stochastic integrate and fire regime can be described as a random process and therefore the time of firing for the nth spine, T_n, is a random variable. We can then define the associated, cumulative probability of firing as:

$$P_n(t) = P(t > T_n) \ . \tag{7.1}$$

So P is the probability that the spine located at x_n, fired at time T_n before time t, given in short as $P_n(t)$.
We need the equation describing the change of probability to take a form that reflects the way in which we expect the spine to react to voltage in the cable, V, and the spine head, U. As either the voltage in the cable, at the spine, or in the spine heads increases so P_n should approach 1 as the spine is likely to fire; just as observed in Chapter 4, if the voltage is high enough the spines fire. Due to this nature of the system, we can write:

$$\frac{dP_n}{dt} = k(V(x_n,t))(1-P_n) \ , \ P_n(0) = 0 \ . \tag{7.2}$$

Here $k(V(x_n,t))$ is a rate parameter, and is chosen as a function of the local voltage in the cable:

$$k(V(x_n,t)) = \frac{k_{max}V^N}{\theta^N + V^N} \ . \tag{7.3}$$

Here $k_{max} = 200$ and is chosen to fit the system behaviour, and $\theta = \frac{-U(x_n,t)}{0.044} + 1$, is the threshold that the voltage in the cable must reach for the spine at that point to fire. Figure 7.1 was obtained by setting the voltage in a spine head in the SDS model and increasing the voltage in the cable until the spine fired on the next time step of the simulation. This was done for $U_n \in [0,h]$, recall h is the firing threshold for the spine head voltage in the IF process, to obtain the straight line equation for θ. Since we consider only one firing event in each spine, the spine head voltage will never be larger than threshold ($U_n \leq 0.04$) therefore $\theta > 0$. This form of $k(V)$ arises from the following properties of the integrate and fire dynamics in the spine heads. When the voltage in the cable at the position of the spine is small we expect that the probability of firing is also small and so $k(V)$, should be small. When the voltage in the cable is high we expect the probability of firing to be high and so $k(V)$ should also be high.

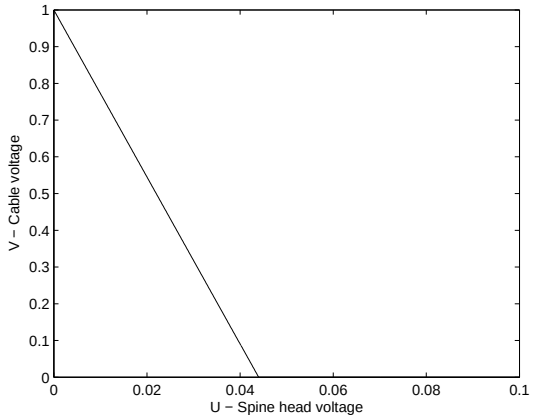

Figure 7.1: Threshold voltage in the cable as a function of, U, the voltage in the spine head, we require both U_n and V_n to determine the threshold θ in Equation (7.3).

Also if the voltage is high in the cable but the spine has yet to fire then the probability that it will fire at some later time will increase, this agrees with our intuition about the system and what is observed in direct simulation. The rate parameter cannot be a function of V solely since if we think of two spines, n and m say, both with the same large voltage in the cable at points x_n and x_m but $U_n < U_m$ then the probability of firing will be higher for spine m than for spine n and the function k must reflect this. The function given above (Equation (7.3)), the Hill function, satisfies these assumptions. This form of the function k is the same as in [54] but we have a time dependent threshold $\theta(t)$ instead of a constant value.

By definition we have that the probability distribution function associated with the random variable T_n given by:

$$p_n(t) = \frac{dP_n}{dt} \ . \tag{7.4}$$

First note that from Equation (7.2), we can integrate to find an expression for P_n:

$$\begin{aligned} \int_0^t \frac{dP_n}{(1-P_n)} &= \int_0^t k(V(s))ds \\ -\ln(1-P_n) &= \int_0^t k(V(s))ds \\ \text{Hence } P_n &= 1 - e^{-\int_0^t k(V(s))ds} \ , \end{aligned}$$

and so we have an explicit expression for the probability distribution:

$$p_n(t) = k(V)\exp\left(-\int_0^t k(V(x_n,s))ds\right). \tag{7.5}$$

However we cannot say that Equation (7.5) is a true probability distribution function since there is some small chance that a spine may never fire, i.e. $\int_0^\infty p_n(t)dt = P_n^\infty \leq 1$.

7.1.2 Expected firing times

Now that we have an expression for the probability distribution function, PDF, of the firing times at a given site, x_n, we can work out some other properties of the system that are of interest. The expected firing time of each spine is of interest since we can then determine if there is a travelling wave present and at what speed this wave is travelling. First we can define the probability distribution of firing times for site n on the assumption that a firing event does occur at the nth site, denoted $(t|n)$. Starting from the standard equation for conditional probability density function:

$$p_n(t|n) = \frac{p_n(t) \cap p_n(t_n)}{p_n(t_n)} = \frac{p_n(t)}{P_n^\infty},$$

and so the expected time of firing can be given by:

$$\mathbb{E}(T_n) = \frac{1}{P_n^\infty} \int_0^\infty t p_n(t) dt. \tag{7.6}$$

This is the expected (or mean) time of firing for site n given that the spine at this site will fire at some point in the future. We can use the definition of the moments; $m_k = \int_0^\infty t^k p_n(t)dt$, with $k = 0, 1, 2$, are the zeroth, first and second moments respectively for the nth spine, to give:

$$\mathbb{E}(T_n) = \frac{m_1}{m_0}, \tag{7.7}$$

and for the variance of the firing times:

$$\text{Var} = \mathbb{V}(T_n) = \frac{m_2}{m_0} - (\frac{m_1}{m_0})^2. \tag{7.8}$$

7.1.3 Probability of sequential or non-sequential firing

We are interested in propagation of a signal from one end of the dendrite to the other by means of sequential firing of spines as discussed previously in Section 3.4. This is our condition that must be satisfied for a travelling wave to be present. Therefore we need to consider the probability of a spine firing given that its neighbour has fired previously. We can also look at the probability of firing out of order as a measure of this propagation. If the probability of firing out of order is low then this means we are more likely to see successful propagation of the wave. To assess whether we have sequential firing or not we simulated the system for 100 realisations and recorded the number of times each spine fired at each time step. This gives a numerical estimate of the probability of firing at each moment in time and since the spine fires for a length

of time τ_S then the probability of firing in the deterministic or low noise case is one for a length of time τ_S. Therefore each point on the curve is the probability that the spine is firing at that point in time. We can visualise the probability of sequential firing by plotting the probability curves for the neighbouring spines of interest, if the curves overlap then there exists a certain probability that the spines will fire out of sequence, see Figure 7.2 to Figure 7.4 for some examples of these plots. Plot (a) in each of these figures shows an overlap which is due to the discretisation of the system and not to an out of order firing event.
The subsequent figures are for a short cable studded with 37 spines and an input strength of $\eta_0 = 1$, which was the value used in Chapter 4 where we looked at the effect of noise on the SDS model, and for different values of noise intensity ν. Figure 7.2 and Figure 7.3 show, for selected pairs of spines, the probability of firing as a function in time and for different levels of multiplicative white noise intensity, the form of the multiplicative noise is $g(U) = U^2$.

Figure 7.2 shows the probability of firing at each time step for spine 3, solid line, and spine 4, dashed line, and the noise intensity increases in each plot. As expected, as the noise level increases there is more probability of firing out of sequence, but there is also less probability that the spines will fire at all. This can also be seen in Figure 7.3 and Figure 7.4 for pairs of spines 17, 18 and 35, 36 respectively, where as the noise increases the probability profile becomes so small that there is little probability of firing at the end of the cable. This is apparent where the amplitude of the peaks decrease as the noise intensity increases, and the probability of firing plots for neighbouring spines starts to overlap more as the noise intensity increases, e.g. consider the plots for spines 3 and 4 which overlap a little when $\nu = 0.1$ but clearly overlap considerably when $\nu = 10$. This agrees with the previous results, in Section 4.4.1, of low-level noise having little effect on the propagation and mid-level noise killing propagation.

We can look at the conditional probability that spine 3, for example, fires before a later site n given that spine 3 does fire, i.e.:

$$P(t_3 < t_n | \text{spine 3 fires}) = \frac{1}{P_3^\infty} \int_0^\infty P_3(t_n) p_n(t_n) dt_n + 1 - P_n^\infty. \tag{7.9}$$

Equation (7.9) is constructed with the following terms:

- $1 - P_n^\infty$ = the probability that spine n does not fire, since we need to take into consideration that spine n may never reach threshold,
- $\frac{P_3(t_n)}{P_3^\infty} = \int_0^{t_n} \frac{p_3(t_3)}{P_3^\infty} dt$: is the probability that spine 3 fires in the interval $[0, t_n]$ given that it does fire at some time in $[0, \infty)$,
- $\int_0^\infty p_n(t_n) dt_n$: the probability that spine n fires at some time in $[0, \infty)$.

We can also consider the probability that there is a firing event at spine n and not at spine 3: $P_n^\infty(1-P_3^\infty)$, is unlikely to occur since P_3^∞ is almost always 1 for the value of η_0 used in the SDS model. When we consider, $P(t_3 < t_4|\text{spine 3 fires})$ we find that at low noise sequential firing is very nearly guaranteed. However at higher noise levels we cannot say that the firing will be sequential. Also as η_0 increases the probability of sequential firing decreases, but the probability of spine four firing but not spine 3, in all cases, is zero or very close to zero.

7.1.4 Extent of propagation

We can also consider the extent of propagation (N_e, the number of the last spine to fire before propagation fails) along the cable. The point at which the wave fails to propagate is when all spines up to the final spine, n say, fire but the spine immediately following it does not, i.e. spine $(n+1)$ fails to fire, so again this agrees with our earlier definition of a successful travelling wave in Chapter 4. The probability that a wave reaches, at least, spine n is the same as the probability that spine n fires:

$$P(N_e \geq n) = P_n^\infty, \tag{7.10}$$

and the probability that the wave reaches spine n but not spine $(n+1)$ is $P(N_e = n) = P_n^\infty - P_{n+1}^\infty = m_0^n(1-m_0)$. So the expected extent of propagation is given by:

$$\mathbb{E}(N_e) = \sum_n (P_n^\infty - P_{n+1}^\infty). \tag{7.11}$$

Now that we have the extent of propagation and the expected firing times for certain parameter values, we can use them to calculate a speed for the wave. If, for example, the wave is expected to reach spine, $n > 3$, then we can use:

$$c = \frac{x_n - x_3}{\mathbb{E}(t_n) - \mathbb{E}(t_3)} \tag{7.12}$$

as an estimate of the wave speed.

7.2 Simulation of SDS model and data collecting

In order to check that the analysis in Section 7.1 agrees with the behaviour of the SDS model observed in Chapter 4 we collect the expected/mean values of the voltage in the cable and the voltage in the spine heads. We can then proceed to the results of the analysis, e.g. probability of firing and expected extent of propagation, after using the mean voltages in the equations of Section 7.1. The SDS model was simulated as previously described in Chapter 3 and Chapter 4, then the data was collected,

$\mathbb{E}(V(x,t))$, $\mathbb{E}(U_n(t))$, and a distribution of firing times, $\mathbb{E}(T_n)$, for a range of values of ν, the strength of the multiplicative white noise in the spine heads, and for a range of values of input strength (of injected pulse), η_0, see Section 2.8 in Chapter 2. For each combination of ν and η_0 a total of 100 realisations were simulated and the average values recorded. Therefore the data, e.g. V, at a point x along the cable consists of contributions from all previous firing events at spines with $x_n \leq x$. Using these voltages we can apply the equations described in Section 7.1 to get the results laid out in the results Section 7.2.1.

7.2.1 Results

Figure 7.5 to Figure 7.7 show the probability distributions for a range of η_0, ν and at different spines.

As is expected the peaks of the distributions occur at greater times the further one looks along the cable, this is only natural since if propagation occurs we expect it to happen with some finite speed. For example in Figure 7.5, spine 3, the top left plot for $\eta_0 = 1$ (dashed line) peaks at approximately 0.9 and in Figure 7.6, spine 18, the top left plot for $\eta_0 = 1$ (dashed line) peaks at approximately 13.

The level of noise in the system also greatly effects the probability distributions. The noise can stop propagation, since the graphs show a long delay, or require a large input before a sizable peak is seen, e.g at $\nu = 1$ spine 3, Figure 7.5, has quite a strong peak, but at spine 18, Figure 7.7 you require a greater input to see a peak, and at 18 this peak is very small.

The figures indicate that there are two regions of noise that give different behaviours; at lower noise intensities the wave behaves close to the deterministic behaviour and at higher levels the noise terminates wave propagation.

Figure 7.8 shows the probability of spines 3, 18, 36, firing in infinite time. It can be seen that, at all levels of noise, $P_n^\infty = 1$ can be achieved if there is a strong enough input pulse, η_0. Again the three regions of noise give different results: low noise requires little input to get firing, mid range requires the larger inputs to achieve firing further along the cable and at high noise the input required decreases again. For $\eta_0 = 1$ we can see the behaviour observed in Chapter 4, i.e. at mid levels of noise $P^\infty < 1$, see Figure 7.8.

The mean firing time, of a spine n, decreases as the strength of the input pulse η_0 increases, see Figure 7.9. This is as expected since in the absence of any active properties or noise in the system, a larger input will have more of an impact along the cable due to the diffusive properties of the cable equation. As noise in the system increases there is an increase in the expected firing time, $\mathbb{E}(T_n)$.

This expected time difference suggests that there is a maximum delay for each level of noise and input level. This property could be used to determine whether a firing event

is due to the input/previous firing event or if it is purely noise induced. The results we found using this methodology were in agreement with the full simulation of the system, as expected since we had to start with the full simulation to get the voltages required for this analysis. It is encouraging to know that the probabilistic representation can extract the correct information but it does not save any computing time, in fact it requires more, and we may as well interpret the data from the simulations directly. We show in the subsequent Section 7.2.2 that we can use Equation (7.2), Equation (7.6) etc, along with a reduced simulation to extract the overall behaviour of the system and save vast computing time.

Using Equation (7.12) and the expected firing times as shown in Figure 7.9 we can calculate the expected speed of the wave with different strengths of noise in the spine heads. We look at Figure 7.10 where we deal with noise intensity values that are small and do not pose any problems with voltage values leaving the range of $[0, 1]$. We can see that the speed increases as ν increases, this is in agreement with previous results shown in Chapter 4 as measured by the level set method and the freezing method in Figure 4.8. Here the expected firing time of the third spine, $\mathbb{E}(T_3)$, is used to calculate the speed and poses the same problem as discussed in the level set method in Section 4.4.1 (shown in Figure 4.8): where the first point used in the level set method is taken close to the start of the cable then we get an artificial effect, seen as small hump in speed plot, from the initial conditions on U. However the plot here, Figure 7.10 agrees with Figure 4.8, so we know that using expected firing times to calculate speed is a valid method.

7.2.2 Speed measured using reduced cable dynamics

This section shows how we can use the voltage evolution at one spine, with noisy IF dynamics, to capture the overall behaviour of the SDS model under the influence of white noise in the spine heads.

We look at the voltage in the cable at one spine, spine n, at x_n under the assumption that the previous two spines, at x_{n-1} and x_{n-2} have fired. To construct the voltage in the cable given these firing events we use the series solution given in [109] instead of a direct numerical simulation.

Using Equation (2.22) we can obtain the voltage in the cable by multiplying the input to the cable, which is the voltage from the spine firing $\frac{Dr_a}{r}(\hat{V}(x_n, t) - V(x_n, t))$, by Green's function derived for the cable as in Section 2.2.3 and integrating over the time interval of interest. Here n is the spine number and so we sum over all the spines (it will be two here) to ensure the firing event from each spine contributes to the

voltage in the cable, Equation (7.14).

$$V(x,t) = \frac{Dr_a}{r} \sum_n \int_0^t G(x - x_n, t - s)[\hat{V}(x_n, s) - V(x_n, s)]ds, \tag{7.13}$$

can be simplified under the assumption that $\frac{Dr_a}{r}$ is small, see [109] for detailed description, and we obtain:

$$V(x,t) = \sum_n H(x - x_n, t - T_n), \tag{7.14}$$

where x_n is the position of the nth spine, and T_n is the firing time of the nth spine.

$$H(x,t) = A_\epsilon(x, t - \min(t, \tau_s)) - A_\epsilon(x,t)\ , \tag{7.15}$$

where τ_s is the length of the pulse injected into the cable when a spine fires and

$$\begin{aligned} A_\epsilon(x,t) &= \frac{\eta_0}{4}\sqrt{\frac{1}{\epsilon D}}\exp(-|x|\sqrt{\frac{\epsilon}{D}})\text{erfc}(\frac{-|x|}{\sqrt{4Dt}} + \sqrt{\epsilon t}) \\ &+ \exp(|x|\sqrt{\frac{\epsilon}{D}})\text{erfc}(\frac{|x|}{\sqrt{4Dt}} + \sqrt{\epsilon t}). \end{aligned} \tag{7.16}$$

which $\epsilon = \frac{1}{\tau}$, τ is the time constant of the cable and D is the diffusion coefficient.

We use the sum, Equation (7.14), to evaluate the voltage at the spine of interest given that the previous two spines have fired, i.e. spines at $x_n - x_{n-1} = d$ and $x_n - x_{n-2} = 2d$. We then use the stochastic integrate and fire dynamics to evaluate the voltage in the spine, therefore we can apply the previous methodology to obtain the probability of firing and the expected time of firing. The speed of the wave is now $c = d/\mathbb{E}(T)$.

Figure 7.11 shows the same behaviour as seen in the full SDS model Chapter 4, with the speed of the wave reducing as the noise intensity increases and the dynamics of the full cable have been greatly reduced to those of just one spine and 2 firing events.

7.3 Conclusions

We started this chapter by using the mean voltages, **U** and **V**, obtained from full simulation of the SDS model with multiplicative white noise in the spine head dynamics, to check that the probabilistic model proposed for calcium dynamics, in [54], is a suitable representation of the noisy SDS model. We discovered that this probabilistic model, with a modified threshold condition Equation (7.3) to capture the relevance of

both spine head and cable voltage in firing times, is a good representation of the SDS model and agrees with the behaviour observed in the direct simulations of Chapter 4. From Figure 7.2 - Figure 7.4 we observed that for spines at different points along the cable the probability of firing out of order increases as the noise increases, in agreement with the full simulations of Chapter 4. These figures also showed that as the noise increased the probability of firing at all decreases which again agrees with the results that higher levels of noise kills all propagation in the SDS model. We used the probability density for spines at different points along the cable to calculate the speed of the waves as the noise intensity increased. To do this the probability density was used to find the mean firing times $\mathbb{E}(T_n)$, which in turn was used to calculate the speed. This was found to agree with the speed in the full model: as the noise intensity increased the speed decreased. The agreement of the probabilistic model and the full model was encouraging and suggested that there may be a way to capture the mean behaviour of the noisy system without the full set of equations being solved many times. We used the series sum solution of the SDS model, Equation (7.14), to reduce the dynamics from the whole cable to just two previous, neighbouring firing events in an attempt to discover the mean firing time of a third spine and so find the speed of a wave on the whole cable. This method was very quick to simulate and did show the reduced speed as the intensity of the noise increased but the value of the speed was different to that of the full simulation and the change in speed was much smaller over the same range of noise intensities than in the full model. This suggests that while the overall behaviour can be captured by only two previous firing events, the details of the behaviour requires the information from all firing events. Similarly for the branching structure there appears to be no quick method of simulating the behaviour by using a probabilistic model despite the fact that the probability of a wave crossing the branching point and bringing the first spine on the post branch point dendrite to threshold to fire can be written explicitly in terms of the firing events of the two pre branch point spines. The analysis above can be extended to consider the probability of spines firing on a branched structure. On each of the branches the analysis will be exactly as previously described for the unbranched dendrite, with minor differences in the parameters, e.g. resistance, capacitance, spine input strength etc since they may change from branch to branch. These parameter differences and the contributions from all branches at the branch point will affect the structure of the rate constant $k(V)$.

We have a simple branching morphology with 3 branches, one parent branch and two daughter branches, which we label $b1$ and $b2$, respectively. If each daughter branch has m spines then the probability of the first spine on the parent branch firing is given

by:

$$\begin{aligned} p_1(t) &= \int_0^t \int_0^t p_1(t|T_{b1m}, T_{b2m}) p_{b1m}(T_{b1m}) p_{b2m}(T_{b2m}) dt_{b1m} dt_{b2m} \\ &+ (1 - P_{b2m}(t)) \int_0^t p_1(t|T_{b1m}, T_{b2m}) p_{b1m}(T_{b1m}) dt_{b1m} \\ &+ (1 - P_{b1m}(t)) \int_0^t p_1(t|T_{b1m}, T_{b2m}) p_{b2m}(T_{b2m}) dt_{b2m} \end{aligned} \tag{7.17}$$

The three terms of this equation relate to different permutations of firing events which could effect the probability of the wave crossing the branch point and raising the first spine on the parent branch to threshold and so leading it to fire. The first term is the probability density of spine 1 firing given that the last spines on each branch fire, term two is the probability that the last spine on branch one fires but the last spine on branch 2 does not and the final term is the probability density of spine 1 firing conditional on the last spine in branch 2 firing but not the last spine on branch one. To simulate this system, the SDS model as it is outlined in section 3 can be used for the individual branches in this structure but there will be different boundary conditions on the terminal points of branches 1 and 2 and on the starting point of the main branch, i.e. at the branch point. The conditions that need to be satisfied at the branching point are simply those imposed by Kirchhoff's voltage and current laws, see Chapter 2 for the numerical method used to simulate a branched structure such as this. We simulate the branched structure with noise in the spine heads 100 times to create a mean value for the cable voltage, spine head voltage and to obtain the probability of firing as a function of time; to do this we simply record the firing time of each spine for each time step. We know how each branch behaves individually since it is simply a section of straight cable as treated previously in this chapter, but we would like to know how the branch point behaves. The terms of Equation (7.17) cannot be obtained without full simulation of the system, so unlike the single cable case there appears to be no quick method of simulating the whole branched structure.

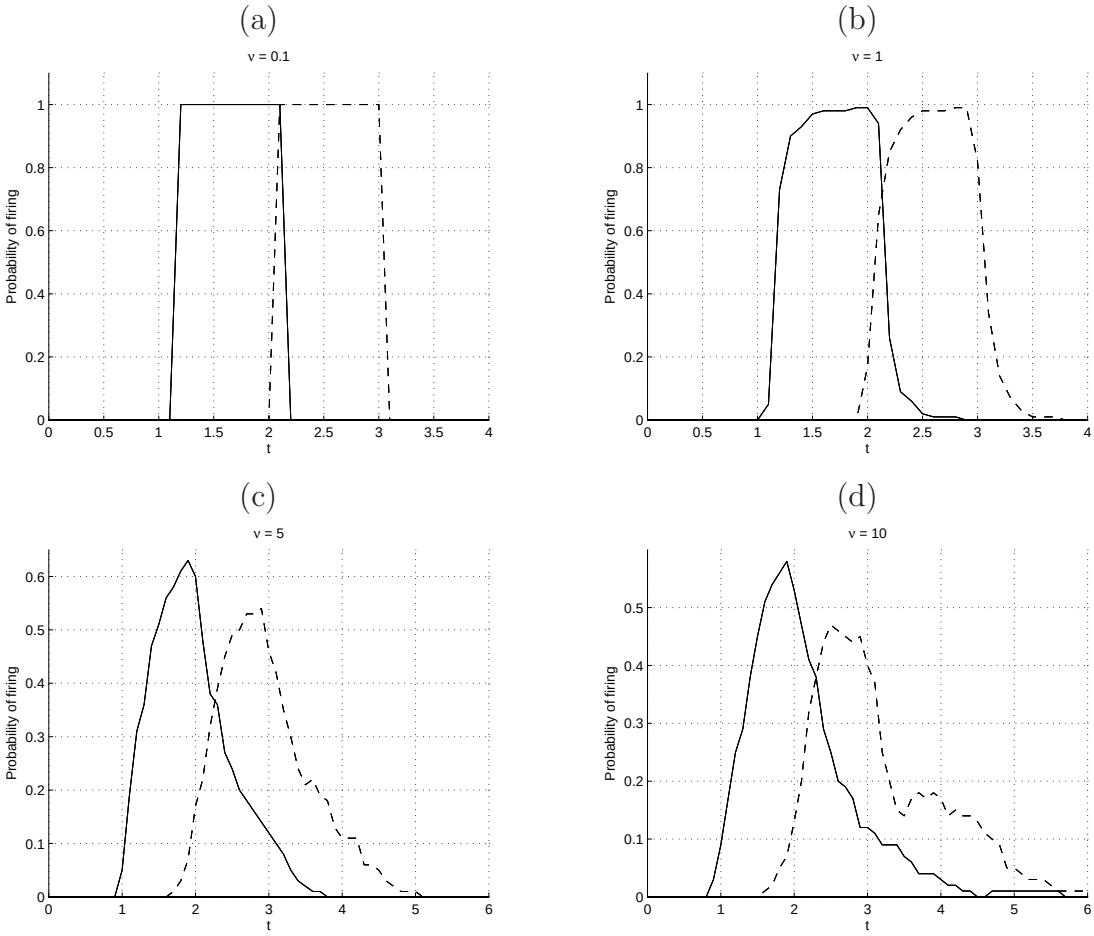

Figure 7.2: This figure shows the probability that the spine is firing, at each point in time, near the start of the cable: spine 3, solid line, and spine 4, dashed line, as the noise intensity increases. The values for the intensity are $\nu = 0.1$ (plot (a)), $\nu = 1$ (plot (b)), $\nu = 5$ (plot (c)) and $\nu = 10$ (plot (d)). Since each spine fires for a length of time τ_S then the probability of firing at low levels of noise (e.g. plot (a)) is one for each point in time for a length of time τ_S. As the noise intensity increases the neighbouring spines have an increased probability of firing out of order, as seen in the overlapping of the curves, and a lower probability of firing at all, as seen in the reduced amplitude of the curves. Note that the overlap in plot (a) is due to the temporal discretisation and not due to an out of order firing event. All other parameters are as described in the parameter list at the start of the thesis. We solve Equation (4.4) along with Equation (4.1), to collect mean values of $V(x,t)$ and $U(x,t)$, with temporal discretisation $\Delta t = 0.1$, $t \in [0, 70] and$ spatial discretisation $\Delta x = 0.08$, $x \in [0, 48]$ (measured in non-dimensional electronic length units) with 37 spines attached along this length. The boundary conditions used are Dirichlet and initial conditions $V(x,0) = 0$, $U_1(0) = U_2(0) = 0.04$ and $U_{n>2} = 0$.

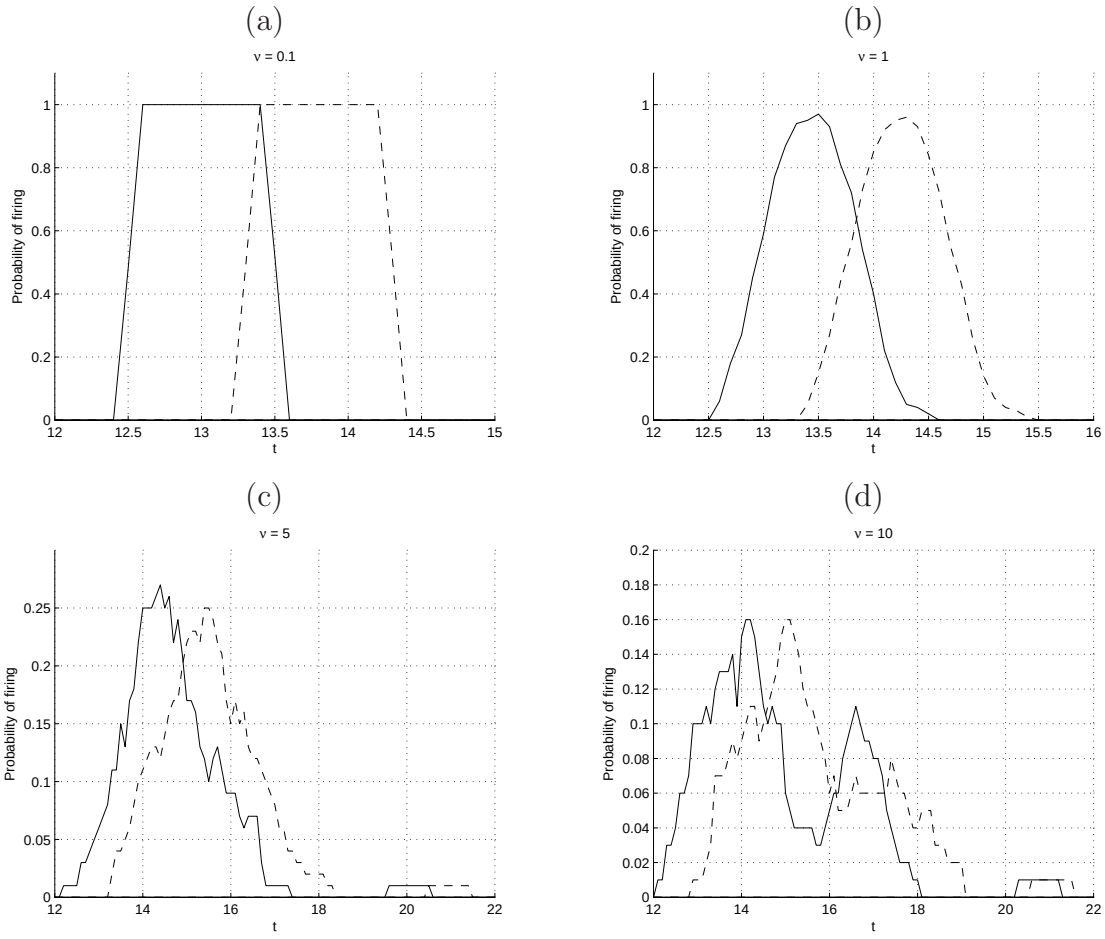

Figure 7.3: This figure shows the probability of firing for mid cable spines 17, solid line, and 18, dashed line, as the noise intensity increases. The values for the intensity are $\nu = 0.1$ (plot (a)), $\nu = 1$ (plot (b)), $\nu = 5$ (plot (c)) and $\nu = 10$ (plot (d)). As the noise intensity increases the neighbouring spines have an increased probability of firing out of order, as seen in the overlapping of the curves, and a lower probability of firing at all, as seen in the reduced amplitude of the curves. All other parameters are as described in the parameter list at the start of the thesis. We solve Equation (4.4) along with Equation (4.1), to collect mean values of $V(x,t)$ and $U(x,t)$, with temporal discretisation $\Delta t = 0.1$, $t \in [0, 70] and$ spatial discretisation $\Delta x = 0.08$, $x \in [0, 48]$ (measured in non-dimensional electronic length units) with 37 spines attached along this length. The boundary conditions used are Dirichlet and initial conditions $V(x,0) = 0$, $U_1(0) = U_2(0) = 0.04$ and $U_{n>2} = 0$.

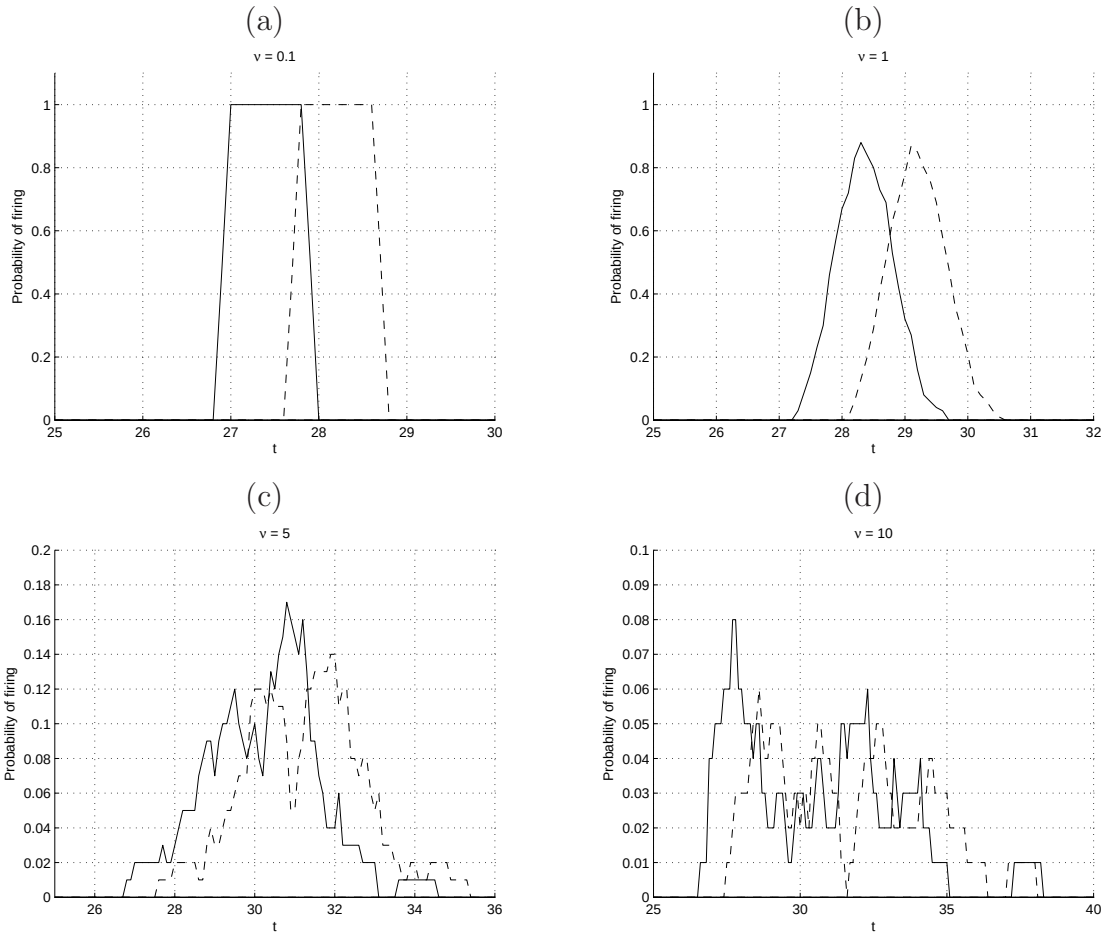

Figure 7.4: This figure shows the probability of firing for mid cable spines 35, solid line, and 36, dashed line, as the noise intensity increases. The values for the intensity are $\nu = 0.1$ (plot (a)), $\nu = 1$ (plot (b)), $\nu = 5$ (plot (c)) and $\nu = 10$ (plot (d)). As the noise intensity increases the neighbouring spines have an increased probability of firing out of order, as seen in the overlapping of the curves, and a lower probability of firing at all, as seen in the reduced amplitude of the curves. All other parameters are as described in the parameter list at the start of the thesis. We solve Equation (4.4) along with Equation (4.1), to collect mean values of $V(x,t)$ and $U(x,t)$, with temporal discretisation $\Delta t = 0.1$, $t \in [0, 70] and$ spatial discretisation $\Delta x = 0.08$, $x \in [0, 48]$ (measured in non-dimensional electronic length units) with 37 spines attached along this length. The boundary conditions used are Dirichlet and initial conditions $V(x,0) = 0$, $U_1(0) = U_2(0) = 0.04$ and $U_{n>2} = 0$.

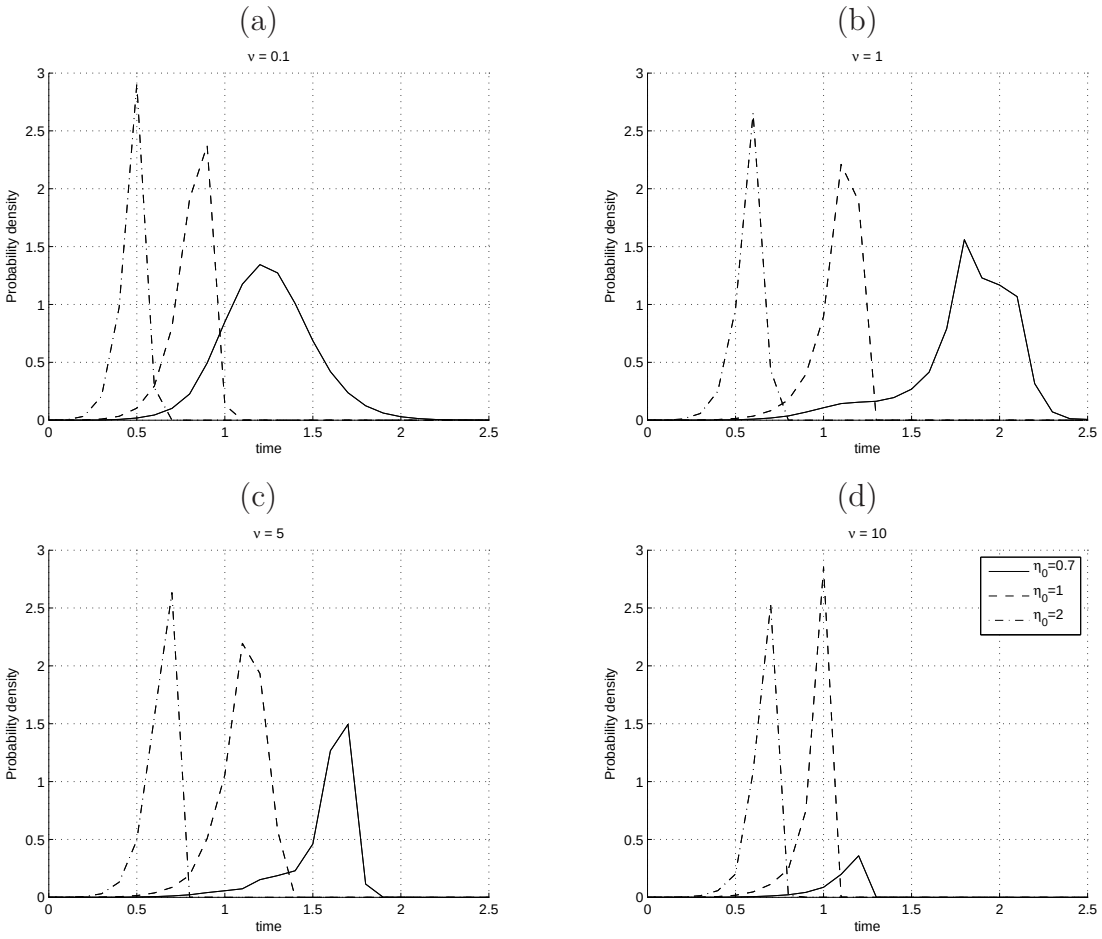

Figure 7.5: Probability distribution for spine 3, $p_3(t)$ for different values of η_0, the strength of the injected voltage, and ν, the strength of the multiplicative noise. Solid line $\eta_0 = 0.7$, dashed line $\eta_0 = 1$ and dot dashed line $\eta_0 = 2$. Plot (a) $\nu = 0.1$, plot (b) $\nu = 1$, plot (c) $\nu = 5$ and plot (d) $\nu = 10$. As the noise intensity increases from plot to plot the curves move further along in time which indicates that the noise is slowing the time to fire. The injected current also affects the time to fire and so shifts the plots backwards in time as the input pulse strength increases. All other parameters are as described in the parameter list at the start of the thesis. We solve Equation (4.4) along with Equation (4.1), to collect mean values of $V(x,t)$ and $U(x,t)$, with temporal discretisation $\Delta t = 0.1$, $t \in [0, 70] and$ spatial discretisation $\Delta x = 0.08$, $x \in [0, 48]$ (measured in non-dimensional electronic length units) with 37 spines attached along this length. The boundary conditions used are Dirichlet and initial conditions $V(x,0) = 0$, $U_1(0) = U_2(0) = 0.04$ and $U_{n>2} = 0$.

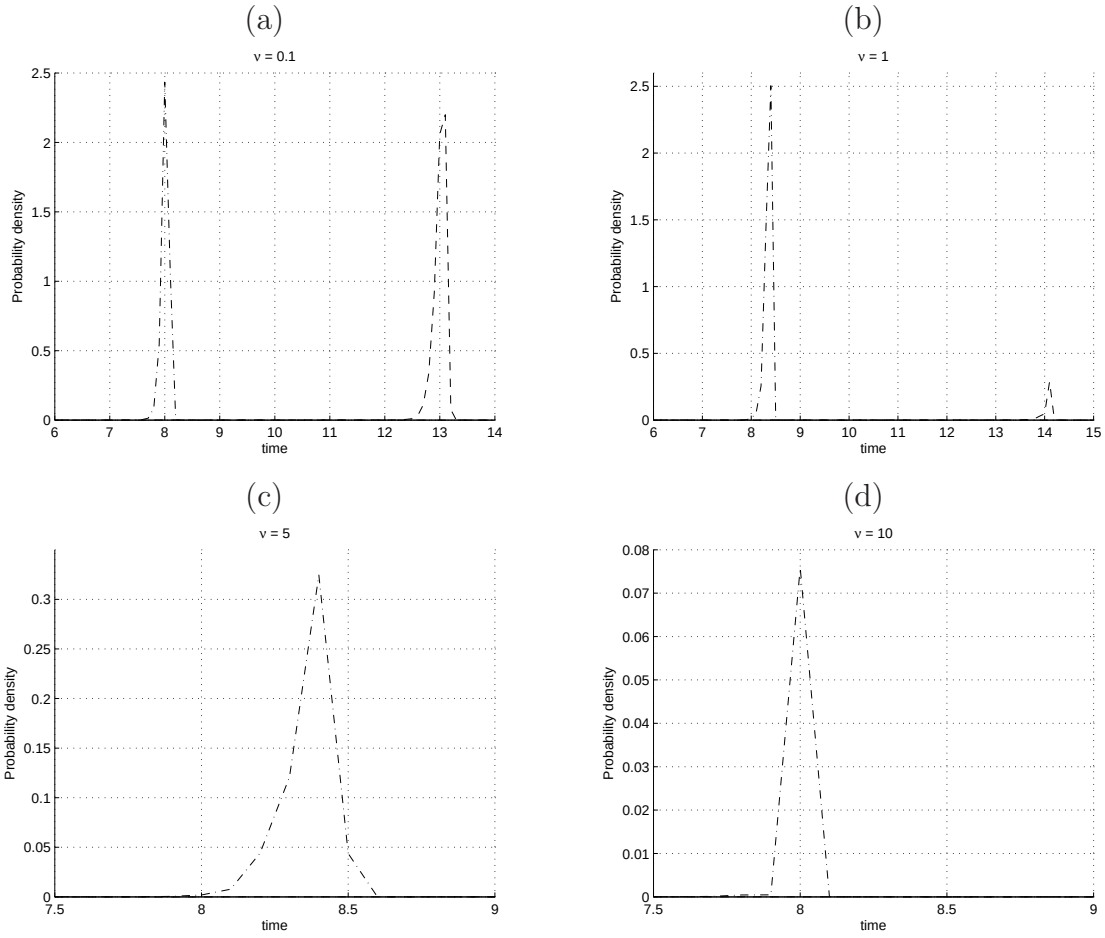

Figure 7.6: Probability distribution for spine 18, $p_{18}(t)$ for different values of η_0, the strength of the injected voltage, and ν, the strength of the multiplicative noise. Solid line $\eta_0 = 0.7$, dashed line $\eta_0 = 1$ and dot dashed line $\eta_0 = 2$. Plot (a) $\nu = 0.1$, plot (b) $\nu = 1$, plot (c) $\nu = 5$ and plot (d) $\nu = 10$. As the noise intensity increases from plot to plot the curves become much smaller in amplitude and so suggest that there is less probability of this spine firing. The curve for $\eta_0 = 0.7$ cannot be seen in this figure since it is not strong enough to support a travelling wave with this parameter configuration and as the noise intensity increases the $\eta_0 = 1$ curve also disappears suggesting again that this pulse is not strong enough to produce a wave which reaches spine 18 when higher levels of noise are present. All other parameters are as described in the parameter list at the start of the thesis. We solve Equation (4.4) along with Equation (4.1), to collect mean values of $V(x,t)$ and $U(x,t)$, with temporal discretisation $\Delta t = 0.1$, $t \in [0, 70] and$ spatial discretisation $\Delta x = 0.08$, $x \in [0, 48]$ (measured in non-dimensional electronic length units) with 37 spines attached along this length. The boundary conditions used are Dirichlet and initial conditions $V(x,0) = 0$, $U_1(0) = U_2(0) = 0.04$ and $U_{n>2} = 0$.

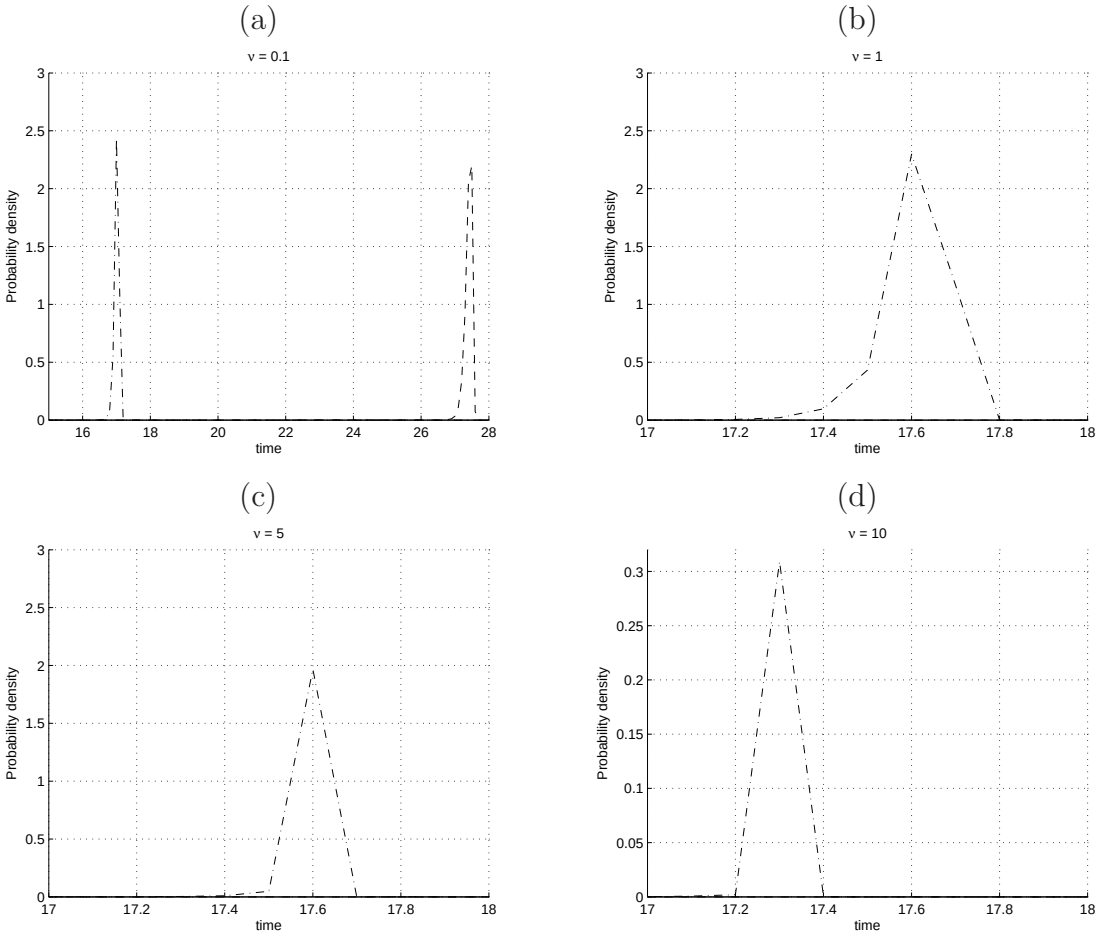

Figure 7.7: Probability distribution for spine 36, $p_{36}(t)$ for different values of η_0, the strength of the injected voltage, and ν, the strength of the multiplicative noise. Solid line $\eta_0 = 0.7$, dashed line $\eta_0 = 1$ and dot dashed line $\eta_0 = 2$. Plot (a): $\nu = 0.1$, plot (b): $\nu = 1$, plot (c): $\nu = 5$ and plot (d): $\nu = 10$. As the noise intensity increases from plot to plot the curves become much smaller in amplitude and so suggest that there is less probability of this spine firing. The curve for $\eta_0 = 0.7$ cannot be seen in this figure since it is not strong enough to support a travelling wave with this parameter configuration and as the noise intensity increases the $\eta_0 = 1$ curve also disappears suggesting again that this pulse is not strong enough to produce a wave which reaches spine 36 when higher levels of noise are present. All other parameters are as described in the parameter list at the start of the thesis. We solve Equation (4.4) along with Equation (4.1), to collect mean values of $V(x,t)$ and $U(x,t)$, with temporal discretisation $\Delta t = 0.1$, $t \in [0, 70] and$ spatial discretisation $\Delta x = 0.08$, $x \in [0, 48]$ (measured in non-dimensional electronic length units) with 37 spines attached along this length. The boundary conditions used are Dirichlet and initial conditions $V(x,0) = 0$, $U_1(0) = U_2(0) = 0.04$ and $U_{n>2} = 0$.

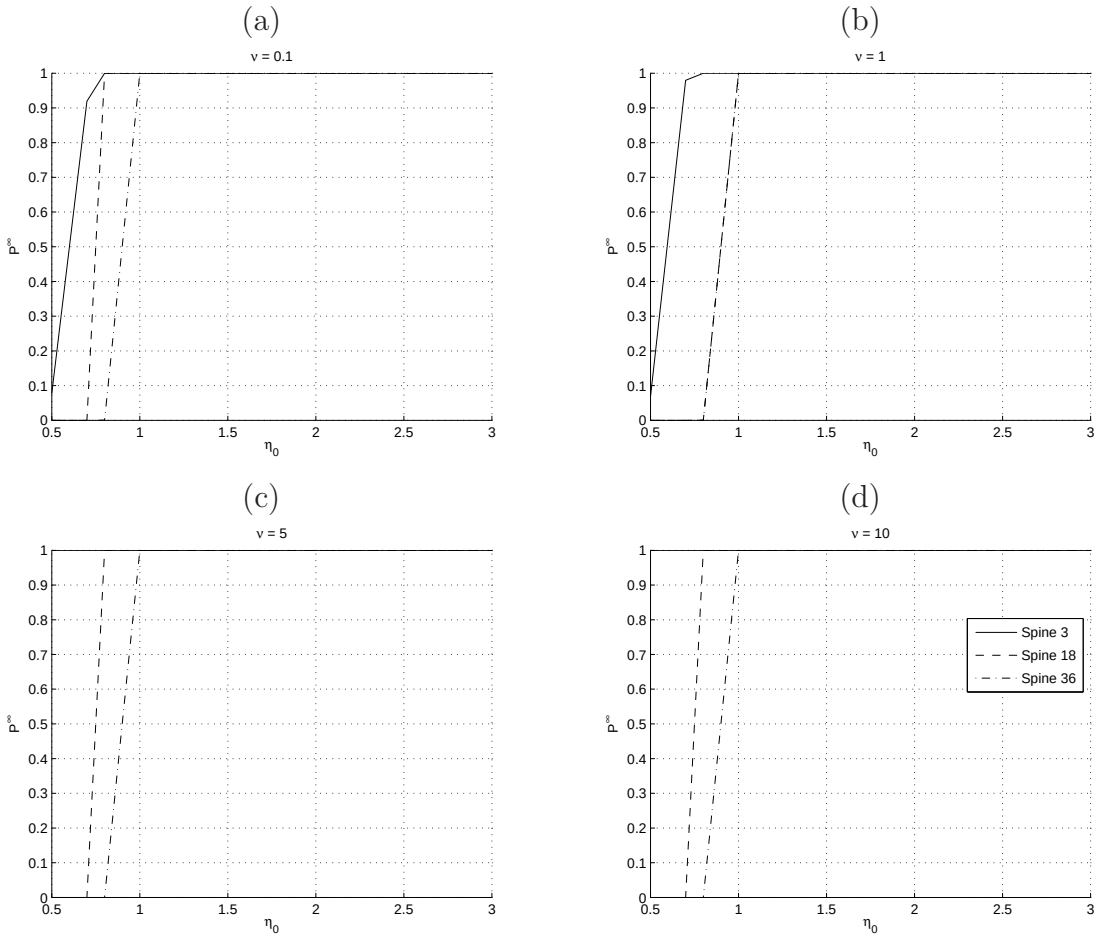

Figure 7.8: Probability of firing in infinite time, P_n^∞, $n = 3, 18, 36$. Spine 3 solid line, spine 18 dashed line and spine 36 dot dashed line. This shows that if the input pulse is strong enough, the spines will always fire at some point in time, even when there is noise in the system. The noise intensity for each plot is: plot (a) $\nu = 0.1$, plot (b) $\nu = 1$, plot (c) $\nu = 5$ and plot (d) $\nu = 10$. All other parameters are as described in the parameter list at the start of the thesis. We solve Equation (4.4) along with Equation (4.1), to collect mean values of $V(x,t)$ and $U(x,t)$, with temporal discretisation $\Delta t = 0.1$, $t \in [0, 70] and$ spatial discretisation $\Delta x = 0.08$, $x \in [0, 48]$ (measured in non-dimensional electronic length units) with 37 spines attached along this length. The boundary conditions used are Dirichlet and initial conditions $V(x, 0) = 0$, $U_1(0) = U_2(0) = 0.04$ and $U_{n>2} = 0$.

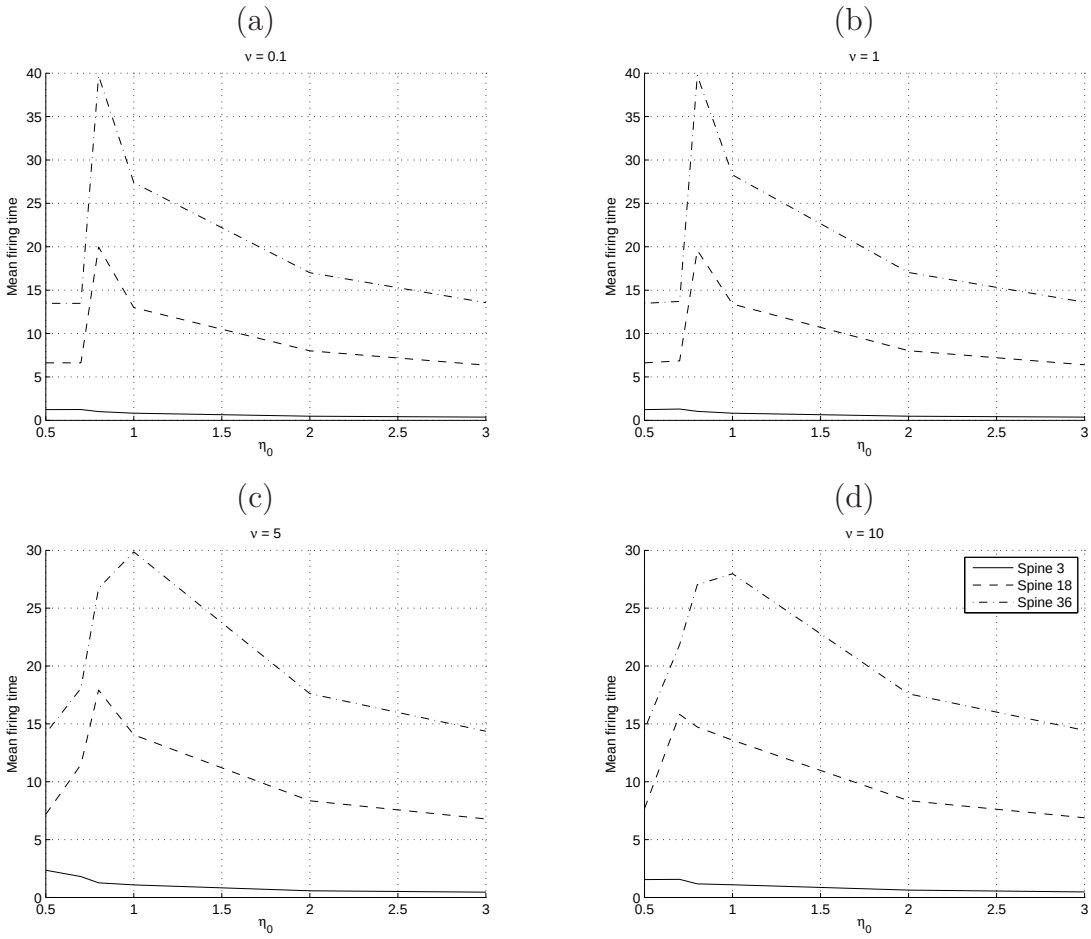

Figure 7.9: This figure shows the mean firing time of spines 3, solid line, 18, dashed line and 36, dot dashed line, as a function of the input pulse strength, η_0, and as the noise intensity increases. As the noise intensity increases the firing time of spines 18 and 36 clearly reduce, this arises from the random, noise induced behaviour at higher noise levels.All other parameters are as described in the parameter list at the start of the thesis. We solve Equation (4.4) along with Equation (4.1), to collect mean values of $V(x,t)$ and $U(x,t)$, with temporal discretisation $\Delta t = 0.1$, $t \in [0, 70] and$ spatial discretisation $\Delta x = 0.08$, $x \in [0, 48]$ (measured in non-dimensional electronic length units) with 37 spines attached along this length. The boundary conditions used are Dirichlet and initial conditions $V(x,0) = 0$, $U_1(0) = U_2(0) = 0.04$ and $U_{n>2} = 0$.

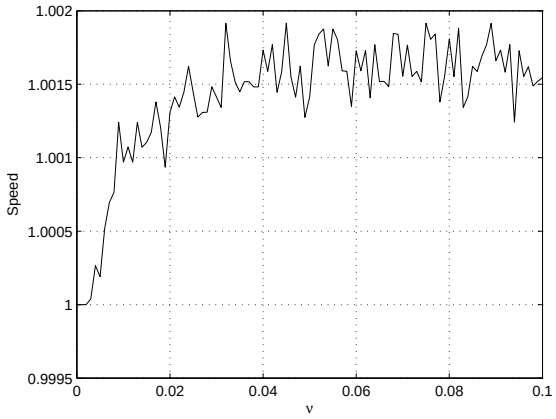

Figure 7.10: Speed of wave calculated using expected firing times, over range of small values of multiplicative noise intensity and input pulse strength $\eta_0 = 1$. All other parameters are as described in the parameter list at the start of the thesis. We solve Equation (4.4) along with Equation (4.1), to collect mean values of $V(x,t)$ and $U(x,t)$, with temporal discretisation $\Delta t = 0.1$, $t \in [0, 70] and$ spatial discretisation $\Delta x = 0.08$, $x \in [0, 48]$ (measured in non-dimensional electronic length units) with 37 spines attached along this length. The boundary conditions used are Dirichlet and initial conditions $V(x, 0) = 0$, $U_1(0) = U_2(0) = 0.04$ and $U_{n>2} = 0$.

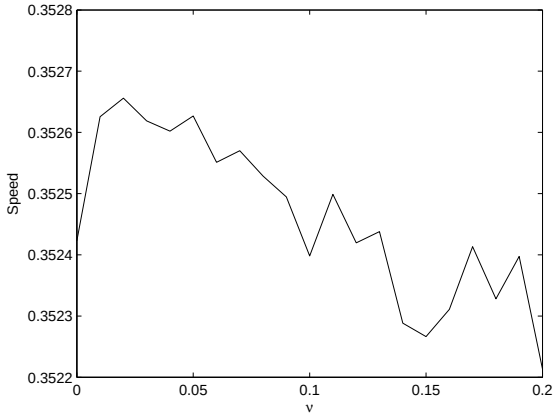

Figure 7.11: Speed of stochastic wave measured using only the expected firing time of one spine given that 2 previous spines have fired.

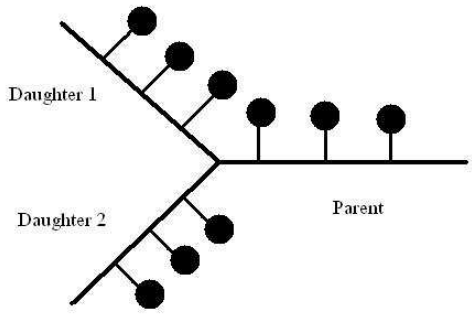

Figure 7.12: Diagram showing the branched structure we are considering, with one parent and two daughter branches.

Chapter 8

Signal processing in the SDS and BR model

8.1 Introduction

A question which must be asked is whether the propagation of travelling waves in the SDS or BR model with noise, contains any useful information, e.g. can it help to carry an input pattern from one end of the cable to the other? It has been shown in the experimental work of Fortune and Rose [28] that the spiny dendrites in the dorsal torus semicircularis of the fish Eigenmannia, have low-pass filtering properties. The SDS model was also shown to have low-pass filtering properties, see [109] that were consistent with those observed experimentally by Rose and Fortune. We now look at the filtering properties with noise in the system and with a noisy input signal. We show that the system is robust to noise in these circumstances i.e. it still supports the low-pass filtering properties when the system is noisy and can recover the mean input frequency when the signal is corrupt. The timing of action potentials is also important in the filtering behaviour since if there is variation in the spike arriving at the end of the cable then the system may not be able to pick out the input frequency, [64] talks of the importance of action potential timing in the neuron in perception and movement of invertebrates. We can also, in a small range of parameters, show that the SDS model for the spiny dendrite can act like a high-pass filter. This allows high frequency input signals to propagate to the end of the cable, the output frequency will be determined by the refractory time of the system and low frequency input signals will not induce travelling waves, therefore no output.

The branched SDS model also shows some processing properties when in the correct parameter ranges. We can show that a single branch point can act as a simple logic gate. In the parameter ranges used throughout most of the previous work the branch point acts as an OR gate, but can behave, with the correct parameters, as an AND gate. The following tables are the truth tables for the AND and OR gate

Input A	Input B	Output
0	0	0
0	1	0
1	0	0
1	1	1

Input A	Input B	Output
0	0	0
0	1	1
1	0	1
1	1	1

Figure 8.1: The truth tables for: left table is the AND logic gate and the right table is the OR logic gate. The AND gate requires 2 inputs to give an output whereas the OR gate only requires one input to give an output.

respectively, where A and B are the input from each branch, i.e. if the last spine on branch A fires the input is 1 (0 if it does not fire), and the output column represents the firing of the first spines after the branch point.

8.2 Measuring the filtering properties of the SDS model

To look at the filtering properties we want to input a train of pulses, of period T, into one end of a length of spiny dendrite, modelled by the SDS model, and measure the period, T_{out}, at the other end of the cable. Here we use a step function to model the pulses, which are on for the same length of time as a firing spine, τ_s, have strength A and the time between them is our input period T:

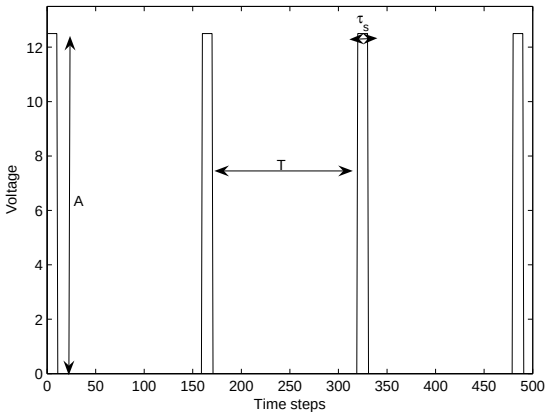

Figure 8.2: Schematic of input pulse train which is injected to the beginning of the cable at the same position as spine one, showing the amplitude of the input pulses, A, and the length of time the pulse is on for, τ_s. T is the period between the pulses.

When we add this injected current to the cable equation we simply get one extra term to solve in Equation (8.1). We choose this form of the input since it is the same as the input (action potential) from a firing spine therefore it is a realistic representation

of an input spike train for the SDS model.

$$\frac{\partial V(x,t)}{\partial t} = D\frac{\partial^2 V(x,t)}{\partial x^2} - \frac{V(x,t)}{\tau} + Dr_a\rho(x)\frac{\hat{V}(x,t) - V(x,t)}{r} + V_{inj}(x_{inj},t) \quad (8.1)$$

Parameters in Equation (8.1) are the same as before and $V_{inj}(x_{inj},t)$ is given by:

$$V_{inj}(x_{inj},t) = \begin{cases} A & t_{on}^k \leq t \leq (t_{on}^k + \tau_s) \\ 0 & (t_{on}^k + \tau_s) \leq t \leq t_{on}^{k+1}, \end{cases}$$

where t_{on}^k's are a sequence of times that the pulse begins and $t_{on}^1 = 0$, $t_{on}^k = t_{on}^1 + k(\tau_s + \frac{T}{\Delta t})$, T is the period of the input signal and Δt is the time step used in the simulation of the the SDS model. The whole system can still be solved as in Chapter 4, with white noise in the spine heads. When we have the full solution for the system with the new injected voltage we need to determine the output frequency/period. To do this we look at the firing times, T_n^m is the mth firing time of spine n, which we choose to be near the end of the cable over all time. When we do this we will get m times which corresponds to each firing event. To get T_{out}, the period of the output signal, we need to find the times between firing events or simply for each m, $t_{out} = T_n^m - T_n^{m-1}$. When this is done for each m we get a value for T_{out} by taking the average of all the t_{out} values.

8.2.1 Noisy input signal

When considering the case where the input signal has some variation in T we choose the input period from a normal distribution of times. We generate an input train of pulses with $T_{in} = T + \sigma\eta(t)$, where $\eta(t) \in \mathcal{N}(0,1)$. We generate the $\mathcal{N}(0,1)$ in Matlab using the 'randn' function which has a mean of zero and a variance of one. We use σ to alter the variance and so our $T_{in} \in \mathcal{N}(T,\sigma)$, i.e. mean T and variance σ. The input mean is chosen to be a variety of values to correspond with a range of low and high frequencies. We then measure the output as outlined in the previous subsection, by looking at the firing times of the final spine and again take the average values to be the final output frequency.

8.3 Results

We first look at the response of the deterministic system to a deterministic input, we have plotted the 'frequency in' (f_{in}) vs 'frequency out' (f_{out}), on a log scale, rather than the period T. Frequency is given by $f = \frac{1}{T}$. It can be seen in Figure 8.3 that the system responds with the same output frequency to the input frequency for low frequency. Then when the system gets close to the refractory time of the spines $\tau_R = 7$,

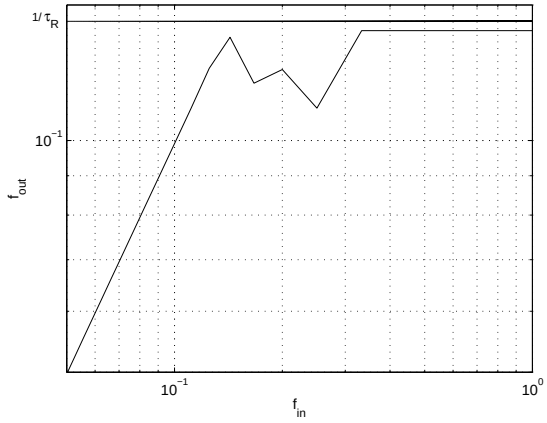

Figure 8.3: Deterministic response of the SDS model, as a low-pass filter, to input spike train with various frequencies, refractory time $\tau_R = 7$. All other parameters are as described in the parameter list at the start of the thesis. We solve Equation (4.4) along with Equation (4.1), to collect mean values of $V(x,t)$ and $U(x,t)$, with temporal discretisation $\Delta t = 0.1$, $t \in [0, 70] and$ spatial discretisation $\Delta x = 0.08$, $x \in [0, 48]$ (measured in non-dimensional electronic length units) with 37 spines attached along this length. The boundary conditions used are Dirichlet and initial conditions $V(x,0) = 0$, $U(x,0) = 0$.

in this case, there is a bit of fluctuation caused by the interplay of the input frequency and the natural frequency caused by the refractory time. When the input frequency becomes faster than the natural frequency then the system can only respond at the frequency determined by τ_R i.e. $f_R = \frac{1}{\tau_R}$ and the graph levels out. We first look at the response of the system to V_{inj}, described by Equation (8.2), with temporal white noise in the spine heads as described by the discretised Equation (4.10), with $g(U) = U(1-U)$. Figure 8.4 shows how the low-pass filtering properties start to break down as the noise in the spine heads increases, the higher noise does not allow the SDS dendrite to transmit the input signal. The linear response in the lower part of the graph, low frequencies, is lost and when f_{in} crosses the natural frequency the response is not always that of the refractory time. The overall trend of the noise is to smooth the graph and remove the fluctuations from the interplay of the input frequency and the natural frequency of the system. The system is, however, robust to low levels of noise.

Figure 8.5 shows that the SDS system is robust to noisy input signals. The system responds with approximately the same frequency as the mean of the input signal up to the refractory time, τ_R, just as the deterministic case, Figure 8.3. After the refractory time has been passed by the mean input frequency, the system again responds roughly at the frequency of the refractory time $\frac{1}{\tau_R}$ as in the deterministic case. The interplay between the refractory time and the input frequency, seen as the fluctuations in Figure 8.3, smooths as the noise in the signal increases. So again the system is able to sort

out the underlying frequency from a noisy signal.

We now briefly look at the SDS model in a high-pass filter configuration. Figure 8.6 shows that the system can also be configured in such a way that it acts like a high-pass filter. For low input frequencies there is no response at the other end of the cable and so $f_{out} = 0$. As the input frequency increases the system does respond albeit only at the natural frequency of the system. This high-pass property is an interplay between the voltage threshold for firing h and the amplitude of the input pulse when a spine fires η_0. The first spine will receive more input from a faster frequency, since the voltage will build up before it can diffuse along the cable, but with a slower frequency the voltage has no opportunity to build up since it is diffusing faster than the input is being received. However if the input amplitude is large then one input alone is enough to bring the first spine to threshold, and fire, so the high-pass property is lost, therefore this phenomenon is only seen when the amplitude and threshold are in the right balance.

8.3.1 Filtering with the BR model

In the BR model there is no way to control the natural refractory scale of the system, or the size of the action potential and so we can only observe the low-pass filtering behaviour. The system also reacts with a frequecy of multiples of the input frequency, e.g. $f_{out} = \frac{1}{2} f_{in}$, making a filtering graph, like Figure 8.3, difficult to plot and understand.

8.4 Branched SDS model as a logic gate

Figure 8.7 shows the branched configuration of 3 lengths of SDS cable that can carry out some simple logic computations. It does this by acting like a logic gate, the AND or OR gates. As such it can take input from the two branches, A and B, and then 'decide' if the signal will proceed any further by either allowing the spine on the parent branch to fire or not; see the truth tables, Figure 8.1. An example of this type of logic behaviour in nature can be found in the developing retina of the mouse ([12]). This paper shows that in early development all pre-synaptic neurons must fire to generate activity on the post-synaptic side of the system, like an AND gate. Later in development this all or nothing set up changes so that the post-synaptic neurons do not require all pre-synaptic neurons to fire to illicit a response, behaviour akin to an OR gate.

8.4.1 Simulating the discretised branched SDS model

The numerical algorithm follows exactly the same steps as for the non-branched SDS model, the only difference is that we have to keep track of the spines firing on separate branches and we use the the method described in Section 3.3.3 to modify the discretisation matrix to include the branch point. The wave is initiated in both the daughter branches, as for the single branch SDS model, and the firing of the spines on both of these branches is stored and contributes to the cable voltage as in the single SDS cable. We keep track of the firing on each branch and observe the spines on the parent branch to see if the signal passes the branch point. We simulate this system when one or other or both of the daughter branches is initially set above threshold to simulate the different configurations of logic inputs, as in Figure 8.1. If the parent branch fires in response to any input then it is an OR gate, but if the parent branch requires both daughter branches to fire to initiate a wave then it is and AND gate. Figure 8.8 shows a wave travelling down the daughter branches to the branch point and inducing a wave in the parent branch. The first two waves on the figure show the voltage on the daughter branches and are both attached to the branch point. Figure 8.8, shows the branched structure in the AND gate configuration and if either one of the daughter branches does not support a wave then the signal will not pass the branch point. To switch to an OR gate situation then we need to change some of the system parameters. The AND gate shown above has the standard parameter values for each branch that have been used in the SDS model throughout this body of work, and we can switch to an OR gate by changing only one of these many parameters. If the threshold for firing in the IF dynamics for the spines of the parent branch is reduced slightly then we can show that if only one of the daughter branches has a travelling wave then the wave will still pass through the branch point and induce a wave in the parent branch. We can also change the value of λ (the space constant) which effectively changes the diffusion constant of the branch, and achieve the same effect of turning the structure from the AND gate to the OR gate. Figure 8.9 show the SDS branching structure acting as an OR gate.

8.5 Conclusion

The aim of this chapter was to investigate how robust the dendrite models were to noise by showing how they process some information which has been very simply encoded as a chain of input pulses with an associated frequency. We started with the SDS model with a configuration of parameters which means the system acts as a low-pass filter, i.e. only signals with low input frequencies can pass along the cable and be observed as a spike train at the opposite end. In the deterministic case the system responds, at low input frequencies, at the same frequency until it nears the

refractory time of the system when there is an interplay between the input and refractory frequencies resulting in a non-linear response until the input frequency exceeds the refractory time when the system responds with a constant output frequency close to the refractory time. When noise is added to the spine heads and the system is again stimulated with a periodic input, we obtained the average response for different levels of noise. Figure 8.4 shows the results of these noisy filters, and the SDS model is very robust to low levels of noise since there is little difference in the response of the deterministic system and plots (a) and (b) of Figure 8.4. Plots (a) and (b) have noise intensities $\nu = 0.01$ and $\nu = 0.1$, both of which support sequential firing and full propagation, as seen in Chapter 4, so it is expected that they will respond accurately to the input frequency. The surprising result is that even at levels of noise where the waves in the SDS model are not always sequential, as in plot (c) $\nu = 0.8$ and plot (d) $\nu = 1$ of Figure 8.4, the system still responds at frequencies very close to the input frequency when f_{in} is below the refractory time. The accuracy is lost as the input frequency exceeds the refractory time and the system no longer responds with a constant frequency of $\frac{1}{\tau_R}$. When the deterministic SDS model is subjected to a noisy input again it shows a remarkable ability to determine the underlying mean frequency. At low levels of noise in the input signal the SDS model responds with the mean frequency up to the refractory time where it responds with a constant frequency, just like a low pass filter. As the noise increases the system loses some accuracy but still remains close to the input frequency. Interestingly the noisier input signals smooth out the response when the input frequency is close to the refractory time, but the system never reaches the refractory time response. We also briefly showed that the SDS model can act as a high pass filter if the parameters of the system are chosen properly, although there is only a small range of parameters where this occurs, suggesting that the natural arrangement for a dendrite (modelled by the SDS model) is that of a low-pass filter. The branched SDS model showed more versatility in the processing capabilities of the SDS model. When arranged such that there are three lengths of SDS dendrite meeting at a single branch point and the distal ends of the two daughter branches are thought of as input sites and the proximal end of the parent branch as the output site, this structure can be used as a logic gate. A simple change in the parameters of each branch can switch the behaviour of the branched SDS model from an AND gate to an OR gate. If each of the branches has the parameters used throughout this work so far then the branched structure acts like an AND gate.

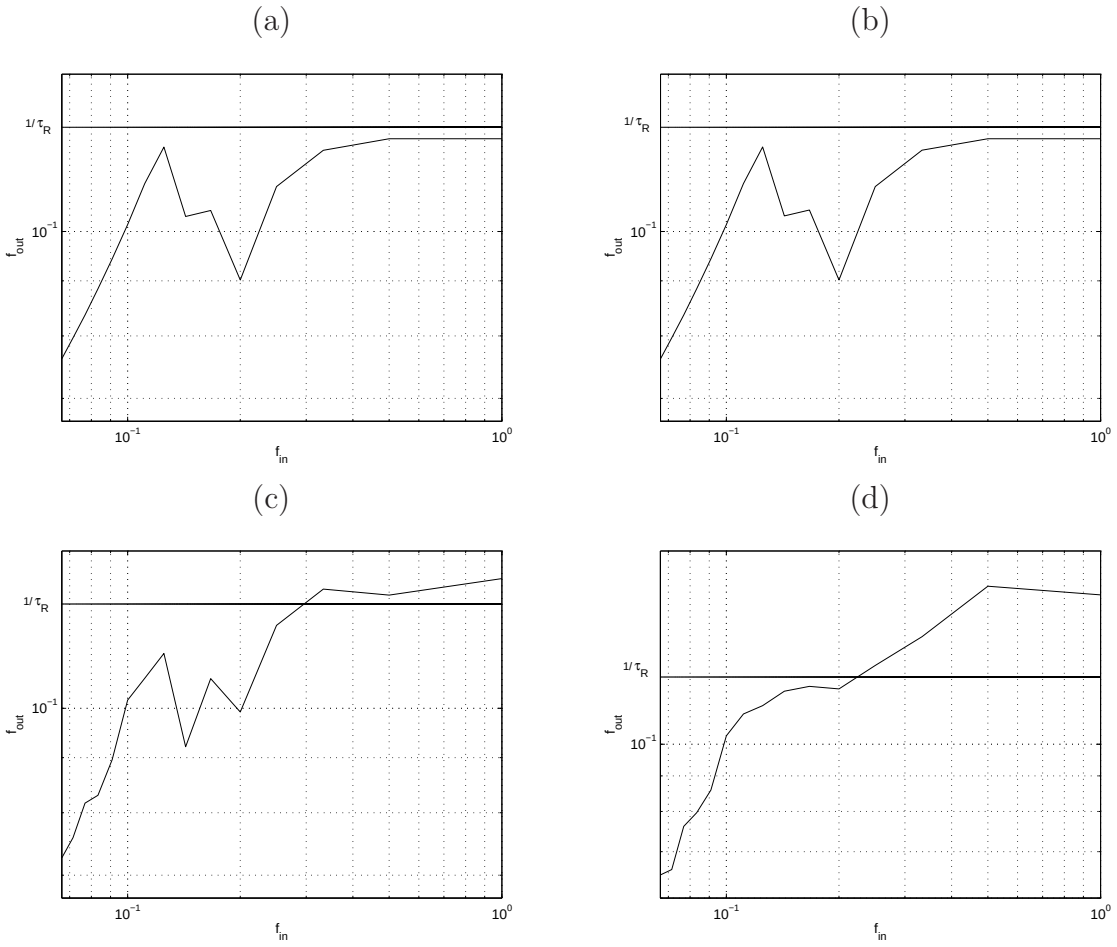

Figure 8.4: These figure show the mean response, $n_{sample} = 100$, of the SDS model with white noise in the spine heads to different frequencies of input signal. The input signal is injected to the cable as a train of voltage steps. Plot (a): shows f_{in} vs f_{out} with $\tau_R = 7$ and the intensity of the noise in the spine heads is $\nu = 0.01$, plot (b): shows f_{in} vs f_{out} with $\tau_R = 7$ and the intensity of the noise in the spine heads is $\nu = 0.1$, plot (c): shows f_{in} vs f_{out} with $\tau_R = 7$ and the intensity of the noise in the spine heads is $\nu = 0.8$, plot (d): shows f_{in} vs f_{out} with $\tau_R = 7$ and the intensity of the noise in the spine heads is $\nu = 1$. All other parameters are as described in the parameter list at the start of the thesis. We solve Equation (4.4) along with Equation (4.1), to collect mean values of $V(x,t)$ and $U(x,t)$, with temporal discretisation $\Delta t = 0.1$, $t \in [0, 70] and$ spatial discretisation $\Delta x = 0.08$, $x \in [0, 48]$ (measured in non-dimensional electronic length units) with 37 spines attached along this length. The boundary conditions used are Dirichlet and initial conditions $V(x, 0) = 0$, $U(x, 0) = 0$.

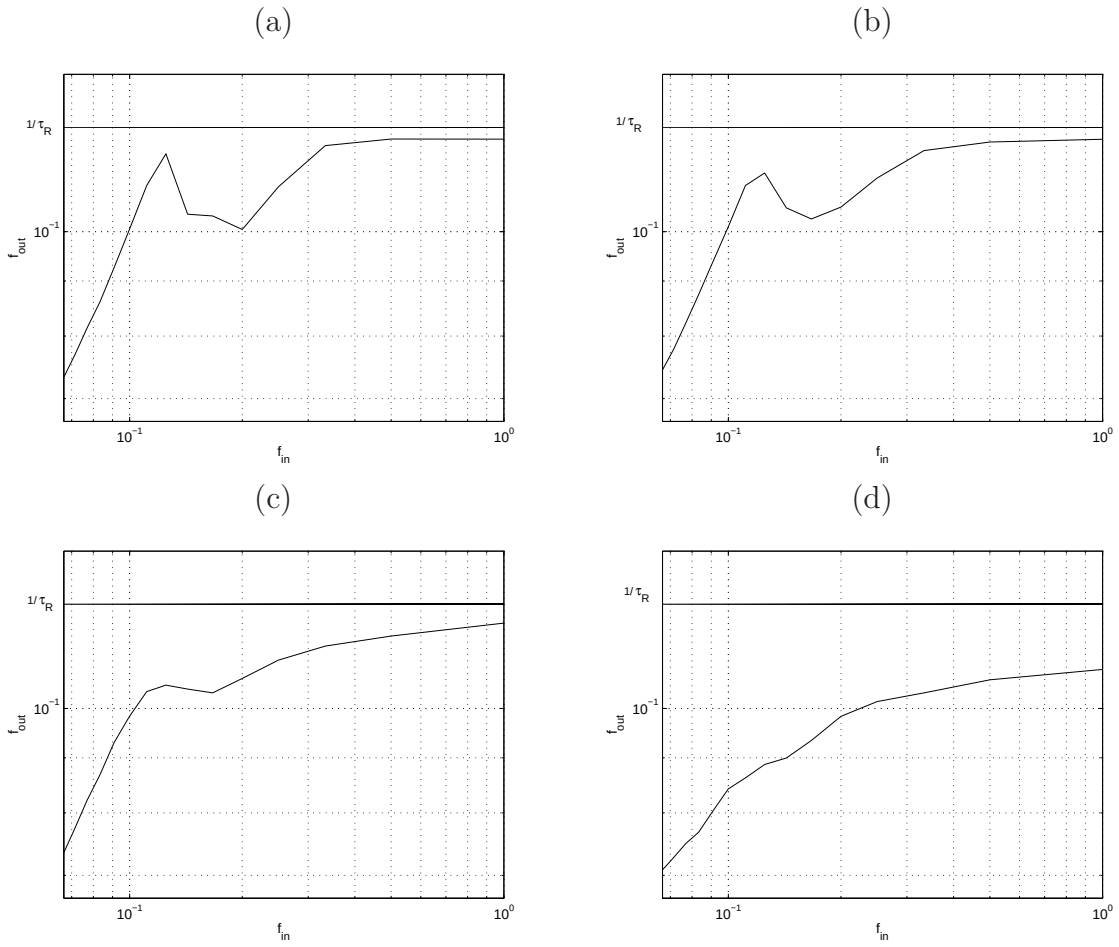

Figure 8.5: This figure shows the SDS model response, f_{out}, to a periodic input, $\mathbb{E}(f_{in})$, that is corrupted with noise. Plot (a) has $\sigma = 0.5$, plot (b) $\sigma = 1$, plot (c) $\sigma = 2$ and plot (d) $\sigma = 5$. As the variation around the mean frequency increases the output frequency smooths out the variation which occurs just before refractory time, τ_R, is reached. Also the frequency stays below the refractory time, which is different to the case where the noise is intrinsic to the system. All other parameters are as described in the parameter list at the start of the thesis. We solve Equation (4.4) along with Equation (4.1), to collect mean values of $V(x,t)$ and $U(x,t)$, with temporal discretisation $\Delta t = 0.1$, $t \in [0, 70] and$ spatial discretisation $\Delta x = 0.08$, $x \in [0, 48]$ (measured in non-dimensional electronic length units) with 37 spines attached along this length. The boundary conditions used are Dirichlet and initial conditions $V(x,0) = 0$, $U(x,0) = 0$.

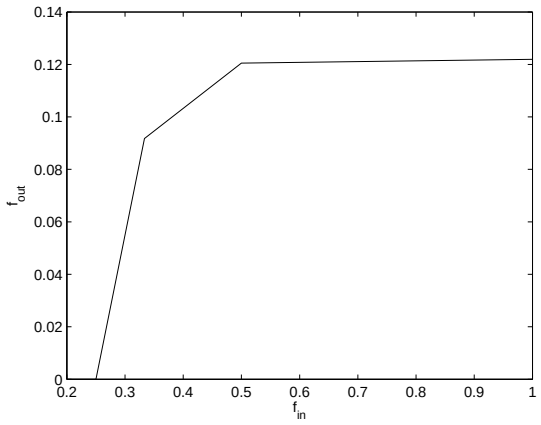

Figure 8.6: This figure shows the response of the SDS model in a high-pass filtering regime. The parameters are arranged such that only high frequency signals can pass to the end of the cable, low frequencies are blocked out.

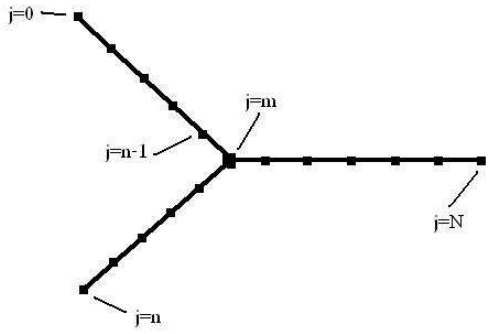

Figure 8.7: Diagram showing how the spatial steps are labelled for use in the spatial discretisation matrix A.

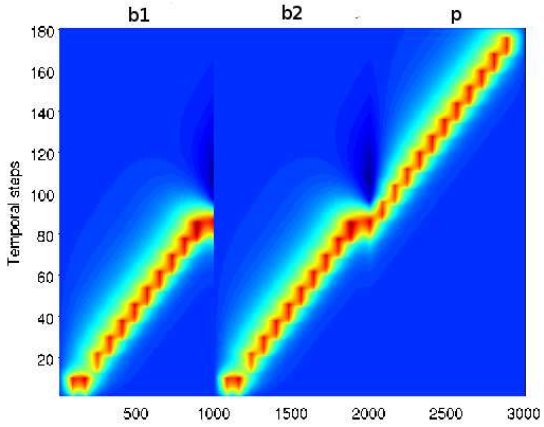

Figure 8.8: Voltage in the branched deterministic SDS model. The first two waves show the voltage in the daughter branches and the third (starting at a later time) is the wave in the parent branch. The first 2 spines on each daughter branch are set above threshold to induce a travelling wave. When these waves reach the branch point the voltage passes across the branch point and raises the voltage in the parent branch to induce firing in the spines here.

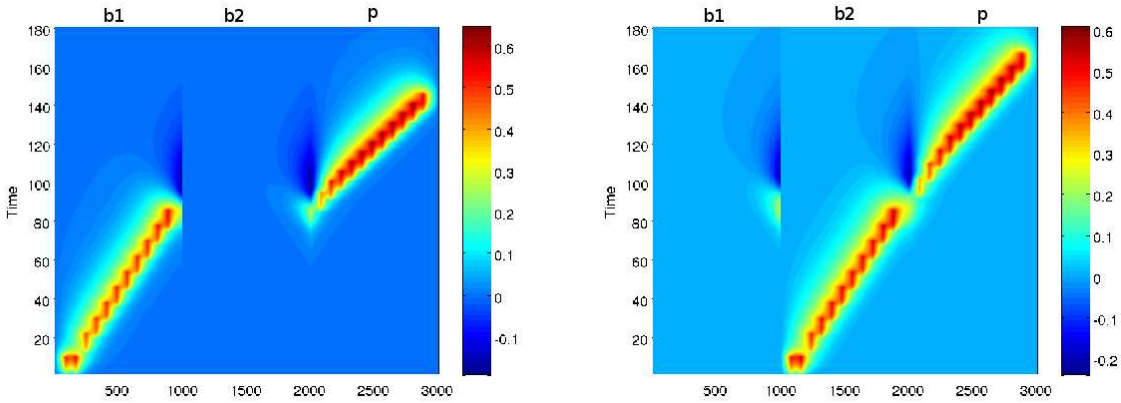

Figure 8.9: The left figure shows the branching structure acting as an OR gate when the first daughter branch has the first two spines set above threshold to induce a travelling wave which crosses the branch point. The right figure also shows the OR gate configuration when the other daughter branch is used to initiate a wave.

Chapter 9

Discussion

We set out to investigate the effects of different types of noise on models of spiny dendrites and have provided a comprehensive comparison of white, temporally and spatially correlated noise in two such models. We investigated the stochastic spike-diffuse-spike model and the stochastic Baer and Rinzel model driven by noise in the spine head and cable dynamics.

When the noise is in the SDS model the speed of any travelling wave decreases as the noise intensity increases but when the noise is in the BR model the speed of travelling waves increases as the noise intensity increases, when the noise is in the spines or spatially correlated in the cable. The main differences between the two models are the dynamics used to describe the evolution of the spine head voltage (integrate and fire dynamics in the SDS model and the Hodgkin Huxley equations in the BR model) and the spine density, $\rho(x)$ (discretely attached equally spaced spines in the SDS model and a constant in the BR model). This difference could be used to decide which model is a more accurate description of the real dendrite if an experiment could be devised in which the speed of an injected pulse travels the length of a dendrite with noise present. In an attempt to discover which of the differences in the models produced the difference in behaviour we investigated the BR model with a spatially dependent density. The form of the density was chosen such that it could be either a constant value or a series of discrete points just as in the BR and SDS models respectively. In the SDS limit where the spines are attached discretely the model can be thought to be the SDS model with HH dynamics in the spine heads and this model does act like the SDS model when we add noise to the system. Therefore we can conclude that the type of spine dynamics is not the reason for the difference in behaviour between the SDS and BR models and we investigate the affect of the spine density and so the spine stem. As we change the spine density from one limit to the other the cases in between are like looking at spines attached to the cable with a spine stem that has an area of attachment to the cable. The speed of the wave in the deterministic version of this model increases from the BR limit to the SDS limit and

there is an optimal value for the spine attachment that gives a maximum value of the speed. When there is noise in the system and we are changing the parameter from BR to SDS limits, the average speed of the wave starts faster than the deterministic wave speed and decreases below the deterministic speed at the SDS limit, in agreement with the previous results from the original SDS and BR models. Although this spatially dependent spine density gives some insight to the importance of the spine stem the model could be improved by a more realistic physical description of the way the spine stems are attached to the cable and perhaps by introducing some random distribution of the spines to investigate how this affects the behaviour. To take this a step further there could even be a simple learning rule introduced which could move the spines in relation to the levels of activity and give a time dependent spine distribution; [114] looks at a simple activity dependent spine plasticity in the BR model, so perhaps this could be extended to include noise. When the noise in the BR or SDS model is correlated, either in time or space, the correlation scale makes little difference to the behaviour of the system e.g. the speed of the stochastic waves in the SDS model as the strength of correlated noise increases decreases just as for white noise. When the noise is temporally correlated in the spine heads of the SDS model or spatially correlated in the cable of the SDS model, for a fixed level of noise intensity, the wave speed increases as the correlation scale increases. However the speed never increases beyond the speed of the deterministic wave. The temporally correlated noise in the spines of the BR model, may not affect the speed of the wave much but it does serve to stabilise waves which were out of order in the white noise case; thereby making the model robust to higher levels of noise.

Additive noise in both the dendrite models can induce synchronous behaviour in the spines. For very small levels of noise the systems are fairly robust to the noise; all waves fully propagate and are only subject to a small change in the speed. As the strength of additive noise increases the spines in the models begin to fire out of order and seemingly in a random fashion until a synchronous behaviour takes over and they all fire simultaneously, similarly observed in [77] and [76]. When the noise in the SDS model is additive and spatially correlated in the spine heads then the correlation scale can play a role in restoring sequential firing that has been destroyed by the noise, e.g. when the noise intensity is fixed a short correlation scale displays the out of order firing but as the correlation scale is increased the wave travels in a sequential fashion. The synchrony, [60], [122], [77], is an interesting phenomena that we observe in this work but have not investigated, and would be a clear place to extend the work by looking at this behaviour in the context of neural networks rather than as a model of a single dendrite or it could be used as means to dendritic democracy since an increase in the correlation scale encourages distal inputs to travel to the proximal end, [108], [39].

We investigated the possibility of representing the SDS model by a probabilistic model in an attempt to find a quick way to simulate the stochastic system. The model investigated, [54], did fit the behaviour of the stochastic SDS model very well as it captured the correct expected firing times, probability of firing out of order and the speed of the wave decreasing as noise intensity increased. Unfortunately this still required full simulation of the SDS model before the probabilistic model equations could be applied. One problem in trying to use this model to find a quick method of simulation is the lack of system parameters explicitly expressed in the model equations. The dynamics were all reduced to a threshold condition in the probability equation and so if we wish to investigate the role of the noise intensity or one of the system parameters, e.g. spine stem resistance r or spine density ρ, then we need to re-simulate the full system to fit the threshold condition again. This problem was complicated when we looked briefly at a branched structure since we now have three sets of parameters to consider. A reduced method would be very useful in this case in particular since the simulation time for a branched structure is considerably longer than that of the single dendrite.

When we looked at the signal processing capabilities of the SDS model we found that it was very versatile and could act as a low or high pass filter and as either an AND or OR logic gate in the branched configuration. The filtering properties are in agreement with previous results and experiments, see [109] and [28], and we showed in this work that not only does the system act as a filter but that this capability is robust to small noise. When the noise is intrinsic to the system the filtering properties remain as the noise intensity increases and even when the noise is high enough to produce out of order firing in the system some of the linear response remains, i.e. the model still responds with an output frequency close to the input frequency although it loses the limiting response of the refractory time when the input frequency is high. Alternatively we looked at a deterministic SDS model processing noisy signals; the input had a mean frequency that was corrupted by different levels of noise. When the noise in the signal is small again the system is robust to these variations and responds with the mean frequency and as the noise increases the system's response loses a bit of accuracy. This result is encouraging since we would expect that real neurons in the brain would have to cope with a lot of surrounding noise and yet signals are still successfully processed by the brain in performing even primitive tasks such as breathing. When the SDS dendrite is used as a three branch structure we can alter the parameters in each branch to change the system from working as an AND gate to an OR gate. We did not look at this configuration of the system with noise and it would be good to know how robust it was to noise. It would also be interesting to investigate if combinations of AND and OR units could be combined in such a way as to produce more complicated logic gate operations. There is experimental evidence

of living neurons working as logic gates, the paper [12] for example shows the same neural circuit working as both an AND gate and an OR gate at different stages of development and [25] used real hippocampal neurons grown on a patterned template to develop AND gates. A possible way to extend our work is to look at the BR model as a logic gate and perhaps add a soma to the SDS model dendrite to see how this affects the processing capabilities and further a series of these units could be coupled together in an attempt to reproduce the results of [25] for example.

We have shown that the SDS and BR models are robust to low levels of noise and that they can be used in a variety of configurations to show some signal processing capabilities. The SDS model is a simple model and it is exciting to see that it can be used in a variety of ways that reflect the real behaviour of neurons. Even when the noise exceeds the levels where clean signals and sequential firing of the spines occur the system displays some interesting behaviour; the noise induced synchrony of diffusively coupled IF units or HH units. There is much more that could be done and we have discussed a few possibilities in this chapter; even without adding in the complications of learning models or somas the basic SDS and BR models can still have more applications. Depending on one's interest the models can be extended to investigate spine motility and plasticity, network properties including noise induced synchrony and signal processing in the form of filters or logic gates. These models are truly versatile and relatively simple to use and simulate, even when stochastic as shown through this work by using simple numerical methods.

Bibliography

[1] M. K. N. Afghan, P. Jung, A. Neiman, and M. Rowe. Stimulus-induced synchronisation in Hodgkin-Huxley model neurons of cat retinal ganglion cells. *Acta Physica Polonica B*, 37(5):1387–1395, 2006.

[2] S. Alonso, F. Sagués, and J. M. Sancho. Excitability transitions and wave dynamics under spatiotemporal structured noise. *Physical Review E*, 65, 2002.

[3] P. Andersen, R. Morris, D. Amaral, T. Bliss, and J. O'Keefe. *The Hippocampus book*. Oxford University Press, 2007.

[4] J. Armero, J. M. Sancho, J. Casademunt, A. M. Lacasta, L. Ramírez-Piscina, and F. Sagués. External fluctuations in front propagation. *Physical Review Letters*, 76(17), 1996.

[5] L. Arnold. *Stochastic differential equations: Theory and applications*. John Wiley and sons, 1974.

[6] S. M. Baer and J. Rinzel. Propagation of dendritic spikes mediated by excitable spines: A continuum theory. *Journal of Neurophysiology*, 65(4):874–890, 1991.

[7] V. Beato, H. Engel, and L. Schimanski-Geier. Pulse trains propagating through excitable media subjected to external noise. *European Physical Journal B-Condensed matter and complex systems*, 53(3), 2007.

[8] T. Bonhoeffer and R. Yuste. Spine motility: phenomenology, mechanisms and function. *Neuron*, 35:1019 – 1027, 2002.

[9] P. Bressloff and S. Coombes. Travelling waves in chains of pulse-coupled integrate-and-fire oscillators with distributed delays. *Physica D*, 130:232 – 254, 1999.

[10] R. L. Burden and J. D. Faires. *Numerical analysis*. Brookes/Cole publishing company, 1997.

[11] B. J. Cao and L. F. Abbott. A new computational method for cable theory problems. *Biophysical Journal*, 64:303 – 313, 1993.

[12] A. R. Chandrasekaran, R. D. Shah, and M. C. Crair. Developmental homeostatis of mouse retinocollicular synapses. *The Journal of Neuroscience*, 27(7):1746–1755, 2007.

[13] C. Chow and N. Kopell. Dynamics of spiking neurons with electrical coupling. *Neural computation*, 12:1643 – 1678, 2000.

[14] P-L Chow. *Stochastic Partial Differential Equations*. Chapman and Hall, 2007.

[15] S. Coombes and P. C. Bressloff. Solitary waves in a model of dendritic cable with active spines. *SIAM Journal on Applied Mathematics*, 61:432–453, 2000.

[16] S. Coombes and P. C. Bressloff. Saltatory waves in the spike-diffuse-spike model of active dendritic spines. *Physical Review Letters*, 91, 2003.

[17] S. Coombes, G. J. Lord, and M. R. Owen. Waves and bumps in neuronal networks with axo-dendritic synaptic interactions. *Physica D*, 178:219 – 241, 2003.

[18] G. Da Prato and J. Zabczyk. *Stochastic equations in infinite dimensions*. Cambridge University Press, 1992.

[19] Y. Dan and M. Poo. Spike timing dependent plasticity of neural circuits. *Neuron*, 44:23 – 30, 2004.

[20] E. Doedel, A. R. Champneys, T. R. Fairgrieve, Y. A. Kuznetsov, B. Sandstede, and X. J. Wang. AUTO-07P. http://indy.cs.concordia.ca/auto, 1997.

[21] C. R. Doering, K. V. Sargsyan, and P. Smereka. A numerical method for some stochastic differential equations with multiplicative noise. *Physics Letters A*, 344:149–155, 2005.

[22] B. Ermentrout and C. Chow. Modelling neural oscillations. *Physiology and behaviour*, 77:629 – 633, 2002.

[23] L. C. Evans. www.math.berkeley.edu/∼evans/sde.course.pdf.

[24] A. A. Faisal, L. P. J. Selen, and D. M. Wolpert. Noise in the nervous system. *Nature reviews neuroscience*, 9:292–303, 2008.

[25] O. Feinerman, A. Rotem, and E. Moses. Reliable neuronal logic devices from patterned Hippocampal cultures. *Nature physics*, 4:967–973, 2008.

[26] O. Feinerman, M. Segal, and E. Moses. Signal propagation along unidimensional neuronal networks. *Journal of neurophysiology*, 94:3406–3416, 2005.

[27] J-M. Fellous, M. Rudolph, A. Destexhe, and T. J. Sejnowski. Synaptic background noise controls the input/output characteristics of single cells in an in vitro model of in vivo activity. *Neuroscience*, 122:811–829, 2003.

[28] E. S. Fortune and G. J. Rose. Passive and active membrane properties contribute to the temporal filtering properties of midbrain neurons in vivo. *The Journal of Neuroscience*, 17:3815–3825, 1997.

[29] L. Gammaitoni, P. Hanggi, P. Jung, and F. Marchesoni. Stochastic resonance. *Reviews of modern physics*, 70, 1998.

[30] J. García-Ojalvo and J. M. Sancho. *Noise in spatially extended systems*. Springer, 1999.

[31] T. C. Gard. *Introduction to stochastic differential equations*. Marcl Pekker inc., 1988.

[32] C. W. Gardiner. *Handbook of stochastic methods: for physics, chemistry and the natural sciences*. Springer-Verlag, 1983.

[33] W. Gerstner and W. M. Kistler. *Spiking neuron models: Single neurons, populations, plasticity*. Cambridge University Press, 2002.

[34] P. Goel and B. Ermentrout. Synchrony, stability and firing patterns in pulse-coupled oscillators. *Physica D*, 163:191 – 216, 2002.

[35] S. S. Goldstein and W. Rall. Changes of action potential shape and velocity for changing core conductor geometry. *Biophysical Journal*, 14:731 – 757, 1974.

[36] B. P. Graham and A. van Ooyen. Mathematical modelling and numerical simulation of the morphological development of neurons. *BMC neuroscience*, 7, 2006.

[37] S. Guan, Y. Lai, C. Lai, and X. Gong. Understanding synchronisation induced by "common noise". *Physics Letters A*, 353:30–33, 2006.

[38] D. Halliday, R. Resnick, and J. Walker. *Fundamentals of physics*. John Wiley and Sons, 2007.

[39] M. Häusser. Synaptic function: Dendritic democracy. *Current Biology*, 11(1), 2001.

[40] M. Haüsser, N. Spruston, and G. J. Stuart. Diversity and dynamics of dendritic signalling. *Science*, 290, 2000.

[41] D. J. Higham. An algorithmic introduction to numerical simulation of stochastic differential equations. *SIAM Review*, 43(3):525–546, 2001.

[42] D. J. Higham and N. J. Higham. *Matlab Guide*. SIAM, 2000.

[43] M. Hines. Efficient computation of branched nerve equations. *International journal of bio-medical computing*, 15:69 – 76, 1984.

[44] A. L. Hodgkin and A. F. Huxley. A quantitative description of membrane current and its applications to conduction and excitation in nerve. *Journal of physiology*, 117:500–544, 1952.

[45] Y. Horikawa. Noise effects on spike propagation in the stochastic Hodgkin-Huxley models. *Biological cybernetics*, 66:19–25, 1991.

[46] T. M. Hospedales, M. C. W. van Rossum, B. P. Graham, and M. B. Dutia. Implications of noise and neural heterogeneity for vestibulo-ocular reflex fidelity. *Neural computation*, 20:756–778, 2008.

[47] J. P. Hoyt. *A brief introduction to probability theory*. International textbook Co., 1967.

[48] J. J. B. Jack, D. Noble, and R. W. Tsien. *Electric current flow in excitable cells*. Oxford Science Publications, 1975.

[49] J. Jacod and P. Protter. *Probability essentials*. Springer, 2000.

[50] A. D. Dorval Jr. and J. A. White. Channel noise is essential for perithreshold oscillations in enthorinal stellate neurons. *Journal of neuroscience*, 25(43):10025–10028, 2005.

[51] S. Kádár, J. Wang, and K. Showalter. Noise-supported travelling waves in sub-excitable media. *Nature*, 391:770–772, 1998.

[52] H. Kasai, M. Matsuzaki, J. Noguchi, N. Yasumatsu, and H. Nakahara. Structure stability function relationships of dendritic spines. *Trends in neuroscience*, 26(7), 2003.

[53] W. E. Kaufmann and H. W. Moser. Dendritic anomalies in disorders associated with mental retardation. *Cerebral Cortex*, 10, 2000.

[54] J. P. Keener. Stochastic calcium oscillations. *Mathematical Medicine and Biology*, 23:1–25, 2006.

[55] P. E. Kloeden and E. Platen. *Numerical solution of stochastic differential equations*. Springer-Verlag, 1992.

[56] C. Koch. *Biophysics of computation: Information processing in single neurons*. Oxford University Press, 1999.

[57] C. Koch and I. Segev. *Methods in neuronal modeling, 2nd Edition: From ions to networks*. MIT Press, 1998.

[58] C. Koch and I. Segev, editors. *Methods in neuronal modelling: from ions to networks*, chapter 14. MIT Press, 1998.

[59] E. Kreyszig. *Advanced engineering mathematics*. John Wiley and Sons, 1999.

[60] C. Laing and G. Lord, editors. *Stochastic methods in neuroscience*, chapter 5. Oxford University Press, 2010.

[61] C. Laing and G. Lord, editors. *Stochastic methods in neuroscience*, chapter 9. Oxford University press, 2010.

[62] C. Laing and G. Lord. *Stochastic methods in neuroscience*. Oxford University Press, 2010.

[63] C. Laing and G. Lord, editors. *Stochastic methods in neuroscience*, chapter 4. Oxford University Press, 2010.

[64] C. Laing and G. Lord, editors. *Stochastic methods in neuroscience*, chapter 11. Oxford University press, 2010.

[65] C. R. Laing. Rotating waves in rings of coupled oscillators. *Dynamics and stability of systems*, 13(4):305–318, 1998.

[66] B. Lindner, J. Garcia-Ojalvo, A. Neiman, and L. Schimanski-Geier. Effects of noise in excitable systems. *Physics reports*, 392:321 – 424, 2004.

[67] B. Lindner, L. Schimansky-Geier, and A. Longtin. Maximizing spike train coherence or incoherence in the leaky integrate and fire model. *Physical Review E*, 66, 2002.

[68] K.A. Lindsay, J. R. Rosenberg, and G. Tucker. Analytical and numerical construction of equivalent cables. *Mathematical biosciences*, 184:137 – 164, 2003.

[69] G. Lord and V. Thümmler. Freezing stochastic travelling waves. Technical Report 08-010, Bielefeld University, 2008.

[70] G. J. Lord and S. Coombes. Traveling waves in the Baer and Rinzel model of spine studded dendritic tissue. *Physica D*, 161:1 – 20, 2002.

[71] S. Luccioli, T. Kreus, and A. Torcini. Dynamical response of the Hodgkin-Huxley model in the high-input regime. *Physical Review E*, 73, 2006.

[72] E. Manjarrez, J. G. Rojas-Piloni, I. Méndez, L. Martínez, D. Vélez, D. Vazquez, and A. Flores. Internal stochastic resonance in the coherence between spinal and cortical neuronal ensembles in the cat. *Neuroscience Letters*, 326, 2002.

[73] A. Manwani and C. Koch. Detecting and estimating signals in noisy cable structures, i: Neuronal noise sources. *Neural Computation*, 11:1797–1829, 1999.

[74] E.A. Martens, C. R. Laing, and S. H. Strogatz. Solvable model of spiral wave chimeras. *Physical Review Letters*, 104, 2010.

[75] The MathWorks. Matlab. www.mathworks.com.

[76] K. A. Newhall, G. Kovacic, P. R. Kramer, and D. Cai. Cascade-induced synchrony in stochastica;;y-driven neuronal networks. *Physical review E*, To Appear.

[77] K. A. Newhall, G. Kovacic, P. R. Kramer, D. Zhou, A. V. Rangan, and D. Cai. Dynamics of current-based poisson driven integrate-and-fire neuronal networks. *Communication Math Science*, 2010.

[78] E. A. Novikov. Functionals and the random-force method in turbulence theory. *Soviet physics JEPT*, 20(5):1290–1294, 1965.

[79] J. M. Ogden, J. R. Rosenberg, and R. R. Whitehead. *Modeling in the neurosciences:from ionic channels to neural networks*, chapter 7. Harwood Academic Publishers, 1999.

[80] B. Øksendal. *Stochastic differential equations: An introduction with applications.* Springer, 2007.

[81] R. Osan and B. Ermentrout. The evolution of synaptically generated waves in one- and two-dimensional domains. *Physica D*, 163:217–235, 2002.

[82] K. Pakdaman, S. Tanabe, and T. Shimokawa. Coherence resonance and discharge time reliability in neurons and neuronal models. *Neural networks*, 14, 2001.

[83] R. R. Poznanski, editor. *Modelling in the neurosciences: From ionic channels to neural networks*. Harwood Academic Publishers, 1999.

[84] R. R. Poznanski, editor. *Biophysical neural networks: Foundations of integrative neuroscience*. Mary Ann Liebert Inc., 2001.

[85] R.R. Poznanski. A generalized tapering equivalent cable model for dendritic neurons. *Bulletin of mathematical biology*, 53:457 – 467, 1991.

[86] C. Prevot and M. Rockner. *A concise course on stochastic differential equations*. Springer, 2007.

[87] W. Rall. Theory of physiological properties of dendrites. *Ann. N.Y. Acad. Sci.*, 96:1071 – 1092, 1962.

[88] K. F. Riley, M. P. Hobson, and S. J. Bence. *Mathematical methods for physics and engineering*. Cambridge university press, 2006.

[89] J. Rinzel and J. B. Keller. Travelling wave solutions of a nerve conduction equation. *Biophysical journal*, 13, 1973.

[90] J. C. Robinson. *An introduction to ordinary differential equations*. Cambridge University Press, 2004.

[91] A. Rocco, J. Casademunt, U. Ebert, and W. van Saarloos. Diffusion coefficient of propagating fronts with multiplicative noise. *Physical Review E*, 65, 2001.

[92] A. Roth and M. Haüsser. Compartmental models of rat cerebellar Purkinjie cells based on simultaneous somatic and dendritic patch-clamp recordings. *Journal of Physiology*, 535:445–472, 2001.

[93] R.R.Poznanski, editor. *Biophysical neural networks*, chapter 15. Mary Ann Liebert Inc., 2000.

[94] M. Rudolph and A. Destexhe. Correlation detection and resonance in neural systems with distributed noise sources. *Physical Review Letters*, 86(16):3662–3665, 2001.

[95] M. Rudolph and A. Destexhe. A fast conducting stochastic integrative mode for neocortical neurons in vivo. *Journal of Neuroscience*, 23:2466–2476, 2003.

[96] M. A. Santos and J. M. Sanchos. Front dynamics in the presence of spatiotemporal structured dynamics. *Physical Review E*, 64, 2001.

[97] M. Schatzman. *Numerical analysis: A mathematical introduction*. Oxford, 2002.

[98] A. Scott. *Neuroscience: A mathematical primer*. Springer-Verlag, 2002.

[99] I. Segev and W. Rall. Excitable dendrites and spines: Earlier theoretical insights elucidate recent direct observations. *TINS*, 21:453–460, 1998.

[100] T. Shardlow. Numerical simulation of stochastic PDEs for excitable media. *Journal of computational and applied mathematics*, 175:429–446, 2005.

[101] T. Shimokawa, K. Pakdaman, and S. Sato. Time-scale matching in the response of a leaky integrate-and fire neuron model to periodic stimulus with additive noise. *Physical Review E*, 59, 1999.

[102] M. Steriade. Sleep, epilepsy and thalamic reticular inhibitory neurons. *Trends in neuroscience*, 28(6):317–324, 2005.

[103] D. C. Sterratt and A. van Ooyen. Does a dendritic democracy need a ruler? *Neurocomputing*, 58-60:437–442, 2004.

[104] E. Steur, I. Tyukin, and H. Nijmeijer. Semi-passivity and synchronisation of diffusively coupled neuronal oscillators. *Physica D*, 238:2119 – 2128, 2009.

[105] N. G. Stocks. Suprathreshold stochastic resonance in multilevel threshold systems. *Physical Review Letters*, 84, 1999.

[106] N. G. Stocks and R. Mannella. Generic noise-enhanced coding in neuronal arrays. *Physical Review E*, 64, 2001.

[107] R. F. Thompson. *The Brain: An introduction to neuroscience*. W H Freeman and Company, 1985.

[108] Y. Timofeeva, S. J. Cox, S. Coombes, and K. Josić. Democratization in a passive dendritic tree: an analytical investigation. *Journal of computational neuroscience*, 25:228–244, 2008.

[109] Y. Timofeeva, G. J. Lord, and S. Coombes. Spatio-temporal filtering properties of a dendritic cable with active spines: A modelling study in the spike-diffuse-spike framework. *Journal of Computational Neuroscience*, 2006.

[110] R. E. L. Turner. Travelling waves in neural models. *Journal of mathematical fluid dynamics*, 7:S289–S298, 2005.

[111] P. S. Ulinski, E. G. Jones, and A. Peters. *Cerebral cortex*. Kluwer Academic, 1999.

[112] A. van Ooyen, editor. *Modeling neural development*. The MIT Press, 2003.

[113] D. W. Verzi. Modelling activity dependent synapse restructuring. *Bulletin of mathematical biology*, 2003.

[114] D.W. Verzi, M.B. Rheuben, and S.M. Baer. Impact of time dependent changes in spine density and spine shape on the input-output properties of a dendritic branch: a computational study. *Journal of neurophysiology*, 93:2073 – 2089, 2005.

[115] P. Vetter, A. Roth, and M. Haüsser. Propagation of action potentials in dendrites depends on dendritic morphology. *Journal of Neurophysiology*, 85:926–937, 2001.

[116] Y. Wang, D.T.W. Chik, and Z.D. Wang. Coherence resonance and noise induced synchronisation in globally coupled Hodgkin-Huxley neurons. *Physics review E*, 61:740–746, 2000.

[117] R. W. Williams and K. Herrup. The control of neuron number. *Annual Review of Neuroscience*, 11:423–453, 1988.

[118] R. y Cajal. *Les Nouvelles idées sur la structure de systeme nerveux chez l'homme et chez les vertébrés*. Reinwald, 1894.

[119] L.C. Yeung, G.C. Castellani, and H.Z. Shouval. Analysis of the intraspinal calcium dynamics and its implications for the plasticity of spiking neurons. *Physical Review E*, 69, 2004.

[120] R. Yuste and T. Bonhoeffer. Morphological changes in dendritic spines associated with long term synaptic plasticity. *Annual review neuroscience*, 24:1071 – 1089, 2001.

[121] R. Yuste and W. Denk. Dendritic spines as a basic functional units of neuronal integration. *Nature*, 375:682–684, 1995.

[122] C. Zhou and J. Kurths. Noise-induced synchronization and coherence resonance of a Hodgkin-Huxley model of thermally sensitive neurons. *CHAOS*, 13(1):401–409, 2003.